MOLECULAR THERMODYNAMICS OF NANOSCALE COLLOID-POLYMER MIXTURES: CHEMICAL POTENTIALS AND INTERACTION FORCES

A Thesis
Presented to
The Academic Faculty

By

Krishna Tej Marla

In Partial Fulfillment
of the Requirements for the Degree
Doctor of Philosophy in Chemical Engineering

Georgia Institute of Technology
August, 2004

MOLECULAR THERMODYNAMICS OF NANOSCALE COLLOID-POLYMER MIXTURES: CHEMICAL POTENTIALS AND INTERACTION FORCES

Approved by:

Dr. J. Carson Meredith, Advisor

Dr. Charles A. Eckert

Dr. Clifford L. Henderson

Dr. Rigoberto Hernandez

Dr. Peter J. Ludovice

DATE APPROVED: 6 August 2004

I want to know God's thoughts; the rest are details.

- Albert Einstein

Dedicated

To my parents

who have

enlightened me about the highest pursuits in life

edified me with the knowledge to seek them

lit up the path for me to follow…

ACKNOWLEDGEMENTS

My graduate school experience has been truly rewarding and enriching and I would like to thank all the people who have made this possible. I would like to express my deepest gratitude to my advisor Dr. J. Carson Meredith for his guidance, patience, support, encouragement, approachability and motivation during the past four years. His emphasis on critical thinking and fundamental understanding and his work ethic and attitude towards research have been an ideal model for me to follow. His optimism and calm approach were a panacea in times of 'research crises'. I have had the privilege of being his first graduate student, something that I would always cherish.

I would like thank my thesis committee members, Dr. Charles Eckert, Dr. Cliff Henderson, Dr. Rigoberto Hernandez and Dr. Pete Ludovice for volunteering to be on my committee and providing valuable suggestions on various aspects of this work. I would also like to thank members of the Meredith Research group for creating an enjoyable working environment. I would especially like to thank Joe Sormana for being a good friend and also for all the entertainment in the office. I would like to acknowledge Dr. Santanu Chattopadhyay for all his help in the lab. I would also like to thank friends that I made in Atlanta: Augustin and Subramanian for helping me get settled when I first landed here, Karthik for being a wonderful roommate, and Niket for all his *fundaes*.

I am most grateful to my parents, who have instilled in me the value of knowledge and education, taught me to pursue the right goals and provided me with everything that I need to achieve them. I would also like to thank my brother, Vishnu, for being a role model of hard-work and perseverance and also for being a constant source of strength and motivation. I would like to thank my wife, Geetanjali, for her unwavering support and

understanding, immense patience, and the peace and happiness that she has brought into my life. I am truly blessed to have you as my partner in life. Thank you for being my best friend and sharing my goals.

Finally, I thank God for His infinite grace and making everything possible.

TABLE OF CONTENTS

LIST OF TABLES

LIST OF FIGURES

SUMMARY

Nanoscale colloidal particles display fascinating electronic, optical and reinforcement properties as a consequence of their dimensions. Stable dispersions of nanoscale colloids find applications in drug delivery, biodiagnostics, photonic and electronic devices, and polymer nanocomposites. Most nanoparticles are unstable in dispersions and polymeric surfactants are added generally to improve dispersability and control self-assembly. However, the effect of polymeric modifiers on nanocolloid properties is poorly understood and design of modifiers is guided usually by empirical approaches. Monte Carlo simulations are used to gain a fundamental molecular-level understanding of the effect of modifiers properties on the thermodynamics and interaction forces of nanoscale colloidal particles. A novel method based on the expanded ensemble Monte Carlo technique has been developed for calculation of the chemical potential of colloidal particles in colloid-polymer mixtures (CPM). Using this method, the effect of molecular parameters like colloid diameter, polymer chain length, colloid-polymer interaction strength, and colloid and polymer concentrations, on the colloid chemical potential is investigated for both hard-sphere and attractive Lennard-Jones CPM. The presence of short-chain polymeric modifiers reduces the colloid chemical potential in attractive as well as athermal systems. In attractive CPM, there is a strong correlation between polymer adsorption and colloid chemical potential, as both show a similar dependence on the polymer molecular weight. Based on the simulation results, simple scaling relationships are proposed that capture the functional dependence of the thermodynamic properties on the molecular parameters. The polymer-induced interaction

forces between the nanoparticles have been calculated as a function of the above parameters for freely-adsorbing and end-grafted homopolymer modifiers. The polymer-induced force profiles are used to identify design criteria for effective modifiers. Adsorbing modifiers give rise to attractive interactions between the nanoparticles over the whole parameter range explored in this study. Grafted surface modifiers lead to attraction or repulsion based on the polymer chain length and grafting density. The polymer-induced attraction in both adsorbing and grafted modifiers is attributed primarily to polymer intersegmental interactions and bridging. The location of the thermodynamic minimum corresponding to the equilibrium particle spacing in nanoparticle-polymer mixtures can be controlled by tuning the modifier properties.

CHAPTER 1

INTRODUCTION

In 1915 Wolfgang Ostwald described colloid science as a "*world of neglected dimensions*" as it deals with structures that are much larger than atoms and molecules, but are considerably smaller than macroscopic objects that can be directly perceived. About a century later with the rediscovery of nanoparticles, this "world" referred to by Ostwald is at the forefront of scientific research endeavor and technological innovation. Exploitation of nanoparticles and nanostructured materials is expected to lead to "breakthroughs in areas such as nanoelectronics, healthcare and medicine, materials and manufacturing, chemical, biotechnology, agriculture, information technology and national security".[1] Generally, polymers and surfactants must be added to nanoparticles to improve dispersability and direct self-assembly. Unfortunately, robust molecular models of these complex multiscale nanoparticle-polymer mixtures are unavailable and a detailed understanding of the effects of polymeric modifiers on nanocolloid properties is lacking. The objective of this work is to develop a fundamental molecular understanding of the thermodynamic properties and interaction forces in these nanoscale colloid-polymer systems. This chapter provides a brief overview of the recent theoretical and modeling efforts directed towards studying various aspects of these systems. The motivation and

specific aims of this work are also described. In addition, an outline of the thesis summarizing the work in the remaining chapters is presented.

1.1 BACKGROUND AND MOTIVATION

The colloidal domain of matter, broadly defined as particles of sizes ranging from 1 nm to 1μm, is ubiquitous in natural and man-made materials. The size range of colloids is more or less defined by the importance of Brownian motion – the translational diffusion of particles arising from constant bombardment of the molecular species in dispersion medium. The upper size limit is largely determined by the size at which external force fields, such as gravity, dominate the effects of Brownian motion. This Brownian motion allows the statistical mechanical treatment of these systems and ensures that a suspension of such particles can thermodynamically seek the lowest free-energy state. In addition, colloids are also characterized by their innate ability to either remain dispersed in solution, or randomly aggregate, or organize themselves into ordered arrays, depending on the nature of the governing interparticle forces and the medium. The traditional applications of colloids range from paints, coatings and foods to a multitude of manufacturing processes.

In the recent past, advances in physical and chemical sciences have led to the development of sophisticated analytical methods such as electronic, atomic and scanning probe microscopy, X-ray and neutron scattering, and electrochemistry, which are capable of probing and manipulating materials on a nanometer scale. These methods, combined with the development of simple, reproducible and quite general techniques to manufacture nanometer-sized colloidal particles have catapulted nanotechnology to the

frontier of physical science research. Nanoscale particles offer size-dependent, tunable, and different chemical and physical properties than bulk materials, which form the basis for new technologies. Stable dispersions of these colloidal particles have already found a wide array of fascinating applications such as genetic or biological probes in drug discovery and screening, quantum dots for biochemical sensing, catalysts and polymer nanocomposites. On the other hand, their size and ability to self-organize makes these nanocolloids ideally suited for the creation of three-dimensional structures with feature sizes of the order of the wavelengths of electrons or photons. This self-assembly approach provides an inexpensive, thermodynamically driven "bottom-up" alternative to the fabrication of electronic devices, similar to the one used by nature to construct complex biological architectures. Harnessing these potential applications hinges on understanding and manipulating the phase behavior and interaction forces of nanoparticle dispersions.

Colloidal forces such as van der Waals (VDW), Coulombic, depletion and solvation could exist between nanoparticles suspended in a liquid. Nanoparticles tend to be fairly unstable in solution due to the ubiquitous attractive VDW forces between them. In addition, due to the large surface areas of these nanoparticles in dispersion, the interfacial free energy between the particle and the solvent tends to dominate the equilibrium and dynamic behavior of these systems. Control over these interactions can be achieved by chemical or physical modification of the surface and bulk properties of the colloidal particles and by tuning the solvent in which they are dispersed. There are two common approaches to stabilizing colloids, electrostatic and steric. In electrostatic stabilization, the attractive van der Waals forces are overcome by repulsive interactions

between the ions (and the associated counter ions) adsorbed on the particles. Steric stabilization is achieved by polymeric modifiers that are either adsorbed or grafted to the surface of the colloidal particles. When two such polymer-coated particles approach each other, the compression of the polymer layers results in an increased osmotic pressure and this is the origin of the repulsive force which keeps the particles at distances large enough to counter the VDW attractions, resulting in colloid stabilization. While polymeric modifiers (surfactants) have been used traditionally for stabilization of colloids, their ability to screen the interparticle VDW attraction also makes them well suited for controlled self-assembly applications. For example, changing the length of the polymeric modifiers can provide almost atomic-scale control over the spacing of nanoparticles in a colloidal crystal.[2] Short-chain organic modifiers are also used for passivating and capping reactive end-groups on nanoparticle surfaces.

Colloid-polymer systems have been studied extensively (mostly with regard to stabilization and flocculation applications) in the macroscopic limit of large colloidal particles and long polymer chains. However, a detailed understanding of how exactly these polymeric modifiers influence the thermodynamics and interaction forces in *nanoscale* systems is still lacking. At these size scales, particle curvature effects become increasingly important and in addition, the modifiers used are short-chain polymers (or oligomers) with characteristic dimensions similar to the colloidal nanoparticles. In this regime, questions like, how the physical and chemical properties of the modifiers affect the free-energy properties and phase-behavior of the colloids and how the polymer-induced forces compare with the bare nanoparticle interactions, remain unanswered. Thus, the design of appropriate modifiers for dispersion and controlled self-assembly

applications is guided usually by empirical approaches or previous work. As in other areas of materials and chemical processing, there is a critical need for physically-sound models of the effects of these organic surface modifiers on the nanoparticle thermodynamics and forces. These models would enable the rational molecular design of modifiers for specific applications, could be used to compare and interpret experimental data at different process conditions and would catalyze the discovery of synthetic routes to novel "designer materials" based on colloidal phenomena.

1.2 MODELING OF COLLOID-POLYMER SYSTEMS: A REVIEW

Over the past few decades, various aspects of colloid-polymer mixtures (CPM) including phase behavior, structure and interaction forces have been studied extensively using a combination of theoretical, experimental and simulation approaches. CPM are generally three-component systems composed of solid colloidal particles, macromolecules and solvent. The solvent molecules are generally much smaller than the colloids and polymers and hence theoretical and simulation approaches treat the solvent as a background continuum which can influence the effective interactions between the other two components. The primary complicating factor in studying these systems is the large length and time scale separations between colloids and polymers. For example, consider the simplest model of CPM where the colloids are treated as hard spheres and the polymers are treated at the microscopic Kuhn segment level. In this case, even though the radius of gyration (R_g) of the polymer chains may be of similar dimensions to the colloid size, the number of degrees of freedom required to model the polymer is several orders of magnitude higher than that needed for the colloid. Another complexity is the strong size asymmetry found in these systems ranging from the traditional problem of

large colloids and small polymers, to small particles and large macromolecules. In addition, there are also various colloid-polymer forces that are generally present including VDW attractions, Coulombic and repulsive excluded volume forces, which are of varying range and magnitudes. These factors make it extremely challenging to develop a unified theoretical approach for treating CPM, valid over all the relevant size and composition regimes. Despite several decades of theoretical and simulation efforts, it still remains a major challenge to achieve a fundamental and predictive understanding of the structure, thermodynamics and interaction forces of CPM over the entire parameter range of experimental and technological importance. Depending on the phenomena of interest and the target applications, simplifying assumptions are required usually to model these systems.

1.2.1 Theory

The earliest theoretical model of CPM was developed by Asakura and Oosawa, (AO)[3, 4] who in their seminal work on colloid-polymer mixtures, modeled the polymers as ideal spherical particles with respect to each other (phantom hard spheres) and hard spheres with respect to the colloids. This model was able to explain successfully the entropy-driven depletion attraction observed in hard-sphere CPM. Using this model, the CPM could be treated as an effective one-component fluid (colloid) model where the polymers enter implicitly through a pair-decomposable AO depletion potential. This approach was extended by Gast *et al* [5] to study the phase behavior of CPM and assign the nature (i.e. colloidal gaseous, liquid and solid state) of the coexisting phases. Lekkerkerker *et al* [6] later constructed a two-component mean field-like theory based on an AO-like model, which accounted for polymer partitioning at phase separation and

predicted the existence of three phase regions for a range of polymer and colloid concentrations. The AO model has been further treated by liquid state theory,[7] has been extended to non-homogeneous situations[8,9] and to perturbatively include non-ideality.[10] However, the AO model is valid only in the limit of dilute polymer solutions and for $\sigma_c >> R_g$, where σ_c is the colloid diameter. In the opposite limit of the AO model, where the colloidal particles are very small compared to the polymer chains, it is possible to integrate out the polymer degrees of freedom in the presence of small particles and field-theoretic approaches have been used successfully to obtain important insights in these systems.[11-14] The above two approaches are relevant only for the two limiting cases, $\sigma_c >> R_g$ and $\sigma_c << R_g$.

A promising approach, capable of treating the wide range of relevant length scales and geometric asymmetries in CPM is liquid-state theory. These liquid-state types of theories are well developed,[15] and have been applied to colloidal dispersions[16] and polymers.[17-19] The liquid-state theories for polymeric systems are referred to as PRISM theories (polymer reference interaction site model). In addition, liquid-state approaches can incorporate the polymer correlation length dependence as a function of polymer concentration and the flexibility of polymers that allows them to adjust their configuration in voids between the colloidal spheres. The main problem, however, is that this approach requires appropriate closure relations for the colloid-polymer interactions (reasonable closures exist for colloid-colloid and polymer-polymer correlations). Recently, Fuchs and Schweizer (FS) developed a general two-component macromolecular liquid-state integral equation approach to study the structure and thermodynamic properties of mixtures of hard-sphere colloids and flexible Gaussian

polymer chains.[20-22] They use a simple one-parameter extension of the Percus-Yevick closure for the colloid-polymer direct correlation function, that accounted for the non-local entropic repulsions between the polymer segments and the colloid. The FS approach is applicable to all size asymmetry ratios and over the whole range of colloid and polymer densities. The structure, phase behavior and other thermodynamic properties predicted by the FS model are in good agreement with experimental data.[23, 24]

Another approach that combines the AO model and liquid-state theory was developed by Louis and co-workers.[25-27] In their approach, the polymer chains are approximated as 'soft colloids' i.e. the detailed intersegmental interactions are replaced by an effective interaction between the centers-of-mass (CM) of the polymer coils. This effective interaction potential was obtained by inverting the radial distribution functions (from simulations) of the CM of the polymer coils. This methodology predicts many features of CPM quite well[28,29] and would potentially enable large multi-scale simulations of colloid-polymer mixtures, which are currently intractable. A key feature of all these above approaches and studies is that they consider only the simplest realization of colloid-polymer mixtures – hard sphere colloids and flexible polymer chains under athermal 'good solvent' conditions. The ubiquitous van der Waals attractions that exist in these systems are not accounted for in these models. Hence the results of these studies are relevant to mixtures of colloids and non-adsorbing polymers, where the only interactions that exist are polymer-induced depletion attraction and excluded volume repulsion. The introduction of attractive interactions of variable strength and spatial range induce significant changes in the mixture structure, thereby making the theoretical treatment of CPM using liquid-state theories a very difficult task. For example, if strong attractions (or

non-contact repulsions) exist between the polymer segments, then collective phenomena like polymer adsorption can occur which are difficult to capture using standard closure approximations. These problems could be overcome by using advanced computer simulation techniques, which are reviewed in the next section. Also, it should be noted that all of the above studies are directed towards understanding the thermodynamics, phase behavior and structure of CPM.

Colloid-polymer systems have also been studied extensively from another important perspective – polymer adsorption on colloidal surfaces and the resultant interaction forces. These studies are relevant to stabilization, flocculation and self-assembly of colloidal particles using polymeric surface modifiers, which are either adsorbed or end-grafted to the surface of the particles. Theoretical approaches to modeling structure and interaction forces between colloidal particles coated with polymeric modifiers are based broadly on either scaling analysis[30] or self-consistent field (SCF) theory. These approaches for treating adsorbing and end-grafted polymers are reviewed in detail in chapters 4 and 5 of this thesis. Most of the scaling and SCF-based studies focus invariably on flat and macroscopic colloidal surfaces and high molecular weight (long chain) polymers. However, in the case of nanoscale colloidal particles, the curvature effects become important and the often used Derjaguin approximation is no longer expected to hold. In addition, low molecular weight polymeric modifiers are used, where R_g of the polymer chains is of the same size range as σ_c. Also, as in the case of theoretical phase behavior studies of CPM, the colloid-polymer and the polymer-polymer VDW attractions are most often neglected in the calculation of interaction forces.

1.2.2 Simulation

Computer simulation methods are broadly classified into two categories (i) molecular dynamics in which the trajectories of the particles are calculated through Newton's equations of motion and (ii) Monte Carlo (MC) based methods in which the trajectories are tracked by performing a random walk through state space. Although computer simulations of CPM are computationally very intensive, they offer the advantage of explicitly accounting for the polymer internal degrees of freedom (that are important in CPM when $\sigma_c \approx R_g$) and allow the use of realistic interaction potentials. For calculating equilibrium thermodynamic properties of CPM, the MC technique is preferred usually as it is not constrained to follow the 'real' dynamics of the system, thereby avoiding the long relaxation times associated with polymeric systems. The ultimate goal of a MC simulation is that of obtaining accurate averages of the quantities of interest. To accomplish this, the MC recipe must be able to efficiently and effectively sample equilibrium conformations of the system, which contribute significantly to the final average properties, by proposing random trial moves. The trial moves are accepted with a Boltzmann probability that holds the appropriate thermodynamic properties at specified values.[31] The main challenge in simulating CPM is to propose non-overlapping trial moves for efficient sampling of equilibrium conformations. For polymers, the difficulty arises because their natural dynamics are dominated by topological constraints (for example, chains cannot cross and chain connectivity constraints) and hence any algorithm based on the real motion of macromolecules will be inefficient. Hence, many 'unphysical' Monte Carlo moves have been proposed to improve sampling of polymer conformations. The configurational continuum bias (CCB) algorithm[32-34] is one such

method in which the polymer chains are re-grown in low-energy conformations avoiding overlaps with surrounding molecules, thereby facilitating fast equilibration. MC simulations methods for polymeric systems have been reviewed comprehensively.[35]

With regard to simulating the phase behavior of CPM, one of the most important requirements is accurate calculation of the chemical potentials of both, polymers and colloids. The chemical potential is defined as the free energy of inserting a molecule (or a macromolecule/particle) into the system of interest, relative to a reference state. However, it is difficult to insert long chain molecules due to the high probability of overlap resulting in inefficient chemical potential calculation. This limitation can be overcome combining the CCB with the expanded ensemble technique for calculating polymer chemical potentials.[36] The idea is to define additional thermodynamic states and perform the chain insertion incrementally, rather than all at once, resulting in improved acceptance rates. This expanded ensemble technique has been used to simulate athermal chains in a pore,[37] bulk phase behavior[38] and adsorption of chains onto an attractive surface[39] in a supercritical fluid-polymer solution. The problem with calculating colloid chemical potentials is similar in nature (to the polymers) due to the large size of the particles, which results invariably in steric overlaps and low insertion probabilities. While chemical potentials of colloidal particles in CPM have not been simulated previously, the expanded ensemble technique could, in principle, be extended to colloids by using the colloid diameter as the expansion variable. Accurate calculation of colloid and polymer chemical potentials would enable full-scale phase behavior simulations of CPM. Although there have been a few previous simulation studies of the phase behavior of

CPM,[40, 41] they consider only athermal colloid-polymer systems (like most theoretical studies).

Computer simulations have also been widely used to study polymer adsorption on colloidal surfaces and interaction forces between polymer-coated colloids using both molecular dynamics and MC techniques. However, all these studies address either one or some combination of the following simplified situations:

i. large planar colloidal surfaces and relatively low molecular weight polymers (Derjaguin limit)[42-47]
ii. extremely small particles and long polymer chains (star polymer limit)
iii. hard-sphere polymer chains (good solvent conditions)
iv. $\sigma_c \approx R_g$, but colloid-polymer attractive interactions are neglected [48]
v. colloid-colloid attractive interactions are neglected

The applicability of most of these simulation studies is restricted to situations in which the VDW dispersion forces have been masked out either due to the effect of solvent or temperature conditions.

1.3 OBJECTIVES AND OUTLINE

A key issue in nanoscale materials and chemical processing is the need for thermodynamic models for colloid-polymer systems over the mesoscopic scale (~1 – 100 nm). A breakthrough in rational predictive strategies for nanoscale structural material synthesis would be the development of molecular-models that account for the effect of surfactants on the thermodynamic properties and interaction forces of nanoparticles. Theoretical approaches for calculating the thermodynamic properties and phase behavior of these systems are still in their infancy and treat only the simplified athermal cases. An

important advance would be to develop simulation algorithms that can accurately calculate the free-energy properties of attractive colloid-polymer systems in this size regime. Towards this goal, a method for accurate estimation of the chemical potential of organically modified nanoscale colloidal particles using Monte Carlo simulations has developed in this work. The chemical potential yields molecular-level insight into the effect of organic modifiers on the free energy of transferring particles from one phase to another. These potentials are the stepping-stone towards simulation of the full phase behavior and self-assembly of nanoparticles into crystalline arrays. Particle chemical potentials from simulations could also be used to develop accurate equation of state models for colloidal and nanoparticle systems.

Apart from the computationally intensive nature of these simulations, the most significant challenge is the large number of variables that affect the phase behavior of these systems. These include polymer chain length (molecular weight), polymer concentration, colloid size, colloid concentration, temperature (solvent effect) and the interaction energy parameters. In this work, the effect of each of these parameters has been investigated individually while holding the others constant. Although this is an arduous task, it will help provide a fundamental understanding of the dependence of colloid thermodynamics on each individual parameter. This knowledge could be used by experimentalists to juxtapose the effect of two or more variables in order to design optimal modifiers for a particular application. In addition, the effect of various molecular parameters on the polymer-induced interactions forces between the nanoparticles has also been investigated. Two different types of polymeric modifiers – freely adsorbing homopolymers and end-grafted polymers have been studied. The primary goal of this

work is to develop a fundamental understanding of the various molecular parameters on the thermodynamics and interactions forces in nanoscale colloid-polymer systems, which would eventually enable rational and predictive design of polymeric modifiers for self-assembly and stabilization of nanoscale colloidal systems. The outline of the thesis and objectives of each of the studies in the subsequent chapters are described below.

In Chapter 2, a novel algorithm based on the expanded ensemble Monte Carlo (EEMC) method is proposed for calculation of colloid chemical potentials (μ_c) in CPM. The statistical mechanical equations that form the basis of the algorithm are described in detail. The method, shown to be superior to conventional Widom[49] particle insertion, is validated by performing simulations of hard-sphere (HS) colloid-solvent (monomer) mixtures and comparing the chemical potentials to a theoretical equation of state. The infinite dilution colloid chemical potentials for HS colloid-polymer mixtures are calculated as a function of colloid diameter (σ_c) and polymer chain length (n) and compared to a recent integral equation model.[20, 21] Physical interpretations of the diameter and chain-length dependence of μ_c are discussed and empirically-derived function is presented for describing the μ_c as a power law function of R_g/R.

In Chapter 3, the EEMC method is extended to calculating colloid chemical potentials in a dilute dispersion of freely adsorbing homopolymers. The simulations are performed in the canonical NVT ensemble. The effects of σ_c, n colloid-polymer interaction strength and the polymer concentration on μ_c and polymer adsorption are investigated. A correlation between polymer adsorption and nanoparticle free energy is established. A simple scaling model for the physical dependence of μ_c on contributions from particle size and modifier chain length is proposed. This model reflects the physics

that connects chemical potential of nanoparticles with chain adsorption, that is observed in the simulations and could be used to compare, interpolate or extrapolate experimental data, as well as to motivate modeling efforts. In addition, the adsorption calculations are compared to the scaling theory of Aubouy and Raphael[50] in order to ascertain the applicability of this theory to the mesoscopic size range studied in the simulations.

In Chapter 4, the polymer-induced interaction force between two nanoparticles dispersed in a dilute solution of freely adsorbing homopolymers is calculated in the full thermodynamic equilibrium condition. The expanded grand canonical Monte Carlo method is used to simulate the equilibrium partitioning of polymer chains between the bulk phase and the colloid-polymer region. The force-distance profiles and polymer adsorption are calculated as a function of σ_c, n and polymer-particle adsorption energy. Based on the correlation between polymer adsorption and the force profiles, the dominant mechanism which leads to attraction or repulsion in these systems is proposed. The results are compared to the force profiles in the flat-wall limit to underscore the effect of particle curvature in nanoscale CPM.

The interaction forces between the nanoparticles with polymeric modifiers that are end-grafted irreversibly to the particle surface are studied in Chapter 5. In addition to the molecular parameters mentioned above (σ_c, n and polymer-particle adsorption energy), the effect of grafting density (ρ_a) on the polymer-induced force profiles between the nanoparticles is investigated using NVT Monte Carlo simulations. The conformational properties of the grafted polymer chains are also calculated and correlated to the observed force profiles. Based on the interplay between the various molecular

parameters, the physical mechanisms that lead to attraction or repulsion in the force profiles are identified.

While the colloid chemical potentials calculated in Chapters 2 and 3 are in the infinite dilution limit, Chapter 6 studies the effect of finite colloid concentrations on chemical potential using the EEMC method. The trends in the μ_c are correlated to the colloid-colloid, $g_{cc}(r)$, and colloid-polymer, $g_{cp}(r)$, radial distribution functions. In addition, the $g_{cc}(r)$ obtained from the simulations are inverted using the Ornstein-Zernike technique supplemented with closure approximations to obtain effective one-component colloid potentials. This coarse-graining procedure allows the binary CPM to be represented as pure one-component colloidal systems, thereby providing a route to large multiscale simulations of CPM.

1.4 REFERENCES

(1) http://www.nano.gov

(2) Murray, C. B.; Kagan, C. R.; Bawendi, M. G. *Science* **1995,** 270, 1335-1338.

(3) Asakura, S.; Oosawa, F. *J. Polym. Sci.* **1958,** 33, 183.

(4) Asakura, S.; Oosawa, F. *J. Chem. Phys.* **1954,** 22, 1255-1256.

(5) Gast, A. P.; Hall, C. K.; Russel, W. B. *J. Colloid Interface Sci.* **1983,** 96, 251-267.

(6) Lekkerkerker, H. N. W.; Poon, W. C. K.; Pusey, P. N.; Stroobants, A.; Warren, P. B. *Europhys. Lett.* **1992,** 20, (6), 559-64.

(7) Louis, A. A.; Finken, R.; Hansen, J. P. *Europhys. Lett.* **1999,** 46, (6), 741-747.

(8) Schmidt, M.; Lowen, H.; Brader, J. M.; Evans, R. *Phys. Rev. Lett.* **2000,** 85, (9), 1934-1937.

(9) Brader, J. M.; Evans, R. *Europhys. Lett.* **2000,** 49, (5), 678-684.

(10) Warren, P. B.; Ilett, S. M.; Poon, W. C. K. *Phys. Rev. E: Stat., Nonlinear, Soft Matter Phys.* **1995,** 52, (5-B), 5205-13.

(11) Eisenriegler, E. *Phys. Rev. E: Stat., Nonlinear, Soft Matter Phys.* **1997,** 55, (3-B), 3116-3123.

(12) Eisenriegler, E. *J. Chem. Phys.* **2000,** 113, (12), 5091-5097.

(13) Eisenriegler, E.; Hanke, A.; Dietrich, S. *Phys. Rev. E* **1996,** 54, (2), 1134 - 1152.

(14) Eisenriegler, E. *J. Phys.: Condens. Matter* **2000,** 12, (8A), A227-A232.

(15) Hansen, J. P.; McDonald, I. R., *Theory of Simple Liquids*. 2nd ed.; Academic: London, 1986.

(16) Agterof, W. G. M.; Van Zomeren, J. A. J.; Vrij, A. *Chem. Phys. Letters* **1976,** 43, (2), 363-7.

(17) Chatterjee, A. P.; Schweizer, K. S. *Macromolecules* **1998,** 31, (7), 2353-2367.

(18) Schweizer, K. S.; Curro, J. G. *Adv. Poly. Sci.* **1994,** 116, (Atomistic Modeling of Physical Properties), 319-77.

(19) Schweizer, K. S.; Curro, J. G. *Adv. Chem. Phys.* **1997,** 98, 1-142.

(20) Fuchs, M.; Schweizer, K. S. *Europhys. Lett.* **2000,** 51, 621-627.

(21) Fuchs, M.; Schweizer, K. S. *Phys. Rev. E* **2001,** 64, 021514.

(22) Fuchs, M.; Schweizer, K. S. *J. Phys.: Condens. Matter* **2002,** 14, R239-R269.

(23) Ramakrishnan, S.; Fuchs, M.; Schweizer, K. S.; Zukoski, C. F. *Langmuir* **2002,** 18, (4), 1082-1090.

(24) Ramakrishnan, S.; Fuchs, M.; Schweizer, K. S.; Zukoski, C. F. *J. Chem. Phys* **2002,** 116, 2201.

(25) Louis, A. A.; Bolhuis, P. G.; Hansen, J. P.; Meijer, E. J. *Phys. Rev. Lett.* **2000,** 85, (12), 2522-2525.

(26) Bolhuis, P. G.; Louis, A. A. *Macromolecules* **2002,** 35, (5), 1860-1869.

(27) Bolhuis, P. G.; Louis, A. A.; Hansen, J. P.; Meijer, E. J. *J. Chem. Phys.* **2001,** 114, (9), 4296-4311.

(28) Bolhuis, P. G.; Louis, A. A.; Hansen, J. P. *Phys. Rev. Lett.* **2002,** 89, (12), 128302.

(29) Louis, A. A.; Bolhuis, P. G.; Meijer, E. J.; Hansen, J. P. *J. Chem. Phys.* **2002,** 117, (4), 1893-1907.

(30) de Gennes, P. G., *Scaling Concepts in Polymer Physics*. ed.; Cornell University Press: Ithaca, 1979; p 324.

(31) Allen, M. P.; Tildesley, D. J., *Computer Simulation of Liquids*. ed.; Clarendon Press: Oxford, 1987; p.

(32) Frenkel, D.; Smit, B., *Understanding Molecular Simulations: From Algorithms to Applications*. ed.; Academic Press: San Diego, Calif., 1996; p 450.

(33) Mooij, G. C. A. M.; Frenkel, D. *Mol. Phys.* **1991,** 74, (1), 41-47.

(34) de Pablo, J. J.; Laso, M.; Suter, U. W.; Cochran, H. D. *Fluid Phase Equilib.* **1993,** 83, 323-331.

(35) de Pablo, J. J.; Escobedo, F. *Adv. Chem. Phys.* **1999,** 105, 337-367.

(36) Escobedo, F.; de Pablo, J. J. *J. Chem. Phys.* **1995,** 103, (7), 2703-2710.

(37) Escobedo, F. A.; de Pablo, J. J. *J. Chem. Phys.* **1997,** 106, (23), 9858-9868.

(38) Gromov, D. G.; de Pablo, J. J.; Luna-Barcenas, G.; Sanchez, I. C.; Johnston, K. P. *J. Chem. Phys.* **1998,** 108, (11), 4647.

(39) Meredith, J. C.; Johnston, K. P. *Langmuir* **1999,** 15, 8037-8044.

(40) Meijer, E. J.; Frenkel, D. *J. Chem. Phys* **1994,** 100, (9), 6873.

(41) Meijer, E. J.; Frenkel, D. *Physica A* **1995,** 213, 130-137.

(42) Lai, P. Y.; Binder, K. *J. Chem. Phys.* **1991,** 95, (12), 9288-99.

(43) Toral, R.; Chakrabarti, A.; Dickman, R. *Phys. Rev. E: Stat., Nonlinear, Soft Matter Phys.* **1994,** 50, (1), 343-8.

(44) Murat, M.; Grest, G. S. *Phys. Rev. Lett.* **1989,** 63, (10), 1074-7.

(45) Murat, M.; Grest, G. S. *Macromolecules* **1989,** 22, (10), 4054-9.

(46) Dijkstra, M. *Thin Solid Films* **1998,** 330, 14-20.

(47) Yethiraj, A.; Hall, C. K. *Macromolecules* **1990,** 23, 1865-1872.

(48) Toral, R.; Chakrabarti, A. *Phys. Rev. E: Stat., Nonlinear, Soft Matter Phys.* **1993,** 47, (6), 4240-6.

(49) Widom, B. *J. Chem. Phys* **1963,** 39, (11), 2808-2812.

(50) Aubouy, M.; Raphael, E. *Macromolecules* **1998,** 31, 4357-4363.

CHAPTER 2

SIMULATION OF NANOCOLLOID CHEMICAL POTENTIALS IN A HARD-SPHERE POLYMER SOLUTION: EXPANDED ENSEMBLE MONTE CARLO

A novel application of the expanded ensemble Monte Carlo (EEMC) simulation method to calculation of the chemical potential of nanocolloidal particles in colloid-polymer mixtures is presented. This approach uses an expanded canonical ensemble in which the colloidal particle diameter is an additional ensemble variable, allowed to vary between zero and the maximum colloid size desired. Using a hard-sphere model system, we demonstrate that this approach is superior to the Widom method for calculating chemical potentials in colloid-polymer systems. Specifically the EEMC leads to lower uncertainties and is capable of calculating accurate colloid chemical potentials for particle sizes where Widom insertion fails due to overlap. The EEMC method is applied to calculate the colloid chemical potential for an infinitely dilute colloidal particle (hard-sphere) in a dilute polymer (hard-sphere chain) solution over a wide range of relative sizes, $0.1 < R_g/R < 12$, where R_g is the polymer radius of gyration and R is the colloid radius. The simulation results are compared to the predictions of models developed by others: an integral equation model (FS) [Fuchs and Schweizer, *Europhys. Lett.* **51**, 621

(2000)] and a field theoretic (FT) approach [Eisenriegler *et al*., *Phys. Rev. E*. **54**, 1134, 1996]. Very good agreement is observed with the FS model over a wide range of R_g/R values, whereas the FT model agrees well only at large R_g/R. An empirical power law function is found to represent the simulation results well, potentially useful for analysis of free energy data for colloid-polymer mixtures.

2.1 INTRODUCTION

Dispersions of nanoscale colloidal particles play an important role in advanced materials synthesis and processing, with examples that include nanoparticle-filled polymers, self-assembled nanolattices of magnetic or quantum dot particles for sensors and electronics, and colloidal crystals for optical and photonic devices. In many experimental approaches to dispersion and self-assembly of nanoscale colloids, surfactants in the form of oligomers or polymers are added in order to improve dispersability or to control the onset of self-assembly. A few recent examples include noble metal nanoparticles stabilized with poly (2-hydroxyl methacrylates),[1] two- and three-dimensional arrays of Pd or CdSe nanocrystals modified with alkanethiols,[2, 3] and polymer-silica nanocomposites that mimic natural organic-inorganic materials.[4, 5] For lyophilic colloids, self-assembly can be driven by entropic packing forces, or in the presence of dissolved nonadsorbing polymer, entropic depletion forces.[6, 7] The development of molecular-based approaches to describing such self-assembly behavior is of intense current interest.[6-13]

Due to extremely large surface areas, the interfacial free energy between the colloid and the continuous phase can dominate the equilibrium and dynamic behavior of these systems. Molecular-based approaches that account accurately for the size,

chemistry, and structure of modifiers at the colloidal surface could be used for rational design of modifiers that lead to desired phase behavior and self-assembly. However, robust molecular models (active over large size ranges) of the effects of organic modifiers on the thermodynamic and transport properties of colloids are not generally available. Thus, the selection of appropriate organic modifiers (materials synthesis) or the understanding of their effects on colloid properties (materials characterization) is guided usually by empirical approaches or previous work. As in other areas of materials and chemical processing, accurate models for thermodynamic properties and phase behavior are critical to a scientific description and exploration of complex colloid-organic modifier systems.

One of the most important thermodynamic properties related to predicting colloid dispersability, self-assembly, and phase behavior is the chemical potential. A number of molecular-based equations of state have been developed that can describe accurately the thermodynamic properties of hard-sphere (HS) mixtures, including *colloid-solvent* mixtures. Perhaps the most well-known are the Carnahan-Starling[14] equation of state and its derivatives.[15-17] The HS system is an important fundamental model since it allows exploration of purely entropic configurational effects in the absence of attractive intermolecular potentials. This consideration is important for the calculation of chemical potentials, μ, since the configurational contribution (averaging over possible configurations Ω) is the most difficult part of the calculation. For example, for hard-spheres in a canonical ensemble, $\mu = -T(\partial S/\partial N)_{V,T} = -k_B T(\partial \ln Q/\partial N)_{V,T} = \Sigma_E\, \Omega(N,V,E)$, where Q and Ω are the canonical and microcanonical partition functions, respectively, N is the number of molecules, and V is the volume. In addition, the HS system is a

reasonably good model of the "good solvent" condition for colloid dispersions and polymer solutions.

In addition, a number of HS colloid-polymer models have been proposed. One recent and promising approach is that of Fuchs and Schweizer (FS),[9-11] which utilizes an integral equation combined with closure relationships based upon models of the colloid-colloid, polymer-polymer (PRISM), and colloid-polymer (modified Percus-Yevick) correlation functions. This model has recently been compared favorably to both phase behavior measurements[18] and osmotic compressibility measurements[19] for an athermal colloid-polymer-solvent system. Other approaches to developing equations of state and studying the phase behavior of colloid-polymer mixtures include field theoretic methods[8] and mean field theory.[12] However, due to computational difficulties with simulating colloid-polymer mixtures, these models have not been tested by comparing insertion chemical potentials to simulation studies. Such a comparison is critical in order to ascertain the model accuracy, range of applicable polymer and colloid sizes, and to guide future improvements.

The chemical potential is the free energy of inserting a molecule, or collection of molecules in the case of a colloidal particle, into the system of interest, relative to a reference state. The traditional approach to calculating μ from simulation is the Widom method,[20] in which a test molecule is inserted in the system multiple times at random positions. The interaction energy, U_0, between the test particle and the rest of the system is related to chemical potential via $\beta\mu = -\ln\langle\exp(-\beta U_0)\rangle$, where $\beta = 1/k_B T$ and $\langle\cdots\rangle$ denotes an ensemble average. While this approach works very well for small molecules and at moderate densities, severe difficulty arises for larger molecules like polymers or

molecular aggregates such as colloids. When a large polymer or colloid is inserted randomly into a fluid, the probability of overlap with existing molecules is very high. Thus, the Widom method would sample almost exclusively the high-energy (overlap) contributions, while sampling very few of the lower energy cases where the polymer or colloid is successfully inserted. As a result the accuracy and efficiency of chemical potential measurement is very low, and becomes intractable above a critical particle size and system density. From our own Widom calculations for colloids (Figure 2.3), we find this point to be approximately $\rho\sigma_c/\sigma_s \approx 0.3$, where ρ is the number density, σ_c is the colloid diameter, and σ_s is the solvent diameter.

A number of approaches have been taken to overcome these sampling limitations in free energy calculations during Monte Carlo simulations. The *expanded ensemble* (EE) method is one such approach, developed originally for calculating the Helmholtz free energy at any temperature.[21] In this method, additional ensemble variables are introduced in order to define a reversible and efficient path between the two states at which free energy measurement is desired. The additional states are sampled during the simulation according to probabilities determined from the partition function. The approach has been adapted for the calculation of the chemical potential of polymers.[22, 23] This method overcomes the problem of low insertion probabilities by allowing chain length of the test chain, the expansion variable, to be varied between zero and full length. Hence, the insertion of the test chain occurs in gradual steps, rather than all at once, and the incremental chemical potentials are summed to obtain the total potential.[22, 24, 25] This technique has been used to calculate the *polymer* chemical potential for a single chain in a colloidal medium.[26]

In this chapter, we have applied the EE approach to the calculation of colloid chemical potentials in HS colloid-solvent and colloid-polymer mixtures. In our approach, the colloid diameter is the expansion variable and is allowed to vary between zero (fully removed) and full size via discrete increments and decrements. In this work, as the colloid is gradually inserted, the incremental chemical potentials associated with each diameter are calculated. These incremental chemical potentials can be summed to obtain the total colloid chemical potential, as we show below. The use of diameter increments in expanded ensemble calculations has been demonstrated previously, for example in calculating free energy properties of single-component fluids.[27, 28] What is novel here is the application of diameter-increment EEMC to colloid-polymer mixtures. We first describe the adaptation of the EE to colloid-polymer systems. Then we present validation studies for HS colloid-solvent (monomer) mixtures. Since entropic excluded volume interactions are the reason that traditional Widom methods fail for colloids, the HS model provides a stringent test of the efficiency of the EE method presented here. Finally, we present the chemical potential for HS colloid-polymer mixtures at infinite dilution as a function of both colloid diameter and polymer chain length. We compare our calculations to both the FS integral equation theory[9-11] and field theoretic calculations,[8] and we discuss physical interpretations of the diameter and chain-length dependence of the colloid chemical potential. Finally, an empirically-derived function is presented for describing the colloid chemical potential as a power law of R_g/R.

2.2 SIMULATION DETAILS

In this work the EE method is applied to calculate the infinite dilution chemical potential of a colloid in pure solvent and in a dilute polymer solution. The simulations were performed in a cubic box with conventional periodic boundary conditions. In all cases, our system (depicted in Figure 2.1) consisted of a single colloidal particle (hard sphere, diameter σ_c) dispersed in either a pure HS solvent or a dilute HS polymer (or oligomer) solution. The polymer chains are fully flexible and consist of tangent HS segments with a constant bond length of σ_p. The polymer segment density ρ_p is maintained constant for all the simulations at $\rho_p = 0.05$, which corresponds to a packing fraction of $\Phi = 0.026$. However the polymer chain length was varied from n = 2 (oligomeric) to n = 60 to observe the effect of the chain length on the colloid chemical potential. The radius of gyration (R_g) and the reduced polymer concentration (c_p/c_p^*) values for the different chain lengths of polymer are shown in Table 2.1, where c_p is the polymer-molecule number density and c_p^* is the polymer-molecule number density at the dilute to semi-dilute crossover (where polymer coils begin to interact). The effect of colloid size on the chemical potential was also studied by varying σ_c from $1\sigma_p$ to $15\sigma_p$. In all of the simulations, the box length L (typically $40\sigma_p$) was greater than $n/2$ and σ_c, to prevent artificial intrachain or intraparticle interactions. We verified by a series of trial simulations at various box sizes and constant density that these artifacts do not appear for L/σ_c ratios above 2.5.

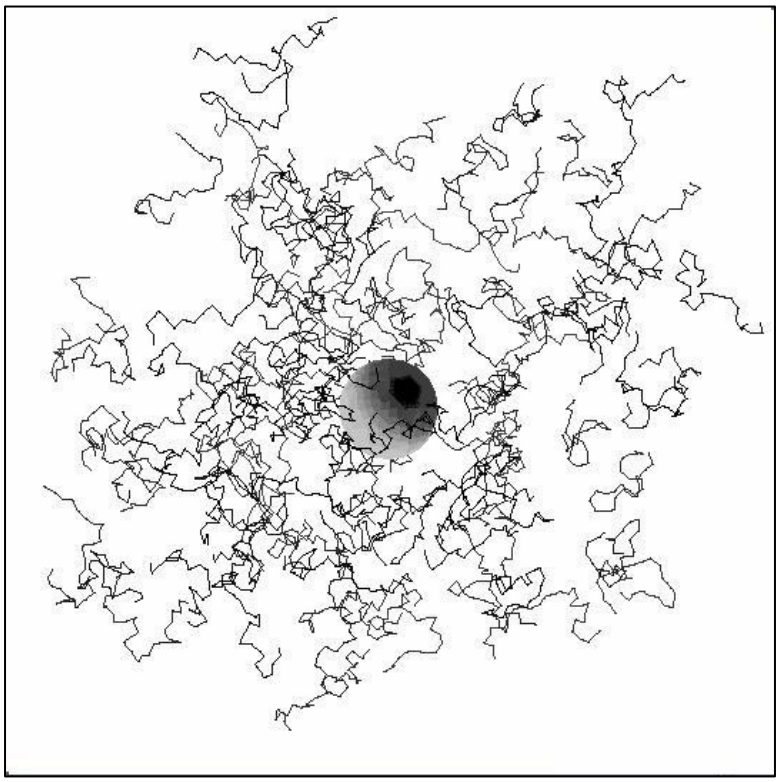

Figure 2.1: Configuration snapshot of the simulation box showing the single colloidal particle ($\sigma_c = 10$) and the polymer chains. ($n = 30$, $\rho_p^* = 0.05$).

2.2.1 Expanded Ensemble simulations for chemical potential

The generalized formulation of the EE and its application to the calculation of the chemical potentials and phase equilibria of polymers[21-23] can be found in the literature. Here we describe the EE method as applied to the calculation of the chemical potential of colloidal systems, or more generally, mixtures of large and small "particles". The diameter of the colloidal particle is allowed to vary from zero (fully removed) to full size by attempting discrete particle size increments and decrements. These size increments and decrements are accepted or rejected according to a Metropolis acceptance criterion described below. Thus, in contrast to the Widom[20] or inverse-Widom methods,[29] the particle is not inserted or deleted *all at once,* but in a number of more efficient partial steps. A predefined number of intermediate diameters of the particle is allowed by prescribing them as the different "states" of the EE. Incremental chemical potentials, calculated at each diameter describe the free energy of increasing diameter from d_i to d_{i+1}. The full chemical potential is recovered by summing the incremental values from zero to the desired particle size.

The canonical partition function for a pure colloid – solvent mixture in an EE is given by

$$\Omega = \sum_{y=1}^{D} Q(n_s, n_c, y, V, T)\exp(\psi_y) \tag{2.1}$$

where n_c and n_s are the total number of colloid and solvent molecules, V is the volume, T is the temperature and y is the state of the particle. Particle diameters of 0 and $\sigma_{c\,full}$ correspond to y = 0 and D, respectively. During the EE simulation, the state of the

particle changes by ± 1, which implies an increase or decrease by one step size. The transition moves take place between the neighboring *y* states. Particle size increments ($y \rightarrow y+1$) and decrements ($y \rightarrow y-1$) are attempted with equal frequency during the course of the simulation. When an end state is reached ($y = 0$ or $y = D$), the particle is either fully removed or fully added. Upon full removal the particle is added back at a random position with diameter zero. The particle size increments or decrements are accepted with a Metropolis criterion [30] that is given as

$$P(y \rightarrow y+\Delta) = \min\left[1, \frac{T(y+\Delta \rightarrow y)}{T(y \rightarrow y+\Delta)} \frac{p(y+\Delta)}{p(y)}\right] \tag{2.2}$$

where $T(y+\Delta \rightarrow y)$ is the probability of a transition from $y \rightarrow y+\Delta$ and $p(y+\Delta)$ is the probability of observing the system at state $y+\Delta$. For any two states of a system at y and $y+\Delta$ in a canonical EE, it has been shown that [22]

$$\frac{p(y+\Delta)}{p(y)} = \exp\left(-\beta\left[U_p(y+\Delta) - U_p(y)\right]\right)\exp\left(\psi_{y+\Delta} - \psi_y\right) \tag{2.3}$$

where $U_p(y)$ is the total interaction energy between the particle in state *y* and the rest of the system. The transition probabilities are given by:

$$T(y+\Delta \rightarrow y) = \frac{1}{NS} \tag{2.4}$$

where *NS* is the number of neighboring states to $y+\Delta$. In the case of colloid particles the number of neighboring states is always 2 except for the states $y = 0$ and $y = D$, in which case the number of neighboring states is one.

The efficiency of the diameter moves is controlled by the ψ_y preweighting factors, which set the frequency at which each particle diameter is visited. An efficient simulation results in a uniform distribution of states. For a uniform sampling of the particle diameters the probability of visiting each intermediate particle diameter d_i and d_{i+1} must be equal. Under this condition it can be shown that

$$\psi_{d_i} - \psi_{d_k} = \beta\mu_c^{ex}(d_i) - \beta\mu_c^{ex}(d_{i+1}) \tag{2.5}$$

The preweighting factors are calculated using eq 2.5 during a series of short trial simulations, prior to the longer averaging steps. Within a few million attempted moves, the factors converge onto a set of values that yield essentially uniform sampling of colloid diameters. We explored a number of uniform particle diameter increments between $\sigma_{c,full}$ / 30 to $\sigma_{c,full}$ / 5, and we found that the preweighting factors remain the same. For the averaging runs we used $\sigma_{c,full}$ / 20 as the increment. The set of preweighting factors is very sensitive to the maximum particle size ($\sigma_{c,full}$), particularly for $\sigma_{c,full}$ more than 10 times the size of a polymer segment. We were able to simulate colloid diameters up to a size of $\sigma_{c,full}$ = 15 times the polymer segment diameter by performing the simulations in two stages. First colloid diameters from 0 to 10 were simulated with one optimized set of preweighting factors. Then, colloid diameters from 10 to 15 were simulated with a different set of preweighting factors optimized from trial runs using colloid diameters from 10 to 15.

During the course of the simulation, incremental chemical potentials, $\beta\mu_c^{ex}$, associated with each diameter increment *i*, are calculated by $\beta\mu_c^{ex} = -\ln\langle\exp(\Delta E / k_B T)\rangle$,

where ΔE is the energy between the particle with diameter d_{i+1} and the rest of the system. These incremental values are stored and summed at the end of the run to obtain the total particle chemical potential. To validate the above EE formulation we calculated the chemical potentials of a pure HS solvent and of HS colloids in a pure solvent using the EE method. These results were compared with those obtained from the conventional Widom method and predictions from the Boublik-Mansoori-Carnahan-Starling-Leland (BMSCL)[14-16] equation of state and virial equation of state.

Our primary system of interest was a colloid in a dilute polymer solution. The EE formulation for this system is similar to that outlined above except that in this case the EE is applied to both chains and the particle, so that the chemical potential of the chain and the colloid may be calculated. The EE partition function for a homopolymer-colloid mixture consisting of N homopolymer chains, M colloid particles, one k-mer polymer and one particle at diameter state j is

$$\Omega = \sum_{j=1}^{D} \sum_{k=1}^{P} Q\left(N+M, V, T, a_j, b_k\right) \exp\left(\psi_j + \psi_k\right) \tag{2.6}$$

where $a_1 = 0$, $a_D = \sigma_{c\ full}$ and for any other intermediate state, a_j is an integer between 0 and D. Similarly for the chain $b_1 = 0$ and $b_P = n$, where n is the chain length of the polymer. In our case, which involves one-segment increments, we have $P = n + 1$ states and b takes integer values between 0 and n. The chemical potential of the polymer is calculated in an EE using a formulation similar to that as described above, except that a preselected number of *intermediate chain lengths* correspond to the states of the EE, presented elsewhere[22, 23].

Molecular rearrangement of polymer chains and translation of the colloidal particle are also performed to achieve thermal equilibrium. Chain displacements are attempted using the continuum configurational bias (CCB) algorithm, in which a portion of the chain is cut and regrown into a favorable energy configuration after scouting various positions. The details of the CCB algorithm are presented elsewhere.[31-34] The colloid particle is moved via random displacement accepted with the standard Metropolis Monte Carlo criterion[30].

2.2.2 Simulation statistics

In most cases 10 x 10^6 to 20 x 10^6 equilibrium steps and 60 x 10^6 to 120 x 10^6 averaging steps were used for statistical averaging of the properties of interest. In this work one MC step corresponds to one attempted move. Trial moves are performed at prescribed frequencies selected to yield acceptable number of moves for both polymer and colloid. The frequency of attempted moves was 10% colloid displacement, 10 % EE colloid moves, 40% CCB and 40% EE chain moves, which gave a good convergence to equilibrium. The statistical error for the conformational properties of the chains was taken as the root-mean square fluctuation divided by the square root of the number of independent blocks.[35] The error in the chemical potential was calculated based on the statistical inefficiency parameter s,[35] which is defined as

$$s = \frac{\lim}{\tau_b \to \infty} \frac{\tau_b \sigma_b^2}{\sigma^2} \tag{2.7}$$

where τ_b is the block size, σ_b^2 is the variance of block averages of length τ_b about the overall mean $\beta\mu_c^{ex}$ value, and σ^2 denotes the variance of all sampled $\beta\mu_c^{ex}$ values about

the mean. The statistical error in chemical potential for a simulation of length *Nsteps* Monte Carlo steps is then given by $\Delta\beta\mu_c^{ex} = (s/Nsteps)^{1/2} \times \sigma$. Note that the error bars have been omitted for all figures unless they were larger than the symbols representing the data points.

2.3 MODELS AND ANALYTICAL EXPRESSIONS

2.3.1 Infinitely dilute hard sphere colloid in a pure solvent

The Boublik-Mansoori-Carnahan-Starling-Leland (BMSCL) equation of state[14-16] can be used to calculate the chemical potential of a pure HS solvent as well as that of an infinitely dilute HS solute in a HS solvent. This equation of state is derived from solutions of the Percus-Yevick (PY) integral equation for the radial distribution function of a mixture of hard spheres. There are two well-known routes for calculating the equation of state from a radial distribution function. The first is obtained from differentiation of the logarithm of the configuration integral to give the virial equation and the other is the compressibility equation derived from fluctuations in the grand canonical ensemble.[16] The BMSCL equation of state is derived by taking a linear combination of the two solutions of the PY equation. The BMSCL expression for the chemical potential of an infinitely dilute hard colloidal sphere of diameter σ_c dissolved in a solvent of diameter σ_s is[36]

$$\beta\mu = 2\frac{\eta d^3}{(1-\eta)^3} + 3\frac{\eta d^2}{(1-\eta)^2} + 3\frac{\eta d\left(-d^2+d+1\right)}{1-\eta} + \left(-2d^3+3d^2-1\right)\ln(1-\eta) \quad (2.8)$$

where $d = \sigma_c/\sigma_s$ and $\eta = (\pi/6)(N/V)\sigma_s^3$ is the packing fraction of the solvent.

2.3.2 Colloid-polymer mixtures

Recently Fuchs and Schweizer developed a general two-component macromolecular liquid state integral equation approach to study the structure and thermodynamic properties of mixtures of HS colloids and flexible polymer chains.[9-11] A simple one-parameter extension of the PY closure for the colloid-polymer direct correlation function is proposed, that accounts for the non-local entropic repulsions between polymer segments and colloid (due to chain connectivity constraints). The form of the correlation function is $\hat{c}_{cp}(q) = \hat{c}^{s}_{cp}(q) \big/ (1 + q^2 \lambda^2)$ with $c^{s}_{cp}\left(r > \left(\sigma_c + \sigma_p\right)/2\right) = 0$, which accounts for the excluded volume on the local scale by fixing $c^{s}_{cp}(r)$ from the HS excluded volume condition. The carat (^) denotes a Fourier transform. The non-locality length λ captures the rearrangement of the polymer chains close to the colloidal particle and is determined by enforcing the thermodynamic consistency condition i.e., the chemical potential for inserting a single polymer into a colloidal suspension calculated from the compressibility and the free energy charging routes should be equal. Since the exact determination of λ is difficult, an approximate interpolation formula is used,

$$\lambda^{-1} = \xi^{-1} + \frac{1 + 2\phi_c}{1 - \phi_c} \frac{1}{\lambda_1 \sigma_c} \tag{2.9}$$

where $\lambda_1 = \left(\sqrt{5} - 1\right)/4$, ϕ_c = colloid packing fraction, and ξ is the polymer correlation length. The polymer chains are described with the assumption of Gaussian single chain statistics and a mean field approximation to the polymer correlations with self-avoidance.

The free energy of insertion of an infinitely dilute colloid HS into a polymer solution as derived from the FS model is given by

$$\beta\delta\mu_c = \frac{\pi c_p \sigma_c^3 \xi_c^2}{6\xi^2}\left(1+\frac{9+36\lambda_1}{6\lambda_1}\left(\frac{\xi}{\sigma_c}\right)+\frac{6}{\lambda_1}\left(\frac{\xi}{\sigma_c}\right)^2\right) \tag{2.10}$$

where σ_c is the colloid diameter, polymer size $\xi_c = R_g/\sqrt{2}$, where R_g is the radius of gyration, $\xi = \xi_c/(1+2\varphi_p)$ and $\varphi_p = 2\pi c_p \xi_c^3$ is the reduced polymer concentration . This equation was used for our system at hand and the chemical potentials were compared to our simulations. The radius of gyration (R_g) values of the polymer chains used in this expression were calculated from simulations for each relevant system (Table 2.1) and agreed well with those of other workers.[37, 38] We also compared our simulation results with predictions from the field theoretic (FT) continuum approach of Eisenreigler and co-workers, the details of which are found in the literature.[8]

Table 2.1: Polymer radius of gyration, R_g, and reduced polymer concentration c_p/c_p^* at different chain lengths used in the simulations. The polymer segment density is maintained constant at 0.05.

Chain Length (*n*)	R_g	c_p/c_p^* (= $(4\pi/3)\rho_p R_g^3$)
5	1.05	0.049
10	1.71	0.104
20	2.70	0.206
30	3.49	0.299
40	4.18	0.384
50	4.79	0.461
60	5.36	0.533

2.4 RESULTS

2.4.1 Pure solvent simulations

In order to test the code and validate the method we first simulated a pure HS solvent and calculated the chemical potential at different densities using the EE and Widom method and compared the results with the predictions from the BMCSL equation of state. Figure 2.2 shows a plot of $\beta\mu_c^{ex}$ for a pure solvent system at different densities. We observe that the results from the three methods compare almost exactly with each other, validating the accuracy of the EE method.

2.4.2 Infinitely dilute hard sphere colloid in a pure solvent

Figure 2.3 shows a plot of infinite dilution chemical potential of a HS colloid in a HS solvent at different colloid particle sizes. The solvent density (ρ_S^*) was maintained constant at 0.05. The EE simulation results are compared with the Widom results and the predictions of the BMSCL equation of state. The diameter ratio d is the ratio of the diameter of the colloid particle σ_c to that of the solvent molecules σ_s. From the plot we observe that the simulated (EE and Widom) $\beta\mu_c^{ex}$ and those predicted from the BMCSL equation of state are within 2% of each other up to $d = 6$. However, beyond $d = 6$, the Widom method fails. This is because for $d > 6$, every attempted random insertion of the whole particle results only in steric overlaps, i.e., an infinite chemical potential. The EE method, on the other hand, gives values in agreement with BCMSL over the whole range of d values that we explored (up to $d = 12$). The acceptance rate for the EE particle moves was about 10%.

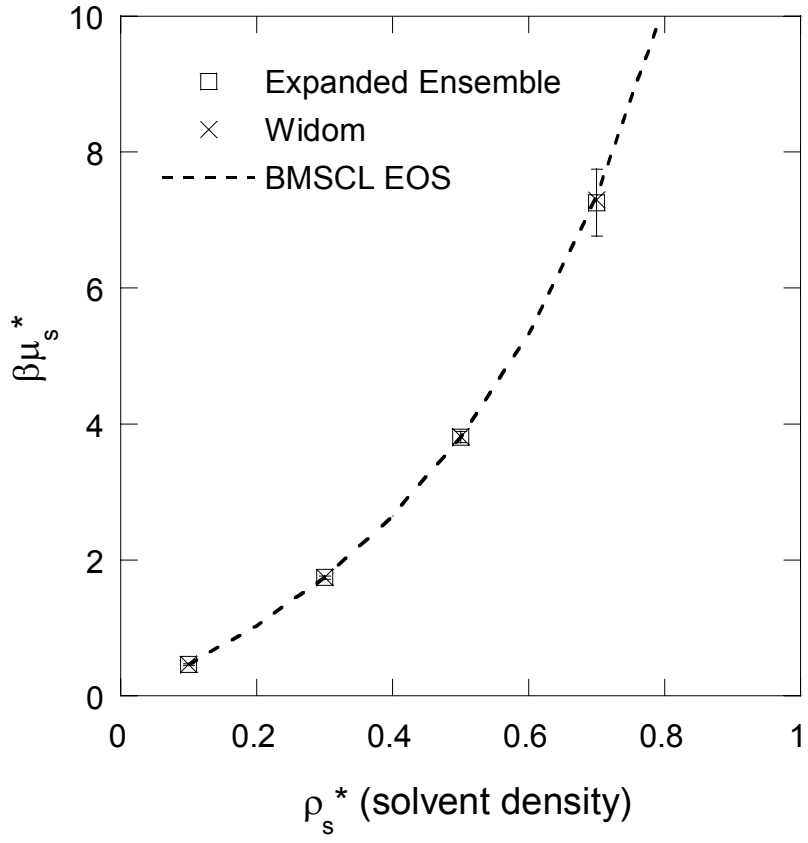

Figure 2.2: Solvent excess chemical potential $\beta\mu_s^{ex}$ vs. solvent density for pure hard sphere monomer. The points are calculated with the expanded ensemble and Widom methods and the line is the BMSCL equation of state.

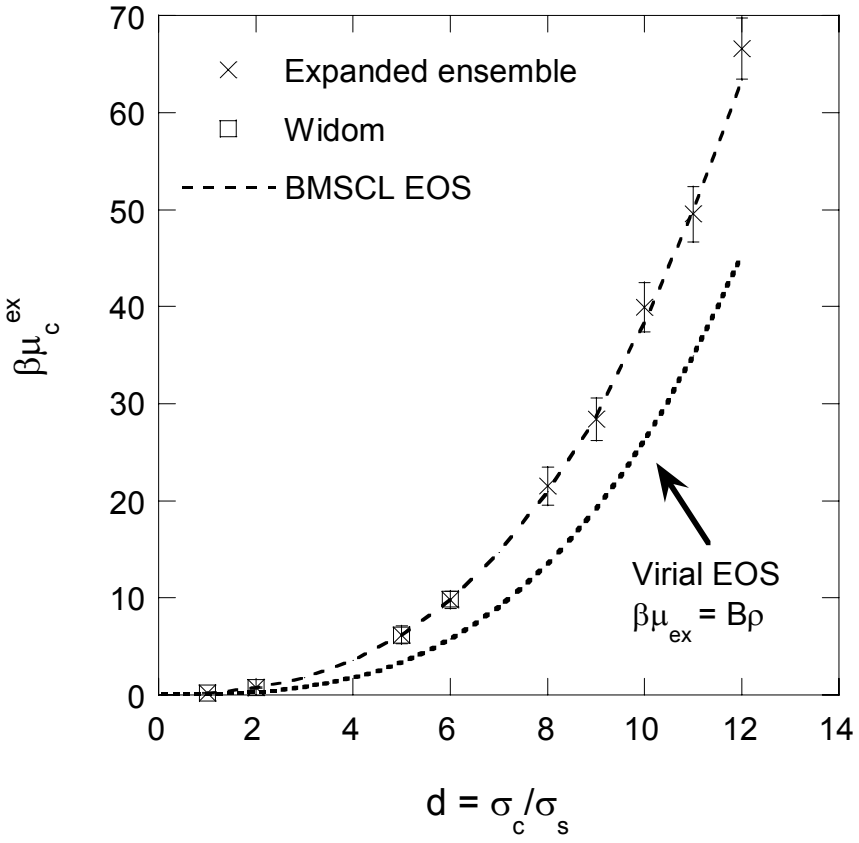

Figure 2.3: Infinite dilution hard sphere colloid chemical potential $\beta\mu_c^{ex}$ vs. diameter ratio in a pure hard sphere monomer ($\rho_s^* = 0.05$). The points are calculated with the expanded ensemble and Widom methods and the dotted line is the BMSCL equation of state. The virial equation of state, truncated after the second (linear) term is also shown.

The dependence of chemical potential on particle size can be represented exactly by a third order polynomial ($R^2 = 1$). The dependence of chemical potential on particle diameter is an excluded volume effect for a HS system, and a physical significance can be assigned to each of the terms in the cubic polynomial. For a binary mixture of unequally sized hard spheres, the virial equation of state presents a sound theoretical framework for relating intermolecular potentials to mixing rules for the virial coefficients. The chemical potential from the virial equation taking only the second order term is given by $(\mu - \mu_0)/RT = B\rho$. For a mixture of the colloid and solvent the second virial coefficient is given by: $B = y_c^2 B_{cc} + 2y_c y_s B_{sc} + y_s^2 B_{ss}$, where B_{cc}, B_{ss}, B_{sc} are the colloid-colloid, solvent-solvent and colloid-solvent second virial coefficients which are known exactly for HS systems.[39] Substitution of these second virial coefficients leads to:

$$(\mu - \mu_0)/RT \cong \rho(c_1\sigma_c^3 + c_2\sigma_s\sigma_c^2 + c_3\sigma_s^2\sigma_c + c_4\sigma_s^3) \qquad (2.11)$$

The coefficients in eq 2.11 are related algebraically to B_{cc}, B_{ss}, and B_{sc}. The chemical potential for different colloid particle sizes obtained from eq 2.11 is plotted in Figure 2.3 for comparison. Although the virial equation of state fails to match the simulations quantitatively, it yields insight into the physical significance of each of the terms in the cubic polynomial. The first term corresponds to the colloid sphere excluded volume, the second term corresponds to the excluded shell about the colloid, the third term is the contribution due to the excluded shell about the solvent and the last term is the solvent molecule excluded volume.

2.4.3. Infinitely dilute hard sphere colloid in a dilute hard sphere polymer solution.

Figure 2.4 shows a plot of $\beta\mu_c^{ex}$ vs. the colloid diameter obtained from two different types of simulations at a constant polymer chain length of n = 20. Initially a single simulation was performed for a colloid diameter of 15. Since the EE method enables calculation of the incremental chemical potential, it was possible to calculate $\beta\mu_c^{ex}$ for smaller colloid diameters (1 to 14) from the incremental $\beta\mu_c^{ex}$ that were accumulated during this single large 15σ particle simulation ('+' symbols). Individual simulations were then performed for the smaller colloid diameters to obtain *independent* values of $\beta\mu_c^{ex}$ (open squares). We observe that the chemical potentials obtained by the two methods are equal within experimental uncertainty. This result satisfies a necessary thermodynamic criterion of path independence for a state function, and provides a stringent test for the EE method. It also brings out another advantageous feature: a single simulation for a large colloid diameter yields chemical potentials for smaller diameters, eliminating the need to run separate simulations for the smaller diameters.

Figure 2.5 shows the infinite dilution chemical potential, $\beta\mu_c^{ex}$ versus the colloid diameter σ_c for polymer chain lengths of $5 < n < 60$. In general $\beta\mu_c^{ex}$ increases as a cubic polynomial in σ_c for all chain lengths, reflecting the increase in the probability of overlaps and excluded volume. The cubic polynomial results from the various contributions to the colloid-polymer excluded volume, discussed above in the context of the virial expression. Figure 2.5 compares the simulation results with the predictions from the FS model, eq 2.10. The FS model compares very well with the simulations except that at chain lengths above 30 the FS model slightly overpredicts the chemical potential, and at chain lengths less than 30, the predictions are slightly lower than the simulated results.

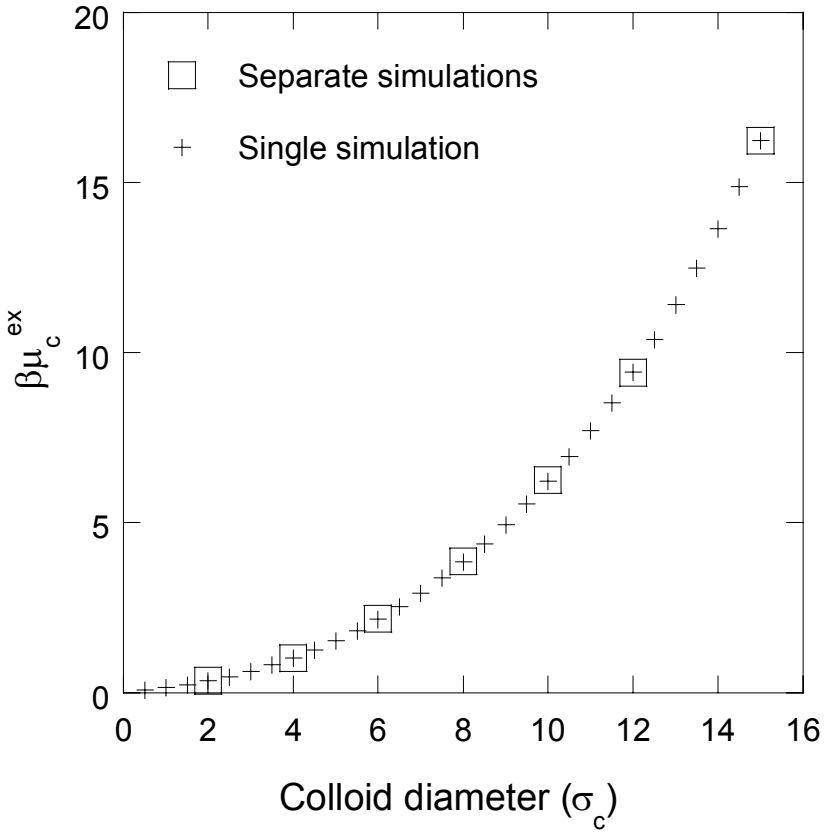

Figure 2.4: Infinite dilution hard sphere colloid chemical potential $\beta\mu_c^{ex}$ vs. colloid diameter in a dilute hard sphere polymer solution (chain length = 20, ρ_p^* = 0.05.) The '+' symbols are results from a single simulation for diameter = 15σ, whereas the squares represent $\beta\mu_c^{ex}$ values at the maximum diameter from individual simulations at colloid diameters of 2, 4, 6, 8, 10, 12 and 15.

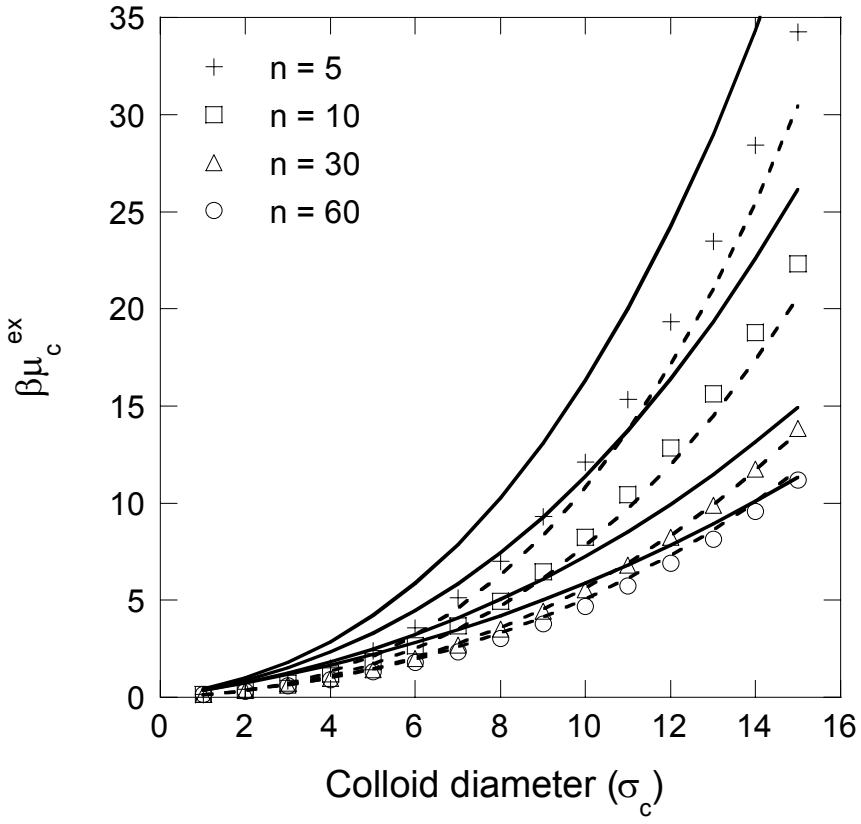

Figure 2.5: Infinite dilution hard sphere colloid chemical potential $\beta\mu_c^{ex}$ vs. colloid diameter (σ_c) in a dilute hard sphere polymer solution at different polymer chain lengths (n) (ρ_p* = 0.05). The symbols represent results from simulations. The dotted lines are predictions from the FS model (eq 2.10) and the solid lines are predictions from the FT approach.

The maximum deviation between the simulated and FS chemical potentials over a range spanning particle sizes from 5 to 15 and chain lengths from 5 to 60 is 12 %. The largest deviations occur at low chain lengths where the FS analytical model is not expected to hold quantitatively due to the assumed PRISM thread limit ($\sigma_p \rightarrow 0$) for intramolecular polymer structure. The results in Figure 2.5 suggest that the FS theory (eq 2.10) slightly underestimates the entropic penalty associated with the colloid-polymer excluded volume for $n < 30$, and slightly overestimates it for $n > 30$.

A similar observation has been reported in a recent paper in which the experimentally determined osmotic compressibility of an athermal colloid-polymer suspension was compared to predictions from the FS model.[19] At low R_g/R, the osmotic compressibility (second derivative of free energy with colloid composition) is underpredicted and at high R_g/R it is overpredicted. To facilitate discussion, our results from Figure 2.5 have been replotted versus the relative polymer-to-colloid size parameter, R_g/R, in Figure 2.6. Our results cover a similar range of R_g/R values as the osmotic compressibility measurements. In Figure 2.6 the under- and overprediction of $\beta\mu_c^{ex}$ from FS model is observed at low and high R_g/R values, respectively, an observation complimentary to the under- and overprediction of osmotic compressibility. The authors of that work suggest that at low R_g/R the underprediction of osmotic compressibility is due to the form of the closure approximations necessary for the integral equations, deviations from which are expected to be largest at low R_g/R. In the limit of small R_g the "thread" polymer model used in the FS formulation, which results in infinitesimally thin segments, is sure to result in deviations. On the other hand, when $R_g >> R$, Fuchs, Schweizer, and coworkers have attributed overprediction of osmotic

compressibility to the assumed Gaussian coil chains used in the theory,[19] which are less expanded than realistic self-avoiding walk chains. In the limit of $R_g >> R$, only an internal part of the chain needs to be rearranged in order to insert a small colloidal particle, and since the Gaussian coil is more dense, this rearrangement requires a higher free energy compared to the self-avoiding walk, resulting in a higher prediction of the free energy of insertion. We attribute these same factors at low and high R_g/R, respectively, to the minor quantitative deviations of the FS theory from the simulated $\beta\mu_c^{ex}$ values. In addition, complimentary under- and overpredictions of the phase boundaries in athermal colloid-polymer mixtures have been reported.[18]

Results from a field theoretic (FT) model (solid lines) are also shown in Figure 2.5 for comparison.[8] The deviations between the FT model and the simulations decrease from about 40% for n = 10 to 2% for n = 60. In other words the FT model shows very good agreement with the simulation results for longer chain lengths and larger particle sizes. This trend is expected as the FT approach should become exact only in the $n \rightarrow \infty$ limit, whereas the FS model is more broadly applicable to a wide range of chain lengths and particle sizes. Starting from small R_g/R values, the colloidal insertion chemical potential decreases sharply with increasing R_g/R, but begins to level off for $R_g/R > 1$. Ultimately at $n \rightarrow \infty$ the chain length dependence is expected to disappear. This is an interesting result since it tells us that firstly, even in the absence of attractive energetics, a large reduction in the colloid chemical potential can be brought about by adding short chain polymers (modifiers) and secondly, increasing polymer (modifier) chain length beyond a particular value yields little additional reduction in chemical potential. In addition, the chemical potential reduction effect from adding polymer chains increases as

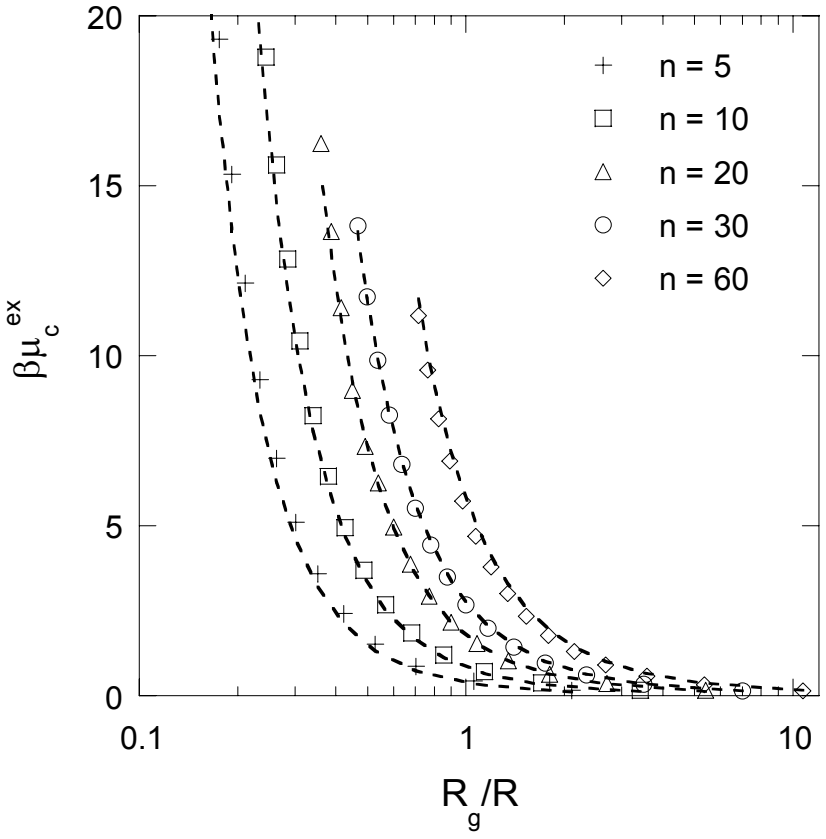

Figure 2.6: Infinite dilution hard sphere colloid chemical potential $\beta\mu_c^{ex}$ versus the relative size, R_g/R, in a dilute hard sphere polymer solution at different polymer chain lengths (n) ($\rho_p^* = 0.05$). The symbols represent results from simulations. The dotted lines shown for comparison are predictions from eq 2.10.

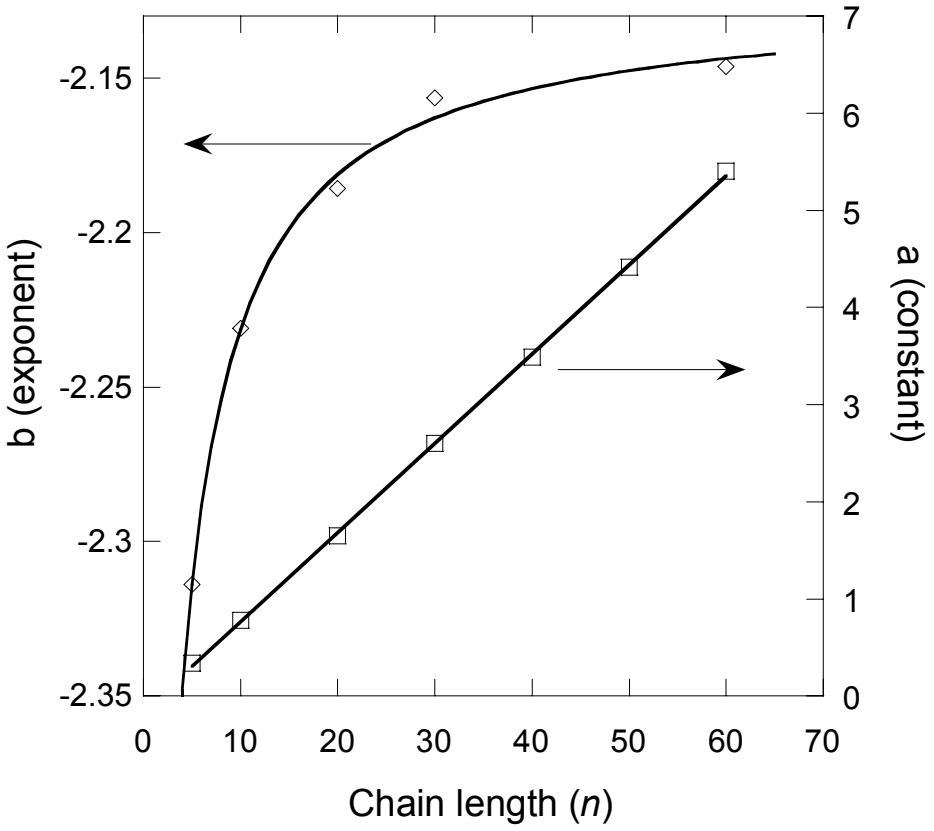

Figure 2.7: The empirical power law constant, a, and exponent, b, versus chain length, n, from the proposed expression $\beta\mu_c^{ex} = a(R_g/R)^b$.

particle size increases, e.g., at small R_g/R. These insights may help to explain the mechanism by which organic modifier chain-length can affect the dispersion and self-assembly behavior of nanocolloids in a good solvent.

In an effort to use the simulation and modeling results in Figures 2.5 and 2.6 to obtain simplified "practical" models for comparing or interpolating experimental data, it is worthwhile to consider the mathematical properties of the functional dependence of $\beta\mu_c^{ex}$ on R_g/R. This dependence is an inverse cubic polynomial, $\beta\mu_c^{ex} \sim (R_g/R)^{-1} + (R_g/R)^{-2} + (R_g/R)^{-3}$, based on simulation results and the FS and FT models. In general, an inverse cubic polynomial becomes a single-term power law, $a(R_g/R)^b$, in the limit of $R_g/R << 1$. In fact, the polynomial also reduces to another power law at the opposite limit of $R_g/R >> 1$. This mathematical behavior suggests that $\beta\mu_c^{ex}$ might be represented reasonably by a simple power function of the form $\beta\mu_c^{ex} = a(R_g/R)^b$, since much of our data is in the small R_g/R range. With this motivation, we carried out power law regressions of $\beta\mu_c^{ex}$ at each n value for $R_g/R < 1$. The fits are of a very high quality, with $r > 0.999$ in all cases. The power law constants and exponents depend solely on chain length and are given in Figure 2.7. In particular, the constant a is a nearly perfect line with respect to n and the exponent b is fitted by a saturation function, $b = c_1 + c_2 n/(c_3 + c_4 n)$, where the c_i are regression parameters. If the power law scaling holds for the $0.1 < R_g/R < 10$ range explored in the simulations, then a plot of $\beta\mu_c^{ex}$ versus $a(R_g/R)^b$ should collapse all of the data to a single master line. Figure 2.8 shows this plot for chain lengths of $5 < n < 60$, and indicates that the power law scaling holds very well over our R_g/R range. Although completely empirical in nature, Figure 2.8 suggests that the relative size, R_g/R, might be considered a type of scaling variable for the insertion chemical potential. However, we caution that

there is little physical motivation for expecting such a scaling function, and considerably more theoretical and experimental work would be required to demonstrate that the relationship in Figure 2.8 is a true scaling law of the sort often encountered in polymeric systems, e.g., $R_g = an^b$. Nevertheless, even as an empirical function, the power function in R_g/R could be of practical value as a superposition 'rule' for measurements of free energy properties of colloid-polymer mixtures. For example, with knowledge of the parameters a and b, investigators could interpolate or extrapolate free energy values measured at one set of R_g and R to another set of sizes.

Figure 2.9 shows the colloid-polymer pair correlation function $g_{cp}(r)$ at different chain lengths for $\sigma_c = 10$. The dotted lines are from EEMC simulations and the solid lines are from the integrated form of the full polymer segment density profile close to a single sphere from the FS (PRISM) model.[9]. The inset in each plot shows the g_{cp} profile at very small distances from the colloidal particle. The plots depict quantitatively that FS model always underpredicts g_{cp} close to the colloidal particle, due to the assumed PRISM thread limit ($\sigma_p \rightarrow 0$). However, the PRISM profiles capture the essential qualitative features of the simulation profiles.

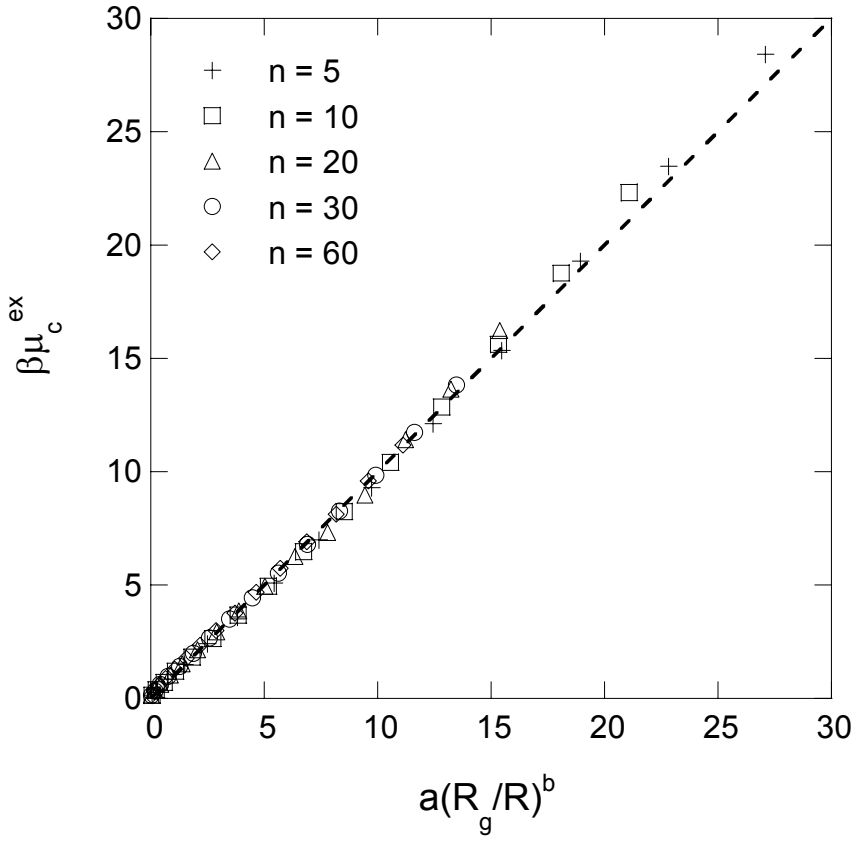

Figure 2.8: Infinite dilution hard sphere colloid chemical potential $\beta\mu_c^{ex}$ versus the scaled relative size term, $a(R_g/R)^b$. The dotted 45º line is shown for comparison to indicate the quality of the empirical power law scaling relationship.

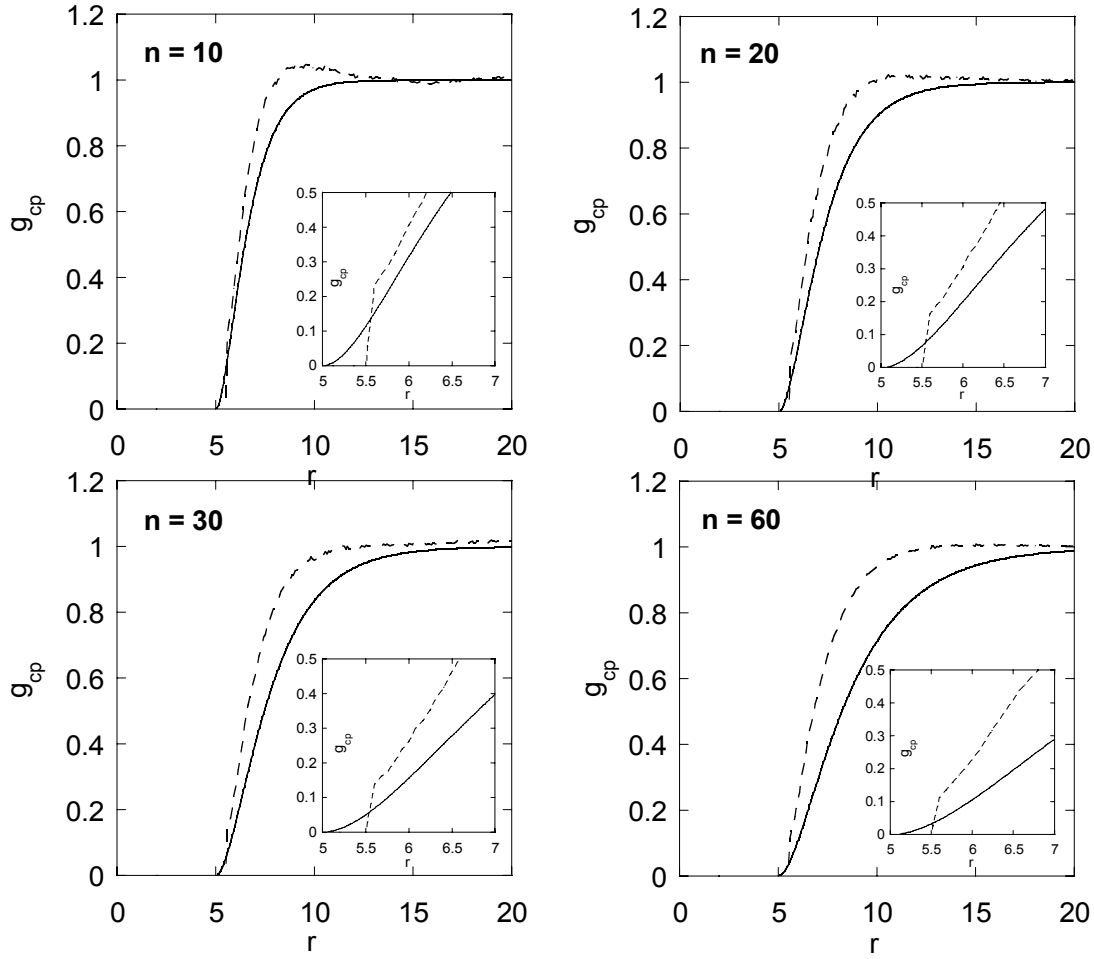

Figure 2.9: Colloid-polymer direct correlation function, $g_{cp}(r)$ at different chain lengths (n) and $\sigma_c = 10$. The dotted lines are from the EE simulations and the solid lines are predictions for the full $g_{cp}(r)$ from the FS model.

2.5 CONCLUSIONS

A new formalism is presented for direct calculation of the chemical potential of nanocolloidal particles in nanocolloid-polymer mixtures. The goal of this effort is to develop simulation tools that can lead to molecular-based approaches for the design of organic modifiers that influence and control stability, phase behavior, and self-assembly of nanoscale colloids. Monte Carlo simulations are performed in an EE whose states are defined by the diameter of the colloidal particle. During the course of the EEMC simulation, incremental chemical potentials are generated as the diameter of the colloidal particle varies between zero and maximum diameter. We have shown that when the incremental chemical potentials from zero to particle size σ_c are summed, the correct chemical potential at size σ_c, measured independently, is recovered. This incremental method provides the unique advantage of generating chemical potentials for smaller diameters from a single simulation for a large colloid diameter. This is a significant advantage considering the computational demands of colloid-polymer simulations. The HS model system, which provides a stringent test for the efficiency of EEMC chemical potential calculations, has been used to show that the EEMC method accurately calculates colloid chemical potentials beyond σ_c values where the Widom method fails. The close agreement of our results with the BMSCL EOS for the chemical potential of an infinitely-dilute colloid in a HS solvent serves to validate further the EEMC method.

The EEMC method was applied to calculate the infinite dilution colloid chemical potential in HS colloid-polymer mixtures as a function of the *colloid diameter* and *polymer chain length*. Taking a single model chain segment to represent several "real polymer" repeat units (≈ 5 nm), the model colloid diameters examined here would range

from 5 nm to 75 nm. Thus our results are relevant to nanocolloids dispersed in a dilute (5 volume %) solution of oligomers or polymers. The results agree well with the FS[9-11] model, except that the FS model slightly underpredicts the chemical potential for $n < 30$ and slightly overpredicts it for $n > 30$. We believe that the minor quantitative deviations are due primarily to the assumed Gaussian intramolecular polymer structure factor in the model. The FS model appears to capture the essential qualitative physics exactly, as has been shown in previous work as well.[18, 19] The FT approach of Eisenriegler et al.[8] also agreed well with our results in the limit of large particle sizes ($\sigma_c = 15$) and long polymer chains ($n > 40$), which is expected based upon the limiting assumptions of the field theoretic approach.

In the limit of small R_g/R, the dependence of the colloid chemical potential on the polymer chain length was found to be represented well by a power scaling law of the form $\beta\mu_c^{ex} = a(R_g / R)^b$, where a and b are parameters that depend purely on the polymer chain length (n). In fact, this relationship was found to describe chemical potentials reasonably well for $0.1 < R_g/R < 10$. This empirical relationship is merely a mathematical consequence of taking the $R_g/R < 1$ limit for an inverse cubic polynomial. However, it may prove to be useful in interpolating and extrapolating experimental and simulation results for free energy properties of colloid-polymer mixtures, in a manner similar to that of time-temperature superposition relationships for viscoelastic properties.

The addition of short chains ($n < 20$) brings about a large reduction in the colloid chemical potential, compared to pure monomer solvent at the same volume fraction. However, this free-energy reducing effect diminishes asymptotically for longer chains ($n > 30$). This behavior shows that even in the absence of attractive colloid-polymer

interactions that might lead to enhancements in dispersability, there is an entropically-derived benefit to dispersing nanocolloids in oligomer or polymer solutions, rather than solvent alone.

2.6 REFERENCES

(1) Mayer, A. B. R.; Mark, J. E. *Polymer* **2000,** 41, 1627-1631.

(2) Murray, C. B.; Kagan, C. R.; Bawendi, M. G. *Science* **1995,** 270, 1335-1338.

(3) Thomas, P. J.; Kulkarni, G. U.; Rao, C. N. R. *J. Phys. Chem. B.* **2000,** 104, 8138-8144.

(4) Lu, Y.; Tang, Y.; Sellinger, A.; Lu, M.; Huang, J.; Fan, H.; Haddad, R.; Lopez, G.; Burns, A.; Sasaki, D. Y.; Shelnutt, J.; Brinker, C. J. *Nature* **2001,** 410, (913-917).

(5) Sellinger, A.; Weiss, P. M.; Nguyen, A.; Lu, Y.; Assink, R. A.; Gong, W.; Brinker, C. J. *Nature* **1998,** 394, 256-260.

(6) Meijer, E. J.; Frenkel, D. *J. Chem. Phys* **1994,** 100, (9), 6873.

(7) Meijer, E. J.; Frenkel, D. *Physica A* **1995,** 213, 130-137.

(8) Eisenriegler, E.; Hanke, A.; Dietrich, S. *Phys. Rev. E* **1996,** 54, (2), 1134 - 1152.

(9) Fuchs, M.; Schweizer, K. S. *Europhys. Lett.* **2000,** 51, 621-627.

(10) Fuchs, M.; Schweizer, K. S. *Phys. Rev. E* **2001,** 64, 021514.

(11) Fuchs, M.; Schweizer, K. S. *J. Phys.: Condens. Matter* **2002,** 14, R239-R269.

(12) Lekkerkerker, H. N. W.; Poon, W. C. K.; Pusey, P. N.; Stroobants, A.; Warren, P. B. *Europhys. Lett.* **1992,** 20, (6), 559-564.

(13) Sear, R. P.; Frenkel, D. *Phys. Rev. E* **1997,** 55, (2), 1677-1681.

(14) Carnahan, N. F.; Starling, K. E. *J. Chem. Phys* **1969,** 51, (2), 635.

(15) Boublik, T. *J. Chem. Phys* **1970,** 53, 471.

(16) Mansoori, G. A.; Carnahan, N. F.; Starling, K. E.; Leland, T. W. *J. Chem. Phys* **1971,** 54, (4), 1523.

(17) Yoon, B. J.; Baeck, K. K.; Jeon, S., I. *Chem. Phys. Lett.* **1999,** 301, 481.

(18) Ramakrishnan, S.; Fuchs, M.; Schweizer, K. S.; Zukoski, C. F. *J. Chem. Phys* **2002,** 116, 2201.

(19) Ramakrishnan, S.; Fuchs, M.; Schweizer, K. S.; Zukoski, C. F. *Langmuir* **2002,** 18, (4), 1082-1090.

(20) Widom, B. *J. Chem. Phys* **1963,** 39, (11), 2808-2812.

(21) Lyubartsev, A. P.; Martsinovski, A. A.; Shevkunov, S. V.; Vorontsov-Velyaminov, P. N. *J. Chem. Phys* **1992,** 96, (3), 1776-1783.

(22) Escobedo, F.; de Pablo, J. J. *J. Chem. Phys.* **1995,** 103, (7), 2703-2710.

(23) Wilding, N. B.; Muller, M. *J. Chem. Phys* **1994,** 101, (5), 4324.

(24) Kumar, K. S. *J. Chem. Phys* **1992,** 97, (5), 3550-3556.

(25) Kumar, K. S.; Szleifer, I.; Panagiotopoulos, A. Z. *Phys. Rev. Lett.* **1991,** 66, (22), 2935-2938.

(26) Escobedo, F.; de Pablo, J. J. *Mol. Phys.* **1996,** 89, 1733-1754.

(27) Attard, P. *J. Chem. Phys* **1993,** 98, 2225-2231.

(28) Kaminsky, R. D. *J. Chem. Phys* **1994,** 101, (6), 4986-4994.

(29) Shing, K. S.; Gubbins, K. E. *Mol. Phys.* **1981,** 43, (3), 717--721.

(30) Metropolis, N.; Rosenbluth, A. W.; Rosenbluth, M. N.; Teller, A. H.; Teller, E. *J. Chem. Phys* **1953,** 21, (6), 1087-1092.

(31) de Pablo, J. J.; Laso, M.; Suter, U. W.; Cochran, H. D. *Fluid Phase Equilib.* **1993,** 83, 323-331.

(32) Mooij, G. C. A. M.; Frenkel, D. *Mol. Phys.* **1991,** 74, (1), 41-47.

(33) Rosenbluth, M. N.; Rosenbluth, A. W. *Trans. Faraday Soc.* **1955,** 62, 3319.

(34) Siepmann, J. I. *Mol. Phys.* **1990,** 70, (6), 1145-1158.

(35) Allen, M. P.; Tildesley, D. J., *Computer Simulation of Liquids*. 1st ed.; Oxford University Press: Clarendon,Oxford, 1987; p 385.

(36) de Souza, L. E. S.; Stamatopoulou, A.; Ben-Amotz, D. *J. Chem. Phys* **1994,** 100, (2), 1456.

(37) Dautenhahn, J.; Hall, C. K. *Macromolecules* **1994,** 27, (19), 5399.

(38) Gan, H. H.; Eu, B. C. *J. Chem. Phys* **1999,** 110, (6), 3235.

(39) Prausnitz, J. M.; Lichtenthaler, R. N.; de Azevedo, E. G., *Molecular Thermodynamics of Fluid-Phase Equilibria*. 3rd ed.; Prentice-Hall PTR: Upper Saddle River, New Jersey, 1996; p 860.

CHAPTER 3

NANOSCALE COLLOIDS IN A FREELY ADSORBING POLYMER SOLUTION: A MONTE CARLO SIMULATION STUDY

A key issue in nanoscale materials and chemical processing is the need for thermodynamic and kinetic models covering colloid-polymer systems over the mesoscopic length scale (~ 1 nm to 100 nm). We have applied Monte Carlo simulations to *attractive* nanoscale colloid-polymer mixtures towards developing a molecular basis for models of these complex systems. The expanded ensemble Monte Carlo (EEMC) simulation method is applied to calculate colloid chemical potentials (μ_c) and polymer adsorption (Γ) in the presence of freely adsorbing Lennard-Jones (LJ) homopolymers (surface modifiers). Γ and μ_c are studied as a function of nanoparticle diameter (σ_c), modifier chain length (n) and concentration, and attractive strength over $0.3 < R_g/\sigma_c < 6$ (R_g is the polymer radius of gyration). In the attractive regime, nanocolloid chemical potential decreases and adsorbed amount increases as σ_c or n are increased. The scaling of Γ with n from the simulations agrees with the theory of Aubouy and Raphael

(*Macromolecules* **1998**, *31*, 4357) in the extreme limits of R_g/σ_c. When R_g/σ_c is large, the "colloid" approaches a molecular size, interacts only locally with a few polymer segments and $\Gamma \sim n$. When R_g/σ_c is small, the system approaches the conventional colloid-polymer size regime where multiple chains interact with a single particle, and $\Gamma \sim \sigma_c^2$, independent of n. In contrast, adsorption in the mesoscopic range of R_g/σ_c investigated here is represented well by a power law $\Gamma \sim n^p$, with $0 < p < 1$ depending on concentration and LJ attractive strength. Likewise, the chemical potential from our results is fitted well with $\mu_c \sim n^q \sigma_c^3$, where the cubic term results from the σ_c–dependence of particle surface area ($\sim\sigma_c^2$) and LJ attractive magnitude ($\sim\sigma_c$). The q-exponent for μ_c ($\mu_c \sim n^q$) varies with composition and LJ attractive strength, but is *always very close* to the power exponent for Γ, ($\Gamma \sim n^p$). This result leads to the conclusion that in attractive systems, polymer adsorption, and thus polymer-colloid attraction, dominates the μ_c dependence on n, providing a molecular interpretation of the effect of adsorbed organic layers on nanoparticle stability and self-assembly.

3.1 INTRODUCTION

Nanoscale colloidal particles, as well and inorganic phases synthesized in situ in organic materials, display fascinating electronic, optical, thermal, and reinforcement properties as a consequence of their dimensions. Stable dispersions of nanoscale colloids may find applications in drug delivery, medical diagnostics, nanopatterning and nanocomposites. The self-assembly of nanoparticles into ordered crystalline arrays offers an attractive route to fabrication of a new generation of optical and electronic devices. These nanostructures can be prepared not only via nucleation and arrested growth processes, but also as equilibrium products, allowing thermodynamic control of crystal lattice structure and feature size. Most nanoparticles are unstable in dispersions unless synthesis and dispersion involves the use of an organic stabilizing agent (oligomeric or polymeric).[2] Recent examples of common organically-modified nanocolloid systems include dodecylthiol mediated synthesis and assembly of Ag_2S nanoparticles,[3] self-assembled structures of long-chain alkane capped silver and silica nanoparticles,[4] noble metal nanoparticles stabilized with poly (2-hydroxyl methacrylates),[5] and two and three-dimensional superstructures of metal nanocrystals modified with alkanethiols.[6,7] The properties of organically-modified nanoparticles are linked intimately to phase behavior, which in turn is controlled by molecular parameters: particle size, modifier size, and molecular interactions. Unfortunately, robust molecular based models of these complex multiscale mixtures are still in their infancy and relationships between molecular parameters and nanoparticle phase behavior are determined often by trial-and-error experimentation.

Recently, there have been numerous theoretical and simulation studies directed towards developing molecular-based approaches to describing parameter-structure-property relationships in colloid-modifier (polymer) systems.[1,8-15] However, most of the theoretical and simulation approaches focus on the simplest realization of these colloid-polymer systems: hard spheres and freely-jointed polymer chains under athermal solvent conditions. The introduction of long-range forces, such as van der Waals attractions or Coulombic interactions, complicates greatly the theoretical treatment of these systems. A major contribution to this complexity is the adsorption of surface modifiers and the subsequent change in their available conformations. For simple HS colloid-solvent mixtures, many models are based upon the Carnahan-Starling equation of state[17] and its derivatives.[18,19] For colloid-polymer mixtures, a recent PRISM-based model developed by Fuchs and Schweizer[14,20,21] accounts correctly for many aspects of HS structure and thermodynamics, as indicated by comparison to phase-behavior and osmotic compressibility experiments[13,22] and simulations.[23] Other approaches to developing equations of state and studying HS colloid-polymer mixtures include field-theoretic methods[11] and mean field theory.[10] A number of simulation studies of these model HS colloid-polymer systems have also been performed to determine structure, interparticle forces and phase behavior.[8,9,12,23-25] While knowledge gained from studies of HS systems is useful for near athermal experimental conditions, many processes involve attraction during adsorption, self-assembly and consolidation processes. Unfortunately, investigation of nanocolloid structure and thermodynamics with attractive models is very limited, and the choice of organic surface modifier in many experiments remains empirical. The primary factor that complicates model development in attractive polymer-

colloid systems is that nanoparticle interfacial free energy is a function of the amount and conformation of adsorbed polymer.

Towards this goal, we recently developed a novel application of the expanded ensemble Monte Carlo (EEMC) simulation method[28-30] that allows accurate calculation of the chemical potentials of organically-modified nanoparticles.[23] Knowledge of the modifier chain length, concentration and particle size dependence of chemical potential can be used to predict conditions under which nanocolloids disperse, flocculate, or self-assemble. The traditional Widom-based methods[26,27] for calculating μ from simulations fail in the case of organically-modified colloidal systems due to low insertion probabilities. The EEMC method[28-30] is a powerful approach that overcomes these sampling limitations in free energy calculations. We have demonstrated previously the use of the EEMC method for calculating nanoparticle chemical potentials in the presence of HS nonadsorbing modifiers.[23] In the present chapter, we apply the EEMC method to the calculation of nanocolloid chemical potentials in the presence of freely adsorbing (attractive) polymeric modifiers. The Lennard-Jones (LJ) homopolymer is used to model freely adsorbing modifiers, as it is a simple model that incorporates both attraction and adsorption effects. The LJ model represents van der Waals dispersion interactions present in all nanoparticle-polymer systems, allowing accurate physical conclusions to be drawn without sacrificing generality. The rest of the chapter is organized as follows: In section 3.2 we describe briefly the simulation details and methodology of EEMC calculations. A validation study of pure LJ solvent (monomer) is presented in section 3.3, followed by detailed results and discussions of colloid chemical potential and polymer adsorption in LJ colloid-polymer systems as a function of nanocolloid size, polymer chain length

(molecular weight) and concentration, and colloid-polymer interaction strength. Based on the results, we develop a simple model for the physical dependence of chemical potential on contributions from particle size and modifier chain length. In addition, the adsorption calculations are compared to the scaling theory of Aubouy and Raphael[1] in order to ascertain the applicability of this theory to the mesoscopic size range studied here.

3.2 SIMULATION DETAILS

3.2.1 Model and simulation methodology

In this study the EEMC method is applied to calculate the infinite dilution chemical potential of a nanocolloidal particle in the presence of freely (reversibly) adsorbing polymeric surface modifiers. The polymeric modifiers are modeled as self-avoiding random walk chains in continuum. The chains are fully flexible and consist of tangent LJ segments with a constant bond length of σ_p. The segment-segment LJ potential is cut at r_c and shifted such that the energy is zero for $r_c \geq 2.5\sigma_p$ as shown in equation (3.1),

$$u(r_{ij}) = \begin{cases} 4\varepsilon_{ij}\left[\left(\frac{\sigma_{ij}}{r_{ij}}\right)^{12} - \left(\frac{\sigma_{ij}}{r_{ij}}\right)^{6} - \left(\frac{\sigma_{ij}}{r_c}\right)^{12} + \left(\frac{\sigma_{ij}}{r_c}\right)^{6}\right] & r \leq r_c, \\ 0 \quad r > r_c \end{cases} \qquad (3.1)$$

where $\sigma_{ij} = (\sigma_i + \sigma_j)/2$ is the size parameter and ε_{ij} is the LJ interaction energy parameter. In all cases, the system consisted of a single colloidal particle dispersed in a dilute polymer (or oligomer) solution. Two types of interactions are considered; segment-segment for non-bonded polymer sites and colloid-segment. The colloid-segment interactions are modeled using the full LJ potential *without any cutoff*. Since the system

has only one colloidal particle, using cutoff did not offer any significant advantage in terms of computational effort.

The 6-12 LJ potential is not a physically exact model for colloid-polymer segment interactions, since a correct potential would involve the integration of the LJ potential between each atom in the particle and a polymer segment, resulting in a much longer ranged attraction. For example, this integration would yield a potential proportional to $\sim[(\sigma/r)^9 - (\sigma/r)^3]$ for the segment-colloid interaction.[48,49] The integration causes an increase in the range of the potential, increasing the number of polymer segments interacting with the colloid and the overall attractive magnitude (Figure 3.4). However, the form of the potential does not change, leading to some interesting generalizations from the 6-12 potential to other power-law potentials of the same form, e.g., $(\sigma / r)^n - (\sigma / r)^m$. Most notably, we examine below the effects of changing the colloid diameter, σ_c, on polymer adsorption and colloid chemical potential. In in a generic power-law potential, an increase in σ results in a linearly proportional increase in the r-position of the energy minimum and in the attractive magnitude (integrated area under the potential). This result is general for the power-law potential, and it can be shown that arbitrary changes in the n or m exponents *will not affect the linear dependence of the attractive range* on σ_c, as long as $n, m > 1$. Since adsorption and chemical potential in the *attractive colloid-polymer regime* depend primarily on the magnitude and range of the potential (proportional to σ_c), the basic trends observed below should extend to other power-law polymer-colloid potentials, including attractive Coulombic (electrostatic) and Hamaker (integrated LJ) potentials. Of course, the generalization requires that other factors,

including the chain entropy and its n- and σ_c-dependence, as well as the ε_{cs} and ε_{ss} interactions are held constant.

The variables are reduced in the usual manner, i.e., $T^* = Tk_B/\varepsilon_{ss}$, $\rho_p^* = \rho_p\sigma_p^3$, where ε_{ss} is the segment-segment interaction parameter and ρ_p is the polymer segment density. The polymer segment density is defined as $\rho_p = Mn/V$, where M is the number of chains and V is the volume of the simulation box. All the simulations were performed at a constant reduced temperature of $T^* = 3.0$. This temperature is above the upper critical solution 'theta' temperature (UCST) of LJ polymer chains, known from previous simulations, to be 2.5[31] thereby eliminating any effects of polymer phase transitions. In addition, it mimics the good solvent condition for the polymer chains. The solvent is not included explicitly in the simulations. The effect of solvent could be modeled by changing the reduced temperature and thereby varying the relative importance of the attractive and repulsive interactions.

In this work, the effect of polymer chain length (n), polymer density (ρ_p), colloid particle size (σ_c) and colloid-segment interaction energy (ε_{cs}) is investigated. Simulations are performed at three different values of polymer segment density $\rho_p = 0.05$, 0.1, 0.15. The polymer chain length was varied from $n = 5$ to $n = 30$ to study the effect of chain length on colloid chemical potential and polymer adsorption on the colloid surface. The chain lengths considered, though they may seem short, are quite realistic since more often than not low molecular weight or short chain polymers are used for surface modification purposes. For example, Sperry and co-workers used hydroxyethyl cellulose (HEC) polymer to demonstrate entropically-driven reversible flocculation of polymer latices.[32]

In order to make a correlation between the chain lengths used in our simulations and 'real world' experiments we can utilize the concept of an equivalent freely jointed chain. Consider an equivalent Gaussian chain of length $\hat{n}$ and segment length $\hat{l}$.[33] Then $\hat{n}\hat{l}^2$ = R_{eed}^2, $\left(\hat{n}\hat{l}\right)^2 = l_f^2$, and $\hat{n} \approx l_f^2/R_{eed}^2$, *where* l_f is the fully extended chain length and R_{eed} is the polymer end-to-end distance. For the largest molecular weight of HEC used in Sperry's paper $\hat{n} \approx 1.985^2/0.22^2 = 81$ and similarly for the smallest polymer used we get n ≈ 4.5, where R_{eed} and l_f are in μm. It must be noted that the equivalent chain lengths for the self-avoiding walk chains will be slightly larger than those calculated above for the Gaussian chains. In addition, surface force apparatus measurements on polybutadiene have shown that an 'alkane-like' to 'polymer-like' transition can be observed at $n > 20$.[34] The radius of gyration (R_g), end-to-end distance (R_{eed}), and the reduced polymer concentration (c_p/c_p^*) for different chain lengths of polymer studied are shown in Table 3.1, where c_p is the polymer-molecule number density and c_p^* is the critical polymer-molecule number density at which the polymer molecules start to overlap and entangle with each other (dilute to semi-dilute crossover). For all chain lengths, the simulations are confined to the dilute polymer regime as shown by the (c_p/c_p^*) values in Table 3.1. The colloid particle diameter (σ_c) was varied from $1\sigma_p$ to $10\sigma_p$ to investigate the effect of particle size on the chemical potential. These values correspond to a ratio of R_g/σ_c values ranging from 0.3 to 6.0. The effect of colloid-segment interaction energy was also explored by varying ε_{cs} from $0.005\varepsilon_{ss}$ to $1.5\varepsilon_{ss}$. ε_{ss} is maintained constant at $\varepsilon_{ss} = 1$ in this study. All the simulations were carried out in a cubic box with standard periodic boundary conditions. Figure 3.1 shows a configurational snapshot of the simulation box for $\sigma_c = 10$ and $n = 20$.

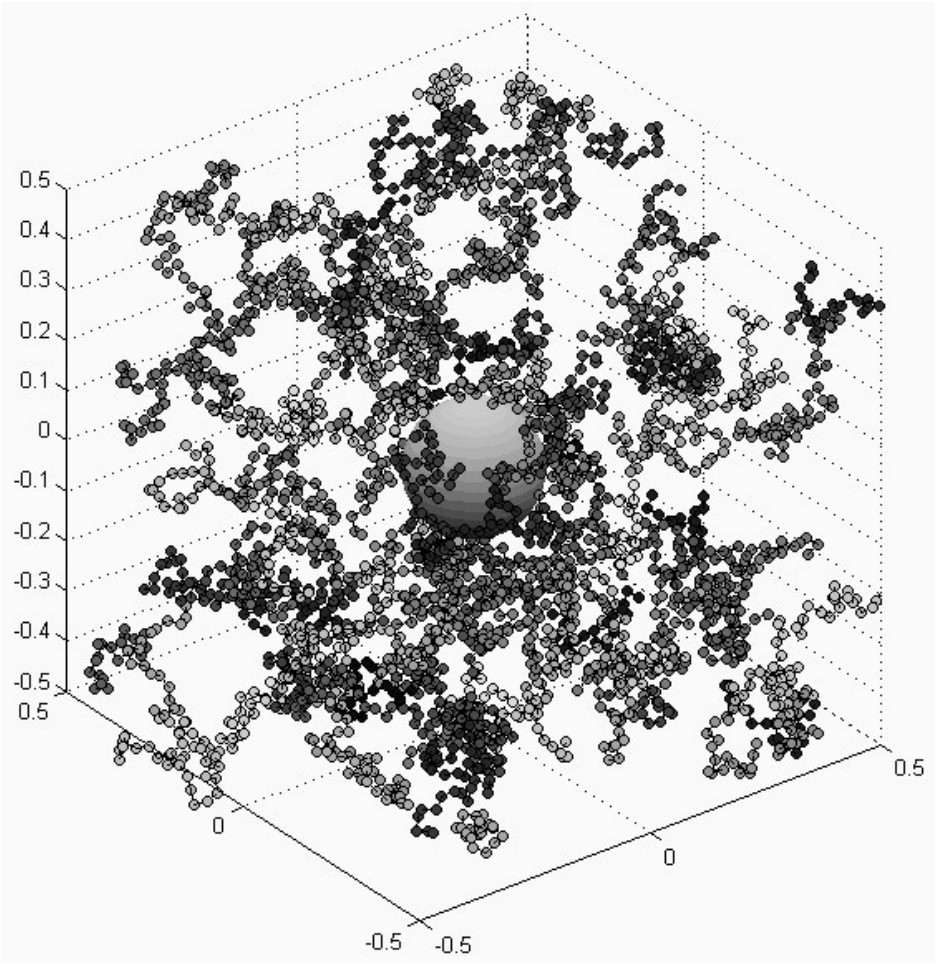

Figure 3.1: Configuration snapshot of the simulation box showing the single colloidal particle ($\sigma_c = 10$) and the polymer chains. ($n = 20$, $\rho_p^* = 0.05$).

Table 3.1: Polymer radius of gyration, R_g, end-to-end distance R_{eed}, and reduced polymer concentration c_p/c_p^* at different chain lengths and polymer segment densities used in the simulations.

	n	R_g	R_{eed}	$c_p/c_p^* = (4\pi/3)(\rho_p/n)Rg^3$
$\rho_p^* = 0.05$	5	1.02	2.37	0.044
	10	1.58	3.82	0.083
	20	2.38	5.79	0.142
	30	2.99	7.26	0.187
$\rho_p^* = 0.1$	5	1.01	2.36	0.086
	10	1.57	3.82	0.162
	20	2.37	5.81	0.278
	30	2.98	7.31	0.368
$\rho_p^* = 0.15$	5	1.00	2.36	0.126
	10	1.56	3.82	0.240
	20	2.36	5.82	0.416
	30	2.98	7.34	0.555

3.2.2 Expanded Ensemble Monte Carlo simulations

The complete details of the application of the EEMC method to calculation of the chemical potential of colloidal particles in colloid-polymer mixtures is outlined in a recent paper.[23] However, a brief summary of the method is presented here for the purpose of completeness. The basic idea of the expanded ensemble is that additional ensemble variables are introduced in order to define a reversible and smooth path between the two states of the system at which the free energy measurement is desired.[28-30,35] In the case of colloidal particles, the diameter of the tagged particle is the expansion variable, and all diameters from zero to full size are sampled as the simulation proceeds. Thus the particle

is not inserted or deleted all at once, but rather one predefined step size at a time.[36,37] These size increments or decrements are accepted or rejected according to a Metropolis-type acceptance criterion.[23] During the course of the simulation, incremental chemical potentials, $\beta\mu_c^{ex}$, associated with each diameter increment d_i to d_{i+1}, are calculated by $\beta\mu_c^{ex} = -\ln\langle\exp(-\Delta E / k_B T)\rangle$, where ΔE is the energy between the particle with diameter d_{i+1} and the rest of the system. These incremental chemical potentials are stored and summed at the end of the run to obtain the total particle chemical potential. In our simulations, we use the EE method to calculate the chemical potentials of both, colloidal particles and the polymeric modifiers. The details of the application of the EE to calculation of chemical potentials of polymer chains are described in reference 28.

In order to achieve thermal equilibrium in the simulation box, translation of the colloidal particle and molecular displacements of the polymer chains are also performed. Chain displacements are attempted with the continuum configurational bias (CCB) algorithm, in which a portion of the chain is regrown in a low-energy conformation that avoids overlaps with neighboring segments. The details of the CCB algorithm are given elsewhere.[38-40] The colloid particle is moved via random displacement accepted with the standard Metropolis Monte Carlo criterion.[41] The simulations are initiated by first randomly inserting a full-size colloidal particle in the simulation box and then growing the polymer chains individually, while avoiding overlap with the particle and each other. During the simulation, trial moves are performed at prescribed frequencies selected to yield acceptable number of moves for both polymer and colloid. Moves were attempted according to the following prescription that gave good convergence to equilibrium: 10% colloid displacement, 10 % EE colloid moves, 40% CCB and 40% EE chain moves. In

most cases, (20-40) x 10^6 equilibrium steps and (60-120) x 10^6 averaging steps were required to obtain statistically significant averages of chemical potential, polymer end-to-end distance and segment density distributions. In this chapter, one MC step corresponds to one attempted move. The statistical error in the chemical potential was based on the statistical inefficiency parameter.[42] The typical box side (l_b) chosen to be $40\sigma_p$ was greater than or $n/2$ to avoid any self- interaction between chain segments or particles through the periodic boundary conditions. It was verified by a series of trial simulations that these artifacts do not appear for $l_b/\sigma_c > 2.5$.

3.3 RESULTS

3.3.1 Pure LJ solvent simulations

To verify the accuracy of the code, we first simulated a pure LJ monomer (solvent) and calculated the chemical potential using the EE and the Widom method[26]. These results were also compared with the well-known Johnson equation of state for LJ monomers.[43] Figure 3.2 shows a plot of the LJ solvent excess chemical potential $\beta\mu_s^{ex}$ vs. solvent density ρ_s* for two different temperatures (a "repulsive" high temperature and a lower temperature where attraction occurs). The simulations were performed for the cut and shifted LJ potential shown in equation 3.1. The results from the three methods are in very good agreement with each other over the entire range of densities from 0.1 to 1.0, verifying the accuracy of the code and the EE method. Note that error bars have been omitted in all the figures unless they were larger than the symbols representing the data points. The error bars seen in Figure 3.2 are for the Widom results, which show large

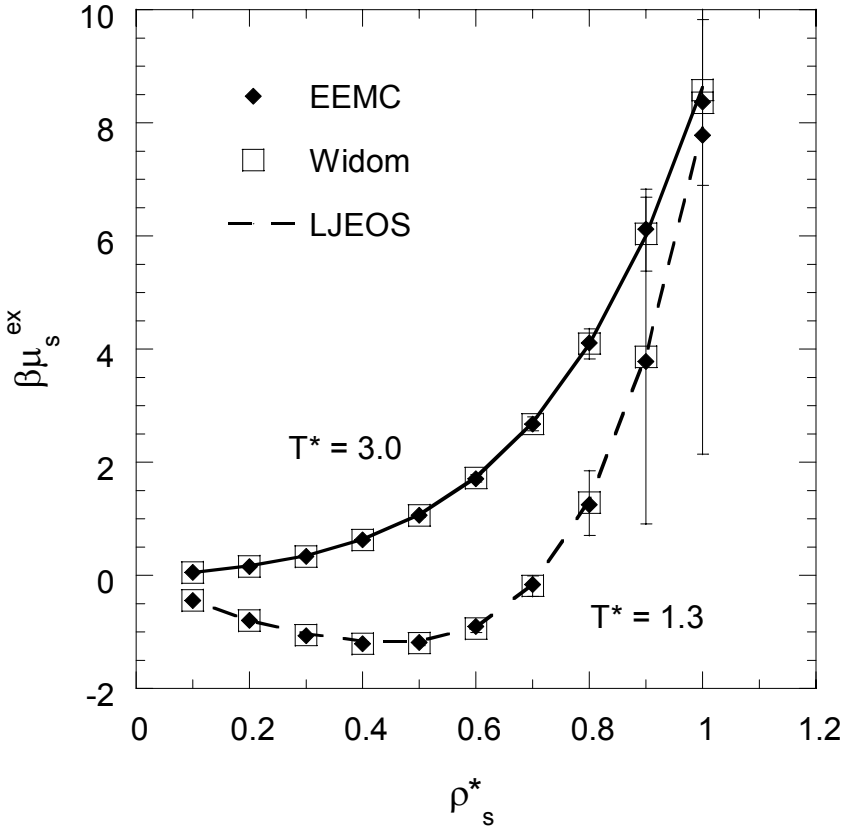

Figure 3.2: Solvent excess chemical potential $\beta\mu_s^{ex}$ vs. solvent density at T* = 3.0 and T* = 1.3 for pure Lennard-Jones monomer. The points are calculated with the expanded ensemble and Widom methods and the line is the Johnson equation of state.

fluctuations due to sampling problems at high densities. These sampling problems are not observed in the EEMC method.

3.3.2 Infinitely dilute colloid in a dilute freely adsorbing polymer solution

A. Particle size effects

Figure 3.3 shows a plot of infinite dilution colloid chemical potential ($\beta\mu_c^{ex}$) vs. the colloid diameter for polymer chain lengths of $5 \leq n \leq 30$ at two values of the polymer segment density (ρ_p* = 0.05, 0.15). The colloid-segment interaction energy (ε_{cs}) is maintained constant at $\varepsilon_{cs} = 1.0\varepsilon_{ss}$ in this plot (i.e. equivalent segment-segment and colloid-segment energy parameters). The markers in the figure are results from the simulations and the lines passing through them are power-law regressions, explained in detail in section 3.3.2 F. In general $\beta\mu_c^{ex}$ decreases with increasing σ_c for all chain lengths and polymer densities. Increasing the colloid particle diameter at constant ε_{cs} results in an increase in the range of the LJ potential energy. As a result, a larger number of polymer chains come under the attractive influence of the colloidal particle, resulting in a lower chemical potential. Figure 3.4 shows a plot of the LJ attractive energy vs. particle size, obtained by integrating the area of the LJ attractive region from $(\sigma_c + \sigma_p)/2$ to $l_b/2$. The magnitude of the LJ attractive energy increases linearly with the particle size suggesting that the effect of particle size on the LJ potential contributes a linear decrease in chemical potential. However, the $\beta\mu_c^{ex}$ data in Figure 3.3 shows a cubic dependence on particle size for all chain lengths and polymer densities. We propose that this cubic dependence arises from a combination of the linear dependence of LJ attractive energy on σ_c and a σ_c^2 contribution due to the surface area of the colloid (surface area controls total

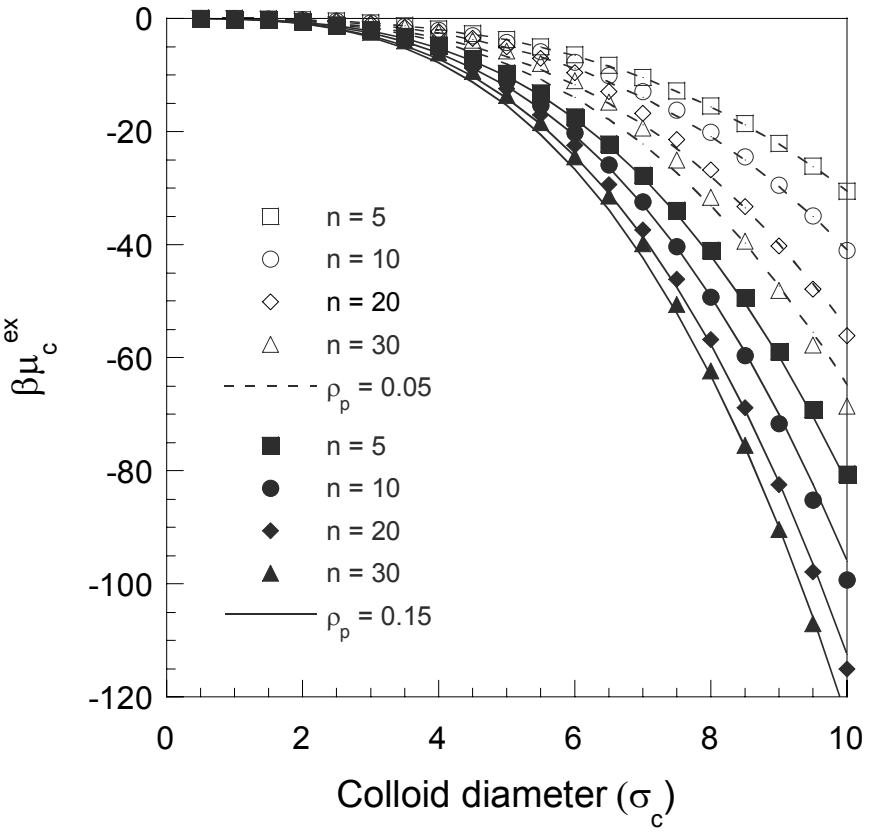

Figure 3.3: Infinite dilution colloid chemical potential $\beta\mu_c^{ex}$ vs. colloid diameter (σ_c) in a dilute LJ polymer solution at different polymer chain lengths (n). The unfilled open symbols are for $\rho_p^* = 0.05$ and the dark filled symbols are for $\rho_p^* = 0.15$. The lines are predictions from scaling relationships of the form $\beta\mu_c^{ex} = c\sigma_c^{3.0}n^b$. Dotted lines correspond to $\rho_p^* = 0.05$ and solid lines correspond to $\rho_p^* = 0.15$. The interaction energy parameter ε_{cs} is kept constant at $1.0\varepsilon_{ss}$.

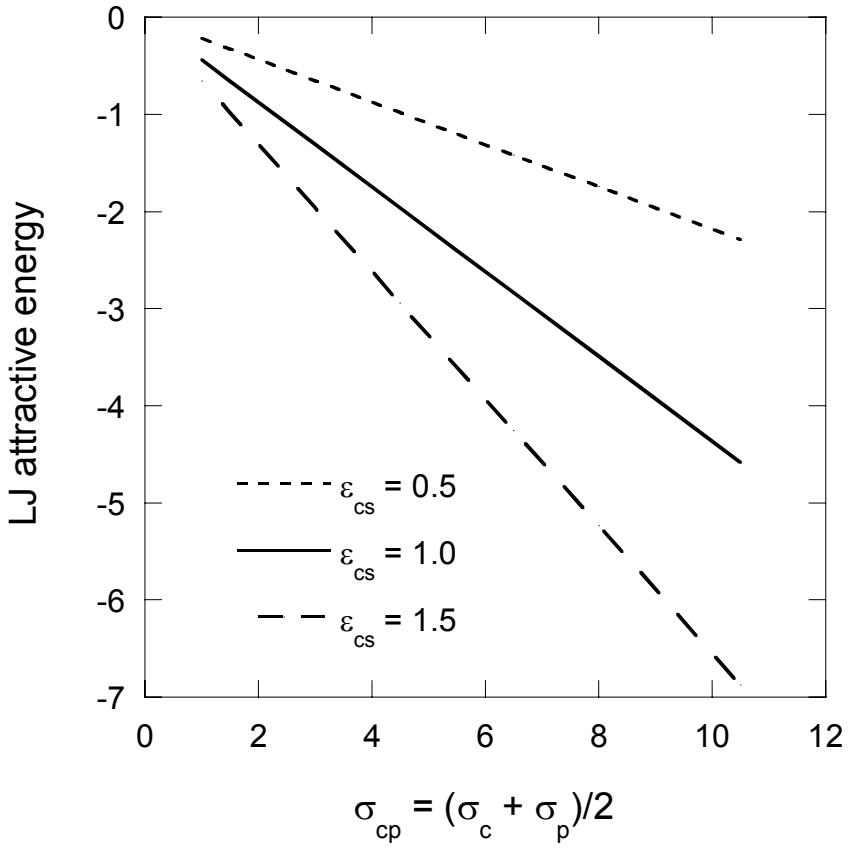

Figure 3.4: Integrated Lennard-Jones attractive energy vs. the σ_{cp} for different values of the colloid-segment interaction parameter (ε_{cs}).

number of polymer segments that can adsorb). This hypothesis is explored in greater detail in section 3.3.2 F.

B. Chain length effects

The effect of chain length of adsorbing modifiers on particle chemical potential is shown in Figure 3.5. The plot shows the variation of $\beta\mu_c^{ex}$ with n for $\rho_p^* = 0.05$ and 0.15. The plots for chain length and particle size effects at $\rho_p^* = 0.1$ show similar trends and hence have been omitted from Figures 3.4 and 3.5. At each polymer density, we also investigated the chain length effects for colloid diameters of 1, 5, and 10. In all the cases, $\beta\mu_c^{ex}$ decreases with increasing chain length, but this effect is most pronounced for the large particles and is hardy noticeable when the particle diameter is equal to the monomer diameter. It must be noted here that for a constant polymer segment density, increasing the chain length means that we have less number of chains in the simulation box. This results in less excluded volume for the particle due to chain connectivity constraints on the location of polymer segments, thereby making it easier to insert the particle. However, in addition to the decrease in excluded volume due to chain connectivity constraints, increased chain adsorption on the particle surface with increasing n also leads to lowering of particle chemical potential. As the chain length is increased, the entropy loss associated with chain adsorption decreases and hence more chain segments get adsorbed on or close to the particle surface. These combined effects result in the particle getting a larger number of attractive interactions, thereby lowering chemical potential.

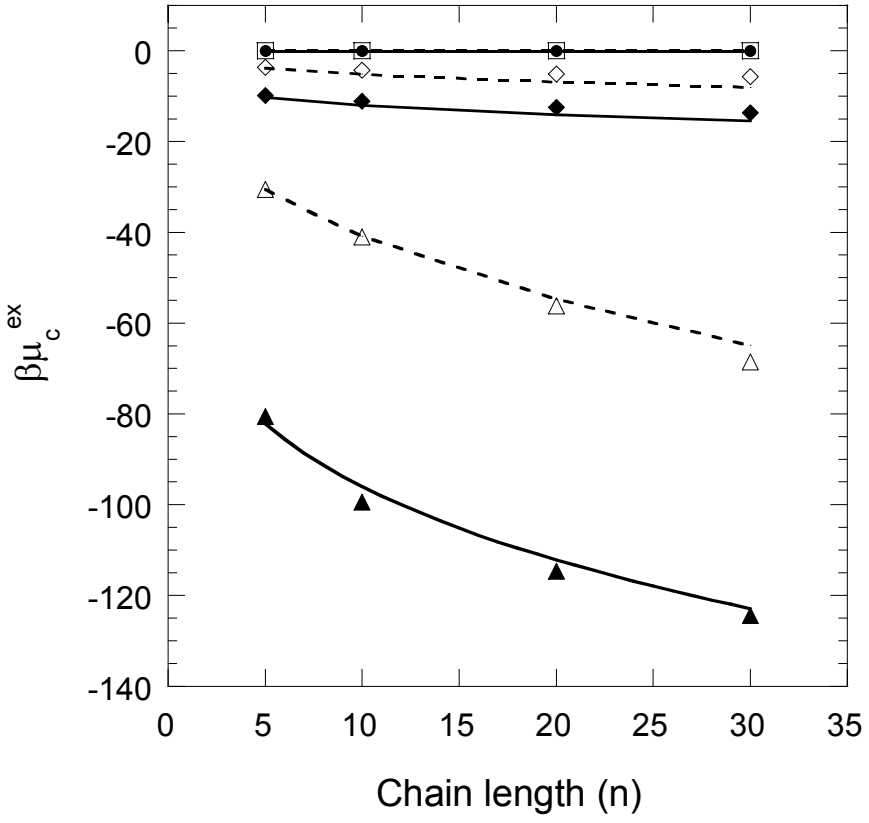

Figure 3.5: Infinite dilution colloid chemical potential $\beta\mu_c^{ex}$ vs. polymer chain length (n) in a dilute LJ polymer solution at different colloid diameters (σ_c). The symbols represent different values of polymer segment density (ρ_p*) and colloid diameter (σ_c). The unfilled open symbols are for ρ_p* = 0.05 (□ $\sigma_c = 1\sigma_p$; ◇ $\sigma_c = 5\sigma_p$; △ $\sigma_c = 10\sigma_p$) and the dark filled symbols are for ρ_p* = 0.15 (● $\sigma_c = 1\sigma_p$; ◆ $\sigma_c = 5\sigma_p$; ▲ $\sigma_c = 10\sigma_p$). The lines are predictions from scaling relationships of the form $\beta\mu_c^{ex} = c\sigma_c^{3.0}n^b$. Dotted lines correspond to ρ_p* = 0.05 and solid lines correspond to ρ_p* = 0.15. The interaction energy parameter ε_{cs} is kept constant at $1.0\varepsilon_{ss}$.

C. Effect of interaction energy parameter (ε_{cs})

Figure 3.6 shows a plot of $\beta\mu_c^{ex}$ vs. σ_c for different values of the colloid-segment interaction parameter ranging from $\varepsilon_{cs} = 0.005\varepsilon_{ss}$ to $1.5\varepsilon_{ss}$, with chain length maintained constant at $n = 20$. At ε_{cs} values of 0.005 and 0.05, the colloid chemical potential $\beta\mu_c^{ex}$ *increases* with increasing diameter. In this case the colloid-segment attractive energy is very small compared to the segment-segment interaction energy. As a result there is a depletion of polymer segments near the surface and entropic or excluded volume effects dominate the colloid chemical potential. In a recent paper we showed that for the case of *nonadsorbing* modifier chains represented by the hard-sphere potential, $\beta\mu_c^{ex}$ increases with σ_c via a cubic polynomial dependence on σ_c.[23] The cubic polynomial results from the various contributions to the colloid-polymer excluded volume. A similar argument is applied for the low ε_{cs} values here, and in these cases $\beta\mu_c^{ex}$ also shows an exact cubic polynomial dependence on σ_c. For ε_{cs} values of 0.1 and 0.25, $\beta\mu_c^{ex}$ increases to positive values initially with σ_c, passes through a maximum, and then starts decreasing to negative values at higher colloid diameters. As presented above, the LJ potential is modified by changing either the colloid particle diameter or the energy parameters ε_{cs} and ε_{ss}. Changing the particle size (physical effect) varies the range of the LJ attractive energy and changing the energy parameters (chemical effect) varies the strength of the interaction. At ε_{cs} = 0.1 and 0.25, the colloid-segment interaction energy is still quite weak compared to the segment-segment interaction and the entropic effects discussed above dominate initially. However, as the colloid diameter increases, the range of the LJ attractive energy increases, and the colloidal particle interacts with more polymer segments leading to a decrease in the chemical potential. At higher ε_{cs} values of 0.5 and

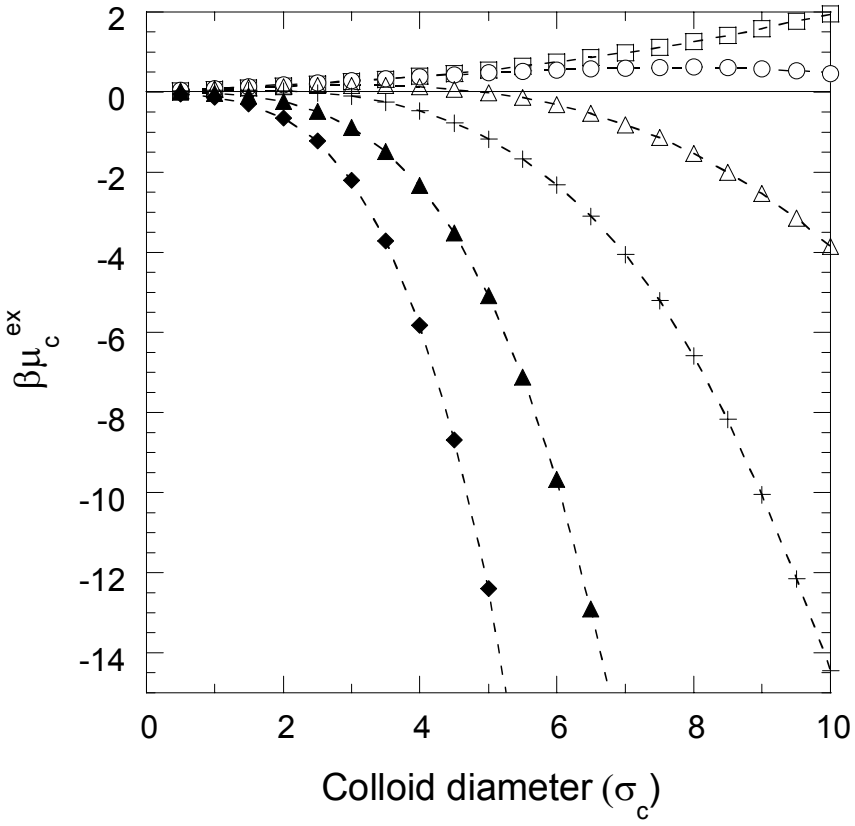

Figure 3.6: Infinite dilution colloid chemical potential $\beta\mu_c^{ex}$ vs. colloid diameter (σ_c) in a dilute LJ polymer solution for different values of the colloid-segment interaction energy parameter (ε_{cs}) at $\rho_p^* = 0.05$, $n = 20$. The symbols refer to different values of ε_{cs}: □ $\varepsilon_{cs} = 0.005$; ○ $\varepsilon_{cs} = 0.1$; △ $\varepsilon_{cs} = 0.25$; + $\varepsilon_{cs} = 0.5$; ▲ $\varepsilon_{cs} = 1.0$; ◆ $\varepsilon_{cs} = 1.5$. The dotted lines are a guide to the eye.

1.0 and 1.5, $\beta\mu_c^{ex}$ decreases monotonically as σ_c^3 increases. Here, the colloid-segment attraction overcomes the entropic excluded volume effects, thereby leading to a negative chemical potential.

D. Colloid-segment pair distribution profiles

The colloid-polymer segment pair distribution profiles enable us to corroborate the trends observed for the colloid chemical potential with the molecular structure. Note that the abscissa in all the pair distribution profiles is the distance from the center of the colloidal particle measured in units of the polymer segment diameter σ_p. Figure 3.7 shows the effect of changing the colloid diameter on the colloid-segment pair distribution function g_{cp}(r) for n = 20, $\varepsilon_{cs} = 1\varepsilon_{ss}$ and ρ_p^* = 0.05. The enhancement of the local polymer segment density (adsorption) near the colloid surface is greater for larger colloids due to the increased range of the LJ attraction. Figure 3.8 compares the g_{cp}(r) profiles at different polymer chain lengths for a constant colloid diameter of $\sigma_c = 10\sigma_p$, $\varepsilon_{cs} = 1\varepsilon_{ss}$ and ρ_p^* = 0.05. At constant particle size, the increase in local polymer segment density near the colloid surface is greater for longer polymer chains. The loss in configurational entropy due to adsorption is lower for longer chains, leading to increased adsorption. Figure 3.9 depicts the effect of strength of the colloid-segment interaction parameter (ε_{cs}) relative to the polymer segment-segment interaction parameter at $\sigma_c = 10\sigma_p$, n = 20 and ρ_p^* = 0.05. At ε_{cs} values of 0.005 and 0.05, there is depletion of polymer segments near the colloidal particle and g_{cp}(r) = 1 in the bulk region away from the particle. For ε_{cs} = 0.1 and ε_{cs} = 0.25, the thickness of the depletion layer decreases and the bulk density is achieved within a few segment diameters from the particle surface.

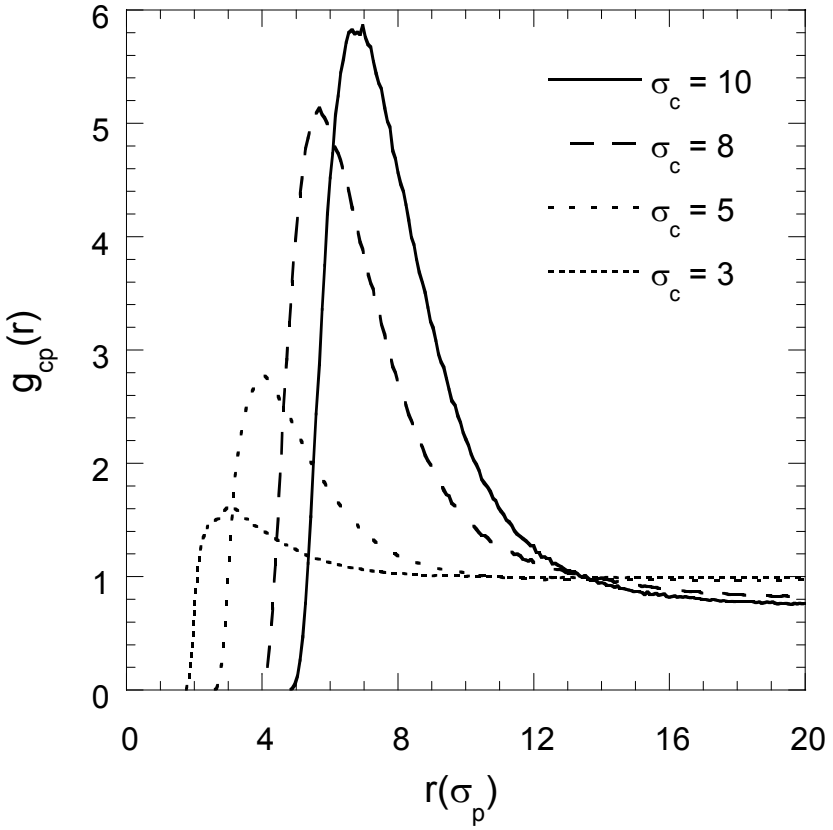

Figure 3.7: Colloid-segment radial distribution profiles for different particle sizes at n = 20, ρ_p* = 0.05 and ε_{cs} = 1.0. The abscissa is the radial distance from the center of the particle expressed in units of a single segment diameter (σ_p).

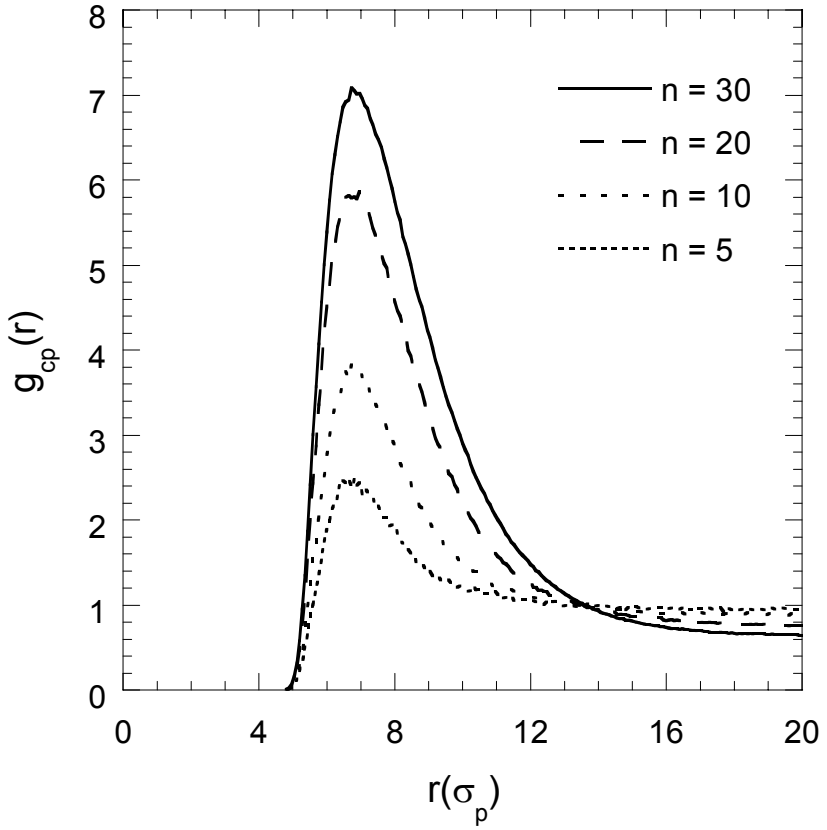

Figure 3.8: Colloid-segment radial distribution profiles for different chain lengths at $\sigma_c = 10$, $\rho_p^* = 0.05$ and $\varepsilon_{cs} = 1.0$. The abscissa is the radial distance from the center of the particle expressed in units of a single segment diameter (σ_p).

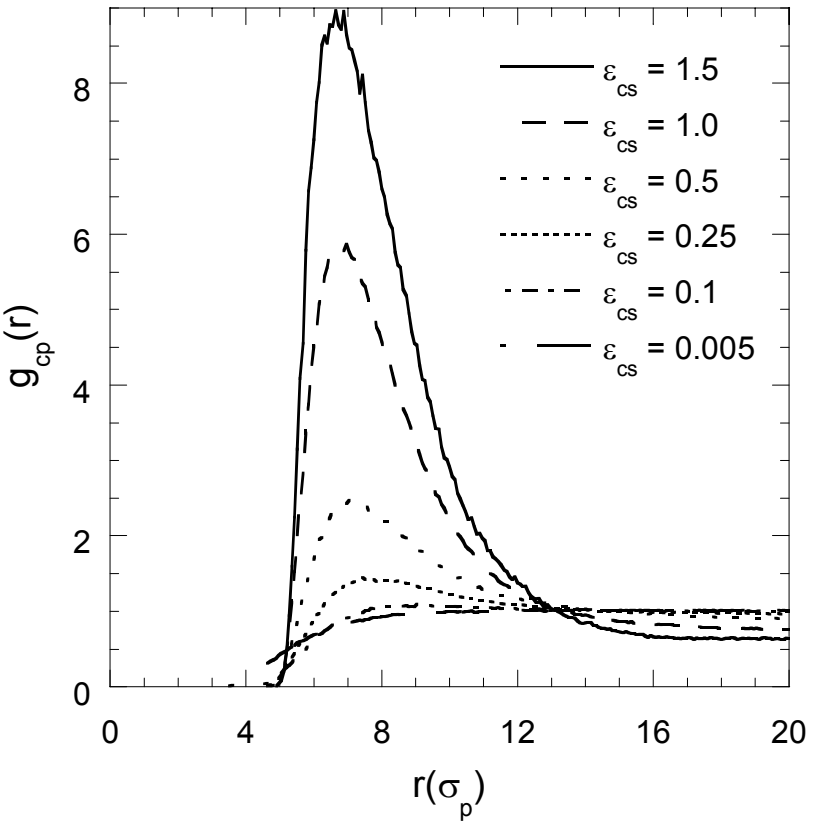

Figure 3.9: Colloid-segment radial distribution profiles for different values of the colloid-segment interaction energy parameter ε_{cs} at $\sigma_c = 10$, $\rho_p^* = 0.05$ and $n = 20$. The abscissa is the radial distance from the center of the particle expressed in units of a single segment diameter (σ_p).

In fact for ε_{cs} = 0.25, there is a slight enhancement of the segment density near the particle. This indicates that the transition from depletion to excess adsorption occurs at ε_{cs} = 0.25, which coincides with the chemical potential changing sign from positive (entropically controlled) to negative (energetic domination) in Figure 3.6. These results confirm the well-known result that there exists a critical interaction energy for excess homopolymer adsorption to occur. For n = 20 and ρ_p* = 0.05, these critical parameters are ε_{cs} = 0.25 and $\sigma_c = 5\sigma_p$ (remember that in our model σ_c adjusts the LJ attraction range) Beyond ε_{cs} = 0.5, there is a very strong increase in g_{cp}(r) near the particle surface. These distribution plots allow the *adsorbed polymer layer structure* to be correlated with the effects of varying the colloid-segment interaction strength on the chemical potential. Namely, we observe that increases in either the colloid-segment attraction (or the colloid diameter) lead to increased polymer adsorption, adding attractive energy to the colloidal chemical potential.

E. Adsorption of polymer chains near the colloid particle

As stated above, the complicating factor behind free energy calculations for colloid-polymer systems in which the colloid is in the same size range as the polymer, is the complex manner in which the particle alters the local density and conformation of polymeric surface modifiers. Below, we will show that the dependence of colloid chemical potential on chain length is due to the change in free energy associated with *adsorption* (or depletion) of the polymer chains on the particle. The effect of chain length on adsorption is examined by spherical integration of the segment density profile close to the particle to yield adsorption isotherms with

$$\Gamma_s = \frac{1}{\pi\sigma_c^2} \int_{\sigma_{cp}/2}^{2.5R_c} \rho_p^*(r) 2\pi r^2 dr \qquad (3.2)$$

where Γ_s is the absolute adsorption of the polymer segments per unit surface area of the particle, σ_{cp} is defined as $(\sigma_c + \sigma_p)/2$, R_c is the radius of the colloidal particle and $\rho_p^*(r)$ is the polymer segment density (averaged over spherical angles θ and ϕ) at a distance r from the center of the particle. The upper limit was chosen to be $2.5R_c$ because the polymer segment density falls approximately to the bulk value at this distance for all particle sizes examined.

Figure 3.10 depicts the absolute adsorption per unit surface area of the particle (Γ_s) as a function of the polymer chain length at different ε_{cs} values, constant particle size (σ_c = 10) and constant polymer segment density (ρ_p^* = 0.05). At ε_{cs} = 0.005 and 0.05, the absolute adsorbed amount is less than the bulk value (obtained by replacing $\rho_p^*(r)$ by bulk polymer segment density in equation 3.2) for all chain lengths, i.e., there is depletion of segments as also indicated in the g_{cp} plots (Figure 3.9). Beyond ε_{cs} = 0.25, the absolute adsorbed amount increases with increasing chain length and is more than the bulk value for all the cases in agreement with the g_{cp} profiles in Figure 3.9. This increase in polymer adsorption is what causes the decrease in colloid chemical potential to more negative values with increasing chain length, in the regime where chains show positive excess adsorption. Also shown in Figure 3.10 are the adsorption isotherms for different ρ_p^* values at ε_{cs} = 1.0. At higher ρ_p^* values, similar Γ_s vs. n are observed except that the increase in Γ_s with chain length is not as profound with increasing ρ_p^* suggesting a reduced dependence on n.

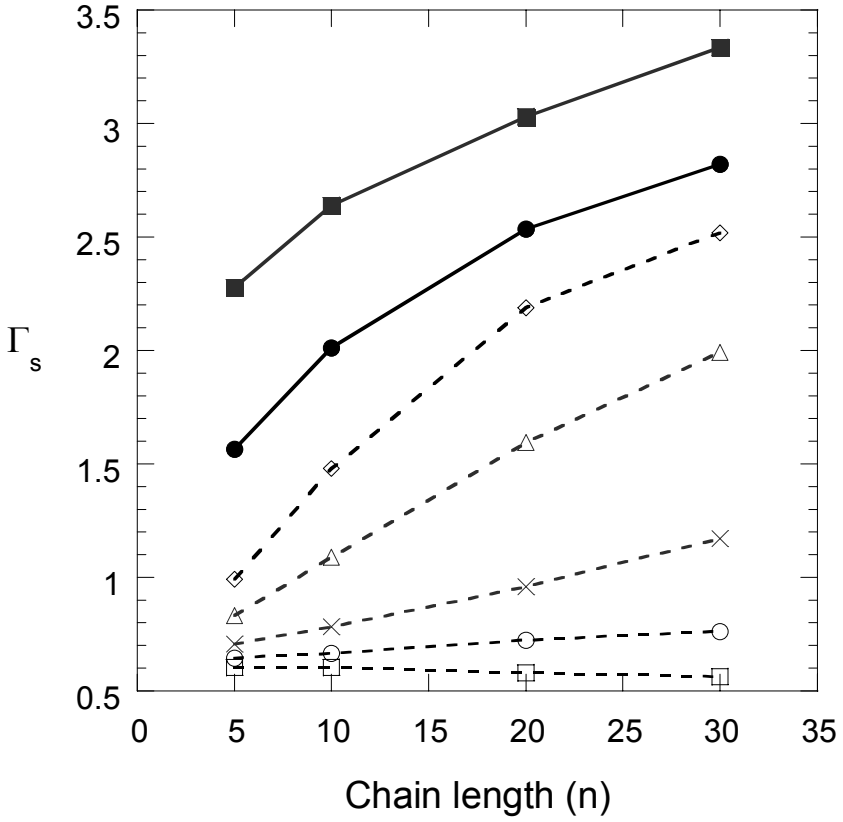

Figure 3.10: Absolute amount adsorbed per unit surface area of particle (Γ_s) calculated from equation (3.2) vs polymer chain length at different values of the colloid-segment interaction energy parameter (ε_{cs}) and different polymer segment densities (ρ_p*). The colloid diameter is kept constant at $\sigma_c = 10$. All the unfilled and open symbols refer to ρ_p* = 0.05 and different ε_{cs} values: ◇ $\varepsilon_{cs} = 1.5$; △ $\varepsilon_{cs} = 1.0$; × $\varepsilon_{cs} = 0.5$; ○ $\varepsilon_{cs} = 0.25$; □ $\varepsilon_{cs} = 0.005$. The remaining dark filled symbols refer to the following: ■ ρ_p* = 0.15, $\varepsilon_{cs} = 1.0$; • ρ_p* = 0.1, $\varepsilon_{cs} = 1.0$. The lines are a guide to the eye.

Figure 3.11 shows Γ_s vs. n at different particle diameters (σ_c) for ρ_p^* = 0.05 and ε_{cs} = 1.0. It should be noted the data for this plot was generated from separate simulations wherein the particle size was held constant for each case and only chain displacements were performed using the CCB and EE methods. For $n \leq 30$ and $\sigma_c \leq 10$, the Γ_s values from these simulations and the EEMC chemical potential simulations were within 5 % of each other, confirming that the measured amount adsorbed is not altered artificially by particle increments or decrements during the EEMC simulations. Since adsorption calculations are relatively inexpensive compared to the chemical potential calculations, we simulated a larger range of particle sizes ($\sigma_c \leq 15$) and chain lengths ($n \leq 50$). Up to σ_c = 12, Γ_s increases with both chain length and particle diameter due to colloid-monomer interaction described earlier in the chapter. Beyond σ_c = 12, as we approach chain lengths greater that 20, Γ_s starts decreasing with particle diameter. We propose that this is due to the two contrasting effects that particle size has on adsorption. The first is the increase in adsorption due to the range of LJ attractive energy and increased surface area available for particle-polymer contact. The second competing effect is the reduction in chain conformational entropy as the particle size increases (curvature decreases); e.g., flatter surfaces offer less available volume as a function of distance from the surface than curved surfaces of the same area. Above σ_c = 12 this entropy loss effect apparently causes adsorbed amount to level-off with increasing chain length. A similar observation for long polymer chains in the presence of nanoparticles has also been reported in previous simulations by Nowicki. [15]

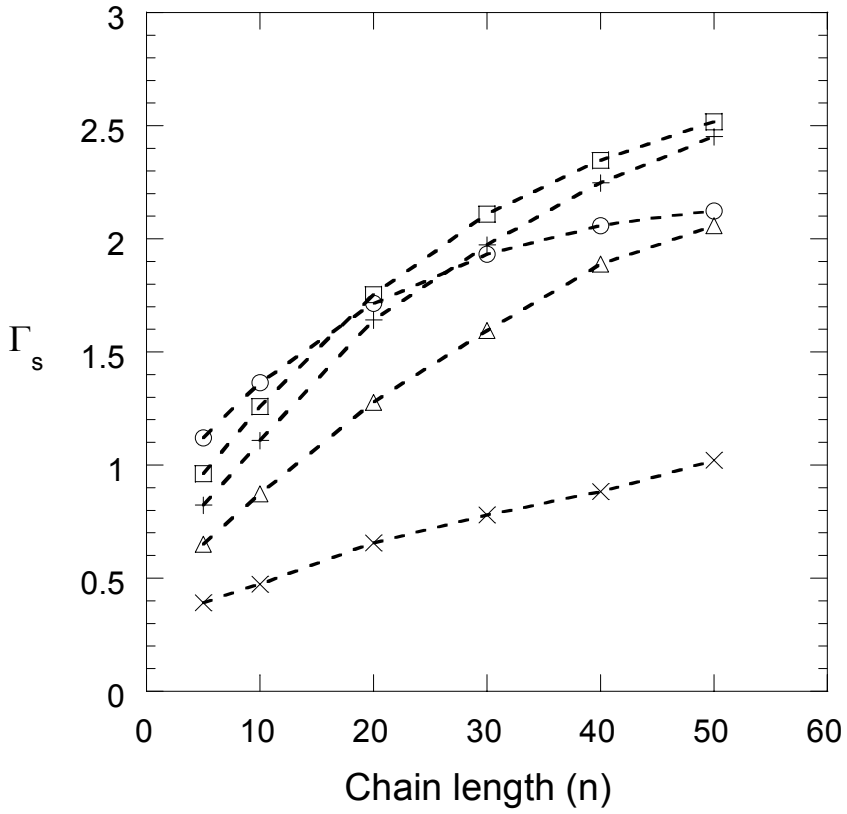

Figure 3.11: Absolute amount adsorbed per unit surface area of particle (Γ_s) calculated from equation (3.2) vs polymer chain length at different colloid diameters (σ_c). ρ_p* = 0.05 and ε_{cs} = 1.0 are kept constant. The symbols refer to different values of σ_c: ○ σ_c = 15; □ σ_c = 12; + σ_c = 10; △ σ_c = 8; × σ_c = 5. The dotted lines are a guide to the eye.

F. Adsorption in the small and large particle extremes

Recently, Aubouy and Raphael[1] developed a scaling approach for describing an arbitrary polymer layer coating a colloidal particle. Their method describes the layer as a statistical ensemble of a population of loops and tails. For various limiting cases, they modeled the reversible adsorption of polymer chains on colloidal particles and developed scaling relations for the adsorption of polymer chains as a function of the colloid radius and polymer chain length. A comparison to our results can be made over certain regimes of adsorption. Consider the plot of Γ_s vs. chain length for $\sigma_c = 5$ in Figure 3.11. At $\sigma_c = 5$ and $n \geq 10$ the system is in the Aubouy regime of $\sigma_c/2 < n^{1/2}$ (small particles relative to polymer size). Our results indicate that for $\sigma_c \ll n^{1/2}$, adsorption increases linearly with chain length, in agreement with the Aubouy and Raphael predicted scaling relationship $\Gamma \sim n$. It must be noted here that since we plot Γ_s ($= \Gamma/\pi\sigma_c^2$) vs. chain length at constant particle diameter in Figure 3.11, the Γ_s and Γ dependency on n will remain the same for a constant σ_c. At larger particle diameters, the plot of Γ_s vs. n becomes nonlinear and seem to approach a saturation limit (flattening out) with increasing n suggesting that Γ_s becomes increasingly chain length independent.

At $\sigma_c = 15$ and $n \geq 30$, the system approaches the Aubouy regime $n^{1/2} < \sigma_c/2 > n^{3/5}$ where the scaling theory predicts that $\Gamma \sim (\sigma_c/2)^2$, independent of chain length. Physically, at larger particle diameters, curvature effect decreases and the particle appears more like a flat wall to the chains. Using a scaling description similar to the one described above, it has been shown previously that in the flat wall limit Γ_s does not depend on chain length.[45] Hence, the scaling predictions are in good agreement with the

simulation results at the extreme range of σ_c and n values explored in this study. However, many nanoparticle-polymer experimental systems correspond to σ_c and n in intermediate σ_c and n values. To explore this correlation between chain adsorption and chemical potential as a function of n in this important intermediate regime, we performed a scaling analysis of the simulation results.

G. Power Law scaling analysis of adsorption and chemical potential

We hypothesize that the chemical-physics of nanocolloid-polymer mixtures can be described by simplified scaling relationships which capture the dependence of structure and thermodynamic properties on physical molecular parameters. These relationships may reflect the physics that connects chemical potential of nanoparticles with chain adsorption, that is observed in the simulations and could be used to compare, interpolate or extrapolate experimental data, as well as to motivate modeling efforts. With this goal, we performed power law regressions of the chemical potential and chain adsorption data using σ_c and n as the functional molecular parameters and obtained relationships of the form $\beta\mu_c^{ex} = c\sigma_c^a n^b$ and $\Gamma_s = c\sigma_c^a n^b$. Table 3.2 shows the c, a and b parameters obtained from regression of chemical potential data for different ε_{cs} values at $\rho_p^* = 0.05$. The results from the hard-sphere simulations (nonadsorbing modifiers) reported in a recent paper[23] were also regressed in the same manner and the exponents are reported in Table 3.2 as well. Table 3.2 also shows the regressed parameters for different ρ_p^* values while keeping ε_{cs} constant at 1. For the hard-sphere case we demonstrated previously that the chemical potential shows a cubic polynomial dependence on σ_c/R_g where R_g is the radius of gyration of the polymer, in agreement with others [14,20,21,23]

Table 3.2: Scaling parameters *a*, *b* and *c* obtained from power-law regression of the chemical potential data to fit an equation of the form $\beta\mu_c^{ex} = c\sigma_c^a n^b$.

	ε_{cs}	c	a	b
$\rho_p^* = 0.05$	Hard-sphere	0.126	2.34	-0.48
	0.005	0.077	1.98	-0.44
	0.050	0.168	1.88	-0.67
	0.250	-4.7E-06	4.72	0.88
	0.500	-0.001	3.58	0.36
	1.000	-0.006	3.40	0.43
	1.500	-0.018	3.18	0.50
$\rho_p^* = 0.05$	1.000	-0.006	3.40	0.43
$\rho_p^* = 0.1$	1.000	-0.020	3.27	0.31
$\rho_p^* = 0.15$	1.000	-0.041	3.15	0.23

(Hence the empirical power law scaling exponents obtained for the HS case may have little physical significance as they are a mathematical consequence of reducing a cubic polynomial to a power law function of the independent molecular parameters) A similar argument could be applied in the LJ freely-adsorbing model explored here, where at very low ε_{cs} values, ε_{cs} = 0.005 and 0.05. At $\varepsilon_{cs} \geq 0.25$, the chemical potential undergoes a transition from being entropically-controlled (positive) to energetically-controlled (negative). When the data in this (attractive) regime are regressed, all the *a* values (colloid diameter exponent) were close to 3.0. We propose that in this regime a physical significance can be attributed to the σ_c exponent. As demonstrated above, the cubic dependence on σ_c can be seen as a product of a linear term (σ_c) and a square term (σ_c^2).

The linear dependence represents a *unit colloid-polymer interaction energy* since the LJ attractive energy varies linearly with the particle diameter (see Figure 3.4). The square term indicates the surface area that controls the space available for chains to adsorb on the particle and, therefore the *number of colloid-polymer segment interactions*. We therefore performed a regression analysis of $\beta\mu_c^{ex}$ vs. n^b by holding a constant at 3.0 and regressing only for the chain length exponents (b) for ε_{cs} values of 0.5, 1.0 and 1.5. These results are shown in Table 3.3. The b values did not change significantly and the regression variance v_r reported in Table 3.3 for the two regressions did not vary significantly either ($v_r = S_r/(N_d-N_p)$, where S_r is the sum of least squares, N_d is the number of data points and N_p is the number of fitted parameters). To demonstrate the quality of these regressions, the predictions from these scaling relations are plotted as lines with the simulation results in Figures 3.3 and 3.5. In addition, if the power law scaling ($\beta\mu_c^{ex} = c\sigma_c^{3.0}n^b$) holds true for the range of data explored, all the $\beta\mu_c^{ex}$ vs. $c\sigma_c^{3.0}n^b$ data should collapse to one master plot (line). We did obtain plots of this nature for all the densities and interaction parameters studied in this work. Although we attribute a physical import to the power law relationships described above, we caution that further experimental and theoretical studies are required to establish that this is a true *scaling law* arising from self-similarity at various length scales. We propose that in the intermediate particle and chain size regime (where the sizes are close) the chain length exponent (b) for chemical potential is related to the chain length dependence of adsorption.

Table 3.3: Scaling parameters *a*, *b* and *c* obtained from power-law regression of the chemical potential data to fit an equation of the form $\beta\mu_c^{ex} = c\sigma_c^{3.0}n^b$. v_r is the regression variance defined as $v_r = S_r / (N_d - N_p)$, where S_r is the sum of least squares, N_d is the number of data points and N_p is the number of fitted parameters.

	ε_{cs}	c	a	b	$v_r(\sigma_c, n)$[f]	$v_r(n)$[g]
ρ_p^*= **0.05**	0.5	-0.005	3.0	0.36	0.03	0.18
	1.0	-0.016	3.0	0.42	0.24	1.44
	1.5	-0.027	3.0	0.50	0.67	2.21
$\rho_p^* = 0.1$	1.0	-0.036	3.0	0.31	0.52	2.05
$\rho_p^* = 0.15$	1.0	-0.057	3.0	0.23	0.52	1.28

[f] Regression variance for regression of the chemical potential data using both colloid diameter (σ_c) and polymer chain length (n) as the regression parameters. (exponents in Table 3.2)

[g] Regression variance for regression of the chemical potential data using only polymer chain length (n) as the regression parameter and keeping the colloid diameter (σ_c) constant at 3.0.

Table 3.4: Regressed power-law parameters *b* and *c* obtained from power-law regression of the $\beta\mu_c^{ex}$ and Γ_s data to a function of the form cn^b. σ_p = 10 and ε_{cs} = 1.0 are kept constant.

	$\beta\mu_c^{ex} = cn^b$		$\Gamma_s = cn^b$	
ρ_p^*	c	b	c	b
0.05	-14.3	0.45	0.37	0.49
0.1	-34.6	0.32	0.93	0.33
0.15	-55.9	0.24	1.62	0.21

In order to demonstrate this, we carried out power law regression of the Γ_s data using σ_c and n as physical molecular parameters and obtained a relationship of the form $\Gamma_s = c\sigma_c^a n^b$. The regression was performed over the same range as the chemical potential data i.e., $n \leq 30$ and $\sigma_c \leq 10$ and for conditions of $\varepsilon_{cs} = 1.0$ and $\rho_p^* = 0.05$. The chain length exponent values obtained were 0.43 and 0.49 for chemical potential and Γ_s regressions respectively. This suggests that the dependence of colloid chemical potential on polymer chain length is basically an adsorption effect when attraction dominates particle-polymer interactions. We also determined how the adsorption and chemical potential scaled with the chain length at different polymer segment densities. For this we maintained the particle size constant at $\sigma_p = 10$ and regressed the $\beta\mu_c^{ex}$ and Γ_s data as a function of chain length only. The regressed chain length scaling exponents obtained at different densities is reported in Table 3.4. For all the three densities studied, the exponents are quite close to each other, further validating the argument that chain adsorption controls the chain-length dependence of $\beta\mu_c^{ex}$. Also, from Table 3.4 we see that the chain length exponent for adsorption decreases with increasing polymer segment density. At low concentrations, a polymer chain would tend to form multiple contacts with the particle as the entropic loss is outweighed by the enthalpic gain. With increasing polymer concentration, the driving force for polymer adsorption, i.e., the difference in local polymer density near the particle surface and the bulk density, increases. It is thought to be entropically favorable for the polymer chains to minimize contacts with the particle surface and extend further into the solution as more chains are adsorbed. As a result, there is a decreased dependence on the chain length with increasing polymer concentration, and ultimately the surface becomes saturated.

H. Polymer chain orientations near the particle surface

In addition to chain adsorption, we also studied the conformations of the chains near the particle surface. For studying the chain orientations near the particle surface we define $R^2_{eed\perp}$ and $R^2_{eed\parallel}$, where $R^2_{eed\perp}$ is the mean-squared end-to-end distance of the polymer chain perpendicular to the surface of the particle and $R^2_{eed\parallel}$ is the mean-squared end-to-end distance parallel to the particle surface. Since we are interested essentially in chain conformations near the particle, we consider only those chains that have at least one monomer segment within the first two monolayers (i.e., within $2\sigma_p$) around the particle. This ensures that we do not take into account chains in the bulk solution. Table 3.5 shows the $R^2_{eed\perp}$ and $R^2_{eed\parallel}$ values at different particle sizes and chain lengths for ε_{cs} = 1.0 and ρ_p* = 0.05. In addition, the number of chains in the first two monolayers (M_2) and the average surface area occupied per chain (A_s) given by $A_s = \pi\sigma_c^2/M_2$ are also reported. For all chain lengths the ratio $R^2_{eed\parallel}/R^2_{eed\perp}$ increases with increasing particle size, indicating that the chains become increasingly flattened. Simulations of athermal chains near a wall show a similar anisotropy that is due solely to entropic effects in the absence of energetics.[46] The particle-monomer attraction provides further incentive of the chains to flatten at the surface. We also observe that for a particular particle diameter, the average number of chains in the first two monolayers (M_2) is almost independent of the chain length for the range of values studied. This implies that the increased adsorption with chain length is not due to an increase in the number of *chains* adsorbed but rather due to the increased particle-segment *contacts* for longer chains.

Table 3.5: End-to-end distance with components normal and perpendicular to the surface of the colloidal particle for chains within $2\sigma_p$ of the colloid surface. M_2 is the number of chains in the first two monolayers, A_s is the average surface area occupied per chain ($A_s = \pi\sigma_c^2/M_2$), and R_{eed}^2 is the average end-to-end distance of all the chains in the simulation box.

n	M	σ_c	M_2	$R^2_{eed\perp}$	$R^2_{eed\parallel}$	$R^2_{eed\parallel} / R^2_{eed\perp}$	R^2_{eed}	A_s
5	640	5	7	1.905	3.716	1.95	5.59	11.22
		8	18	1.839	3.733	2.03	5.59	11.17
		10	27	1.844	3.731	2.02	5.59	11.64
		12	40	1.849	3.724	2.01	5.59	11.31
		15	58	1.882	3.696	1.96	5.59	12.19
10	320	5	6	4.996	9.701	1.94	14.57	13.09
		8	17	4.496	9.974	2.22	14.56	11.83
		10	28	4.381	9.974	2.28	14.53	11.22
		12	42	4.377	9.969	2.28	14.51	10.77
		15	62	4.407	9.890	2.24	14.46	11.40
20	160	5	5	11.785	22.297	1.89	33.63	15.71
		8	17	9.850	23.449	2.38	33.55	11.83
		10	29	9.230	23.613	2.56	33.41	10.83
		12	43	8.920	23.705	2.66	33.21	10.52
		15	63	8.699	23.592	2.71	32.81	11.22
30	106	5	5	19.287	34.570	1.79	53.20	15.71
		8	17	15.264	37.022	2.43	52.93	11.83
		10	28	14.056	37.732	2.68	52.64	11.22
		12	40	13.281	37.797	2.85	52.03	11.31
		15	57	12.301	37.740	3.07	50.93	12.40

Figure 3.12 shows snapshots of the equilibrated configuration of chains within the first two monolayers around the particle for different particle sizes and chain lengths. As has been described above, at large particle sizes and long chain lengths a thick layer of adsorbing chains is formed around the particle with high surface coverage (a, d in Figure 3.12). At smaller chain lengths, the adsorption and consequently the surface coverage is relatively lower (c, f, i in Figure 3.12). In the limit of long chains and small particle diameters (g), the chains adsorb at only a few segments, leaving large sections of the adsorbed chains which do not interact strongly with the surface.

Chain adsorption on the particle surface is a reversible process. To get a quantitative picture of how the reversibility of the chain adsorption/desorption phenomena is affected by chain length and particle size, we define a longevity fraction F_t, as the fraction of chains that never desorb from the particle after adsorption occurs. Figure 3.13 shows a plot of F_t vs. the colloid diameter (σ_c) at different chain lengths. The longevity fraction increases with both σ_c and chain length. At small σ_c and short chain lengths, the chains almost never adsorb permanently ($F_t \approx 0$). This is because for small particles the adsorption energy is not strong enough to overcome the loss in chain entropy upon adsorption and the smaller surface area allows fewer particle-polymer contacts. As a result, polymer adsorption and desorption can proceed quite readily. However, for larger particle sizes and longer chains, there are many particle-polymer contacts and the (unlikely) simultaneous detachment of all the surface contacts is required for a chain to desorb. In addition, it has been shown that although the individual polymer segments desorb easily, the desorption energy required for an entire chain can be very high and increases with chain length.[47]

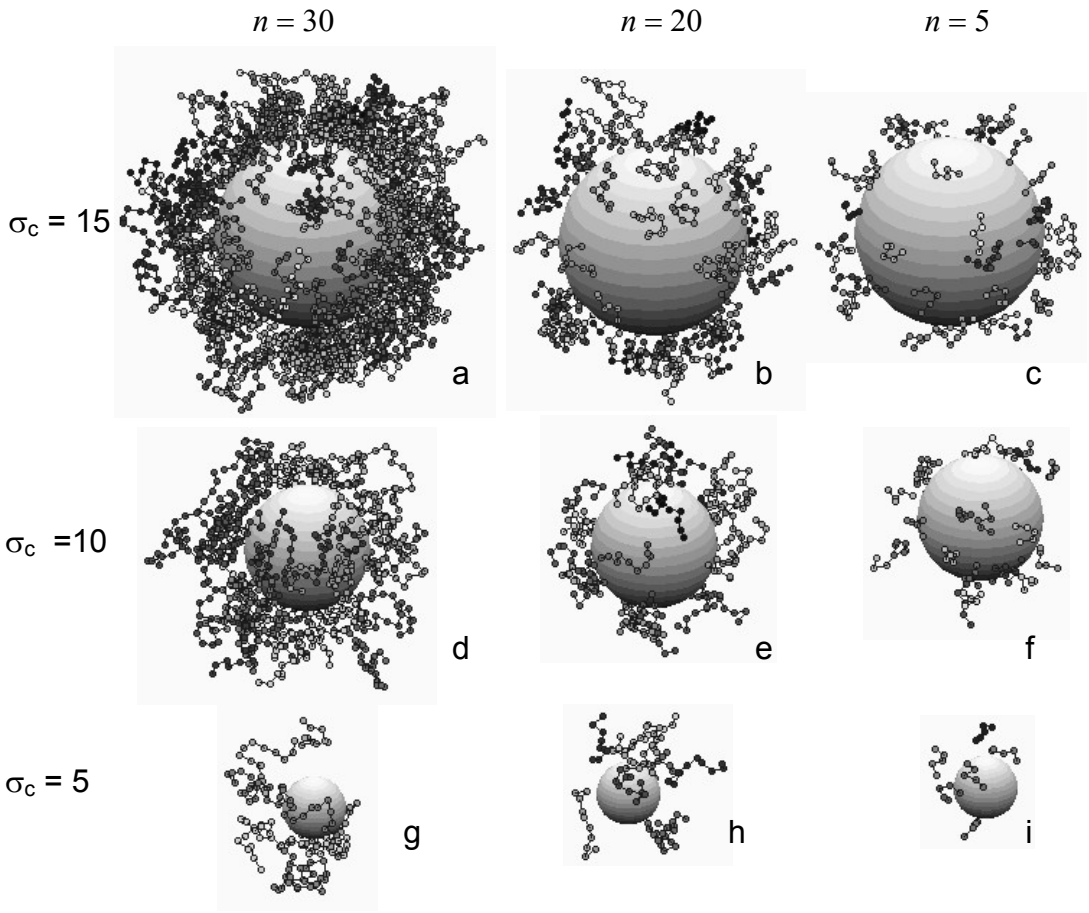

Figure 3.12: Snapshots of the equilibrated configurations for different particle sizes and polymer chains lengths. ρ_p* = 0.05 and ε_{cs} = 1.0. Only polymer chains that are in the first two monolayers around the colloidal particle are shown here.

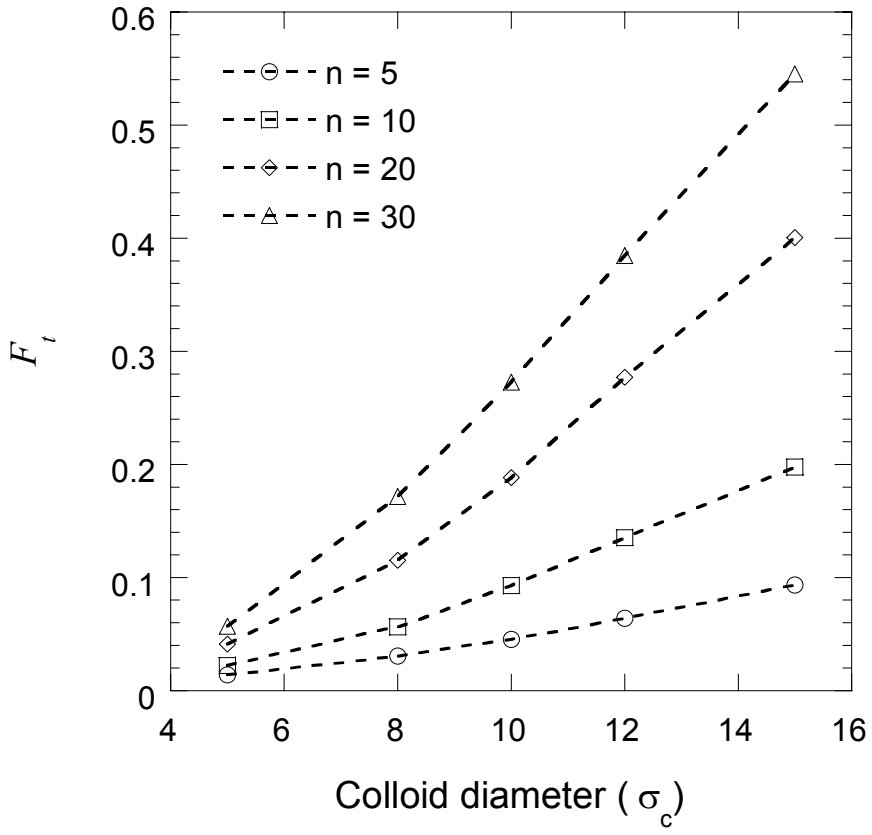

Figure 3.13: Longevity fraction (F_t) defined as the fraction of chains that do not desorb from the particle after adsorption occurs vs. colloid diameter (σ_c) in a dilute LJ polymer solution at ρ_p* = 0.05 and ε_{cs} = 1.0. The lines are a guide to the eye.

3.4 CONCLUSIONS

The EEMC method has been used to calculate the infinite dilution chemical potential of nanocolloidal particles in the presence of reversibly adsorbing LJ homopolymers, the first such calculations via simulations to our knowledge. We have investigated the effect of colloid diameter, polymer chain length, polymer concentration and colloid-polymer interaction energy on the nanocolloid chemical potential. For all polymer chain lengths, the colloid chemical potential decreased and showed a cubic dependence with the colloid diameter. Increasing the chain length of the modifiers also resulted in a decrease in colloid chemical potential. It is noteworthy that the addition of short chain organic modifiers (n < 20) brings about a substantial reduction in the chemical potential, compared to pure monomer solvent at the same volume fraction for both nonadsorbing[23] and freely adsorbing modifiers. For nonadsorbing modifiers, the reduction in chemical potential is *due solely to excluded volume* or entropic contributions. However, in the case of freely adsorbing modifiers (i.e., the attractive polymer-colloid regime), the *reduction in particle chemical potential arises from adsorption*, which is greater for polymer chains than for monomers. The transition of the chemical potential from being entropically controlled (positive) to energetically controlled (negative) occurred at a colloid-polymer interaction energy (ε_{cs}) of 0.25 or ¼ kT. In the attractive regime ($\varepsilon_{cs} \geq 0.25$), the dependence of chemical potential on polymer chain length and colloid diameter was found to be represented well by a power scaling law of the form $\beta\mu_c^{ex} \sim \sigma_c^{3.0} n^b$. The colloid diameter exponent in the above scaling relationship was close to 3.0 for all cases, *independent* of the polymer segment density and ε_{cs}. On the other

hand, the *chain length exponent varied greatly* with polymer segment density and attractive strength. We propose that such power law relationships may be physically meaningful for dilute nanoparticle-polymer systems in which *net* colloid-polymer attraction is dominant as compared to colloid-colloid interactions. A good example is a dilute suspension of silica particles dispersed in toluene with poly (ethylene glycol) (PEG) or poly (methylmethacrylate) (PMMA) surface modifiers.

We believe the most important conclusion is that in *attractive* systems, *chain adsorption dominates the chemical potential* and provides an important molecular interpretation of the effect of adsorbed organic layers on nanoparticle stability and self-assembly. This fact is supported by the similarity between the polymer adsorption and chemical potential dependence on the chain length, confirmed at each polymer concentration investigated (Table 3.4). In addition, the scaling of adsorbance per unit area (Γ_s) with chain length obtained from the simulations agrees well with the scaling theory of Aubouy and Raphael at two extreme regimes of particle size, namely $\sigma_c \ll n^{1/2}$ and $n^{1/2} < \sigma_c/2 > n^{3/5}$.

Because the colloid-polymer attractive magnitude always depends linearly on σ_c, regardless of the exponents in the intersegmental potential, we believe that the correlation between adsorption and chemical potential will hold true for other power law polymer-colloid potentials, including Coulombic (electrostatic) and Hamaker (integrated LJ) potentials in the *attractive colloid-polymer regime*.

3.5 REFERENCES

(1) Aubouy, M.; Raphael, E. *Macromolecules* **1998**, 31, 4357.

(2) Shipway, A. N.; Katz, E.; Willner, I. *CHEMPHYSCHEM* **2000**, 1, 18.

(3) Gai, F.; Lu, Q.; Zhao, D. *Nanolett.* **2002**, 3, 85.

(4) Rensmo, H.; Ongaro, A.; Ryan, D.; Fitzmaurice, D. *J. Mater. Chem.* **2002**, 12, 2762.

(5) Mayer, A. B. R.; Mark, J. E. *Polymer* **2000**, 41, 1627.

(6) Murray, C. B.; Kagan, C. R.; Bawendi, M. G. *Science* **1995**, 270, 1335.

(7) Kulkarni, G. U.; Thomas, P. J.; Rao, C. N. R. *Pure Appl. Chem.* **2002**, 74, 1581.

(8) Meijer, E. J.; Frenkel, D. *J. Chem. Phys.* **1994**, 100, 6873.

(9) Meijer, E. J.; Frenkel, D. *Physica A* **1995**, 213, 130.

(10) Lekkerkerker, H. N. W.; Poon, W. C. K.; Pusey, P. N.; Stroobants, A.; Warren, P. B. *Europhys. Lett.* **1992**, 20, 559.

(11) Eisenriegler, E.; Hanke, A.; Dietrich, S. *Phys. Rev. E* **1996**, 54, 1134

(12) Sear, R. P.; Frenkel, D. *Phys. Rev. E* **1997**, 55, 1677.

(13) Ramakrishnan, S.; Fuchs, M.; Schweizer, K. S.; Zukoski, C. F. *J. Chem. Phys.* **2002**, 116, 2201.

(14) Fuchs, M.; Schweizer, K. S. *J. Phys.: Condens. Matter* **2002**, 14, R239.

(15) Nowicki, W. *Macromolecules* **2002**, 35, 1424

(16) Poon, W. C. K. *J. Phys.: Condens. Matter* **2002**, 14, 859.

(17) Carnahan, N. F.; Starling, K. E. *J. Chem. Phys.* **1969**, 51, 635.

(18) Boublik, T. *J. Chem. Phys.* **1970**, 53, 471.

(19) Mansoori, G. A.; Carnahan, N. F.; Starling, K. E.; Leland, T. W. *J. Chem. Phys* **1971**, 54, 1523.

(20) Fuchs, M.; Schweizer, K. S. *Europhys. Lett.* **2000**, 51, 621.

(21) Fuchs, M.; Schweizer, K. S. *Phys. Rev. E* **2001**, 64, 021514.

(22) Ramakrishnan, S.; Fuchs, M.; Schweizer, K. S.; Zukoski, C. F. *Langmuir* **2002**, 18, 1082.

(23) Marla, K. T.; Meredith, J. C. *J. Chem. Phys.* **2002**, 117, 5443.

(24) Bolhuis, P.; Frenkel, D. *J. Chem. Phys.* **1994**, 101, 9869.

(25) Dickman, R.; Yethiraj, A. *J. Chem. Phys.* **1994**, 100, 4683.

(26) Widom, B. *J. Chem. Phys.* **1963**, 39, 2808.

(27) Shing, K. S.; Gubbins, K. E. *Mol. Phys.* **1981**, 43, 717.

(28) Escobedo, F.; de Pablo, J. J. *J. Chem. Phys.* **1995**, 103, 2703.

(29) Lyubartsev, A. P.; Martsinovski, A. A.; Shevkunov, S. V.; Vorontsov-Velyaminov, P. N. *J. Chem. Phys.* **1992**, 96, 1776.

(30) Wilding, N. B.; Muller, M. *J. Chem. Phys.* **1994**, 101, 4324.

(31) Luna-Bárcenas, G.; Meredith, J. C.; Gromov, D. G.; Sanchez, I. C.; de Pablo, J. J.; Johnston, K. P. *J. Chem. Phys.* **1997**, 107, 1.

(32) Sperry, P. R.; Hopfenberg, H. B.; Thomas, N. L. *J. Colloid Interface Sci.* **1981**, 82, 62.

(33) Flory, P. J. Statistical Mechanics of Chain Molecules; Hanser Publishers: New York, **1988**.

(34) Israelachvili, J. N.; Kott, S. J. *J. Chem. Phys.* **1988**, 88, 7162.

(35) Kumar, K. S.; Szleifer, I.; Panagiotopoulos, A. Z. *Phys. Rev. Lett.* **1991**, 66, 2935.

(36) Attard, P. *J. Chem. Phys*. **1993**, 98, 2225.

(37) Kaminsky, R. D. *J. Chem. Phys*. **1994**, 101, 4986.

(38) de Pablo, J. J.; Laso, M.; Suter, U. W.; Cochran, H. D. *Fluid Phase Equilib.* **1993**, 83, 323.

(39) Siepmann, J. I. *Mol. Phys.* **1990**, 70, 1145.

(40) Mooij, G. C. A. M.; Frenkel, D. *Mol. Phys.* **1991**, 74, 41.

(41) Metropolis, N.; Rosenbluth, A. W.; Rosenbluth, M. N.; Teller, A. H.; Teller, E. *J. Chem. Phys*. **1953**, 21, 1087.

(42) Allen, M. P.; Tildesley, D. J. Computer Simulation of Liquids; 1st ed.; Oxford University Press: Clarendon,Oxford, **1987**.

(43) Johnson, J. K.; Zollweg, J. A.; Gubbins, K. E. *Mol. Phys.* **1993**, 78, 591.

(44) von Goeler, F.; Muthukumar, M. *J. Chem. Phys*. **1994**, 100, 7796.

(45) Aubouy, M.; Guiselin, O.; Raphael, E. *Macromolecules* **1996**, 29, 7261.

(46) Yethiraj, A.; Hall, C. K. *J. Chem. Phys.* **1989**, 91, 4827.

(47) Graessley, W. *Polymer* **1980**, 21, 258.

(48) Israelachvili, J. N. Intermolecular & Surface Forces; 2nd ed.; Academic Press: San Diego, **1991**.

(49) Henderson, D.; Duh, D.-M.; Chu, X.; Wasan, D. *J. Colloid Interface Sci.* **1997**, 185, 265.

CHAPTER 4

SIMULATION OF INTERACTION FORCES BETWEEN NANOPARTICLES IN POLYMER SOLUTION. I. FREELY-ADSORBING HOMOPOLYMERS

The force between two nanoscale colloidal particles dispersed in a solution of freely adsorbing Lennard-Jones homopolymer modifiers is calculated using the expanded grand canonical Monte Carlo simulation method. We investigate the effect of polymer chain length (N), nanoparticle diameter (σ_c) and colloid-polymer interaction energy (ε_{cp}) on polymer adsorption (Γ) and polymer-induced forces ($F_P(r)$) between nanoparticles in the full thermodynamic equilibrium condition. There is a strong correlation between polymer adsorption and the polymer mediated nanoparticle forces. When the polymer adsorption is weak, as in the case of smaller diameters and short polymer chain lengths ($\sigma_c = 5$, $N = 10$), the polymers do not have any significant effect on the bare nanoparticle interactions. The adsorbed amount increases with increasing particle diameter, polymer chain length and colloid-polymer interaction energy. In general, for strong polymer-particle adsorption the polymer-governed force profiles between nanoparticles show short

range repulsion and long ranged attraction suggesting that homopolymers would not be ideal for achieving stabilization in nanoparticle dispersions. The attraction is likely due to bridging as well as polymer segment-segment interactions. The location and magnitude of attractive minimum in the force profile can be controlled by varying N and ε_{cp}. The results show partial agreement and some marked differences with previous theoretical and experimental studies of forces in the limit of flat walls in an adsorbing polymer solution. The difference could be attributed to incorporation of long-ranged colloid-polymer potential in our simulations and the influence of the curvature of the nanoparticles.

4.1 INTRODUCTION

Understanding and manipulating the forces governing nanoscale colloidal phenomena is the key to controlling the phase behavior and stability of nanocolloidal dispersions. Current and potential applications of nanoparticle dispersions range from additives and catalysts to controlled drug-delivery agents and biosensing quantum dots. In addition, the thermodynamically-driven autonomous organization of nanoparticles into well defined superstructures is a promising "bottom-up" fabrication approach to the development of microelectronic, optoelectronic and photonic devices. A common way to achieve control over nanoparticle interactions is to use polymeric surface modifiers which mask out the van der Waals (VDW) forces between the particles. Examples of the use of polymeric surface modifiers in nanoparticle synthesis and dispersions include preparation of colloidal gold nanoparticles using a helical backbone polymer, poly(*N,N*-dihexylcarbodiimide),[1] nanocomposites that include metallic particles with an organic shell of polymer (i.e., polystyrene, poly(dimethylsiloxane), poly(ethyleneoxide), poly(carbodiimides), poly(vinylpyridine), etc.)[2-7] suitable for hierarchical self organization into nanoassemblies,[8,9] and polymer-silica nanocomposites that mimic natural organic-inorganic materials.[10,11] The ability to rationally and predictively design polymeric modifiers that would allow precise control over nanoparticle interactions is an important step towards harnessing the potential applications of colloidal nanoparticles. However, the exact nature and magnitude (relative and absolute) of the polymer mediated forces between these nanoparticles are not very well understood. In addition, experimental determination of polymer-induced nanoparticle forces still remains a challenging task. What is needed is a fundamental understanding of the effects of various

molecular parameters like the nanoparticle size, polymer molecular weight and concentration, and adsorption energy on polymer adsorption and consequently effective interaction forces in these nanoparticle-polymer systems. This would enable us to develop molecular thermodynamic models of these systems which are a precursor to rational predictive strategies for nanoscale structural material synthesis.

Homopolymer adsorption on surfaces and their resultant interactions have been studied extensively using theoretical, experimental and computer simulation approaches as a method of achieving stabilization (as well as flocculation) in macroscopic colloidal particulate systems. For homopolymer adsorption, it is important to distinguish between full thermodynamic equilibrium wherein the chains can leave the gap between the surfaces (being in equilibrium with the surrounding bulk polymer solution) and restricted equilibrium where the polymers between the particles are "trapped" kinetically. Most of the experimental efforts to measure directly the forces between polymer-coated surfaces utilize the surface force apparatus (SFA)[12] and are carried out under some form of restricted equilibrium conditions.[13] Theoretical approaches to modeling these systems can be broadly divided into two categories. One is the self-consistent mean field (SCF) formalism which was first applied to polymer adsorption on surfaces by Scheutjens and Fleer[14] and was later used to calculate free energy of interaction of two surfaces coated with polymers.[15] The SCF method solves for the average equilibrium conformation adopted by a polymer under the influence of the potential imposed by the mean field of the surrounding molecules and the surface. The other approach is based on the density functional theory (DFT) models proposed by de Gennes[16,17] and later developed by Pincus and co-workers.[18,19] In this approach the free energy of the system is expressed as

an integral of a function consisting of a sum of the free energy of a hypothetical system which is homogeneous at the local density of the polymer segments and a term accounting for the variation in the local density, arising from the inhomogeneity of the interfacial profile. The idea here is to calculate the segment density profile that minimizes the integral free energy of the system. Both these approaches have predicted successfully the adsorbed amounts, segment density profiles and force profile between two surfaces in the presence of adsorbing polymers. Theoretical studies based on the above described methods suggest that at full equilibrium, there exists a monotonic attraction between the two polymer-coated surfaces at all separations. At restricted equilibrium, the SCF based theories predict that the interaction force is attractive at large distances and repulsive at short distances.[15] The attraction is primarily due to bridging and in the case of poor solvents, in part due to polymer intersegmental attraction. However, results from the DFT approach suggest that restricted equilibrium would give rise to only monotonic repulsion under good solvent conditions.[16] Both these contrasting results have also been observed experimentally.[13] Monte Carlo (MC) and molecular dynamics (MD) simulation methods have also been used previously to study alkane[20] and polymer solvation forces between flat walls in the limit of "gas-like" as well as "liquid like" polymer densities.[21] Depending on factors such as intermolecular interactions, wall-polymer interactions and polymer segment densities, these solvation forces have been reported to be repulsive, attractive or oscillatory at short separations.

Experimental and theoretical studies invariably involve flat and macroscopic surfaces and high molecular weight (long chain) polymers. The results in flat wall limit can be extended to large spherical surfaces using the Derjaguin approximation which

relates the force profile between two curved surfaces to the interaction free energy between two planar surfaces. However, in the case of nanoparticles the curvature effects become important and the Derjaguin approximation is no longer expected to hold. In addition, the mean size of the polymer chains (i.e., their radius of gyration R_g) used for surface modification in these nanoparticle systems is comparable to the diameter of the particles (and hence would be of relatively low molecular mass). These factors make it important to ask how the polymers change nanocolloidal phenomena, in contrast to larger colloid size ranges.

There have been a few recent studies that calculate the solvation forces between two nanoparticles in Lennard-Jones (LJ) and soft-sphere fluids using MD simulations. Namely Shinto et al[22] varied the fluid-nanoparticle interactions to study the van der Waals and solvation forces between solvophobic and solvophilic nanoparticles. Qin and Fichthorn[23] also performed similar studies in which they represented the nanoparticles as rigidly-fixed clusters of LJ atoms and determined the effect of particle size, shape and roughness on the solvation forces. The force profiles obtained in both these studies are similar in form to those predicted for fluids confined between flat and infinite surfaces (attractive for solvophobic and oscillatory for solvophilic nanoparticles). However, to the best of our knowledge, there have been no reported simulation studies of interaction forces between nanoscale colloidal particles in the presence of freely adsorbing homopolymer modifiers. In this study, we calculate the polymer-mediated interaction force profiles between spherical nanoparticles in the true thermodynamic equilibrium condition using the expanded grand canonical Monte Carlo method. The Lennard-Jones homopolymer is used to model freely adsorbing modifiers, as it incorporates both

attraction and adsorption effects. We investigate the effect of nanoparticle diameter, polymer chain length and the polymer-particle adsorption energy on the force profiles. In addition, we also determine polymer adsorption on the particle surface, and the nature and orientations of the adsorbed layers, and use these results to interpret the force-distance curves. Based on the correlation between polymer adsorption and the force profiles, we propose the dominant mechanism which leads to attraction or repulsion in these systems. These simulations lend important insights into the physics of attractive polymer-nanoparticle mixtures, which are currently unavailable from experimental or theoretical approaches. The objective of this work is to characterize the dependence of polymer adsorption and nanoparticle interactions on the various physical molecular parameters towards the development of rational design criteria for polymer modifiers. The rest of the chapter is organized as follows: In section 4.2 we describe briefly the simulation details and methodology of force calculations. The effect of the various molecular parameters on adsorption of homopolymers on nanoparticles is presented in section 4.3 followed by detailed results and discussion of the polymer-mediated force profiles. We also present a comparison of our results with those obtained for macroscopic colloids in the flat wall limit. Finally we present some concluding remarks in section 4.4.

4.2 SIMULATION METHOD

In this work we have simulated the net binary interaction force between colloidal nanoparticles in the presence of freely (reversibly) adsorbing homopolymer surface modifiers. The polymeric modifiers are modeled as fully flexible Lennard-Jones chains in continuum. The bond length between adjacent segments in a polymer chain is maintained

constant at σ_p. The non-bonded polymer segments interact via the cut and shifted LJ potential shown in eq 4.1,

$$U(r_{ij}) = \begin{cases} 4\varepsilon_{ij}\left[\left(\frac{\sigma_{ij}}{r_{ij}}\right)^{12} - \left(\frac{\sigma_{ij}}{r_{ij}}\right)^{6} - \left(\frac{\sigma_{ij}}{r_c}\right)^{12} + \left(\frac{\sigma_{ij}}{r_c}\right)^{6}\right] & r \le r_c, \\ 0 \quad r > r_c \end{cases} \qquad (4.1)$$

where $\sigma_{ij} = (\sigma_i + \sigma_j)/2$ is the size parameter and ε_{ij} is the LJ interaction energy parameter. The cutoff distance (r_c) has been set to $r_c = 2.5\sigma_p$, and the potential has been shifted to ensure continuity at cutoff. The system consists two spherical colloidal nanoparticles dispersed in a dilute polymer (or oligomer) solution. Three types of interactions are considered; segment-segment for non-bonded polymer sites and colloid-segment and colloid-colloid. The colloid-segment and the colloid-colloid interactions are modeled using the full LJ potential without any cutoff. The simulation variables are reduced in the standard manner, i.e., temperature $T^* = Tk_B/\varepsilon_{pp}$, density $\rho_p^* = \rho_p\sigma_p^3$, where ε_{pp} is the polymer segment-segment interaction parameter, k_B is the Boltzmann constant and ρ_p is the bulk polymer segment density. The polymer segment density is defined as $\rho_p = Nn_p/V$, where N is the polymer chain length, n_p is the number of chains and V is the volume of the simulation box. All the simulations were performed at a constant reduced temperature of $T^* = 3.0$, which mimics the good solvent condition for the polymer chains. In addition, this temperature is above the upper critical solution 'theta' temperature (UCST) of LJ polymer chains, known from previous simulations, to be 2.5[24] thereby eliminating any effects of polymer phase transitions. In our simulations the solvent is not included explicitly and the energetic effects of solvent could be modeled by changing the reduced temperature or the colloid-polymer interaction energy parameter (ε_{cp}). To equilibrate

polymeric modifiers between the bulk phase and the colloid-polymer (CP) region, simulations were performed in a grand canonical ensemble with N, μ_p, V and T^* constant, where μ_p is the polymer chemical potential. Figure 4.1 gives the schematic of the bulk polymer (Figure 4.1a) and the colloid-polymer (Figure 4.1b) simulation boxes. The dimensions of the simulation box are $40\sigma_p$, in the x and y directions and $50\sigma_p$, in the z direction. These box dimensions ensure that there are no artificial interactions between periodic images. Standard periodic boundary conditions apply in all directions. All the simulations were performed at a bulk polymer segment density of ρ_p^* = 0.05. The polymer-mediated nanoparticle interaction forces were calculated for two different particle diameters, $\sigma_c = 10\sigma_p$ and $5\sigma_p$. The effect of homopolymer molecular weight (i.e. chain length) was also studied by considering chain lengths of N = 10 and 30. In addition, the effect of the strength of nanoparticle-polymer interactions (ε_{cp}) on the force distance profiles was explored by varying ε_{cp} from $5\varepsilon_{pp}$ (strong attraction) to completely turning off the colloid-polymer attraction and having only a soft-repulsive interaction (obtained by using only the repulsive term in the LJ potential). ε_{pp} is maintained constant at ε_{pp} = 1 in this study unless specified otherwise.

4.2.1 Expanded Grand Canonical Ensemble Simulations

The equilibrium partitioning of polymer chains between the bulk phase and the colloid-polymer region was simulated using the grand canonical (μVT) ensemble. At the bulk densities and polymer chains lengths that we consider, the trial insertions and deletions of the polymer molecules can be carried out very efficiently in the grand canonical ensemble by combining it with the expanded ensemble method for calculating

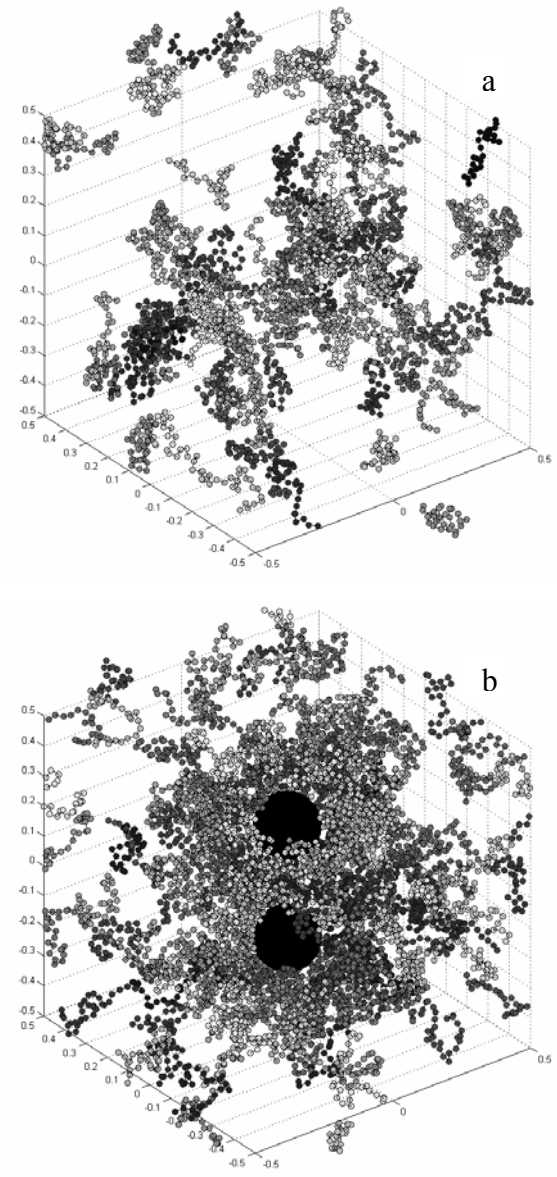

Figure 4.1: Configuration snapshot of the bulk polymer (Figure 4.1a) and the colloid-polymer (Figure 4.1b) simulation boxes. The bulk polymer segment density is $\rho_p^* = 0.05$. The snapshot of the colloid-polymer simulation box is shown for the case of $\sigma_c = 10\sigma_p$, $N = 30$ and colloid surface-to-surface separation distance of $D = 5$.

polymer chemical potentials.[25] The detailed derivation of the expanded ensemble for the calculation of chemical potentials[26] and phase equilibria[25] of polymer systems can be found in the literature. In addition, the details of the expanded grand canonical Monte Carlo method applied to the simulation of homopolymer adsorption on two impenetrable flat surfaces are described in reference.[27] Here, we adopt a similar methodology for simulation of homopolymers adsorbing on spherical nanoscale colloidal particles.

4.2.2 Computational Method

NVT simulations of the bulk polymer solutions were first performed to generate chain chemical potentials at a given temperature (T^*) and bulk polymer density ($\rho_p^* = 0.05$). The chain chemical potential was calculated by using the expanded variable-length chain ensemble.[26] The accuracy of the expanded ensemble code was verified by comparing our chemical potentials to those of previous workers for hard-sphere chains.[26] The nanoparticle-polymer phase was simulated using the expanded grand canonical ensemble by taking the chain chemical potential values from the bulk simulations as set points. For each simulation the two nanoparticles (A & B) were fixed along the z-axis at a specified distance from each other. The polymer chains were then added to the simulation box and the system was allowed to equilibrate until the set point chemical potential is attained. Thermal equilibrium in the simulation box is achieved by performing chain displacements using the continuum configurational bias (CCB) algorithm,[28-30] in which a section of the chain is cut and regrown into low-energy conformations after scouting N_{sp} trial positions. N_{sp} is set to 6 in our simulations. Then the forces due to the polymer chains on each nanoparticle ($F_{AP}(r)$ and $F_{BP}(r)$) were calculated. This ensured that the force at each distance was calculated at "true" thermodynamic equilibrium. Further, the

chain end-to-end distance, orientations of the adsorbed chains with respect to the nanoparticles, and segment density profiles were also calculated. Such individual simulations were performed at each distance to obtain the force-distance profile. The forces were calculated from the nearest centre to centre separation ($r_{c\text{-}c}$) between the nanoparticles of $r_{c\text{-}c} = \sigma_c + 1\sigma_p$ in increments of $1\sigma_p$ up until approximately $r_{c\text{-}c} = 2.5\ \sigma_c$. The forces reported in this chapter are normalized by subtracting the force at "infinite" separation, where the nanoparticle surfaces are far enough not to affect one another significantly. The expanded grand canonical ensemble code was verified by comparing average chemical potentials, densities and chain conformational properties to results from NVT simulations. In most cases (20-40) x 10^6 equilibrium steps and (120 – 180) x 10^6 averaging steps were required at each separation distance to obtain statistically significant averaged values of the properties of interest. In this work, one MC step corresponds to one attempted move. The statistical error in the forces was based on the statistical inefficiency parameter.[31] Note that all error bars have been omitted from the figures unless they were larger than the symbols representing the data points. The details of the all the cases and conditions that were explored in this study are given in Table 4.1, where μ_p is the set chain chemical potential obtained from bulk polymer simulations, $R_{g,bulk}$ and $R_{EED,bulk}$ are the polymer radius of gyration and end-to-end distance respectively in the bulk region and $\rho^*_{p,interface}$ is the equilibrium average polymer segment density in the nanocolloid-polymer simulation box (also referred to as the interface region or colloid-polymer region in this chapter).

Table 4.1: Simulation conditions explored in this study. μ_p is the set point chain chemical potential obtained from bulk simulations and $\rho^*_{p,interface}$ is the equilibrium polymer segment density in the colloid-polymer simulation box. $R_{g,bulk}$ and $R_{EED,bulk}$ are the radius of gyration and end-to-end distance of the polymer chains in the bulk.

Case number	σ_c	n	ε_{cp}	ε_{pp}	μ_p	$\rho^*_{p,interface}$	$R_{g,bulk}$	$R_{EED,bulk}$
1	5	10	1.0	1.0	1.067	0.0516	1.55	3.82
2	5	30	1.0	1.0	3.840	0.0564	2.95	7.29
3	5	30	2.0	1.0	3.840	0.0663	2.95	7.29
4	10	10	1.0	1.0	1.067	0.0603	1.55	3.82
5	10	20	1.0	1.0	2.457	0.0758	2.34	5.80
6	10	30	1.0	1.0	3.840	0.0886	2.95	7.29
7	10	30	2.0	1.0	3.840	0.1125	2.95	7.29
8	10	30	5.0	1.0	3.840	0.1522	2.95	7.29
9	10	30	Rep[f]	1.0	3.840	0.0468	2.95	7.29
10	10	30	0.5	0.5	7.469	0.0616	3.21	7.95
11	10	30	1.0	Rep[f]	14.392	0.0532	3.59	9.18

[f] "Rep" indicates a purely repulsive interaction obtained by using only the repulsive term in the Lennard-Jones 6-12 potential.

4.2.3 Force Calculations

The total polymer mediated interaction force between the colloidal nanoparticles is the sum of the direct nanoparticle-nanoparticle force and the forces acting on the nanoparticles due to the adsorbing polymers. The direct interaction force between the nanoparticles $F_D(r)$ is obtained by

$$F_D(r) = -\frac{\partial U_{cc}(r)}{\partial r} = \frac{48}{r}\left(\left(\frac{\sigma_c}{r}\right)^{12} - 0.5\left(\frac{\sigma_c}{r}\right)^{6}\right) \tag{4.2}$$

The forces on the nanoparticles A and B due to the polymer chains, $F_{AP}(r)$ and $F_{BP}(r)$, are calculated by using a relation similar to eq 4.2,

$$F_{AP,BP}(r) = \sum_{i=1}^{i=Nn_p} -\frac{\partial u_{cp}(r)}{\partial r}, \tag{4.3}$$

where u_{cp} is the colloid-polymer segment interaction potential. The polymer contribution to the interaction force between the nanoparticles is evaluated as an ensemble average over different configurations using [22,23]

$$F_P(r) = \frac{1}{2}\left\langle \hat{\mathbf{r}}_{AB} \bullet \left(F_{AP} - F_{BP}\right)\right\rangle_r \tag{4.4a}$$

$$\hat{\mathrm{r}}_{AB} = \left(\mathrm{r_A} - \mathrm{r_B}\right)/\left|\mathrm{r_A} - \mathrm{r_B}\right| , \tag{4.4b}$$

where $\hat{\mathrm{r}}_{AB}$ is a unit vector pointing from particle B to particle A. In our simulations, the nanoparticles are fixed along the z-axis ($z_A > z_B$) and hence due to symmetry in the (x,y) plane only the z component of force contributes. The total interaction force $F_{TOT}(r)$ is given by $F_{TOT}(r) = F_P(r) + F_D(r)$.

It must be noted here that the use of the LJ pair interaction potential to model the interaction between the colloid and polymer segments is, at best, a gross

oversimplification of reality. However, we believe that the potential does capture the salient features of colloid (or nanoparticle) – polymer systems with primarily dispersive interactions. What is missing here is an accounting for the density of the nanoparticle and an integration of the LJ potential between all the atoms in the nanoparticle and each polymer segment, in the manner of the Hamaker microscopic approach.[12,32] In this case the potential becomes much more long ranged, e.g. $(\sigma/r)^9 - (\sigma/r)^3$. However, the generic feature of the attraction magnitude increasing linearly with colloid size occurs in both the pure and integrated LJ forms. Hence the 6-12 LJ potential, though not quantitatively exact, does approximate the physics of van der Waals interactions in these systems. It is noteworthy to consider the effect of particle diameter on the direct force profiles obtained from differentiating LJ-type power law potentials. Consider a general power-law potential of the form $[(\sigma/r)^m - (\sigma/r)^n]$. For this potential, the force $f(r)$ is given by

$$f(r) = -\frac{\partial U}{\partial r} = \frac{1}{r}\left[m\left(\frac{\sigma}{r}\right)^m - n\left(\frac{\sigma}{r}\right)^n \right] \tag{4.5}$$

The minimum in the force, obtained by setting $\partial f/\partial r = 0$, occurs at

$$r_{\min} = \sigma\left[\frac{m(m+1)}{n(n+1)}\right]^{\frac{1}{m-n}}, \tag{4.6}$$

and is given by,

$$f_{\min} = -n\left(\frac{m-n}{m+1}\right)\left(\frac{n(n+1)}{m(m+1)}\right)^{\frac{n+1}{m-n}}\frac{1}{\sigma} = -\frac{A}{\sigma} \tag{4.7}$$

For m, $n > 0$ and $m > n$, A is always greater than 0. This implies that the magnitude of $f_{\min}$ increases with decreasing particle size. This is illustrated in Figure 4.2 which shows the direct force profile (from eq 4.2) as a function of particle diameter. The plot shows that

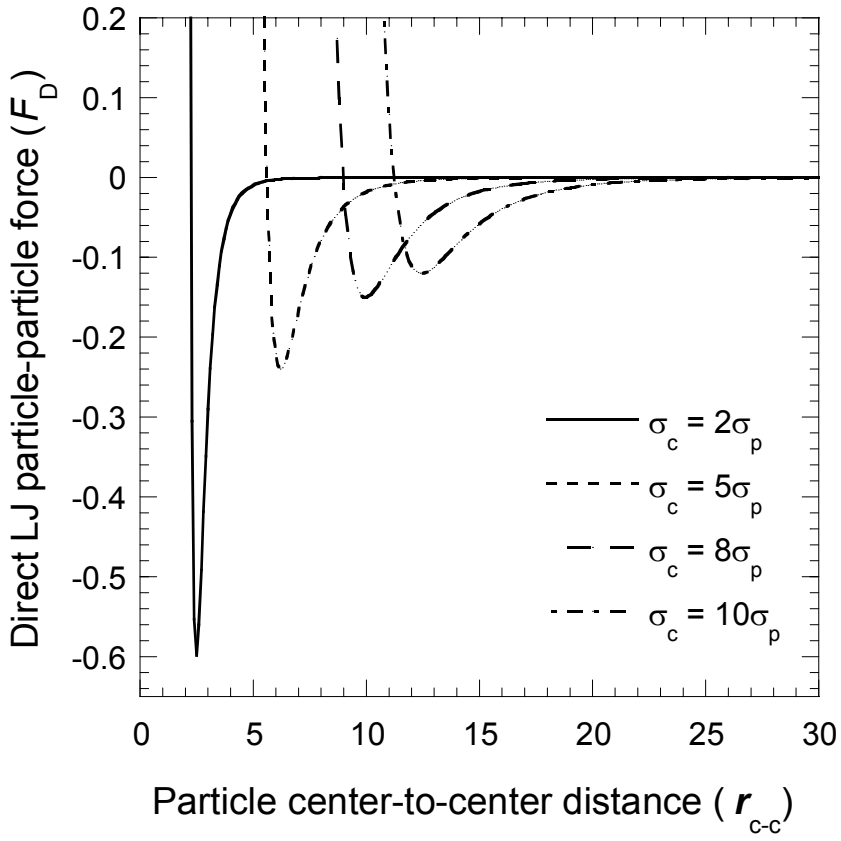

Figure 4.2: Direct LJ interaction force $F_D(r)$ between the two particles versus separation distance at different particle diameters (σ_c). $F_D(r)$ is calculated from eq 4.2.

the minimum in the force profile becomes lower and moves to a closer separation distance as the nanoparticle diameter becomes smaller, making them relatively more difficult to stabilize.

4.3. RESULTS & DISCUSSION

4.3.1 Adsorption of homopolymer modifiers on the colloidal nanoparticles

A. Effect of particle diameter (σ_c) and chain length (N)

The force-distance profile between nanoparticles dispersed in a solution of freely adsorbing homopolymers is correlated strongly with the amount of polymer adsorbed on the nanoparticles and the nature of the adsorbed layers. Hence, we first explore the dependence of adsorption on the various molecular parameters (σ_c, N, ε_{cp}, ε_{pp}) to obtain a better understanding of the physical phenomena that govern the polymer-induced nanoparticle forces. Figure 4.3 shows the polymer segment density profiles in the z-direction in the nanoparticle-polymer simulation box at two particle sizes $\sigma_c = 5\sigma_p$, $10\sigma_p$ and chain lengths $N = 10$, 30. The plots are for a surface-to-surface separation (D) of $5\sigma_p$ between the particles, where D is defined as $D = r_{c\text{-}c} - \sigma_c$ and $r_{c\text{-}c}$ is the centre to centre separation. The locations of the nanoparticle centers are represented by the dashed lines parallel to the y-axis in Figure 4.3. At constant chain length, the local segment density near the particle is greater for larger colloids. Increasing the colloid diameter increases the range of the LJ attraction bringing more chains from the bulk under the attractive influence of the colloidal particle. In addition, the increased surface area available for particle-polymer contacts also enhances adsorption. Consequently, the amount of polymer adsorbed increases with increasing particle diameter. A measure of the attractive

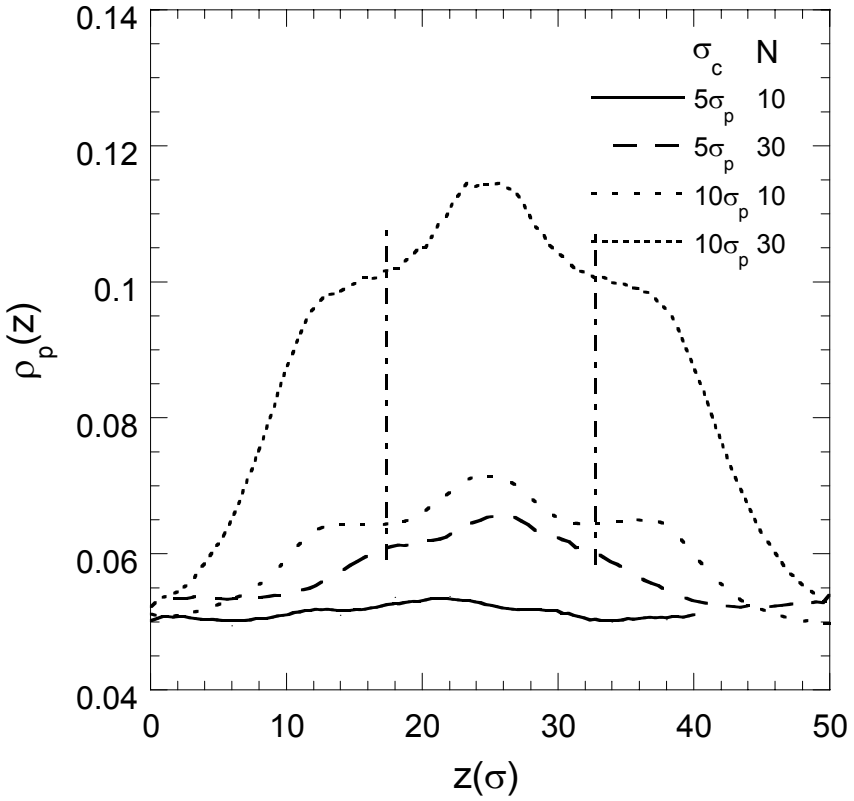

Figure 4.3: Polymer segment density profiles in the *z*-direction in the nanoparticle-polymer simulation box at two particle sizes $\sigma_c = 5\sigma_p$, $10\sigma_p$ and chain lengths $N = 10, 30$. $\varepsilon_{cp} = \varepsilon_{pp} = 1$. The plots are for a surface-to-surface separation (D) of $5\sigma_p$ between the particles, where D is defined as $D = r_{c\text{-}c} - \sigma_c$. The two vertical dashed lines indicate the location of the nanoparticle centers.

influence of the particle diameter is reflected in the $\rho^*_{p,interface}$ values shown in Table 4.1 (cases 2 & 6), where $\rho^*_{p,\ interface}$ for $\sigma_c = 10\sigma_p$ is much higher than the value for $\sigma_c = 5\sigma_p$. Note that the $\rho^*_{p,\ interface}$ values reported in Table 4.1 are averaged over all separations (D) for each specific case. Figure 4.3 also shows that for constant σ_c, the increase in polymer segment density in the colloid-polymer region is greater for longer chains. This is because the entropy loss associated with chain adsorption is lower for longer chains. These trends were also observed recently in simulations of attractive nanoparticle-polymer mixtures.[33]

B. Effect of colloid-polymer interaction energy (ε_{cp})

Figure 4.4 shows the effect of changing the colloid-polymer interaction energy parameter ε_{cp} at $\sigma_c = 10\sigma_p$, $N = 30$, $D = 5\sigma_p$ and $\varepsilon_{pp} = 1$ on the segment density profiles. Varying this parameter allows us to understand the effect of tuning the solvent quality of the polymer. When ε_{cp} is increased compared to ε_{pp}, the polymer has a greater affinity for the particle surface than the polymer solution and this in turn results in increased polymer adsorption. Figure 4.4 also shows the effect of turning off the colloid-polymer attraction wherein only the repulsive part of the LJ 6-12 potential is used to model the colloid-polymer interactions. This is equivalent to the case of suspending nanoparticles in a solution of non-adsorbing polymer solution and as expected there is a depletion of polymer segment density in the vicinity of the nanoparticles. The solvent quality could also be tuned by varying ε_{pp}, while holding ε_{cp} constant. Figure 4.5 shows how the polymer segment density profiles are influenced by changing ε_{pp}, at $\sigma_c = 10\sigma_p$, $N = 30$, $D = 5\sigma_p$ and $\varepsilon_{cp} = 1$. In general, as ε_{pp} is varied from being purely repulsive (hard sphere chains) to $\varepsilon_{pp} = 1$, there is an increase in the polymer segment density in the CP region.

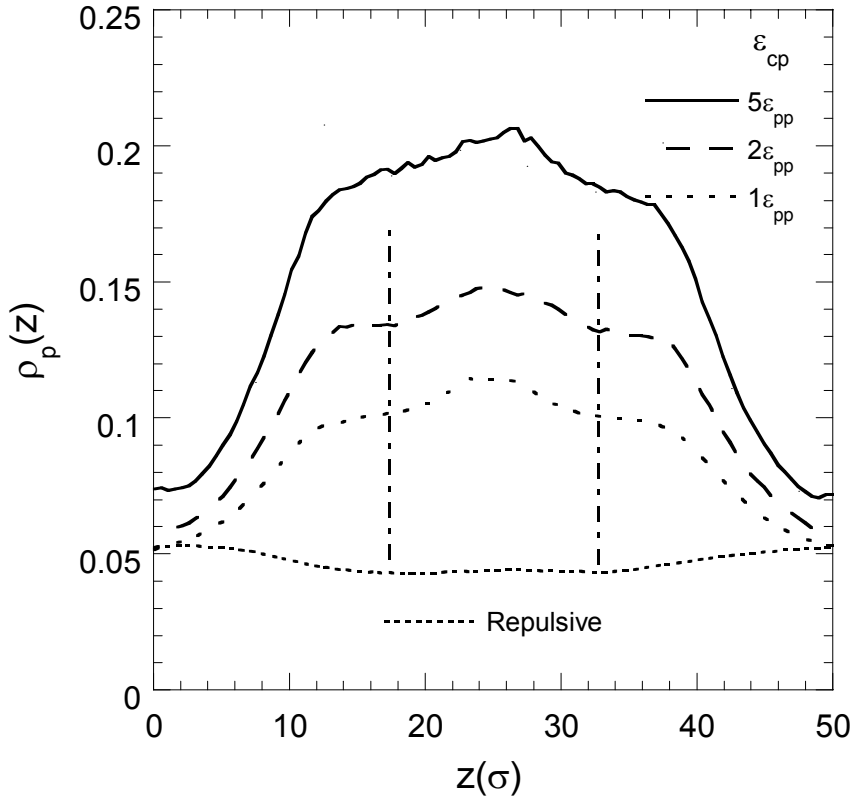

Figure 4.4: Effect of changing the colloid-polymer interaction energy parameter ε_{cp} at $\sigma_c = 10\sigma_p$, $N = 30$ and $\varepsilon_{pp} = 1$ on the polymer segment density profiles in the z-direction in the nanoparticle-polymer simulation box. The plots are for a surface-to-surface separation (D) of $5\sigma_p$ between the particles, where D is defined as $D = r_{c\text{-}c} - \sigma_c$. The two vertical dashed lines indicate the location of the nanoparticle centers.

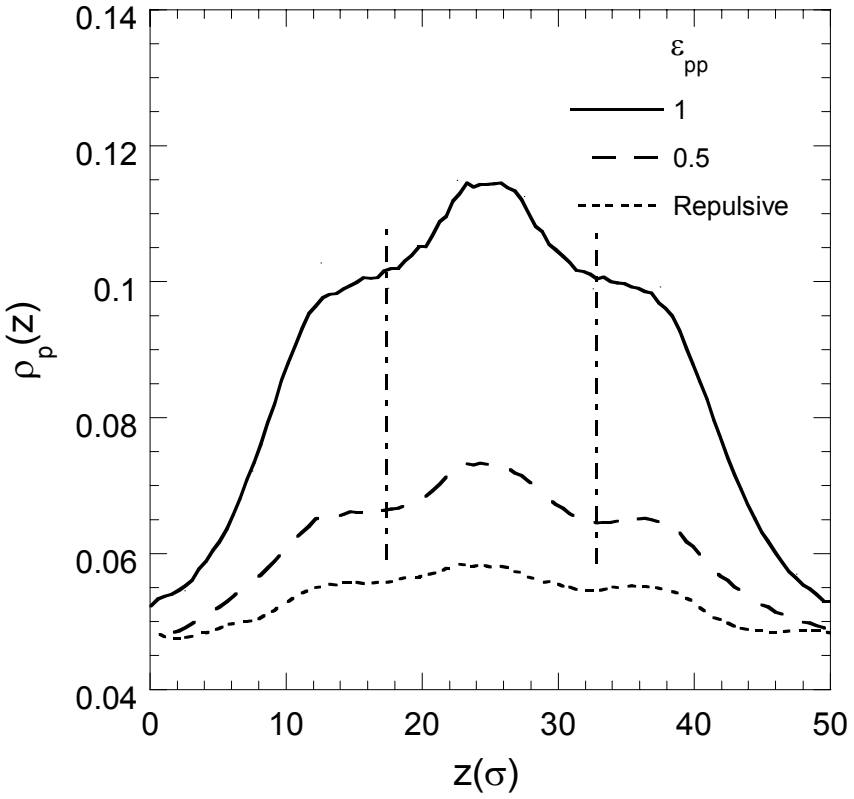

Figure 4.5: Effect of changing the polymer-polymer interaction energy parameter ε_{pp} at $\sigma_c = 10\sigma_p$, $N = 30$ and $\varepsilon_{cp} = 1$ on the polymer segment density profiles in the z-direction in the nanoparticle-polymer simulation box. The plots are for a surface-to-surface separation (D) of $5\sigma_p$ between the particles, where D is defined as $D = r_{c\text{-}c} - \sigma_c$. The two vertical dashed lines indicate the location of the nanoparticle centers.

As ε_{pp} is decreased compared to ε_{cp}, one would expect that the polymer segment density near the particle would progressively increase, which is not the case in Figure 4.5. Although the polymers have a comparatively stronger affinity for the particle surface (when ε_{pp} is decreased compared to ε_{cp}), the decreased polymer segment-segment interaction limits the number of chains that can be adsorbed. At $\varepsilon_{pp} = 1.5$, (plots not shown) we found that the density of polymer in the CP region oscillated between $\rho^*_{p,\,interface} = 0.026$ and 0.16 suggesting that we had reached a coexistence point. This case was not explored further as phase transition effects are beyond the scope of this work. It is interesting to compare the cases of $\varepsilon_{cp} = 2$, $\varepsilon_{pp} = 1$ (Figure 4.4) and $\varepsilon_{cp} = 1$, $\varepsilon_{pp} = 0.5$ (Figure 4.5). The ratio $\varepsilon_{cp} / \varepsilon_{pp} = 2$ for both these cases, however the polymer segment density in the vicinity of the colloid is almost twice in the case of $\varepsilon_{cp} = 2$, $\varepsilon_{pp} = 1$, indicating that the effect of tuning ε_{cp} is significantly different from varying ε_{pp}. A notable feature of all the segment distribution plots in which attraction dominates is that as D decreases, the local polymer segment density in between the planes passing through the centers of the two nanoparticles and perpendicular to the z-axis increases monotonically. For polymer that can freely adsorb-desorb, it would be expected that the polymers would leave the region between the nanoparticles due to entropic considerations as D is reduced. On the other hand, the polymers in this region would also experience doubly strong enthalpic interactions due to the two particles in their close proximity, which could offset the entropic penalty and result in increased adsorption. Changes in the polymer segment density in the interface region can be examined by integrating the segment density profiles to yield adsorption isotherms with,

$$\Gamma_s = \frac{1}{\pi\sigma_c^2} \int_{\sigma_{cp}/2}^{l_b/2} \left(\rho^*_{p,interface}(r) - \rho^*_{p,bulk}(r)\right) 2\pi r^2 dr \qquad (4.8)$$

where Γ_s is the excess adsorption of the polymer segments per unit surface area of the particle, σ_{cp} is defined as $(\sigma_c + \sigma_p)/2$, l_b is the length of the simulation box, and $\rho_{p,interface}^*(r)$ is the polymer segment density in the CP region (averaged over spherical angles θ and ϕ) at a distance r from the center of the particle. Γ_s reported in this study is averaged over both the particles in the simulation box and is reported on a per particle basis.

Figure 4.6 shows a plot of Γ_s versus nanoparticle separation distance (D) for all the cases examined in this study. The effect of particle size and chain length at $\varepsilon_{cp} = \varepsilon_{pp} = 1$ is shown in Figure 4.6a and the effect of colloid-polymer and polymer-polymer interaction energy parameters (ε_{cp} and ε_{pp}) at $\sigma_c = 10\sigma_p$, $N = 30$ is shown in Figure 4.6b. In general, for all cases Γ_s increases very slightly as D decreases for reasons discussed above. Also the excess adsorbed amount increases with σ_c, N, ε_{cp} and ε_{pp} in agreement with the segment density profiles in Figures 4.3, 4.4 & 4.5. When the colloid-polymer attraction is turned off, Γ_s is negative indicating a depletion of polymer chains in the CP region (Figure 4.6b).

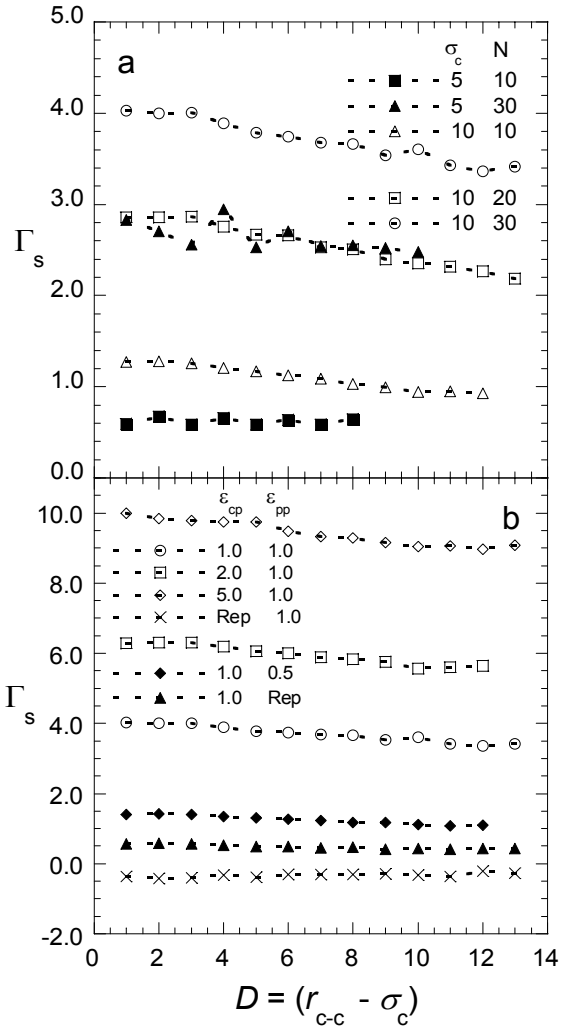

Figure 4.6: Excess adsorbed amount per unit surface area of the particle (Γ_s) calculated from eq 4.8 versus nanoparticle surface-to-surface separation distance (D) for the various cases explored in this study. (a) Effect of particle size and chain length at $\varepsilon_{cp} = \varepsilon_{pp} = 1$. (b) Effect of colloid-polymer and polymer-polymer interaction energy parameters (ε_{cp} and ε_{pp}) at $\sigma_c = 10\sigma_p$, $N = 30$.

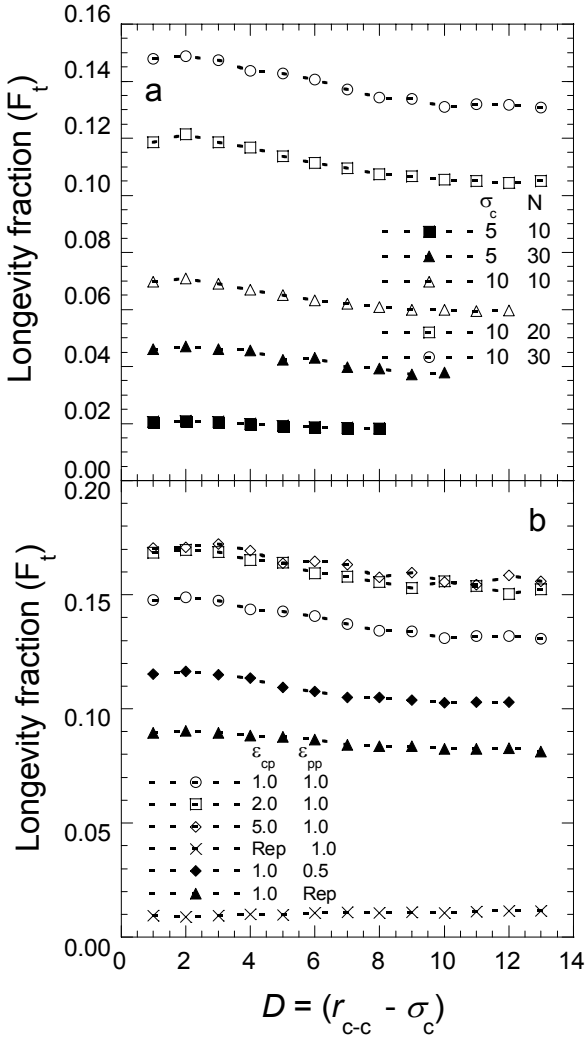

Figure 4.7: Longevity fraction (F_t) defined as the fraction of chains that do not desorb from the particle after adsorption versus separation distance (D) for the various cases explored in this study. (a) Effect of particle size and chain length at $\varepsilon_{cp} = \varepsilon_{pp} = 1$. (b) Effect of colloid-polymer and polymer-polymer interaction energy parameters (ε_{cp} and ε_{pp}) at $\sigma_c = 10\sigma_p$, $N = 30$.

The chain adsorption-desorption phenomenon is a reversible process and a quantitative measure of this reversibility can be obtained by calculating the average longevity fraction (F_t) of the chains. F_t is defined as the fraction of chains that do not desorb from the nanoparticle after adsorption.[33] Figure 4.7 shows a plot of F_t versus separation distance for the various cases explored in this study. For all cases F_t seems to increase marginally with decreasing separation distance between the nanoparticles, which corroborates the argument presented above for increased adsorption as D decreases. The longevity fraction for $\sigma_c = 10\sigma_p$, $N = 30$ is about three times the value for $\sigma_c = 5\sigma_p$, $N = 30$ indicating the relatively stable nature for the adsorbed layer for $\sigma_c = 10\sigma_p$ (Figure 4.7a). In fact for $\sigma_c = 5\sigma_p$, F_t is very close to zero resulting in an adsorbed layer where adsorption-desorption phenomena proceeds quite readily. Also, at a constant particle diameter, F_t is higher for longer chains because of the larger number of polymer-particle contacts that are formed. Although individual polymer segments desorb easily, the desorption energy required for an entire chain can be quite high and increases with chain length. F_t also increases monotonically with increasing ε_{cp} and ε_{pp} (Figure 4.7b) further supporting the trends obtained for adsorption and the segment density profiles. These insights into the adsorption phenomena on spherical nanoparticles will be used to interpret the force profiles observed below.

4.3.2 Polymer induced interaction forces between nanocolloids

A. Effect of nanoparticle diameter (σ_c) and chain length (N)

Figure 4.8 shows a plot of force due to the polymer chains (F_P) between two nanoparticles for diameters of $\sigma_c = 5\sigma_p$ (Figure 4.8a) and $10\sigma_p$ (Figure 4.8b) at different

chain lengths. The direct force between the nanoparticles (F_D) calculated from eq 4.2 is also shown for comparison. In all force profiles the x-coordinate is taken to be $D = (r_{c\text{-}c} - \sigma_c)$. At $\sigma_c = 5\sigma_p$, F_P is very small compared to F_D and is in fact close to zero for both polymer chain lengths $N = 10$, 30 indicating that the polymers do not have a significant effect on the nanoparticle interactions. For $\sigma_c = 10\sigma_p$, the force-distance profile is similar in form and comparable in magnitude to the direct nanoparticle forces (F_D). The attractive minimum in F_P occurs at $D \approx 6$ and then there is a repulsive maximum at $D \approx 2$ for both chain lengths after which the force seems to decrease slightly (at $D \approx 1$). Also, the polymer-induced attractive force is stronger and also the repulsive maximum is higher for $N = 30$ as compared to $N = 10$. As mentioned earlier, the effect of particle size and polymer chain length on the force profile is determined by their effect on polymer adsorption. From results of the adsorption studies, an increase in either σ_c or N results in increased adsorption and a higher $\rho^*_{p,interface}$ which in turn effect an increase in the magnitude of both attraction and repulsion in the polymer mediated force profile. Figure 4.9 shows equilibrated configuration snapshots of the nanoparticle-polymer simulation box for $\sigma_c = 5\sigma_p$, $N = 30$ (Figure 4.9a) and $\sigma_c = 10\sigma_p$, $N = 30$ (Figure 4.9b). The snapshots are for a separation distance of $D = 5$ between the nanoparticles. For $\sigma_c = 10\sigma_p$, a thick layer of adsorbed polymer is formed around the nanoparticles (shaded in dark in Figure 4.9) combined with a dense accumulation of polymers in the interparticle region whereas for $\sigma_c = 5\sigma_p$ there is no significant adsorbed layer and the polymers only form a low density fluid-like field around the particle.

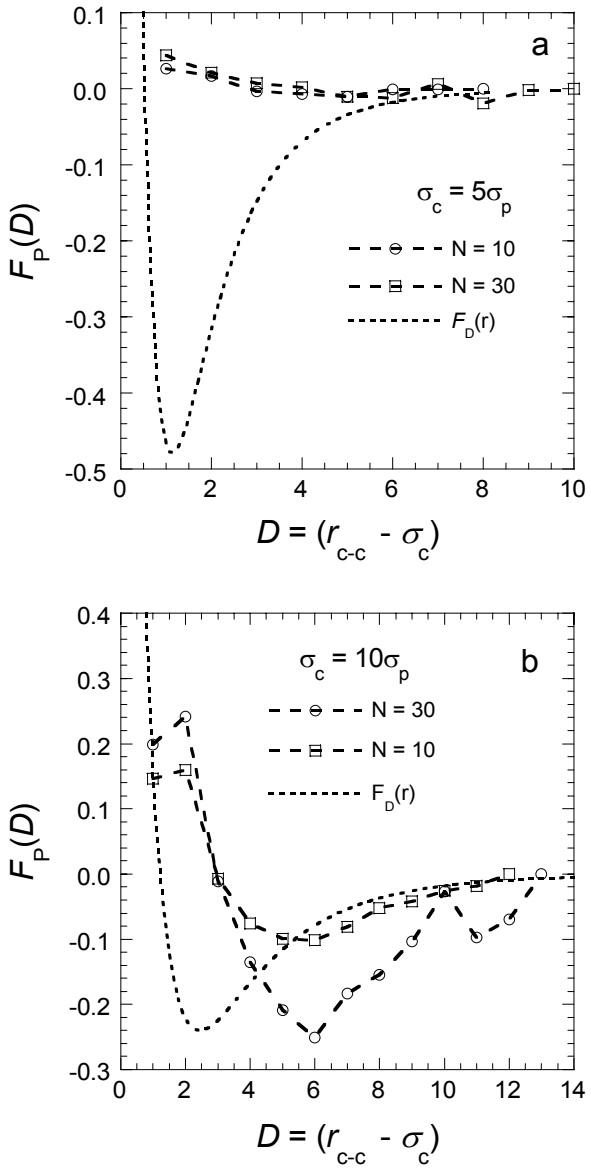

Figure 4.8: Force-distance plots (polymer mediated force $F_P(r)$ vs. D) for diameters of $\sigma_c = 5\sigma_p$ (8a) and $10\sigma_p$ (8b) at different chain lengths. $\varepsilon_{cp} = \varepsilon_{pp} = 1$. The direct force between the nanoparticles (F_D) calculated from eq 4.2 is also shown for comparison.

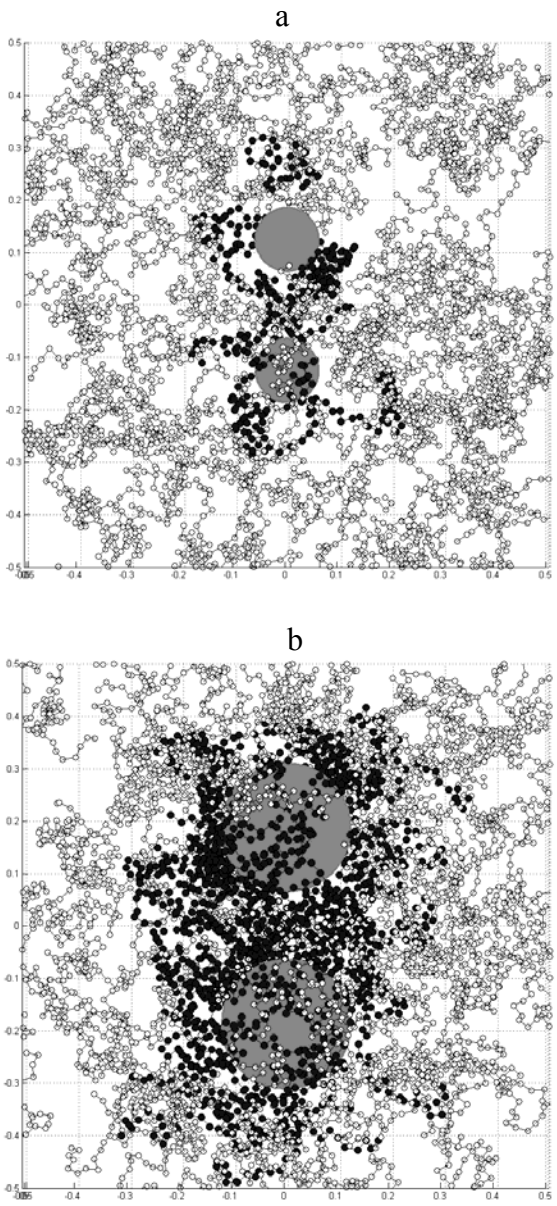

Figure 4.9: Equilibrated configuration snapshots of the nanoparticle-polymer simulation box for $\sigma_c = 5\sigma_p$, $N = 30$ (9a) and $\sigma_c = 10\sigma_p$, $N = 30$ (9b). The snapshots are for a surface-to-surface separation distance of $D = 5$ between the nanoparticles. The polymer chains adsorbed on the nanoparticle surface are shaded in dark and the bulk chains are in white.

The polymer-induced attraction between the nanoparticles may be attributed potentially to (i) bridging, (ii) depletion attraction (iii) interactions between the segments of adsorbed polymer chains or a combination of the above factors. (i) Bridging occurs when segments of an individual polymer chain adsorb on more than one particle surface. For a polymer chain to form a bridge between two particles, the attractive affinity of the polymer chain for the particle surface has to be strong enough to offset the loss in chain configurational entropy upon adsorption. Another condition for bridging is that there have to be vacant adsorption sites on the particle surfaces either due to incomplete coverage or exposed sites that appear during reversible adsorption-desorption. Bridging gives rise to an entropic tension in the polymer chain, and the polymers gain conformational entropy by decreasing the separation between the particle surfaces. This is the origin of bridging attraction between the particles. At $\sigma_c = 5\sigma_p$ for both chain lengths $N = 10$, 30 the adsorption and hence the surface coverage is low which allows for bridging by polymer chains. However, at this particle diameter, the particle polymer attractive energy is very weak and the contribution of bridging to the attraction is at most marginal. This was confirmed by monitoring snapshots of the equilibrated CP simulation box and counting the number of bridging chains. On an average, there was not more than one bridging chain at separations $D \leq 6$, for $\sigma_c = 5\sigma_p$ and $N = 30$. At $\sigma_c = 10\sigma_p$ and $N = 30$, the polymer adsorbs strongly forming a thick layer of adsorbed polymer with high surface coverage. In this situation, bridging would not be expected to occur. However, this inference would be true only under partial equilibrium conditions, wherein the nanoparticles would first be equilibrated at a large distance and then brought closer to each other with the added constraint of a static adsorbed polymer layer. However, since

our study is performed under *true* equilibrium conditions and the adsorption-desorption of polymer is a reversible process, the polymers move in and out of the interface region exposing potential adsorption sites. This leads to the possibility of bridging even under strongly adsorbing conditions. For $\sigma_c = 10\sigma_p$ and $N = 10$, the range over which the bridging attraction occurs decreases as compared to $N = 30$ and this is partially responsible for the minor shift in the force minimum to a closer separation distance (D). The contribution of bridging to the total attraction is expected to be higher for larger particle sizes and longer chains.

(ii) Depletion attraction is due an osmotic force exerted by the polymer on the nanoparticles due to the difference in polymer concentration in the bulk and the region in between the two nanoparticles. Although depletion attraction is associated primarily with non-adsorbing polymer solutions, it has been observed experimentally that short-ranged depletion attraction can occur between surfaces containing weakly adsorbed polymers.[34] The only difference being that the physisorbed layers constitute a new surface which experiences an osmotic depletion attraction with another polymer-coated surface. For $\sigma_c = 5\sigma_p$, the adsorption is weak suggesting that depletion attraction could be acting between the particles contributing to the overall attraction. In addition, the onset of attraction occurs approximately at $D = 2R_g$ for both polymer chain lengths which is consistent with the theoretically expected range of $2R_g$.[35-37] At $\sigma_c = 10\sigma_p$, the adsorption is strong and the polymer segment density between the particle surfaces is higher than on the outside. This almost precludes the possibility of any depletion attraction. Hence, it is unlikely that the depletion effect would contribute significantly to the overall attraction in this case ($\sigma_c = 10\sigma_p$, $N = 10, 30$).

(iii) Attraction that is driven by polymer segment-segment interactions is usually associated with the poor solvent condition wherein polymer segments prefer contact with one another over contact with solvent, resulting in enhanced polymer adsorption on the particle surface. In our case, although the polymers are in the good solvent condition at $T^* = 3.0$, the adsorption is driven by the particle-polymer adsorption energy which increases with σ_c and N. At $\sigma_c = 10\sigma_p$, as the separation distance between the particles is decreased, the polymers already adsorbed to each individual particle experience strong attractive interactions from *both* of the particles. The favorable energetic interactions experienced by the polymers apparently dominate the entropic loss, causing them to prefer this interparticle region. This, in turn results in a large number of favorable polymer segment-segment contacts which further add to the driving force for the polymers to reside in this region. Figure 4.10 shows the segment density profiles in the *z*-direction at different separation distances between the nanoparticles for $\sigma_c = 10\sigma_p$ and $N = 30$. The plots show that the polymer segment density in the central plane of the simulation box, corresponding to the region between the two nanoparticles, increases with decreasing separation distance (D), corroborating the arguments presented above. Hence, at $\sigma_c = 10\sigma_p$, it is likely that the polymer segment-segment interactions are primarily responsible for the attraction in the force profile. However, for $\sigma_c = 5\sigma_p$ the lack of a dense adsorbed layer indicates that segment-segment interactions do not play a significant role in the polymer-induced forces.

Short-range repulsive forces

As the separation between the nanoparticles decreases to $D \leq 3$, the polymer-induced forces pass through zero and become repulsive in nature. At this separation, there is space

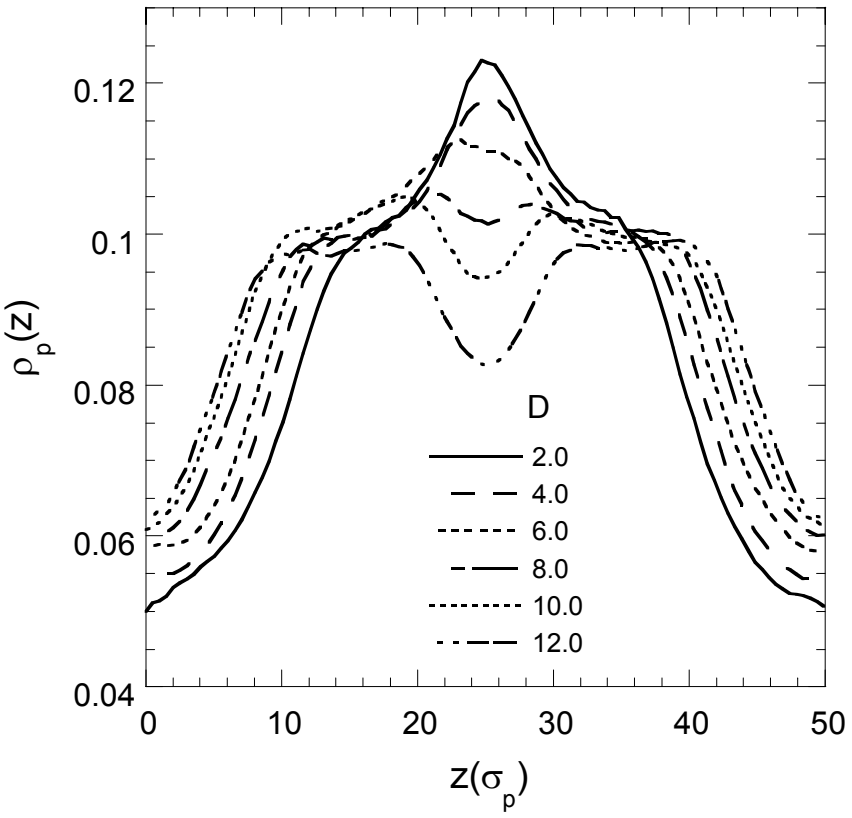

Figure 4.10: Polymer segment density profiles in the *z*-direction in the nanoparticle-polymer simulation box at different nanoparticle surface-to-surface separation (D). $\sigma_c = 10\sigma_p$, $N = 30$ and $\varepsilon_{cp} = \varepsilon_{pp} = 1$.

available only for one physisorbed monolayer on each particle in the region between the particle surfaces. As these monolayers come into contact, entropic steric effects dominate to result in a repulsive force between the particles. Again with increasing σ_c and N, the physisorbed monolayer would be attached more strongly to the surface resulting in stronger repulsive forces as indicated in the force profiles (Figure 4.8).

C. Effect of colloid-polymer interaction energy (ε_{cp})

To explore the hypothesis that segment-segment interactions between adsorbed polymer chains are the primary reason for polymer-induced attraction between spherical nanoparticles, we calculated the force-distance plots (shown in Figure 4.11) for different values of the colloid-polymer interaction strength ranging from $\varepsilon_{cp} = 1\varepsilon_{pp}$ to $\varepsilon_{cp} = 5\varepsilon_{pp}$. The particle diameter, polymer chains length and ε_{pp} were kept constant at $\sigma_c = 10\sigma_p$, $N = 30$ and $\varepsilon_{pp} = 1$, for this study. As ε_{cp} is increased from $1\varepsilon_{pp}$ to $5\varepsilon_{pp}$, the magnitude of the maximum attractive force increases almost linearly with ε_{cp}. However, the location of maximum attraction does not shift significantly and occurs at $D \approx 6$ for all the three cases. The adsorption and polymer segment density between the particles increase with ε_{cp} (see Figures 4.4 and 4.6), resulting in increased attraction due to segment-segment interactions. Although bridging contribution to the attraction is likely to increase with ε_{cp}, it would still be less compared to the segment-segment interactions. To verify this, we determined the average number of bridging chains (n_{bridge}) as a function of separation distance (D) at different values of ε_{cp} and found only a marginal increase in n_{bridge} as ε_{cp} is increased from $1\varepsilon_{pp}$ to $5\varepsilon_{pp}$. On the other hand, $\rho^*_{p,\,interface}$ increased from 0.08 to 0.15 as ε_{cp} is increased from $1\varepsilon_{pp}$ to $5\varepsilon_{pp}$. Also, depletion effect is expected to become

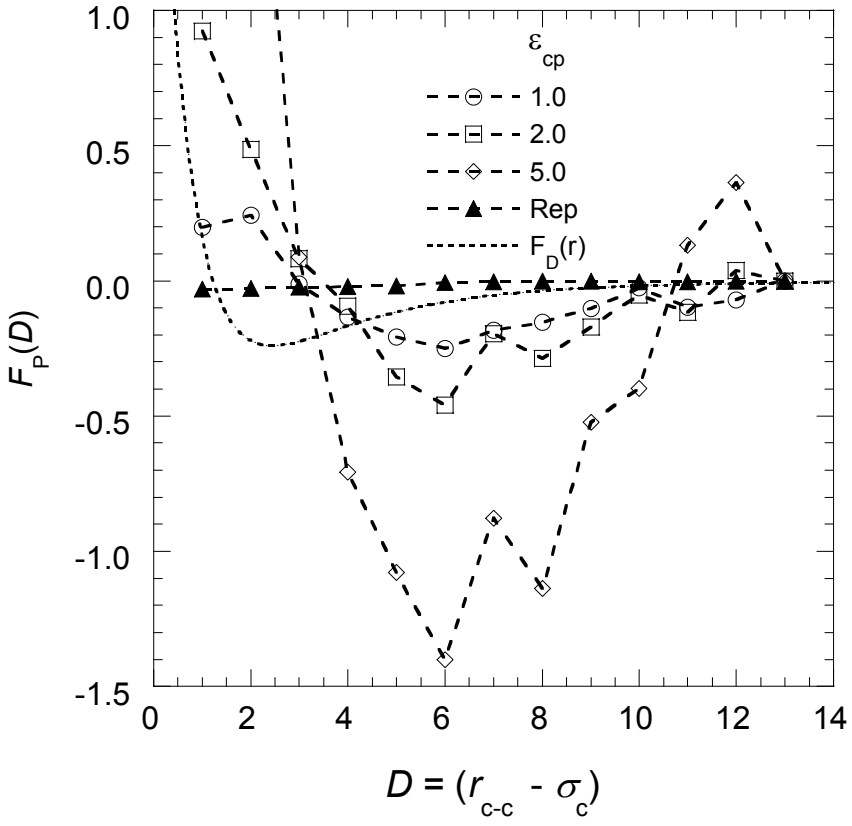

Figure 4.11: Force-distance plots (polymer mediated force $F_P(r)$ vs. D) for different values of the colloid-polymer interaction strength ranging from $\varepsilon_{cp} = 1\varepsilon_{pp}$ to $\varepsilon_{cp} = 5\varepsilon_{pp}$. ($\sigma_c = 10\sigma_p$, $N = 30$ and $\varepsilon_{pp} = 1$). The direct force between the nanoparticles (F_D) calculated from eq 4.2 is also shown for comparison.

progressively insignificant as ε_{cp} increases. It is also noteworthy that as the strength of the colloid-polymer interactions increases, there are relatively more oscillations in the force profiles (for e.g. see the force profile for $\varepsilon_{cp} = 5\varepsilon_{pp}$ between $D = 3$ and $D = 10$). As mentioned before, the increase in polymer segment density in the region between the particles with ε_{cp} results in liquid-like densities in this region and it is likely that the oscillations are due to packing effects. Previous simulations have shown that the solvation forces for LJ nanoparticles in a solvophilic liquid are oscillatory in nature due to packing and molecular structural effects.[22,23] Figure 4.11 also shows the F_P profile for the case of purely repulsive interaction between the nanoparticle and the polymers (non-adsorbing polymer). In this case, $F_P \approx 0$ for $D > 6$ and for $D < 6$, the force is purely attractive for all separations right until the particle surfaces come in contact with each other. These results are consistent with the phenomenon of depletion attraction which is expected to be the solely responsible for attraction in the case of non-adsorbing polymers. The onset of attraction which occurs at $D \approx 2R_g$ is also in agreement with theoretical predictions.[35-37] The magnitude of this attraction however, is very small compared to the adsorbing polymer case and this further supports the argument that depletion effect (though present) does not play a significant role in the attraction mechanism for adsorbing polymers.

D. Effect of polymer-polymer interaction energy (ε_{pp})

Figure 4.12 shows the force-distance profiles for $\varepsilon_{pp} = 0.5$, 1 and the case of soft-repulsive interactions between polymer segments ($\sigma_c = 10\sigma_p$, $N = 30$ and $\varepsilon_{cp} = 1$). As ε_{pp} is reduced from 1 to 0.5, the attractive minimum becomes less negative. Making the polymer-polymer interaction purely repulsive (only excluded volume interactions) has no

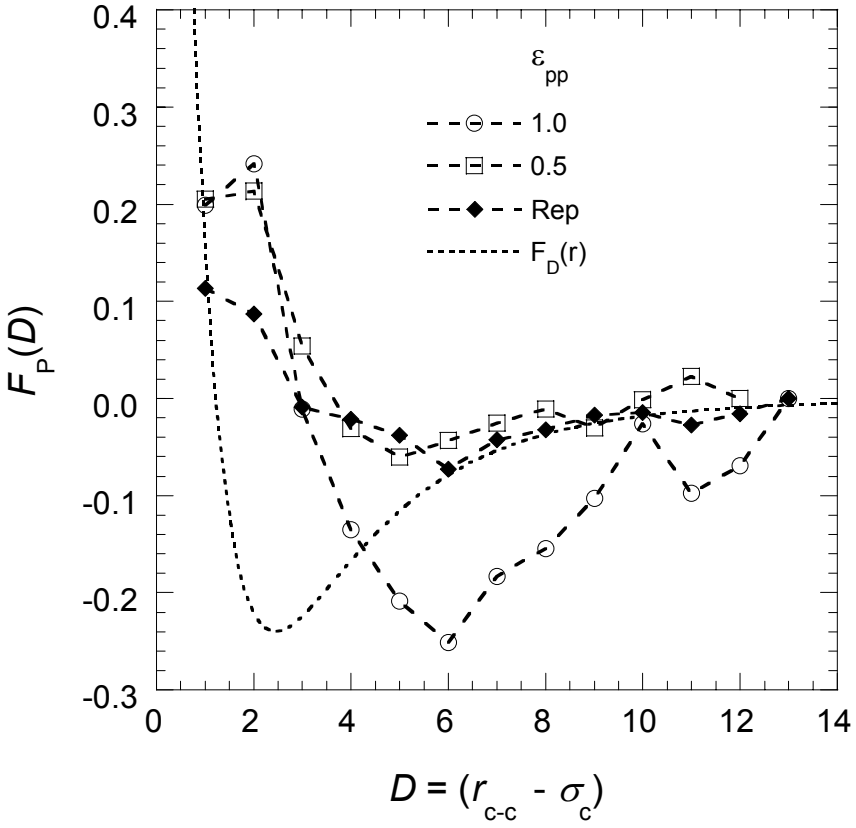

Figure 4.12: Force-distance profiles (polymer mediated force $F_P(r)$ vs. D) for $\varepsilon_{pp} = 0.5$, 1 and the case of soft-repulsive interactions between polymer segments ($\sigma_c = 10\sigma_p$, $N = 30$ and $\varepsilon_{cp} = 1$). The direct force between the nanoparticles (F_D) calculated from eq 4.2 is also shown for comparison.

significant effect on the force profiles. Reducing the value of ε_{pp}, while holding ε_{cp} constant enables us to progressively turn off the contribution of depletion and segment-segment attraction to the polymer-induced particle-particle attraction. The condition of soft-repulsive interactions between polymer segments and $\varepsilon_{cp} = 1$ (attraction between polymer and particle), though not realistic, allows us to isolate polymer-induced attraction due to bridging from other mechanisms. The attraction observed in this case is due solely to bridging and the magnitude of this attraction compared to the case of $\varepsilon_{cp} = 1$, $\varepsilon_{pp} = 1$ indicates that bridging contribution, though significant, is secondary to the effect of segment-segment interaction.

E. Comparison to force profiles in the flat-wall limit

As mentioned earlier in the introduction, most of the previous studies of interactions between layers of adsorbed polymer have been for the case flat walls or macroscopic colloids. It is interesting to make a comparison between the adsorption and force profiles in the flat wall limit to our simulation results for nanoscale colloids in the full equilibrium condition. For flat walls, it has been shown theoretically that there exists a monotonic attraction between two polymer coated surfaces over the entire interaction range.[15,16] The minimum in the free energy occurs when a monolayer of polymer chains in two-dimensional conformations lies flat between the two surfaces. In addition, the adsorbed amount of polymer between the walls passes through a weak maximum and decreases as separation distance decreases until all the chains are "squeezed" out into the bulk.[15] In the case of nanoparticles with strong polymer-particle attraction (for e.g. $\sigma_c = 10\sigma_p$, $N = 30$, $\varepsilon_{cp} = \varepsilon_{pp} = 1$, Figure 4.8b), we see that the polymer-induced force passes through a minimum at approximately $2R_g$ and then becomes repulsive at about $D \approx 3$.

Also, the excess adsorption of polymers Γ_s increases slightly as surface to surface separation D decreases. We propose that this difference is due to the influence of the curvature of the particle on the structure and entropy of the polymer layers. For the same surface to surface distance, flat walls allow significantly less available volume (and hence less conformational entropy) compared to curved surfaces. As a result, the polymers that are in the region between the nanoparticle surfaces lose comparatively less entropy as the surfaces are compressed, while gaining favorable attractive energetic interactions from the particles causing them to prefer this region (see Figure 4.10). This may explain the difference in the adsorption trends between the flat wall and nanoparticle cases. As far as the force profiles are concerned, the monotonic attraction observed in the case of flat walls has been attributed primarily to bridging and depletion. Our results from the investigation of the effect of ε_{cp} and ε_{pp} on the force profiles suggest that in addition to bridging, the polymer segment-segment attraction also contributes significantly to the polymer-induced attraction between the nanoparticles. Also, the repulsion between the nanoparticles observed at short distances is likely due to the steric effects between the strongly adsorbed polymer layers. It is interesting to note in passing that in the case of strong polymer-particle attraction, our simulated nanoparticle force profiles (in the full equilibrium condition) resemble qualitatively the nature of interaction profiles between flat walls with adsorbing polymers in the *restricted equilibrium* condition.[15]

4.4 CONCLUSIONS

In this chapter, we present the first reported simulation study of interaction forces between nanoscale colloidal particles in the presence of freely adsorbing homopolymer modifiers in the full thermodynamic equilibrium condition. Using the expanded grand canonical Monte Carlo simulation method, we have investigated the effect of polymer chain length, colloid diameter and colloid-polymer interaction energy on polymer adsorption and polymer-induced force profiles between two spherical nanoparticles. The results are markedly different from those observed in the macroscopic limit wherein the colloidal particles are represented as flat walls. In general, we found that at small particle diameters and short polymer chains lengths ($\sigma_c = 5\sigma_p$, $N = 10$), the polymers do not adsorb strongly and have no significant effect on the nanoparticle interactions. With increasing particle diameter and polymer chain length ($\sigma_c = 10\sigma_p$, $N = 30$), there is increased adsorption and the polymer-induced forces between the nanoparticles are comparable to the direct nanoparticle VDW forces. Specifically, the polymer-induced forces are repulsive at short separations ($D < 3\sigma_p$) and attractive at larger separations with the attractive minimum at $D \approx 6\sigma_p$. The attractive minimum in the force is lower for longer chains and increasing colloid-polymer interaction energy (ε_{cp}). The attractive forces are attributed primarily to polymer intersegmental interactions and bridging.

These results provide the rationale why adsorbing homopolymers are not a good stabilizer for nanoparticle dispersions. However, it must be noted that in our simulations the bare nanoparticles are fixed initially at a specified distance and polymers are added to the system and allowed to equilibrate after which the force is calculated. While these force-profiles are representative of the true thermodynamic equilibrium condition, the

thermodynamic minimum in free energy (corresponding to polymer-induced nanoparticle flocculation) may not necessarily be achieved in "real-world" experiments. To illustrate this point consider a dilute nanoparticle dispersion in which the added homopolymer modifier adsorbs strongly before the nanoparticles come into contact with each other. If two particles coated with adsorbed polymer collide at Brownian velocities in solution, in addition to the kinetic thermal energy barrier, it is expected that there would be an initial repulsion between the adsorbed polymer layers which may prevent flocculation. In order to verify this, it would be interesting to simulate these nanoparticle-polymer systems in the restricted equilibrium limit using the canonical NVT ensemble. It is also noteworthy that the adsorbing homopolymers shift the minimum in force profile to larger a separation distance between the nanoparticles as compared to the minimum in the bare particle-particle VDW dispersion force (which occurs at $2^{1/6}\sigma_c$ for the LJ potential). The location of the attractive minimum and the thermodynamic minimum (corresponding to $F_P = 0$) could be controlled by varying the polymer chain length and the magnitude of the attractive minimum can be controlled by the colloid-polymer interaction energy parameter. While it is known that self-assembled superstructures of nanoparticles can be prepared as equilibrium products, the ability to control the thermodynamic and force minimum using the above parameters provides a molecular mechanism for nanoparticle self-assembly with controlled lattice spacing which could be potentially useful for photonic and optoelectronic devices.

4.5 REFERENCES

(1) Liu, Y.; Cheng, S. Z. D.; Xing, W.; Jun, H. *Langmuir* **2002**, *18*, 10500-10502.

(2) Jordan, R.; Ulman, A.; Kang, J. F.; Rafailovich, M. H.; Sokolov, J. *J. Am. Chem. Soc.* **1999**, *121*, 1016-1022.

(3) Beecroft, L. L.; Ober, C. K. *Chem. Mater.* **1997**, *9*, 1302-1317.

(4) Corbierre, M. K.; Cameron, N. S.; Sutton, M.; Mochrie, S. G. J.; Lurio, L. B.; Ruehm, A.; Lennox, R. B. *J. Am. Chem. Soc.* **2001**, *123*, 10411-10412.

(5) Fan, X.; Xia, C.; Fulghum, T.; Park, M.-K.; Locklin, J.; Advincula, R. C. *Langmuir* **2003**, *19*, 916-923.

(6) Hashimoto, T.; Harada, M.; Sakamoto, N. *Macromolecules* **1999**, *32*, 6867-6870.

(7) Hicks, J. F.; Young, S.-S.; Murray, R. W. *Langmuir* **2002**, *18*, 2288-2294.

(8) Fox, M. A. *Acc. Chem. Res.* **1999**, *32*, 201-207.

(9) Whitesell, J. K.; Chang, H. K.; Fox, M. A.; Galoppini, E.; Watkins, D. M.; Fox, H.; Hong, B. *Pure Appl. Chem.* **1996**, *68*, 1469-1474.

(10) Lu, Y.; Tang, Y.; Sellinger, A.; Lu, M.; Huang, J.; Fan, H.; Haddad, R.; Lopez, G.; Burns, A.; Sasaki, D. Y.; Shelnutt, J.; Brinker, C. J. *Nature* **2001**, *410*.

(11) Sellinger, A.; Weiss, P. M.; Nguyen, A.; Lu, Y.; Assink, R. A.; Gong, W.; Brinker, C. J. *Nature* **1998**, *394*, 256-260.

(12) Israelachvili, J. N. *Intermolecular & Surface Forces*, 2nd ed.; Academic Press: San Diego, 1991.

(13) Patel, S. S.; Tirrell, M. *Annu. Rev. Phys. Chem.* **1989**, *40*, 597-635.

(14) Scheutjens, J. M. H. M.; Fleer, G. J. *J. Phys. Chem.* **1979**, *83*, 1619-1635.

(15) Scheutjens, J. M. H. M.; Fleer, G. J. *Macromolecules* **1985**, *18*, 1882-1900.

(16) de Gennes, P.-G. *Macromolecules* **1981**, *14*, 1637-1644.

(17) de Gennes, P.-G. *Macromolecules* **1982**, *15*, 492-500.

(18) Klein, J.; Pincus, P. *Macromolecules* **1982**, *15*, 1129-1135.

(19) Ingersent, K.; Klein, J.; Pincus, P. *Macromolecules* **1986**, *19*, 1374-1381.

(20) Dijkstra, M. *Thin Solid Films* **1998**, *330*, 14-20.

(21) Yethiraj, A.; Hall, C. K. *Macromolecules* **1990**, *23*, 1865-1872.

(22) Shinto, H.; Miyahara, M.; Higashitani, K. *J. Colloid Interface Sci.* **1999**, *209*, 79-85.

(23) Qin, Y.; Fichthorn, K. A. *J. Chem. Phys.* **2003**, *119*, 9745-9754.

(24) Luna-Bárcenas, G.; Meredith, J. C.; Gromov, D. G.; Sanchez, I. C.; de Pablo, J. J.; Johnston, K. P. *J. Chem. Phys.* **1997**, *107*, 1-11.

(25) Escobedo, F.; de Pablo, J. J. *J. Chem. Phys.* **1996**, *105*, 4391-4394.

(26) Escobedo, F.; de Pablo, J. J. *J. Chem. Phys.* **1995**, *103*, 2703-2710.

(27) Meredith, J. C.; Johnston, K. P. *Langmuir* **1999**, *15*, 8037-8044.

(28) de Pablo, J. J.; Laso, M.; Suter, U. W.; Cochran, H. D. *Fluid Phase Equilib.* **1993**, *83*, 323-331.

(29) Mooij, G. C. A. M.; Frenkel, D. *Mol. Phys.* **1991**, *74*, 41-47.

(30) Siepmann, J. I. *Mol. Phys.* **1990**, *70*, 1145-1158.

(31) Allen, M. P.; Tildesley, D. J. *Computer Simulation of Liquids*; Clarendon Press: Oxford, 1987.

(32) Henderson, D.; Duh, D.-M.; Chu, X.; Wasan, D. *J. Colloid Interface Sci.* **1997**, *185*, 265-268.

(33) Marla, K. T.; Meredith, J. C. *Langmuir* **2004**, *20*, 1501-1510.

(34) Ruths, M.; Yoshizawa, H.; Fetters, L. J.; Israelachvili, J. N. *Macromolecules* **1996**, *29*, 7193-7203.

(35) Asakura, S.; Oosawa, F. *J. Chem. Phys.* **1954**, *22*, 1255-1256.

(36) Asakura, S.; Oosawa, F. *J. Polym. Sci.* **1958**, *33*, 183.

(37) Vrij, A. *Pure Appl. Chem.* **1976**, *48*, 471-483.

CHAPTER 5

SIMULATION OF INTERACTION FORCES BETWEEN NANOPARTICLES IN POLYMER SOLUTION. II. END-GRAFTED POLYMER MODIFIERS

The interaction forces between nanoscale colloidal particles coated with end-grafted Lennard-Jones homopolymers are calculated using off-lattice Monte Carlo simulations in the NVT ensemble. The effect of chain length (N), nanoparticle diameter (σ_c), grafting density (ρ_a), and colloid-polymer and polymer-polymer interaction energy (ε_{cp} and ε_{pp}) on the polymer-induced forces between the nanoparticles are investigated. The inclusion of attractive dispersion interactions between the colloid and polymeric modifiers result in either long-ranged attraction and short-ranged repulsion, or pure repulsion, depending on the molecular parameters (ρ_a, N, ε_{cp}, ε_{pp}). The polymer-induced attraction could be attributed to bridging and intersegmental interactions. There is a threshold value of ρ_a and N up to which the polymer-induced attraction between the nanoparticles increases. Beyond this threshold, chain entropy and excluded volume effects begin to dominate with increasing ρ_a and N, leading eventually to polymer-induced repulsion, and consequently nanoparticle stabilization.

5.1. INTRODUCTION

Polymers grafted irreversibly to the surface of nanoscale colloidal particles are used widely to either stabilize nanoparticle dispersions or to direct their self-assembly. The structure and physical properties of end-grafted polymers and the interactions between polymer-grafted surfaces have been studied extensively in recent years. The conformations of end-grafted polymers depend on the grafting density and interactions between the segments, surface and solvent. For a non-adsorbing surface at low grafting density, a mushroom structure is observed where the polymer radius of gyration is similar to its bulk dimensions. With increasing grafting density, the polymer chains stretch anisotropically from the surface to avoid a loss in configurational entropy, resulting in a brush-like conformation. When two such polymer brushes approach each other, unfavorable steric overlaps between the polymer segments give rise to an entropic repulsion, which is primarily responsible for the stabilization of colloidal particles. Alternately, attractive interactions between the surface and the tethered polymers results in a different and rather more complex situation. At low grafting densities, the polymers adopt a flat pancake-like conformation to maximize the favorable surface-segment contacts. As the grafting density is increased, the polymer chains form brushes similar to the case of non-adsorbing surfaces. However, the pancake-to-brush transition occurs at a relatively higher grafting density compared to the mushroom-to-brush transition (non-adsorbing surfaces). In addition, attractive interactions between the grafted polymer and the surface can potentially result in bridging attraction between the polymer coated surfaces. This ability of grafted modifiers to either act as stabilizers or facilitate attraction, makes them ideally suited for controlling phase transitions and interaction

forces in nanoscale colloidal systems. Stable dispersions of nanoparticles coated with polymeric modifiers have important applications in areas such as photonics and electronics, chemical and biological sensing, and energy storage. In addition, organically modified nanoparticles also serve as functionalized building blocks for programmed assembly into supramolecular entities.

Most of the theoretical and simulation studies directed towards studying the structure and interactions of end-grafted polymers have focused on long polymer chains grafted onto planar non-adsorbing surfaces. Theoretical approaches for studying these systems include scaling analysis,[1,2] which predict properties like brush height and monomer concentration profiles in good solvent conditions, and self-consistent field (SCF) theories,[3-8] which provide a more detailed description of end-grafted chains and have been used to calculate the free energy of interaction between two flat brushes. These theoretical predictions are in good agreement with the results of Monte-Carlo[9,10] and molecular dynamics simulations.[11,12] Experimental studies of planar polymer brushes using surface force apparatus (SFA),[13-15] neutron reflectivity[16, 17] and small-angle neutron scattering[18,19] have reported parabolic density profiles consistent with theoretical predictions. Both SCF and scaling methods that were developed originally to model chains grafted to a flat interface have also been extended to curved surfaces. The primary effect of curved surfaces is that the volume available to the grafted chains increases with distance from the surface as compared to flat surfaces where the volume available is constant. Chains end-grafted to curved surfaces have been studied mostly in either the star-polymer limit where the polymers are very long compared to the particle diameter or the Derjaguin limit where the range of the interaction is small compared to the particle

radius (small curvature effects). Scaling theory applied to star polymers has shown that the density profile away from the center of the polymer follows a power-law decay as compared to the density profile of a planar polymer layer which is parabolic in shape.[20] This curvature effect which results in differing density profiles eventually leads to changes in the resulting interactions between the polymer brushes as well. Witten and Pincus (WP) used scaling arguments to calculate the interactions between star polymers and proposed a logarithmic form of the interaction potential.[21] More recently, Lin and Gast [22] used a one-dimensional SCF lattice with a modified Derjaguin approximation to investigate the structure and interactions between polymer layers tethered to a spherical interface and obtained interaction profiles different from the WP results in the star-polymer limit.

However, for the case of nanoscale colloidal particles, in addition to curvature effects which become increasingly important, the tethered polymers used for modification purposes are of relatively low molecular weight (short chain) and of the same size range as the particle radius. This regime, intermediate to the star-polymer and the Derjaguin limits, has been relatively unexplored. Wijmans, Leermakers and Fleer (WLF)[23] first used the lattice SCF formalism in two dimensions to calculate the interaction between two polymer coated particles whose radii of curvature are of the same order of magnitude as the polymer layer thickness and found the repulsive interactions to be far less than predicted by Derjaguin approximation. However, SCF studies of polymer coated nanoparticles in a good solvent by Roan[24] show that contrary to predictions from previous studies, the interaction is attractive when the segment "clouds" of the two spheres have just begin to overlap and it can even become purely attractive at

low grafting densities. The reason for these contrasting results is not apparent considering that the studies were performed for similar particle sizes and polymer chains lengths. There has also been a recent simulation study which uses Monte Carlo methods to calculate the pair interaction between two spherical brushes in this intermediate regime.[25] The simulations predict a lower repulsive force at short distances compared to the WLF results. This is because the SCF model does not account for monomer correlations, resulting in a higher monomer concentration at short distances compared to the simulations. The interaction forces obtained from the simulations were modeled by a combination of the WP approach[21] and the Flory theory for dilute polymer solutions.[26] These varied results reflect the need for further theoretical and simulation studies towards understanding the interaction forces and consequently the phase behavior of organically-modified nanoparticles.

In addition, the above studies consider only a repulsive hard-sphere type potential to represent the particle-polymer and polymer-polymer interactions. While knowledge gained from these studies is useful at near athermal or pseudo-hardsphere conditions in which the van der Waals (VDW) dispersion interactions have been masked out due to the effect of "good solvent" or temperature, many nanoparticle self-assembly and consolidation processes involve attractive interactions. These ubiquitous van der Waals dispersion interactions, between the particle and polymer segments and also between the segments themselves, complicate the theoretical and computational treatment. There have been very limited theoretical[27] and simulation studies[28] of polymer-grafted particles that have included attractive monomer-surface interactions even in the simplified planar wall limit. Experimental evidence of attractive interactions between polymer-coated surfaces

is generally associated only with freely adsorbing polymer modifiers.[29] Most of the experimental measurements of force profiles between end-grafted polymers on a flat solid surface report a monotonically increasing repulsive force.[13, 30-34] However, in a recent study, Goodman and co-workers investigated the effect of grafting density and monomer type on the force exerted by spherical polymer brushes in a good solvent on an atomic force microscope (AFM) tip and detected bridging attraction even at high grafting densities in the case of one of the polymers.[35]

In order to design end-grafted polymeric modifiers for stable dispersions or self-assembled structures, we need to model the effect of molecular parameters (polymer chain length, nanoparticle diameter and polymer-particle interaction energy) on the resulting interaction forces. This is critical to the development of rational design criteria for these modifiers leading to the predictive control of nanoparticle phase behavior. In part 1 of this series we examined homopolymer adsorption on and the associated polymer-induced forces between nanoscale colloidal particles. In this chapter we consider the effect of end-grafted polymeric modifiers on the interaction forces between the nanoparticles. Using Monte Carlo simulations, we study the effect of nanoparticle diameter (σ_c), polymer chain length (N), grafting density (ρ_a), and colloid-polymer and polymer-polymer interaction energy (ε_{cp} and ε_{pp}) on the polymer-induced force profiles between the nanoparticles. We identify the physical mechanisms that lead to attraction or repulsion in the force profiles based on the interplay between the various molecular parameters described above. In addition, we also calculate the conformational properties of the grafted polymer chains and relate them to the observed force profiles.

5.2. SIMULATION METHOD

5.2.1 Parameters and Model

We have simulated the interaction between two spherical nanoparticles grafted with Lennard-Jones polymer chains by using three-dimensional off-lattice Monte Carlo simulations in the canonical (NVT) ensemble. Figure 5.1 contains a schematic of the simulation box with two nanoscale colloidal particles that are fixed along the z-axis. Each of the nanoparticles has n_c chains of length N that are grafted at random positions on the nanoparticle surface. In most cases N = 10-30, while a few results are also presented for longer chains of N = 50. To study the effect of grafting density, the number of grafting chains is varied from n_c = 6 to n_c = 55 which correspond to grafting densities ranging from 0.02 to 0.18. The grafting density (ρ_a) is given by $\rho_a = n_c/\pi\sigma_c^2$. Grafting density is reduced generally with respect to the bulk radius of gyration, R_g, with $\rho_a^* = \rho_a \pi R_g^2$. A mushroom or pancake (depending on the polymer-particle interactions) to brush transition occurs generally at a reduced grafting density $\rho_a^* \approx 1$, where chains grafted to a single surface begin to overlap laterally. The grafting densities studied in this work correspond to ρ_a^* values of $0.5 \le \rho_a^* \le 5$, depending on chain length and nanoparticle diameter. Experimental values of ρ_a^* commonly range between 1 and 20.[36]

The polymers are modeled as fully flexible chains with a bond length of σ_p. The polymer segments interact via the Lennard-Jones potential, cut and shifted at $r_c = 2.5\sigma_p$, given in equation 5.1,

$$U(r_{ij}) = \begin{cases} 4\varepsilon_{ij}\left[\left(\frac{\sigma_{ij}}{r_{ij}}\right)^{12} - \left(\frac{\sigma_{ij}}{r_{ij}}\right)^{6} - \left(\frac{\sigma_{ij}}{r_c}\right)^{12} + \left(\frac{\sigma_{ij}}{r_c}\right)^{6}\right] & r \le r_c, \\ 0 & r > r_c \end{cases} \qquad (5.1)$$

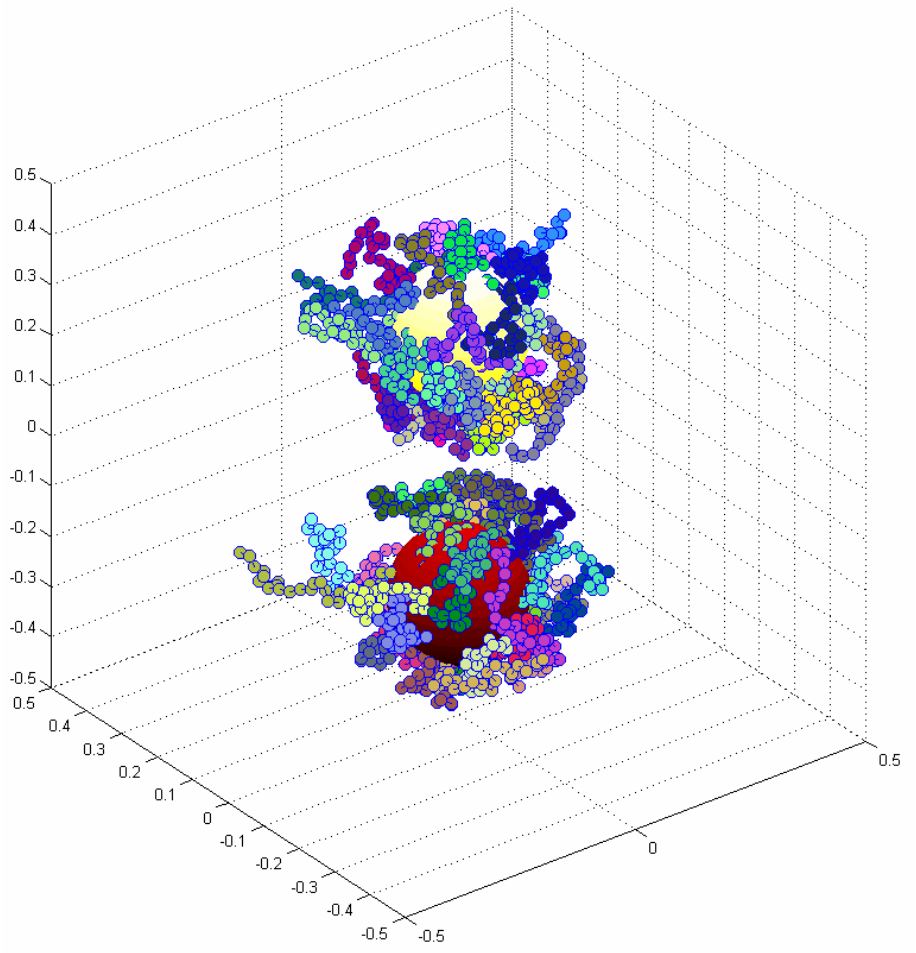

Figure 5.1: Configuration snapshot of the simulation box showing two colloidal nanoparticles with end-grafted polymeric modifiers. ($\sigma_c = 10\sigma_p$, $N = 30$, $\rho_a^* = 3.0$, $T^* = 3.0$)

where $\sigma_{ij} = (\sigma_i + \sigma_j)/2$ is the size parameter and ε_{ij} is the LJ interaction energy parameter. The colloid-colloid and the colloid-polymer interactions are modeled using the full LJ potential without cutoff. However, the interaction between the colloid and the polymer segment that is grafted permanently to the colloid surface is not considered. The temperature was reduced with the LJ parameters in the usual manner, $T^* = Tk_B/\varepsilon_{pp}$, where ε_{pp} is the polymer segment-segment interaction parameter and k_B is the Boltzmann constant. All the simulations were performed at $T^* = 3.0$ (good solvent condition) and $\varepsilon_{pp} = 1$, unless specified otherwise. The polymer-coated nanoparticle interaction forces were calculated for two different particle diameters, $\sigma_c = 10\sigma_p$ and $5\sigma_p$. The effect of the colloid-polymer interaction strength (ε_{cp}) on the force profiles was studied by varying ε_{cp} from $\varepsilon_{cp} = 2\varepsilon_{pp}$ to a purely soft-repulsive interaction between the colloid and polymer segments. The dimensions of the simulation box are $50\sigma_p$ in the x and y directions and $60\sigma_p$ in the z direction, large enough to prevent artificial interactions between periodic images.

5.2.2 Computational details

The simulation was initialized by fixing the two nanoparticles at a specified distance from each other along the z-axis. Grafting sites were then chosen at random on each surface and the first monomer of each polymer chain was fixed permanently at those sites. The remaining N-1 segments of each chain were then grown in a stretched out conformation avoiding overlaps with neighboring chains. The initially stretched conformation facilitates faster equilibrium and helps avoid "locked" configurations. Equilibration of the grafted chains is achieved by two methods for generating chain

conformations. Chain segments 2 through $N/2$ were moved by using the "crankshaft" method, which performs a random rotation about the axis passing through the center of the neighboring segments. The remaining part of the chain farthest from the particle surface, $N/2 + 1$ to N, was moved using the continuum configurational bias (CCB) algorithm. The CCB method consists of cutting a chain at a randomly selected site and regrowing it site by site until the original chain length is restored. The regrowth process involves scouting various trial positions on a spherical surface centered at the previous existing site, favoring non-overlapping low energy configurations at each stage. Details on the computer implementation of the CCB method and its applicability and limitations have been outlined in the literature.[37, 38] After equilibrium is achieved, the forces on each particle ($F_{AP}(r)$ and $F_{BP}(r)$) due to the polymer chains were calculated. Such individual simulations were performed from the nearest centre-to-centre separation ($r_{c\text{-}c}$) between the nanoparticles of $r_{c\text{-}c} = \sigma_c + 2\sigma_p$ in increments of $1\sigma_p$ up until approximately $r_{c\text{-}c} = 2.5\ \sigma_c$. The method and equations used for the force calculation are the same as described in part I of this series. The force profiles reported in this work are normalized by subtracting the force at "infinite" separation, where the nanoparticle surfaces are far enough not to affect one another significantly.

Equilibration required (20-40) x 10^6 Monte Carlo steps (where each step corresponds to one attempted move) depending on the grafting density and chain length. Equilibrium was defined by fluctuations of less than 2% for the energy. Average forces, chain conformational properties and the segment density profiles were collected over (100-160) x 10^6 attempted moves at each separation distance. The statistical error for the conformational properties of the chains was taken as the root-mean square fluctuation

Table 5.1: Simulation conditions explored in this study. ρ_a (= $n_c/\pi\sigma_c^2$) is the grafting density and ρ_a^* (= $\rho_a\pi R_g^2$) is the reduced grafting density. n_c is the number of chains grafted on each colloidal particle. R_g, and R_{EED} are the radius of gyration and end-to-end distance of the end-grafted polymer chains.

Case number	σ_c	N	ε_{cp}	ε_{pp}	$\rho_a^* = \rho_a\pi R_g^2$	$\rho_a = n_c/\pi\sigma_c^2$	n_c	R_g^2	R_{EED}^2
1	10	30	1.0	1.0	0.5	0.02	6	8.05	45.23
2					1.0	0.04	11	8.15	47.33
3					2.0	0.07	22	8.16	48.16
4					3.0	0.11	33	8.33	50.63
5					5.0	0.18	55	8.86	57.90
6	10	30	2.0	1.0	5.0	0.18	55	8.16	48.91
7			Rep[a]	1.0	5.0	0.18	55	9.95	72.11
8			1.0	Rep	5.0	0.18	55	15.82	127.71
9			Rep	Rep	5.0	0.18	55	16.44	137.02
10	10	10	1.0	1.0	0.8	0.11	33	2.42	15.12
11	10	50	1.0	1.0	5.0	0.11	33	14.74	86.19
12	5	10	1.0	1.0	0.8	0.11	8	2.42	14.94
13	5	30	1.0	1.0	3.0	0.11	8	8.54	51.55

[a] "Rep" indicates a purely repulsive interaction obtained by using only the repulsive term in the Lennard-Jones 6-12 potential.

divided by the square root of the number of independent blocks while the statistical error in the forces was based on the statistical inefficiency parameter [39]. Error bars have been omitted from the figures except if they were larger than the symbols representing the data points. Table 5.1 gives the details of all the cases that were investigated in this study.

5.3. RESULTS & DISCUSSION

5.3.1 Effect of grafting density (ρ_a^*)

Figure 5.2 shows the effect of reduced grafting density (ρ_a^*) on the polymer-induced forces (F_P) between the nanoparticles at $\sigma_c = 10\sigma_p$, $N = 30$, $\varepsilon_{cp} = \varepsilon_{pp} = 1$. The direct van der Waals dispersion force between the nanoparticles obtained by

$$F_D(r) = -\frac{\partial U_{cc}(r)}{\partial r} = \frac{48}{r}\left(\left(\frac{\sigma_c}{r}\right)^{12} - 0.5\left(\frac{\sigma_c}{r}\right)^{6}\right), \qquad (5.2)$$

is also shown for comparison. In all force profiles reported in this chapter the x-coordinate is taken to be $D = (r_{c\text{-}c} - \sigma_c)$, which is the nearest surface-to-surface distance between the nanoparticles. For all grafting densities, the force-distance plots show long-ranged attraction and short-ranged repulsion, similar in form and comparable in magnitude to the direct nanoparticle force. The attractive minimum grows deeper and shifts to larger separations with increasing grafting densities up to $\rho_a^* = 3.0$, beyond which the minimum shifts back upward (for $\rho_a^* = 5.0$). The nature and magnitude of the polymer-induced forces between the nanoparticles are a consequence of the competition between attraction due to bridging and intersegmental interactions, and repulsion due to steric interactions between the grafted chains. Bridging occurs due to attractive segment-surface interactions and the presence of exposed adsorption sites on the nanoparticle

surface. At $\rho_a^* = 0.5$, the polymer is in a pancake-like conformation wherein the average distance between the grafting sites is more than the R_g of the polymer chains and the grafted polymers tend to lie flat on the particle surface due to favorable particle-polymer contacts. Although the surface coverage is low (which is favorable for bridging), the small number of grafted chains results in a very low density of bridges formed. In addition, the flattened conformations of the grafted polymers also constrain the amount of bridging that can occur. As ρ_a^* is increased beyond $\rho_a^* = 1.0$, the polymer chains undergo a gradual transition to the brush regime, wherein the excluded volume considerations cause the polymer chains to extend outwards from the surface. It is noteworthy that the pancake (or mushroom) to brush transition for short chains (low molecular weight polymers) is not a very sharp transition and occurs over a broad range of grafting densities.[40] With increasing ρ^*_a, there are more chains available that can form bridges between the two particles. However, there is a progressive decrease in the availability of binding sites on the surface and also an increase in the monomer density in the interparticle region. These competing effects suggest that there is a threshold value of grafting density beyond which the number of bridging chains would be limited by entropic effects. Figure 5.3 shows the average number of bridging chains (n_{bridge}) versus separation distance (D) at different grafting densities. The plots indicate that there is a maximum in n_{bridge} at a grafting density of $\rho_a^* = 3.0$ and a further increase in the grafting density results in a slight decrease in n_{bridge}. The grafting density at which the polymer-induced attraction between the nanoparticles is strongest coincides with the maximum in n_{bridge} (at $\rho_a^* = 3.0$) suggesting that bridging is responsible primarily for the attraction in the force-profiles. Also, at a constant grafting density the number of bridging chains

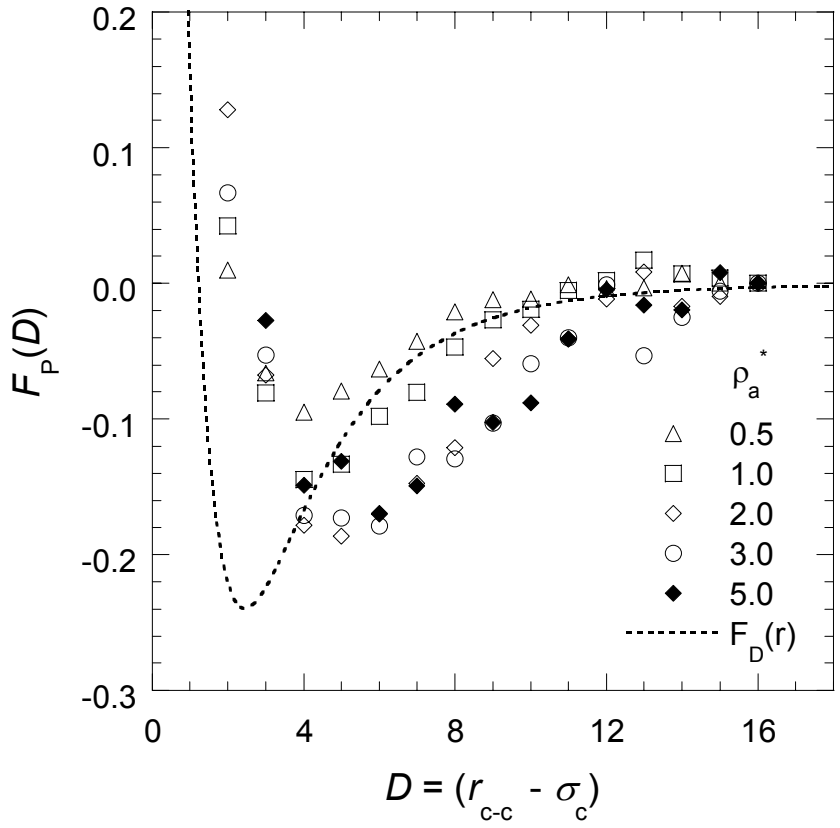

Figure 5.2: Force-distance plots (polymer mediated force $F_P(r)$ vs. D) at different grafting densities ranging from $\rho_a^* = 0.5$ to $\rho_a^* = 5.0$. $\sigma_c = 10\sigma_p$, $N = 30$, $\varepsilon_{cp} = \varepsilon_{pp} = 1$. The direct force between the bare nanoparticles (F_D) calculated from equation 5.2 is also shown for comparison.

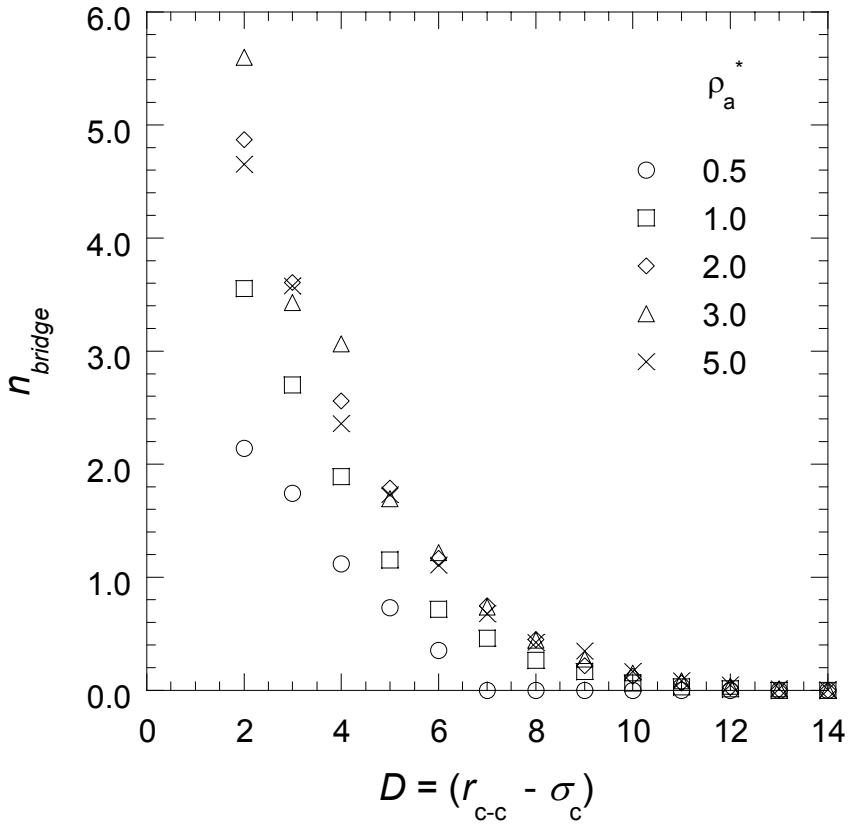

Figure 5.3: The number of bridging chains versus surface to surface separation distance ($D = r_{c\text{-}c} - \sigma_c$) at different grafting densities ranging from $\rho_a^* = 0.5$ to $\rho_a^* = 5.0$. $\sigma_c = 10\sigma_p$, $N = 30$, $\varepsilon_{cp} = \varepsilon_{pp} = 1$.

increases with decreasing interparticle separation suggesting a monotonic attraction in the force profiles. However, at close separations, steric effects dominate the bridging attraction resulting in polymer-induced repulsion between the nanoparticles. While the intersegmental interactions between the grafted polymer chains also contribute to the polymer-induced attraction, it is difficult to quantify exactly the relative contributions of bridging and segmental interactions to the overall attraction. The effect of polymer segment-segment interactions on the polymer-induced forces is explored in greater detail later in this section. The decrease in the magnitude of the attractive minimum as ρ_a^* is increased from $\rho_a^* = 3.0$ to $\rho_a^* = 5.0$ suggests that further increasing the grafting density would eventually result in the repulsive entropic effects dominating the attraction due to both bridging and intersegmental attractions leading to monotonic repulsion in the force-profiles. The separation distance between the nanoparticles at which F_P changes sign (i.e., $F_P = 0$), and the location of the attractive minimum are related closely to the conformations of the end-grafted polymers. The mean squared end-to-end distance (R_{EED}^2) and the radius of gyration squared (R_g^2) of the polymer chains at different grafting densities are shown in Table 5.1. The reported values of R_{EED}^2 and R_g^2 are obtained by averaging over all nanoparticle separation distances at each grafting density. The bulk values of R_{EED}^2 and R_g^2 (for $N = 30$) are 53.2 and 8.96 respectively. For grafting densities upto $\rho_a^* = 3.0$ (at $\varepsilon_{cp} = \varepsilon_{pp} = 1$), the R_{EED}^2 and R_g^2 are less than the bulk values due to the attractive interactions between the nanoparticle and the grafted chains, which cause the polymers to adopt more compact conformations near the particle. However at $\rho_a^* = 5.0$, the R_{EED}^2 is more than the bulk value further validating the argument that the excluded volume effects begin to dominate at this grafting density. The monotonic

increase in R_{EED}^2 and R_g^2 with increasing ρ_a^* is responsible for the shift in the location of the attractive minimum and the thermodynamic minimum (location at which $F_P = 0$) to larger separation distances.

5.3.2 Effect of particle diameter (σ_c) and chain length (N)

Figure 5.4 shows a plot of force due to the grafted chains (F_P) between two nanoparticles for diameters of $\sigma_c = 10\sigma_p$ (Figure 5.4a) and $5\sigma_p$ (Figure 5.4b) at different chain lengths and $\varepsilon_{cp} = \varepsilon_{pp} = 1$. The effect of chain length was studied by keeping the number of grafted chains per particle constant at all chain lengths. This implies that although the grafting density ρ_a (= $n_c/\pi\sigma_c^2$) remained constant at each particle size (ρ_a = 0.1), the reduced grafting density ρ_a^* (= $\rho_a\pi R_g^2$) varied depending on the chain length. At $\sigma_c = 10\sigma_p$, the attractive minimum becomes deeper and shifts to a larger distance as N increases from $N = 10$ to $N = 30$. Further increasing the chain length to $N = 50$ results in the polymer-induced force oscillating between attraction and repulsion for $D > 6\sigma_p$ and being purely repulsive for $D < 6\sigma_p$. In addition, the magnitude of the minimum in F_P is less compared to $N = 30$. Figure 5.5 shows n_{bridge} versus separation distance for all the N and σ_c values corresponding to the force-distance curves in Figure 5.4. For $\sigma_c = 10\sigma_p$, n_{bridge} is higher for longer chains, suggesting that attraction due to bridging increases monotonically with chain length. However, as chain length is increased at constant ρ_a, there are a larger number of polymer segments in the region between the two particles resulting in increased excluded volume effects. The force plots suggest that at $N = 50$, these entropic effects tend to dominate the increased attraction due to bridging and intersegmental interactions, resulting in relatively long range repulsion and a higher

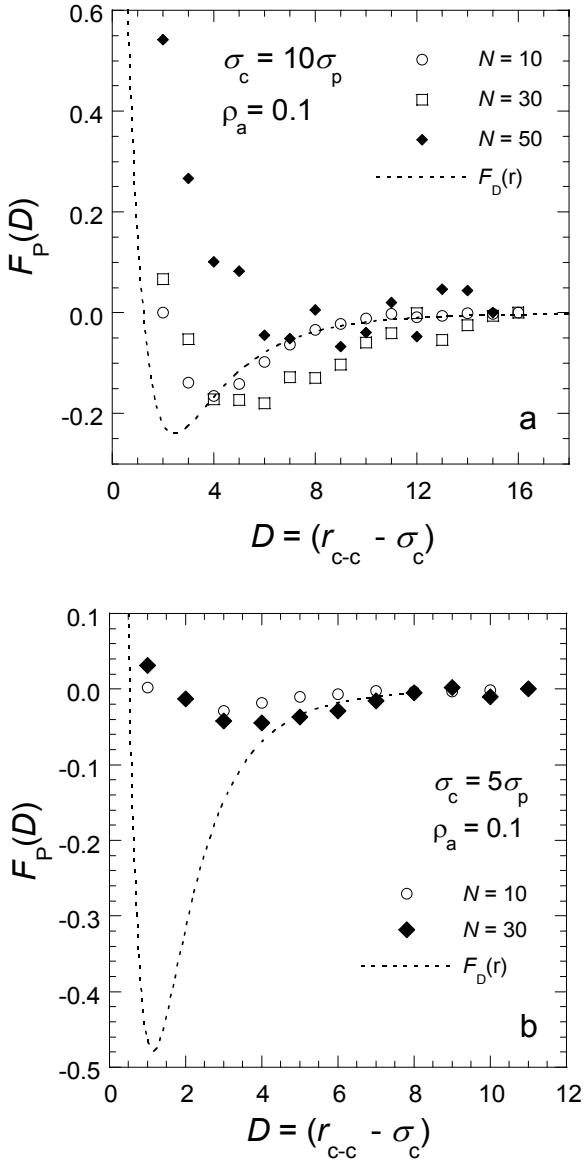

Figure 5.4: Force-distance plots (polymer mediated force $F_P(r)$ vs. D) for diameters of $\sigma_c = 10\sigma_p$ (a) and $5\sigma_p$ (b) at different chain lengths. $\varepsilon_{cp} = \varepsilon_{pp} = 1$. The grafting density is constant at $\rho_a = 0.1$ for all cases. Note however that ρ_a^* varies with σ_c and N (see Table 1). The direct force between the bare nanoparticles (F_D) calculated from equation 5.2 is also shown for comparison.

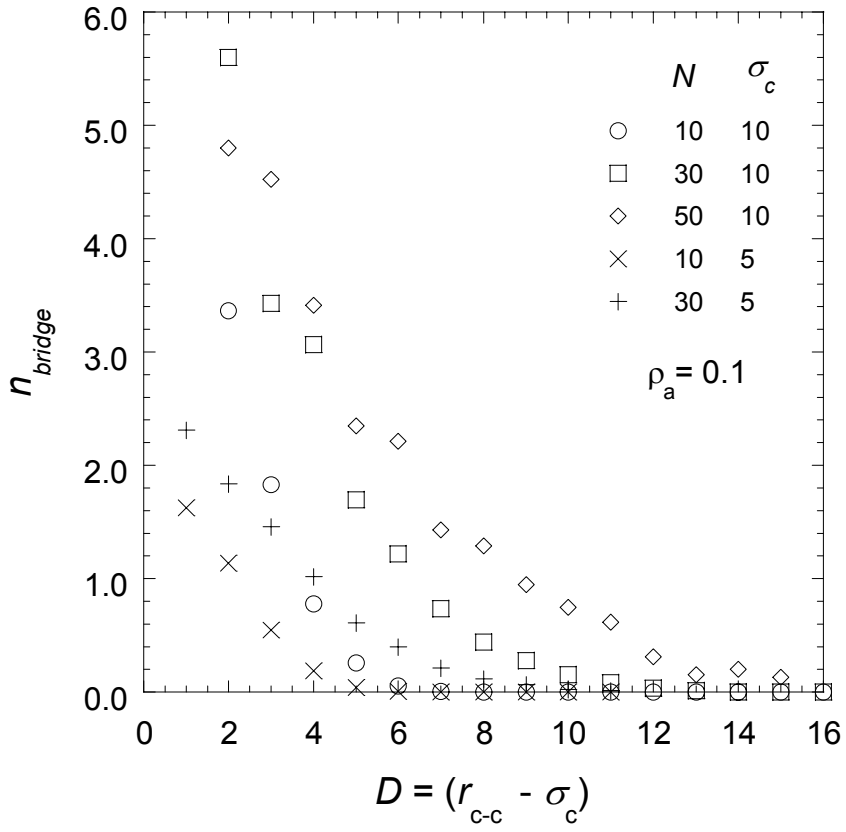

Figure 5.5: The number of bridging chains versus surface to surface separation distance ($D = r_{c\text{-}c} - \sigma_c$) at different σ_c and N corresponding to the force profiles in Figure 4. The grafting density is constant at $\rho_a = 0.1$ and $\varepsilon_{cp} = \varepsilon_{pp} = 1$.

attractive minimum. At $\sigma_c = 5\sigma_p$, the force due to the polymer is very small compared to the direct nanoparticle force for both chain lengths (N = 10 and N = 30). For a constant grafting density (ρ_a = 0.1), the number of grafting chains decreases with decreasing particle size and hence at $\sigma_c = 5\sigma_p$, the polymer-induced attraction is much weaker compared to $\sigma_c = 10\sigma_p$. In addition, the decrease in the magnitude of the LJ attractive energy with σ_c results in a lesser number of bridging chains (shown in Figure 5.5) and consequently a weaker polymer-induced attraction.

5.3.3 Effect of colloid-polymer interaction parameter (ε_{cp})

Figure 5.6 explores the effect of tuning the strength of the colloid-polymer interaction on the force-distance plots at $\sigma_c = 10\sigma_p$, N = 30, ε_{pp} = 1 and ρ_a^* = 5.0. To ensure that the polymers are in the brush regime we use the highest grafting density explored in our simulations (ρ_a^* = 5.0) for this study. In addition, we also ensured that the initial grafting sites were the same for all the cases studied here. As ε_{cp} is increased from $\varepsilon_{cp} = 1\varepsilon_{pp}$ to $\varepsilon_{cp} = 2\varepsilon_{pp}$, the attractive minimum grows deeper due to an increase in the number of bridging chains. The increased colloid-polymer interaction strength causes an increase in n_{bridge}. The number of bridging chains as a function of separation distance at $\sigma_c = 10\sigma_p$, N = 30, ρ_a^* = 5.0 and the different values of ε_{cp} and ε_{pp} explored in this study are shown in figure 5.7. Also, the R_{EED}^2 and R_g^2 decrease with increasing ε_{cp} which results in the transition from attractive to repulsive force occurring at shorter separations. There is no significant difference however in the location of the attractive minimum. We have also studied the effect of turning off the colloid-polymer attraction by using only the repulsive part of the LJ 6-12 potential to model the colloid-polymer interactions. This

allows us to eliminate attraction due to bridging and isolate the effect of polymer intersegmental attractions on the force profiles. The force profile from figure 5.6 shows that beyond $D = 4\sigma_p$, the force due to the polymers is attractive and oscillatory over the entire range of separations up to $D = 16\sigma_p$. It is noteworthy that for all other cases explored in this chapter (wherein F_P is attractive at some distance), the force due to the polymers passes through a minimum and become almost zero at a distance of $D \approx 2.5\sigma_c$. In the present case however, the polymer-induced force is strongly attractive even at $D = 2.5\sigma_c$, The relatively longer range of attraction in F_P could be attributed to the repulsive colloid-polymer interactions which drives the grafted chains to extend out as far as possible from the particle surface. Note that the R_{EED}^2 and R_g^2 values for this case are larger than any case for which there is an attractive interaction between the colloid and the polymer segments (see Table 5.1). In addition, no bridging attraction was observed for this case ($n_{bridge} = 0$). While the force profiles suggest that the polymer intersegmental attractions contribute significantly to the overall polymer-induced attraction between the nanoparticles, it must be noted that the repulsion between the colloid and the polymer segments enhances range and magnitude of the intersegmental attractions compared to the case when $\varepsilon_{cp} = \varepsilon_{pp} = 1$. At $\varepsilon_{cp} = \varepsilon_{pp} = 1$, the polymer segments get favorable attractive interactions with both the colloid as well as with each other, resulting in a competition between bridging and intersegmental attraction. This reduces the relative contribution of intersegmental attractions to the overall attraction.

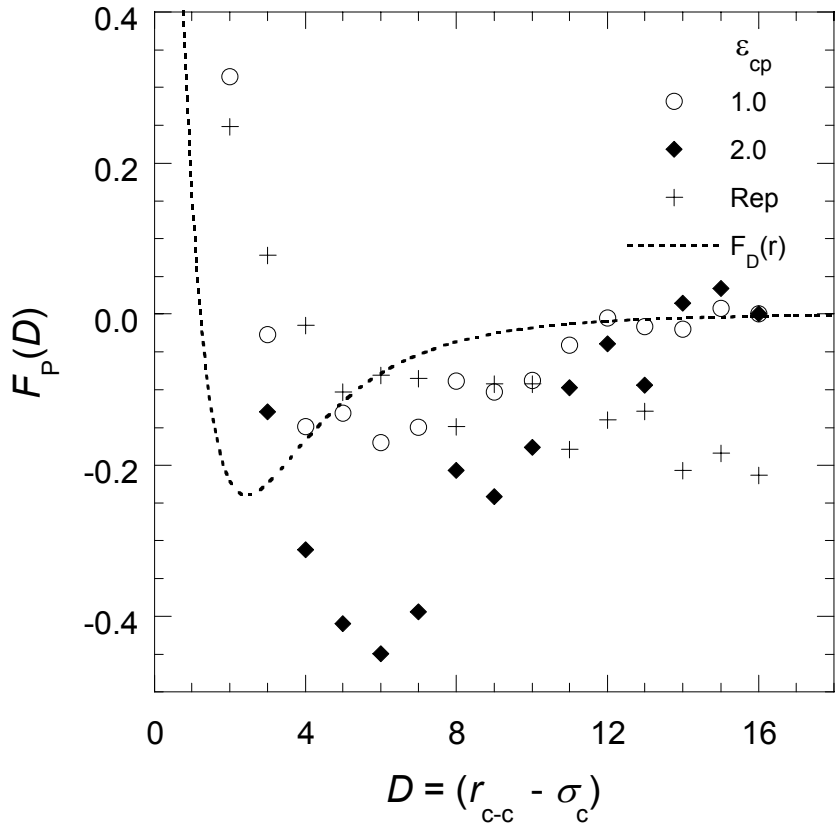

Figure 5.6: Force-distance plots (polymer mediated force $F_P(r)$ vs. D) for different values of the colloid-polymer interaction strength (ε_{cp}). $\sigma_c = 10\sigma_p$, $N = 30$, $\rho_a^* = 5.0$, $\varepsilon_{pp} = 1$ for all cases. "Rep" stands for purely repulsive interaction obtained by using only the repulsive term in the Lennard-Jones 6-12 potential. The direct force between the bare nanoparticles (F_D) calculated from equation 5.2 is also shown for comparison.

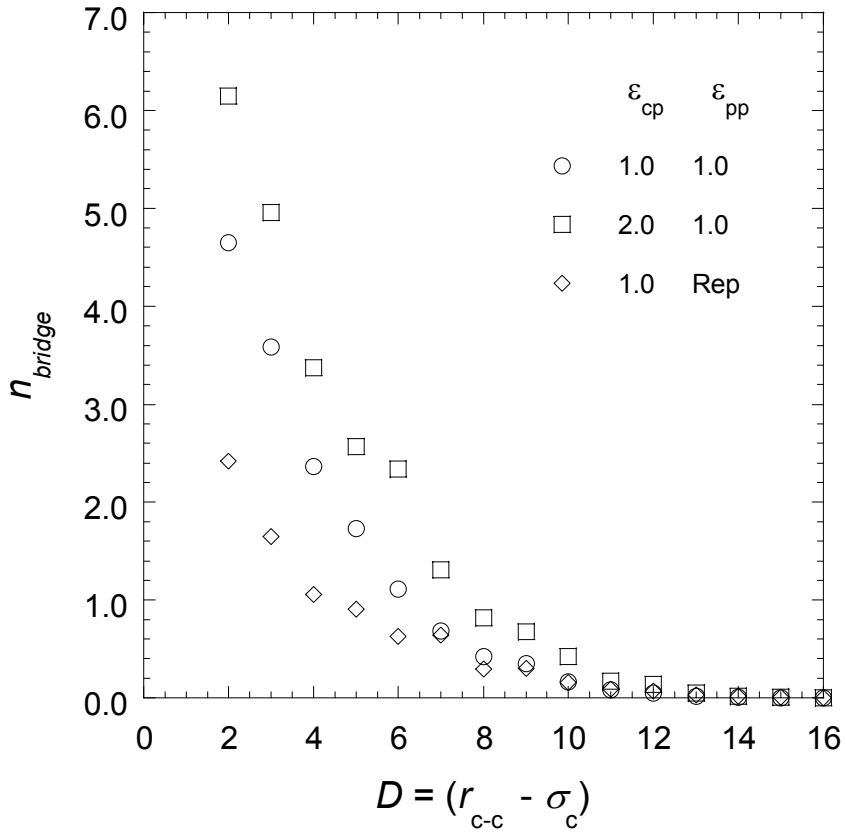

Figure 5.7: The number of bridging chains versus surface to surface separation distance ($D = r_{c\text{-}c} - \sigma_c$) at $\sigma_c = 10\sigma_p$, $N = 30$ and different values of ε_{cp} and ε_{pp}. The grafting density is constant at $\rho_a^* = 5.0$. "Rep" stands for purely repulsive interaction obtained by using only the repulsive term in the Lennard-Jones 6-12 potential.

5.3.4 Effect of polymer-polymer interaction parameter (ε_{pp})

Figure 5.8 shows the force profiles for $\varepsilon_{pp} = 1$ and the case of soft-repulsive interactions between polymer segments ($\sigma_c = 10\sigma_p$, $N = 30$, $\rho_a^* = 5.0$ and $\varepsilon_{cp} = 1$). When the polymer-polymer interactions are purely repulsive, the magnitude of polymer-induced attraction is lower compared to the case of $\varepsilon_{cp} = \varepsilon_{pp} = 1$ because there is no longer any contribution of intersegmental attractions to the overall force profile. The attraction that is observed in this case is solely due to bridging (since $\varepsilon_{cp} = 1$). However, the bridging attraction observed here is less than in the case of $\varepsilon_{cp} = \varepsilon_{pp} = 1$ (see figure 5.7) because the polymer-polymer repulsion restricts the polymer chains from interpenetrating through the opposite grafted layer and attaching to the particle. These results suggest that there is a complex interplay of the effects of ε_{cp} and ε_{pp} and both these parameters need to be accounted for explicitly in order to accurately model these nanoparticle-polymer systems. We also calculated the force profiles for the limiting case of repulsive interactions between both colloid-polymer and polymer-polymer. This represents the condition of athermal polymer chains grafted to a hard colloid surface. As expected, the polymer-induced forces are purely repulsive in agreement with previous simulation results of interactions between spherical brushes modeled using the hard-sphere potential.[25] In addition, the polymer chains are in the most stretched out conformations as the R_{EED}^2 and R_g^2 values for this case are larger than those for any other condition at $\rho_a^* = 5.0$ (see Table 5.1). Also, comparing this athermal system with the case of $\varepsilon_{cp} = \varepsilon_{pp} = 1$ at the same grafting density ($\rho_a^* = 5.0$) suggests that relatively higher grafting densities would

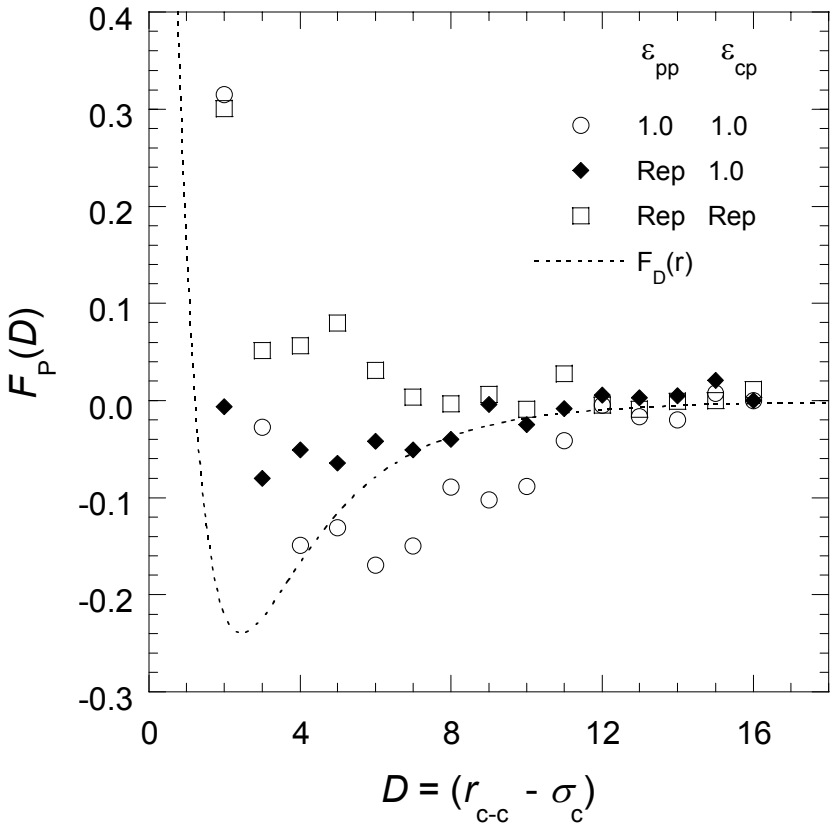

Figure 5.8: Force-distance plots (polymer mediated force $F_P(r)$ vs. D) for different values of the polymer-polymer interaction strength (ε_{pp}). $\sigma_c = 10\sigma_p$, $N = 30$, $\rho_a^* = 5.0$ for all cases. "Rep" stands for purely repulsive interaction obtained by using only the repulsive term in the Lennard-Jones 6-12 potential. The direct force between the bare nanoparticles (F_D) calculated from equation 5.2 is also shown for comparison.

be required for steric stabilization of nanoparticles when the colloid-polymer and polymer-polymer dispersion interactions are taken into account.

Attractive forces between polymer brushes are not observed usually in experimental studies. Most previous experiments report a monotonically increasing repulsive force which decreases exponentially with increasing distance. However, bridging attraction is sometimes observed in the case of *telehelic* (functionalized at both ends) polymers at low surface coverage.[41] These experimental studies are invariably in the limit of flat planar brushes. Recently, Goodman and co-workers used the AFM to measure the interactions between spherical polymer brushes and a silicon nitride tip in aqueous media. They observed a long-ranged bridging force at low grafting density and a monotonically increasing repulsive force at higher grafting densities. In addition, the grafting density at which the bridging force was observed also varied with the polymers used for modification. The authors suggest that in addition to the polydispersity of the polymer that causes the AFM tip to infrequently sample long polymer chains, the curvature of the latex particles may also be partially responsible for the anomalous bridging attraction. While the experimental system is different from our simulations in that we calculate the interaction force between two brushes as compared to the AFM experiments which measure the force between a brush and a surface, a qualitative comparison could still be made. The effect of different polymers used in the experiments could be compared to the effect of varying the colloid-polymer interaction parameter (ε_{cp}) in our simulations. From figure 5.6, at a constant grafting density, the attractive minimum in the force profile grows deeper with increasing ε_{cp} suggesting that a higher grafting density would be required for stabilization. A similar observation has been reported in the

AFM study wherein poly(*N*-isopropylacrylamide) exhibited a stronger affinity for the AFM tip than poly(*N.N*-dimethyacrylamide) at the same grafting density. These results underscore the importance of incorporating van der Waals dispersion interactions in models and theories for studying nanoparticle-polymer systems.

5.4. CONCLUSIONS

The force between two nanoscale colloidal particles coated with grafted polymers has been calculated using continuum Monte Carlo simulations in the NVT ensemble. In contrast to previous hard-sphere models, we demonstrate that the inclusion of dispersion interactions can result in long ranged-attraction as well as short-ranged repulsion in the polymer-induced force (F_P) profiles. The polymer-induced attraction could be attributed to both bridging and intersegmental interactions, the relative contributions of which could be adjusted with ε_{cp} and ε_{pp}. For a constant particle diameter and chain length, there is a threshold value of grafting density (ρ_a^*) up to which the polymer-induced attractive minimum grows deeper monotonically. As ρ_a^* is increased beyond this value, the excluded volume effects begin to dominate the attractive forces leading eventually to purely repulsive forces (and thereby stabilization of the nanoparticles). The effect of increasing ρ_a^* at constant N is similar to the effect of increasing N at constant ρ_a^*. As the particle size is increased from $\sigma_c = 5\sigma_p$ to $\sigma_c = 10\sigma_p$ (at constant ρ_a^* and N) the magnitude of the polymer-induced attraction also increases, suggesting that the grafting density required for stabilization would be higher as the particle diameter increases. By using the simple Lennard-Jones potential to model colloid-polymer and polymer-polymer

interactions, we showed that the force due to the grafted polymers can be attractive and comparable in magnitude to the direct bare colloid-colloid dispersion force.

The ability of end-grafted polymers to induce both attractive and repulsive interactions between nanoparticles make them particularly useful for both self-assembly as well as stabilization purposes. The location and depth of the attractive minimum in the force profiles can be controlled by varying the polymer chain length, grafting density and the colloid-polymer interaction strength. In addition, these parameters also control the particle equilibrium spacing which corresponds to $F_P = 0$. Thus, by tuning the various molecular parameters (ρ_a^*, N, ε_{cp}, ε_{pp}) of end-grafted modifiers, it is perhaps possible to achieve precise control over nanoparticle alignment and spacing in thermodynamically driven self-assembly processes.

Freely adsorbing homopolymer modifiers studied in part 1 of this series also showed a similar dependence of the polymer-induced forces on particle diameter, polymer chain length and colloid-polymer interaction strength. However, over the range of chain lengths, ε_{cp} and ε_{pp} that were investigated, it was found that getting repulsion was more difficult. Hence adsorbing polymers are not ideally suited for stabilization purposes. On the other hand the thermodynamic minimum can be controlled using the same molecular parameters (except grafting density) as with end-grafted modifiers. Finally, we hope that these simulation studies motivate theoretical modeling efforts incorporating the attractive colloid-polymer and polymer-polymer dispersion interactions in nanoscale colloid-polymer systems.

5.5 REFERENCES

(1) Alexander, S. *J. Phys. (Paris)* **1977,** 38, 983-987.

(2) de Gennes, P.-G. *Macromolecules* **1980,** 13, 1069-1075.

(3) Milner, S. T.; Witten, T. A. *J. Phys. (Paris)* **1988,** 49, (11), 1951-62.

(4) Milner, S. T.; Witten, T. A.; Cates, M. E. *Macromolecules* **1988,** 21, (8), 2610-19.

(5) Milner, S. T.; Witten, T. A.; Cates, M. E. *Europhys. Lett.* **1988,** 5, (5), 413-18.

(6) Milner, S. T.; Witten, T. A.; Cates, M. E. *Macromolecules* **1989,** 22, (2), 853-61.

(7) Zhulina, E. B.; Borisov, O. V.; Priamitsyn, V. A. *J. Colloid Interface Sci.* **1990,** 137, (2), 495-511.

(8) Wijmans, C. M.; Scheutjens, J. M. H. M.; Zhulina, E. B. *Macromolecules* **1992,** 25, 2657-2665.

(9) Toral, R.; Chakrabarti, A.; Dickman, R. *Phys. Rev. E: Stat., Nonlinear, Soft Matter Phys.* **1994,** 50, (1), 343-8.

(10) Lai, P. Y.; Binder, K. *J. Chem. Phys.* **1991,** 95, (12), 9288-99.

(11) Murat, M.; Grest, G. S. *Phys. Rev. Lett.* **1989,** 63, (10), 1074-7.

(12) Murat, M.; Grest, G. S. *Macromolecules* **1989,** 22, (10), 4054-9.

(13) Taunton, H. J.; Toprakcioglu, C.; Fetters, L. J.; Klein, J. *Nature* **1988,** 332, (6166), 712-714.

(14) Taunton, H. J.; Toprakcioglu, C.; Klein, J. *Macromolecules* **1988,** 21, (11), 3333-3336.

(15) Tirrell, M.; Patel, S.; Hadziioannou, G. *Proceedings of the National Academy of Sciences of the United States of America* **1987,** 84, (14), 4725-4728.

(16) Cosgrove, T.; Heath, T. G.; Phipps, J. S.; Richardson, R. M. *Macromolecules* **1991,** 24, (1), 94-98.

(17) Field, J. B.; Toprakcioglu, C.; Ball, R. C.; Stanley, H. B.; Dai, L.; Barford, W.; Penfold, J.; Smith, G.; Hamilton, W. *Macromolecules* **1992,** 25, (1), 434-439.

(18) Cosgrove, T.; Ryan, K. *Langmuir* **1990,** 6, (1), 136-142.

(19) Auroy, P.; Mir, Y.; Auvray, L. *Physical Review Letters* **1992,** 69, (1), 93-95.

(20) Daoud, M.; Cotton, J. P. *J. Phys. (Paris)* **1982,** 43, (3), 531-8.

(21) Witten, T. A.; Pincus, P. A. *Macromolecules* **1986,** 19, (10), 2509-13.

(22) Lin, E. K.; Gast, A. P. *Macromolecules* **1996,** 29, (1), 390-7.

(23) Wijmans, C. M.; Leermakers, F. A. M.; Fleer, G. J. *Langmuir* **1994,** 10, (12), 4514-16.

(24) Roan, J.-R. *Phys. Rev. Lett.* **2001,** 86, (6), 1027-1030.

(25) Cerda, J. J.; Sintes, T.; Toral, R. *Macromolecules* **2003,** 36, 1407-1413.

(26) Flory, P. J., *Principles of Polymer Chemistry*. ed.; Cornell University Press: London, 1953; p.

(27) Currie, E. P. K.; Leermakers, F. A. M.; Stuart, M. A. C.; Fleer, G. J. *Macromolecules* **1999,** 32, (2), 487-498.

(28) Grest, G. S.; Murat, M. *Macromolecules* **1993,** 26, (12), 3108-3117.

(29) Patel, S. S.; Tirrell, M. *Annu. Rev. Phys. Chem.* **1989,** 40, 597-635.

(30) O'Shea, S. J.; Welland, M. E.; Rayment, T. *Langmuir* **1993,** 9, 1826-1835.

(31) Yamamoto, S.; Ejaz, M.; Tsujii, Y.; Fukuda, T. *Macromolecules* **2000,** 33, (15), 5608-5612.

(32) Yamamoto, S.; Ejaz, M.; Tsujii, Y.; Matsumoto, M.; Fukuda, T. *Macromolecules* **2000,** 33, (15), 5602-5607.

(33) Yamamoto, S.; Tsujii, Y.; Fukuda, T. *Macromolecules* **2000,** 33, (16), 5995-5998.

(34) Taunton, H. J.; Toprakcioglu, C.; Fetters, L. J.; Klein, J. *Macromolecules* **1990,** 23, 571-580.

(35) Goodman, D.; Kizhakkedathu, J. N.; Brooks, D. E. *Langmuir* **2004,** 20, 2333-2340.

(36) Baranowski, R.; Whitmore, M. D. *J. Chem. Phys.* **1995,** 103, (6), 2343-2353.

(37) Siepmann, J. I.; Frenkel, D. *Mol. Phys.* **1992,** 75, 59-70.

(38) de Pablo, J. J.; Laso, M.; Suter, U. W.; Cochran, H. D. *Fluid Phase Equilib.* **1993,** 83, 323-331.

(39) Allen, M. P.; Tildesley, D. J., *Computer Simulation of Liquids*. 1st ed.; Oxford University Press: Clarendon,Oxford, 1987; p 385.

(40) Carignano, M. A.; Szleifer, I. *Macromolecules* **1995,** 28, (9), 3197-3204.

(41) Eiser, E.; Klein, J.; Witten, T. A.; Fetters, L. J. *Phys. Rev. Lett.* **1999,** 82, 5076–5079.

CHAPTER 6

CALCULATION OF EFFECTIVE-COLLOID PAIR POTENTIALS FOR ATTRACTIVE COLLOID-POLYMER MIXTURES

The expanded ensemble Monte Carlo simulation method is applied to simulate a dispersion of spherical colloidal particles in a dilute freely-adsorbing homopolymer solution. Colloid volume fractions (ϕ_c) ranging from 0.05 to 0.5 were investigated. The colloid-colloid, colloid-polymer radial distribution profiles ($g_{cc}(r)$ and $g_{cp}(r)$) and the colloid chemical potentials ($\beta\mu_c^{ex}$) are calculated. The $\beta\mu_c^{ex}$ first decreases, passes through a minimum and then increases with ϕ_c due to the competition between polymer adsorption and excluded volume effects. It was found that at low ϕ_c, the structure of the colloid-polymer mixture (CPM) is controlled by polymer adsorption. As the ϕ_c is increased, the colloid-colloid interactions dominate the structure of the CPM. The $g_{cc}(r)$ is inverted using the Ornstein-Zernike technique combined with the Duh-Henderson closure approximation to obtain effective one-component colloid potentials. The original $g_{cc}(r)$ were not reproduced exactly by using the effective potentials, possibly due the closure approximations which may not be valid for strongly attractive systems with large size asymmetry.

6.1. INTRODUCTION

Colloid-polymer mixtures (CPM) have been studied extensively in recent years due to their widespread technological applications ranging from paints, coatings and inks to advanced materials and drug delivery. In addition, they also serve as good model systems for studying the strong geometric asymmetry, and large length and time scale separations in complex fluids. The above features of CPM, in addition to the presence of multiple physical forces including attractive van der Waals, Coulomb and excluded volume, are responsible primarily for the novel phase behavior, complex structure and interesting material properties of these systems. The key complicating factor in the theoretical and simulation studies of colloid-polymer mixtures is the large difference in length scales between sizes of the colloid and polymer segments. Even in the simplest model of these systems wherein the colloids are treated as smooth hard spheres and the polymers are represented as non-interacting random-walk chains, there is an order of magnitude difference in the number of degrees of freedom required to model the polymers as compared to the colloidal particles. Hence, large-scale simulations of CPM involving a multitude of polymer chains become intractable if a detailed description of the monomer segments and the internal conformational degrees of freedom of the chains are taken into account. To overcome this problem, the polymers could be represented as simplified single composite particles by tracing out the individual monomer degrees of freedom. The concept was first applied to CPM by Asakura and Oosawa (AO),[1,2] who treated the polymers as ideal spherical particles (mutually penetrable) with respect to each other and hard-spheres with regard to the colloids. This model addressed the question of entropy-driven depletion attraction between hard-sphere colloidal particles in

a nonadsorbing polymer solution. The AO model, valid in the limit of noninteracting polymers or interacting polymers at dilute concentrations, was also used to calculate the phase diagrams of colloid-polymer systems.[3,4] Recently, this concept was extended by Louis and co-workers to repulsive interacting polymer chains in the dilute and semi-dilute limit.[5-8] In their approach, the detailed intersegmental interactions were replaced by an effective interaction between the centers-of-mass (CM) of the polymer coils, obtained by inverting the radial distribution functions for the CM of colloids and polymer chains. They used the hypernetted chain closure (HNC) with Ornstein-Zernike inversion techniques, developed originally for molecular fluids, to derive effective potentials for the polymer-polymer and polymer-colloid interactions in a CPM.[5,6] These potentials were then used to generate phase-diagrams for these coarse-grained models by Gibbs-Ensemble Monte Carlo simulations.[9] In addition, using the two-component model of Louis et al., the depletion interaction between a pair of colloids can be determined from the effective polymer-polymer and colloid-polymer potentials, either by superposition approximations on the one-particle density of the colloids, or by an additional simulations of the effective mixture.[8]

More recently, Guzman and de Pablo[10] showed that an effective one component potential can be defined for colloids dispersed in a repulsive CPM. In this method, the effective interaction potential between the colloidal particles is calculated by inverting the colloid-colloid radial distribution function, $g_{cc}(r)$, obtained from simulations of the binary CPM. The effective potential was then used to simulate pure colloid systems and $g_{cc}(r)$ obtained were in very good agreement to the original $g_{cc}(r)$ of the binary CPM. These coarse-graining methods are an important step towards large-scale simulations of

the structure and phase behavior of colloid-polymer systems. However, most of these studies focus on CPM with purely repulsive interactions. We also note that there have also been numerous other simulation studies[11-14] and theoretical approaches[15-18] that have dealt with various aspects of hard-sphere colloids in a nonadsorbing polymer solution including phase-behavior, interparticle forces and structure. While these studies are vital to the understanding of athermal systems and applications in which depletion interactions are predominant, an important advance would be to account for the ubiquitous van der Waals dispersion interactions in these CPM. The introduction of VDW attractions in colloid-polymer systems complicates the theoretical and model development efforts because of the adsorption of polymers on the colloid surface and the subsequent anisotropy in the polymer conformations. In addition, the nanoparticle free energy also becomes strongly correlated to the amount and conformation of the adsorbed polymers.

In this study, we attempt to extend the coarse-graining approach of Guzman and de Pablo to attractive Lennard-Jones (LJ) colloid-polymer mixtures. We use the expanded ensemble Monte Carlo method[19-21] to simulate colloidal particles in a freely adsorbing polymer solution, in which the radius of gyration (R_g) of the polymer chains is of similar size compared to the colloid radius. The $g_{cc}(r)$ from the simulations is used to calculate the effective one-component potential using the Ornstein-Zernike equation[22] combined with the Duh-Henderson closure.[23] The rest of this chapter is organized as follows: In section 6.2, we outline the details of the binary CPM simulations. Section 6.3 describes the procedure for inverting $g_{cc}(r)$ to obtain effective potentials. The colloid-colloid and colloid-polymer radial distribution plots, colloid chemical potentials and the calculated effective-colloid potentials for the various cases explored in this study are presented in

section 6.4. The analysis of the effective potentials and the effects of the various molecular parameters (colloid diameter, polymer chain length and colloid and polymer concentration) are also presented in this section. Section 6.4 also outlines the limitations of the coarse-graining effective-potential approach for attractive colloid-polymer mixtures. Finally, the main conclusions of this study are summarized in Section 6.5.

6.2. SIMULATION METHODOLOGY

The simulation system consists of spherical colloidal particles dispersed in a dilute solution of freely-adsorbing polymers. The polymer chains were modeled as bead necklace chains with a bead diameter of σ_p. All non-bonded interactions were modeled by the shifted and truncated Lennard-Jones 6-12 potential shown in equation 6.1,

$$U(r_{ij}) = \begin{cases} 4\varepsilon_{ij}\left[\left(\frac{\sigma_{ij}}{r_{ij}}\right)^{12} - \left(\frac{\sigma_{ij}}{r_{ij}}\right)^{6} - \left(\frac{\sigma_{ij}}{r_c}\right)^{12} + \left(\frac{\sigma_{ij}}{r_c}\right)^{6}\right] & r \le r_c, \\ 0 \quad r > r_c \end{cases} \tag{6.1}$$

where $\sigma_{ij} = (\sigma_i + \sigma_j)/2$ is the size parameter and ε_{ij} is the LJ interaction energy parameter. The cut-off for the segment-segment interaction is set to $r_c = 2.5\sigma_p$. The colloid-polymer and colloid-colloid interactions are modeled using the full LJ potential without any cut-off. The LJ energetic parameters for the colloid and polymer are chosen to be symmetric such that $\varepsilon_{pp} = \varepsilon_{cc} = \varepsilon_{cp} = 1$. Simulation variables are reduced in the usual manner; temperature $T^* = Tk_B/\varepsilon_{pp}$, density $\rho_p^* = \rho_p\sigma_p^3$, where ε_{pp} is the polymer segment-segment interaction parameter and k_B is the Boltzmann constant. The temperature is maintained constant at $T^* = 3.0$ (good solvent condition) for all the simulations. The bulk polymer segment density (ρ_p) is given by $\rho_p = Nn_p/V$, where N is the polymer chain length, n_p is

the number of chains and V is the volume of the simulation box. The simulations are performed in the dilute polymer regime as characterized by the reduced polymer concentration (c_p/c_p^*) given by $c_p/c_p^* = (4\pi/3)(\rho_p/N)R_g^3$, where c_p is the polymer-molecule number density, c_p^* is the critical polymer-molecule number density ($1/(4\pi R_g^3/3)$) at which the polymer molecules start to overlap and entangle with each other (dilute to semi-dilute crossover). The number density (ρ_c) and volume fraction (ϕ_c) of the colloidal particles are given by $\rho_c = n_c/V$ and $\phi_c = (\pi\sigma_c^3/6)\rho_c$, where n_c is the number of colloids and σ_c is the colloid diameter.

The colloid-polymer mixture was simulated using the expanded ensemble Monte Carlo method[14,19-21] in a cubic simulation box with standard periodic boundary conditions. The box length was kept constant at $l_B = 40\sigma_p$ unless stated otherwise. Thermal equilibration of the CPM was achieved by translation of the colloidal particle and molecular displacements of the polymer chains. Chain displacements are preformed using the continuum configurational bias algorithm, [24,25] in which a portion of the chain is regrown in a low-energy conformation that avoids overlaps with neighboring segments. Polymer excess chemical potential ($\beta\mu_p^{ex}$) is calculated with the expanded variable-length chain ensemble. [21] The colloid particles are moved via random displacements accepted with the standard Metropolis criterion.[26] In addition, the colloid chemical potential is also calculated using the expanded ensemble method described in a previous paper.[14,27] The basic idea is that incremental chemical potentials are generated as the diameter of the colloidal particles is varied between zero and maximum diameter during the course of the simulation. These incremental values can be summed at the end of the simulation to get the total colloidal chemical potential. It is noteworthy that for large colloidal particles,

random displacement moves result in a very low acceptance rate due to the high probability of overlaps. However, the expanded ensemble method in which the *tagged* colloidal particle is inserted at a random position in the simulation box after being fully removed (when the diameter reaches zero during the increment-decrement process) improves the efficiency of thermal equilibration. Hence it could also be construed as a method for random displacement of colloidal particles in addition to calculation of chemical potentials for large colloid diameters.

In this study, colloid sizes of $\sigma_c = 5\sigma_p$, $10\sigma_p$ and chain lengths of $N = 10$, 30 are considered. The colloid fraction (ϕ_c) is varied from 0.05 to 0.5 depending on the colloid diameter. The effect of polymer segment density is also considered by performing simulations at two different values of polymer segment density, $\rho_p = 0.05$, 0.15. For all cases, we obtained the colloid-colloid, $g_{cc}(r)$, and colloid-polymer segment, $g_{cp}(r)$, radial distribution plots. In addition, averaged values of the colloid and polymer chemical potentials, and the polymer chain conformational properties were also calculated. The statistical error for the conformational properties of the chains was taken as the root-mean square fluctuation divided by the square root of the number of independent blocks while the statistical error in the chemical potentials was based on the statistical inefficiency parameter. [28] The details of all the cases studied in this work are shown in Table 6.1.

Table 6.1: Simulation conditions explored in this study. R_g is radius of gyration of the polymer chains. c_p/c_p^* is the reduced polymer concentration and ϕ_c is the volume fraction of the colloidal particles.

State	σ_c	n	R_g	c_p/c_p^* $= (4\pi Rg^3/3)\rho_p/N$	ϕ_c $= (\pi\sigma_c^3/6)\rho_c$
A1	10	30	2.894	0.169	0.049
A2	10	30	2.851	0.162	0.106
A3	10	30	2.817	0.156	0.205
A4	10	30	2.774	0.149	0.303
A5	10	30	2.753	0.146	0.409
A6	10	30	2.751	0.145	0.515
B1	10	10	1.543	0.077	0.049
B2	10	10	1.534	0.076	0.106
B3	10	10	1.521	0.074	0.205
B4	10	10	1.513	0.073	0.303
B5	10	10	1.510	0.072	0.409
C1	5	30	2.932	0.176	0.026
C2	5	30	2.922	0.174	0.051
C3	5	30	2.917	0.173	0.102
C4	5	30	2.926	0.175	0.153
C5	5	30	2.928	0.175	0.205
C6	5	30	2.946	0.179	0.307
D1	5	30	2.957	0.541	0.02557
D2	5	30	2.951	0.538	0.05113
D3	5	30	2.933	0.528	0.07670
D4	5	30	2.931	0.527	0.10227
D5	5	30	2.926	0.525	0.15340
D6	5	30	2.930	0.527	0.20453

6.3. CALCULATION OF EFFECTIVE POTENTIALS

The Ornstein-Zernike equation which relates the total correlation function ($h(r)$) to the direct correlation function ($c(r)$) for an isotropic one-component fluid is given by[22]

$$h(r) = c(r) + \rho \int c\left(|\mathbf{r} - \mathbf{r}'|\right) h(\mathbf{r}') \mathrm{d}\mathbf{r}', \tag{6.2}$$

where $h(r) = g(r) - 1$ and ρ is the number density. A Fourier transform of equation 6.2 gives an algebraic relation of the form,

$$\hat{h}(k) = \frac{\hat{c}(k)}{1 - \rho \hat{c}(k)}, \tag{6.3}$$

which could be solved to obtain $c(r)$. To connect the correlation functions to the pair potentials, equation 6.2 must be supplemented with a closure relation. A formally exact closure can be written as

$$g(r) = \exp\{-\beta U(r) + h(r) - c(r) + B(r)\}, \tag{6.4}$$

where $\beta = 1/k_B T$ and $B(r)$ is called the bridge function or elementary function and can be expressed as a sum over an infinite set of diagrams that are free of nodal circles. [22] The bridge function is usually written as a functional

$$B(r) = \mathcal{B}(s(r)) \tag{6.5}$$

of the function $s(r) = h(r) - c(r)$. The form of the bridge function depends on the type of the closure approximation. Examples of commonly used closure approximations include the classical Percus-Yevick (PY), hypernetted chain (HNC) and mean-spherical approximation (MSA). The PY approximation is good for strongly repulsive, short range forces, as in the hard-sphere model. On the other hand, the HNC approximation is well-suited for long-range Coulombic potentials, but is unsatisfactory for hard-sphere systems.

While the MSA combines the advantages of the PY and HNC closures, it fails at low temperatures and densities. For our CPM we use the Duh-Henderson closure [23] which was developed for LJ fluids by inverting $\mathcal{B}(s)$ data from molecular dynamics simulations and has been shown to accurately reproduce the gas-liquid phase diagram of LJ fluids.[29] The bridge function for the DH closure is given by

$$\mathcal{B}(s) = -\frac{(9+7s)}{(3+s)(3+5s)} s^2/2;\ s > 0,$$
$$\mathcal{B}(s) = -s^2/2; \qquad s \le 0 \tag{6.6}$$

The two-component CPM can be reduced to a one-component colloid system whose particles interact via an effective potential $U_{\text{eff}}(r)$. This potential is defined by the condition that the one-component radial distribution function $g(r)$ be equal to $g_{cc}(r)$ in the CPM at the same values of ϕ_c and β. The effective potential can be obtained from equation 6.4 by setting $U(r) = U_{\text{eff}}(r)$ to get

$$\beta U_{eff}(r) = -\ln g(r) + h(r) - c(r) + \mathcal{B}(h(r) - c(r)) . \tag{6.7}$$

The colloid-colloid radial distribution function, $g_{cc}(r)$, obtained from simulations of the CPM is used to calculate the direct correlation function, $c_{cc}(r)$, from equation 6.3. This is then combined with the DH closure and substituted in equation 6.7 to get the effective one-component potential $U_{\text{eff}}(r)$. The effective potential due to the freely adsorbing polymers ($V_p(r)$) can then be obtained subtracting the bare colloid-colloid potential $U_{cc}(r)$,

$$V_p(r) = U_{\text{eff}}(r) - U_{cc}(r). \tag{6.8}$$

It is noteworthy that in the low-density limit where $\rho \rightarrow 0$, the OZ relation in equation 6.2 reduces to $h(r) = c(r)$. In this limit, the effective potentials can be derived from the logarithm of the probability of overlaps between two colloidal particles.

6.4. RESULTS & DISCUSSION

6.4.1 Analysis of the radial distribution profiles ($g_{cc}(r)$ and $g_{cp}(r)$)

The colloid-colloid ($g_{cc}(r)$) and colloid-polymer segment ($g_{cp}(r)$) radial distribution functions, obtained from the binary CPM simulations, for the various cases explored in this study (Table 6.1) are shown in Figures 6.1 – 6.4. Consider the $g_{cc}(r)$ profiles for $\sigma_c = 10\sigma_p$, $N = 30$ and $\rho_p = 0.05$ (Figure 6.1). At low ϕ_c, the peak in the $g_{cc}(r)$ plots occurs between $12\sigma_p$ and $13\sigma_p$ corresponding to a particle surface-to-surface separation distance $D = 2\sigma_p$ to $3\sigma_p$ (where $D = r - \sigma_c$). As ϕ_c is increased, the magnitude of this peak decreases and simultaneously the height of another peak which occurs at $D \approx 0$ increases. Also, the $g_{cp}(r)$ plots for the same case (Figure 6.1) indicate a peak at $\approx 1.5\sigma_p$ from the surface of the colloidal particle. This suggests that the peak in the $g_{cc}(r)$ plots which occurs at $D \approx 3\sigma_p$ is due to the adsorbed polymer layers around the particle. At a constant polymer concentration, increasing ϕ_c would result in a decrease in polymer adsorption per particle. This is reflected in the $g_{cp}(r)$ plots where the height of the peak decreases with increasing colloid fraction. Consequently, beyond a certain value of ϕ_c the bare colloid-colloid interactions would dominate the structure of the CPM, giving rise to the peak at $D \approx 0$ in the $g_{cc}(r)$ profiles. Hence, depending on the ratio of colloid-to-polymer concentration, the structure of the CPM is controlled by either the colloid-polymer (low ϕ_c) or colloid-colloid interactions (high ϕ_c). In addition, entropic packing

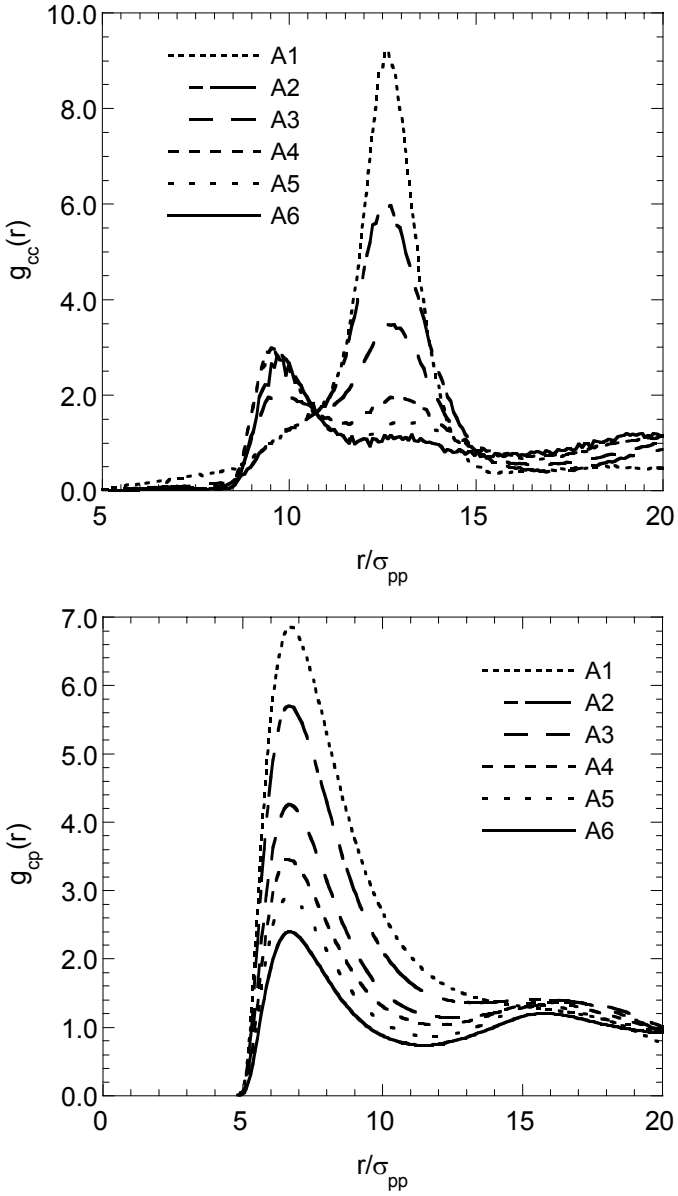

Figure 6.1: The colloid-colloid ($g_{cc}(r)$) and colloid-polymer segment ($g_{cp}(r)$) radial distribution functions, obtained from the binary CPM simulations, for states A1-A6 (Table 6.1). $\sigma_c = 10\sigma_p$, $N = 30$ and $\rho_p = 0.05$.

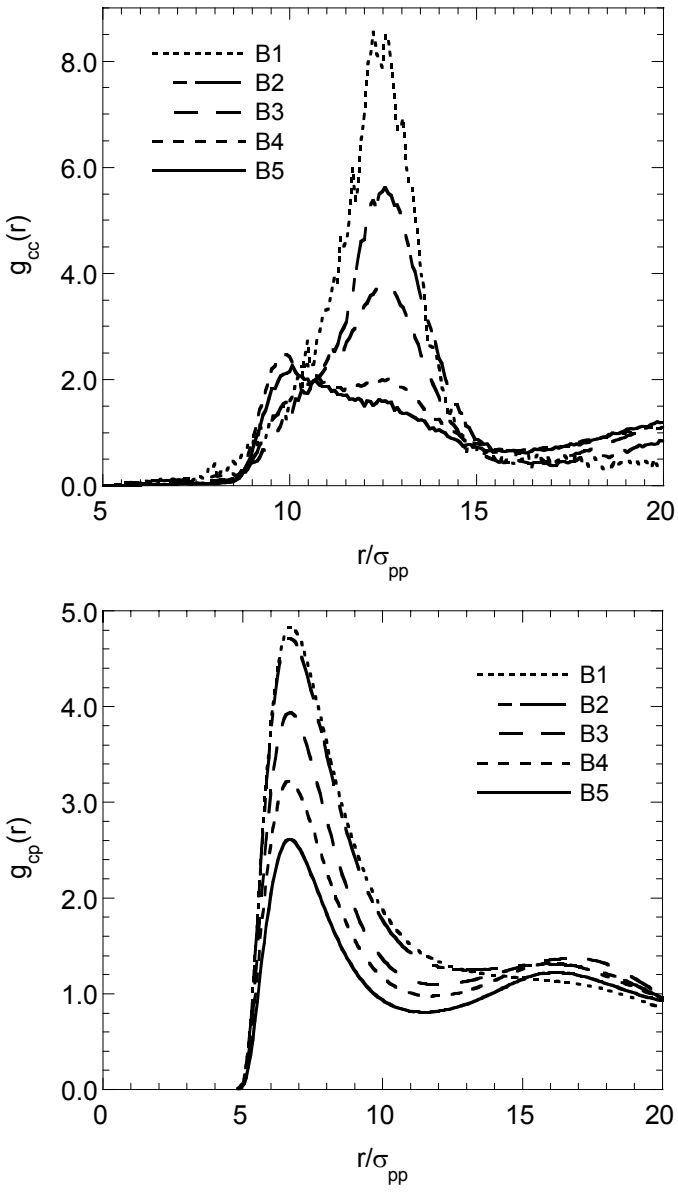

Figure 6.2: The colloid-colloid ($g_{cc}(r)$) and colloid-polymer segment ($g_{cp}(r)$) radial distribution functions, obtained from the binary CPM simulations, for states B1-B5 (Table 6.1). $\sigma_c = 10\sigma_p$, $N = 10$ and $\rho_p = 0.05$.

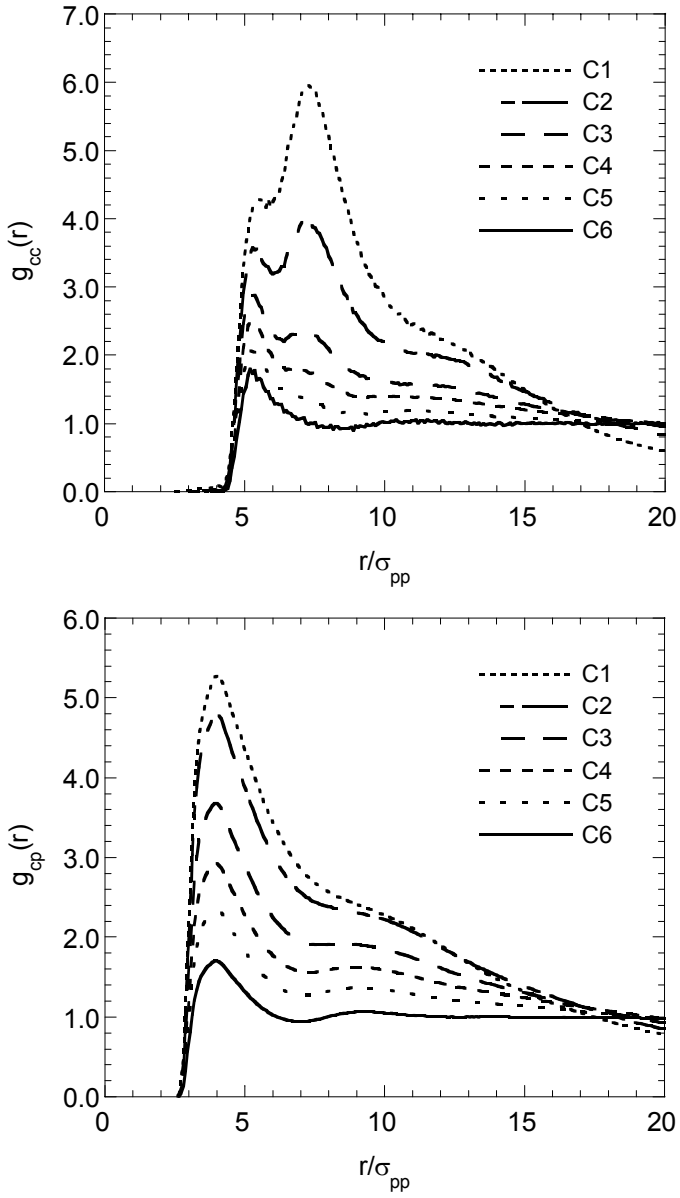

Figure 6.3: The colloid-colloid ($g_{cc}(r)$) and colloid-polymer segment ($g_{cp}(r)$) radial distribution functions, obtained from the binary CPM simulations, for states C1-C6 (Table 6.1). $\sigma_c = 5\sigma_p$, $N = 30$ and $\rho_p = 0.05$.

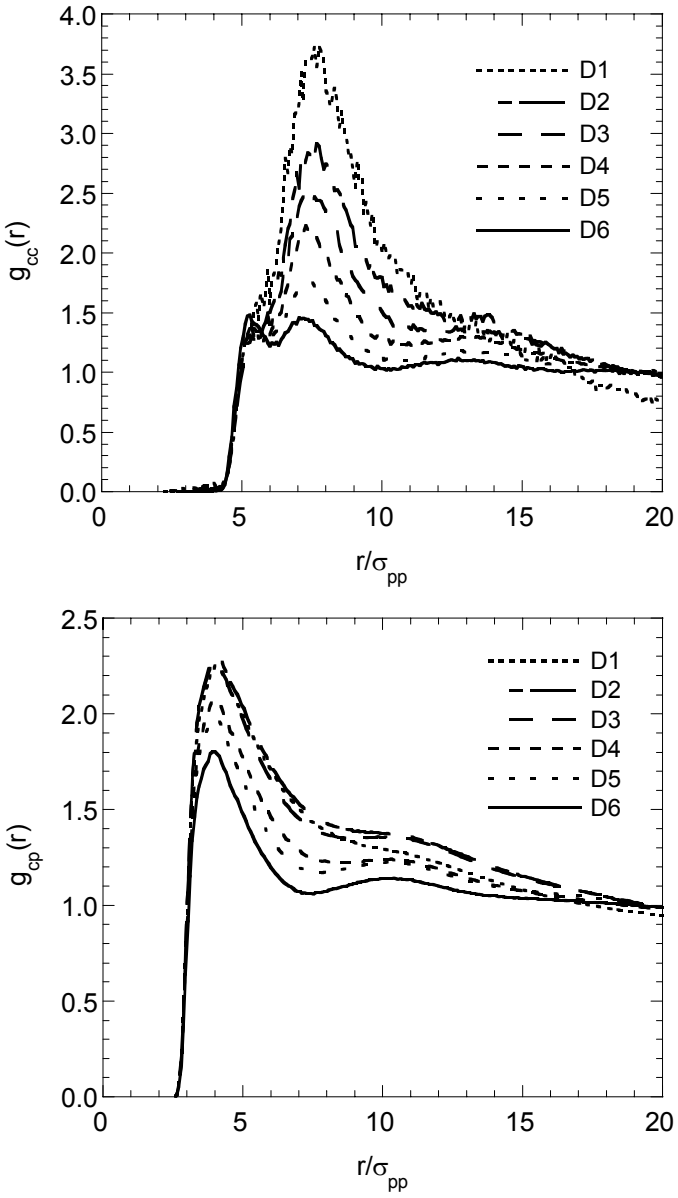

Figure 6.4: The colloid-colloid ($g_{cc}(r)$) and colloid-polymer segment ($g_{cp}(r)$) radial distribution functions, obtained from the binary CPM simulations, for states D1-D6 (Table 6.1). $\sigma_c = 5\sigma_p$, $N = 30$ and $\rho_p = 0.15$.

effects also become important at high ϕ_c values. Even in the limit of purely repulsive hard-sphere colloidal systems, it has been shown that the particles can pack together in order to increase system entropy.[30,31] The addition of LJ attraction between the colloids would only enhance this effect and cause the packing of colloidal particles to occur at lower ϕ_c compared to the hard-sphere case. The above trends in the $g_{cc}(r)$ and $g_{cp}(r)$ plots are also observed for the other cases shown in Figures 6.2 – 6.4. The effect of polymer chain length can be examined by comparing the distribution plots for $N = 30$ (Figure 6.1) and $N = 10$ (Figure 6.2) at $\sigma_c = 10\sigma_p$ and $\rho_p = 0.05$. At constant ϕ_c, there is a greater enhancement of polymer segment density near the particle for longer chains because the loss in chain configurational entropy due to adsorption decreases as N increases (see $g_{cp}(r)$ plots in Figures 6.1 and 6.2). This in turn causes a slight decrease in the height of the peaks at $D \approx 3\sigma_p$ in the $g_{cc}(r)$ plots as N decreases. It is noteworthy that the peaks at $D \approx 0$ remain relatively unaffected with chain length.

The effect of colloid diameter (σ_c) can be studied by comparing the distribution plots for $\sigma_c = 10\sigma_p$ (Figure 6.1) and $\sigma_c = 5\sigma_p$ (Figure 6.3) at $N = 30$ and $\rho_p = 0.05$. Note that the highest colloid volume fraction examined at $\sigma_c = 5\sigma_p$ is $\phi_c = 0.3$ compared to $\sigma_c = 10\sigma_p$ where volume fractions up to $\phi_c = 0.5$ were simulated. This is because for the same ϕ_c, the number of particles required in the simulation box increases by a factor of $(\sigma_{large}/\sigma_{small})^3$. Hence, for smaller σ_c it becomes increasingly difficult to simulate high colloid fractions. Comparing the $g_{cc}(r)$ and $g_{cp}(r)$ profiles (Figures 6.1 and 6.3), we observe that at $\phi_c = 0.3$ (A4 and C6) the peak due to the polymer adsorption at $D \approx 3\sigma_p$ has disappeared for $\sigma_c = 5\sigma_p$ (while it is still present for $\sigma_c = 10\sigma_p$). As σ_c increases, the LJ attractive energy and the range of colloid-polymer attraction increases thereby

resulting in stronger adsorption. Hence the effect of polymers on the structure of the CPM is stronger for larger colloid diameters. This is also evident from the $g_{cp}(r)$ plots where the magnitude of the peaks increases with σ_c at constant ϕ_c.

6.4.2 Effect of colloid volume fraction (ϕ_c) on colloid chemical potential ($\beta\mu_c^{ex}$)

Figure 6.5 shows a plot of $\beta\mu_c^{ex}$ versus ϕ_c for the different σ_c, N and ρ_p values explored in this study. The infinite dilution $\beta\mu_c^{ex}$ values used in the plots are obtained from our previous simulations (Chapter 3).[27] Figure 6.5a shows the $\beta\mu_c^{ex}$ for $\sigma_c = 10\sigma_p$, $\rho_p = 0.05$ and $N = 10$, 30. At constant σ_c, $\beta\mu_c^{ex}$ passes through a minimum and then increases with increasing ϕ_c for both chain lengths. These trends are consistent with the $g_{cc}(r)$ and $g_{cp}(r)$ profiles where increasing ϕ_c at constant ρ_p results in less adsorption per particle, less polymer-particles contacts and thereby a relatively higher $\beta\mu_c^{ex}$. Also the excluded volume increases with increasing ϕ_c, resulting in a higher free energy requirement for particle insertion. At low ϕ_c, the $\beta\mu_c^{ex}$ is lower for longer chains as expected. However, this $\beta\mu_c^{ex}$ reduction effect of chain length is no longer observed with increasing ϕ_c as entropic effects begin to dominate in this region. Also it is noteworthy that minimum in $\beta\mu_c^{ex}$ corresponds to $[(\partial g/\partial\phi_c^2)_{T,P} = 0]$ in the free energy (g) versus concentration diagram. Within the two phase region of the phase diagram $[(\partial g/\partial\phi_c^2)_{T,P} = 0]$ distinguishes the unstable region $[(\partial g/\partial\phi_c^2)_{T,P} < 0]$ from the metastable region $[(\partial g/\partial\phi_c^2)_{T,P} > 0]$.[32] However, the minimum in $\beta\mu_c^{ex}$ is a necessary but not sufficient condition for phase instability. In order to represent a point on the spinodal which lies between the unstable and metastable regions, this minimum has to be preceded

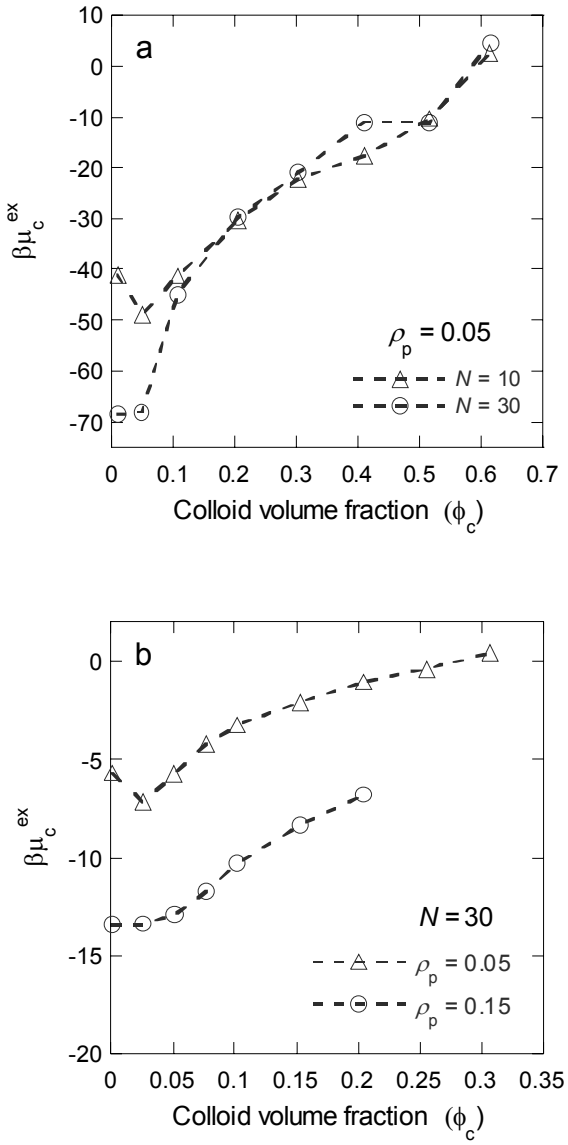

Figure 6.5: Excess colloid chemical potential $\beta\mu_c^{ex}$ versus ϕ_c for the different σ_c, N and ρ_p values explored in this study. (a) shows the $\beta\mu_c^{ex}$ for $\sigma_c = 10\sigma_p$, $\rho_p = 0.05$ and $N = 10$, 30. States A and B in Table 6.1. (b) shows the $\beta\mu_c^{ex}$ at $\sigma_c = 5\sigma_p$, $N = 30$, and $\rho_p = 0.05$, 0.15. States C and D in Table 6.1.

by a maximum which is not the case in above $\beta\mu_c^{ex}$ plots. It is interesting to note that the plot of $\beta\mu_c^{ex}$ versus ϕ_c for $\sigma_c = 10\sigma_p$ and $N = 30$ shows that the $\beta\mu_c^{ex}$ is approximately the same for $\phi_c = 0.4$ and $\phi_c = 0.5$, suggesting that a co-existence point in the phase diagram may exist at these concentrations.

Figure 6.5b presents the $\beta\mu_c^{ex}$ at $\sigma_c = 5\sigma_p$, $N = 30$, and $\rho_p = 0.05$, 0.15. The plots show that the $\beta\mu_c^{ex}$ decreases with increasing ρ_p, due to the increased polymer adsorption. Although the $g_{cp}(r)$ profiles (Figures 6.3 and 6.4) indicate at constant ϕ_c, the peaks are higher for $\rho_p = 0.05$ compared to $\rho_p = 0.15$, it must be noted that these are normalized $g_{cp}(r)$ values. In other words, although the excess adsorption may be lower (for $\rho_p = 0.15$), the total adsorbed amount is higher (observed from the unnormalized $g_{cp}(r)$ plots not shown here). Hence the particle experiences more attractive (negative) polymer-particle contact resulting in a lower chemical potential at $\rho_p = 0.15$. However, further increasing ρ_p would eventually result in a minimum beyond which $\beta\mu_c^{ex}$ would increase with ρ_p. A comparison of the $\beta\mu_c^{ex}$ at different σ_c and all other parameters constant (Figures 6.5a and 6.5b, $N = 30$ and $\rho_p = 0.05$) show that the chemical potential is higher for larger particle diameters, in agreement with the radial distribution plots and previous simulations.[27]

6.4.3 Analysis of polymer-induced effective potentials ($V_p(r)$)

Figures 6.6 – 6.9 show the effective potentials (from equation 6.8) obtained by inverting the colloid-colloid radial distribution plots for the various cases examined in this study. Consider the effective potential plots for $\sigma_c = 10\sigma_p$, $N = 30$ and $\rho_p = 0.05$ (Figure 6.6). In general, there is an attractive minimum in $\beta V_p(r)$ at $D \approx 3\sigma_p$ and a

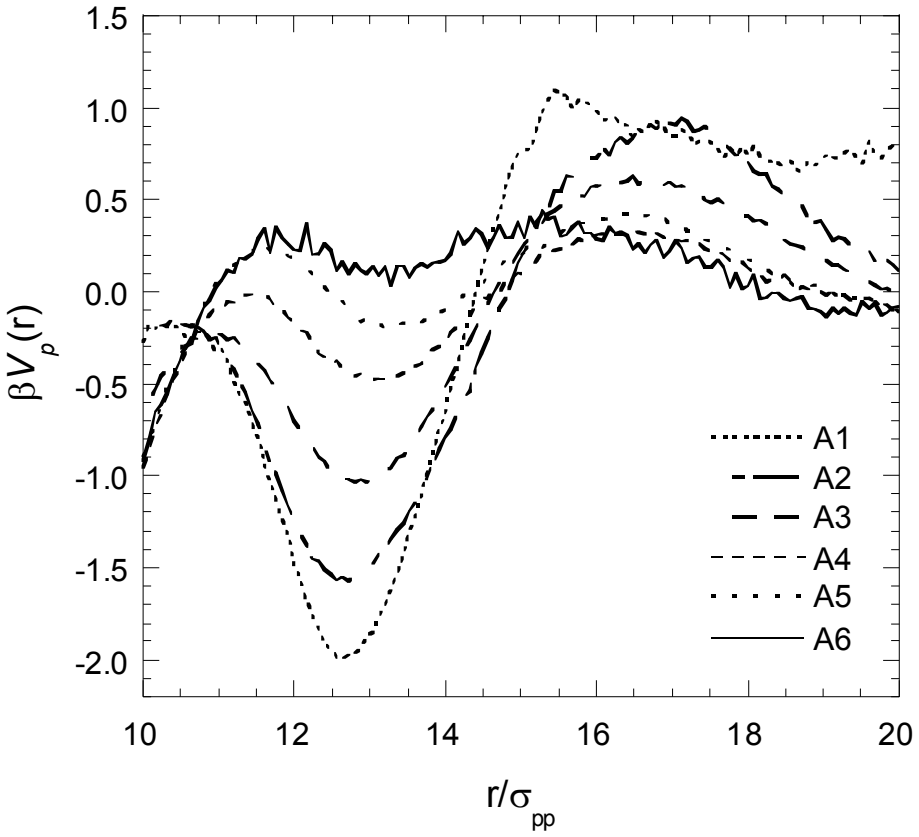

Figure 6.6: The effective one-component colloid potentials, $\beta V_p(r)$, obtained from equation 6.8, for states A1-A6 (Table 6.1). $\sigma_c = 10\sigma_p$, $N = 30$ and $\rho_p = 0.05$.

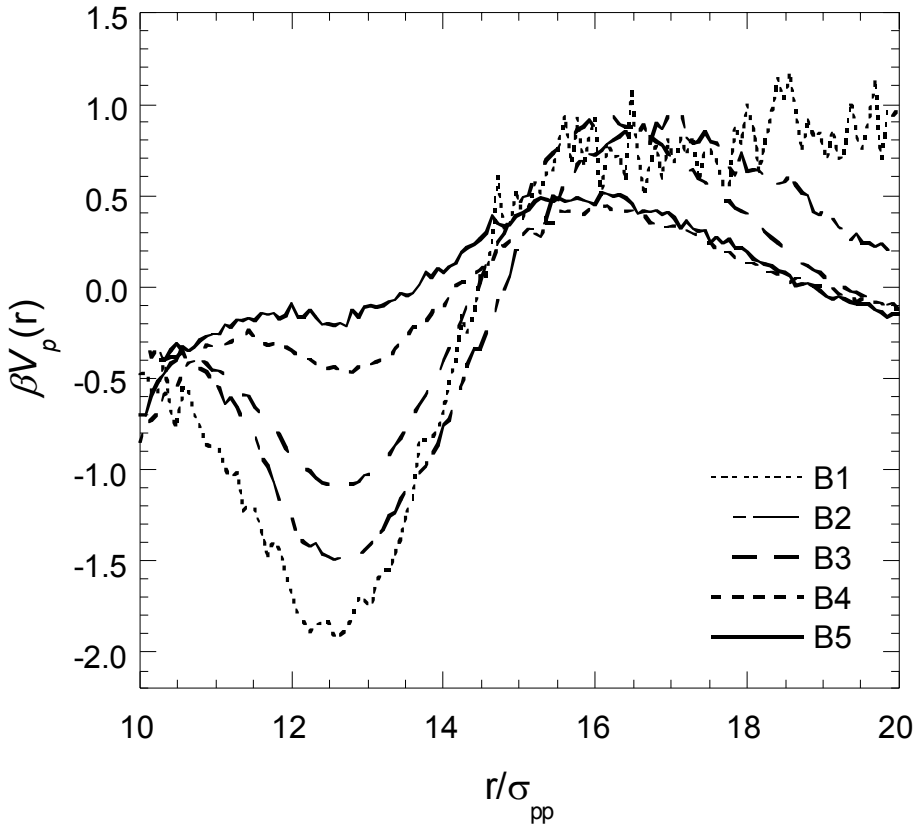

Figure 6.7: The effective one-component colloid potentials, $\beta V_p(r)$, obtained from equation 6.8, for states B1-B5 (Table 6.1). $\sigma_c = 10\sigma_p$, $N = 10$ and $\rho_p = 0.05$.

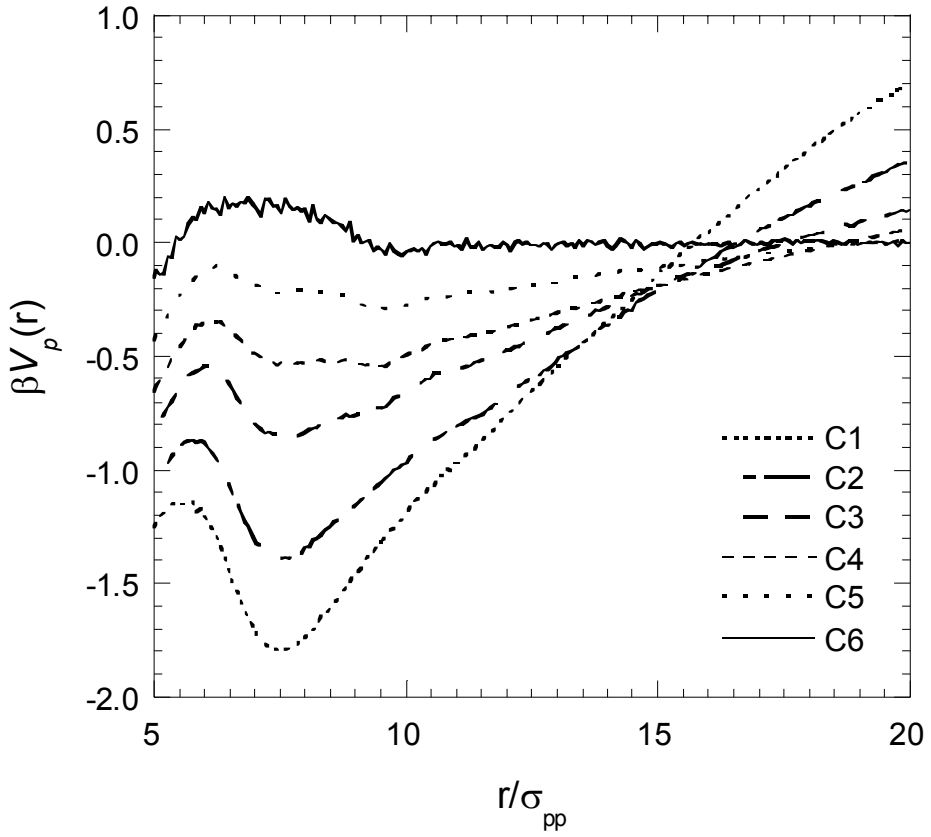

Figure 6.8: The effective one-component colloid potentials, $\beta V_p(r)$, obtained from equation 6.8, for states C1-C6 (Table 6.1). $\sigma_c = 5\sigma_p$, $N = 30$ and $\rho_p = 0.05$.

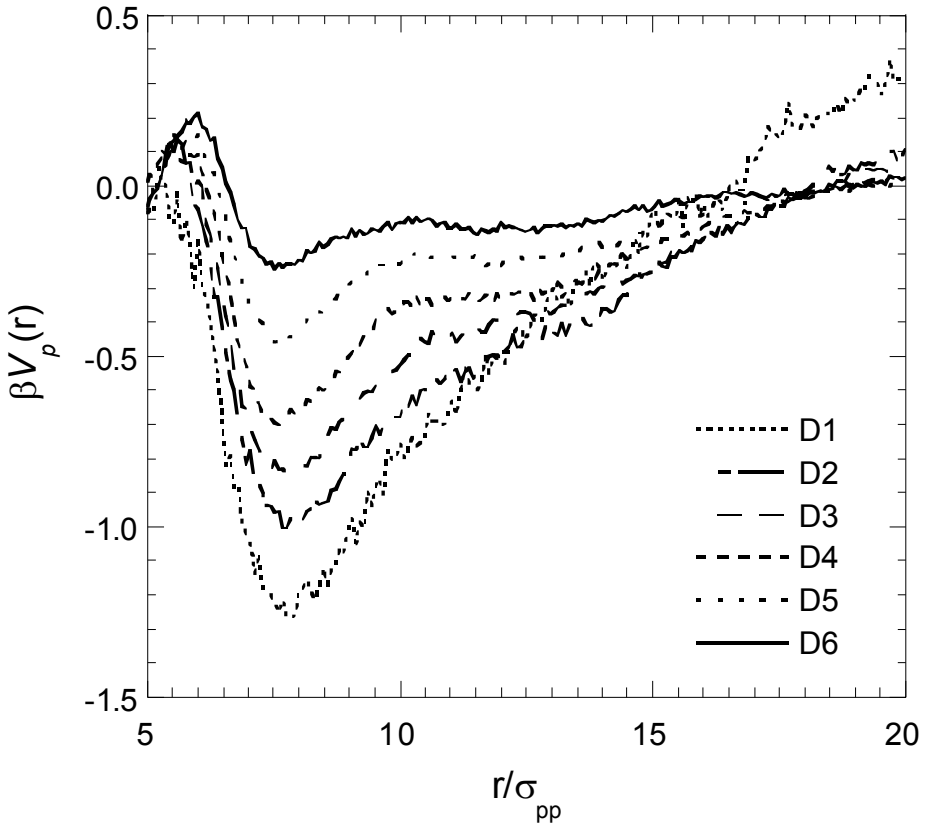

Figure 6.9: The effective one-component colloid potentials, $\beta V_p(r)$, obtained from equation 6.8, for states D1-D6 (Table 6.1). $\sigma_c = 5\sigma_p$, $N = 30$ and $\rho_p = 0.15$.

repulsive maximum between $D \approx 6\sigma_p$ and $D \approx 8\sigma_p$, beyond which there seems to be another small minimum in $\beta V_p(r)$. Also at $D < 3\sigma_p$, the effective potential increases with decreasing separation. This could be ascribed to repulsion between the adsorbed polymer layers. On the other hand, the attractive minimum ($D \approx 3\sigma_p$) could be attributed to a combination of bridging by the adsorbing homopolymers and polymer intersegmental attractions. The nature of the effective potentials is in close agreement to the polymer-induced force profiles between two colloidal particles dispersed in an LJ polymer solution observed in recent simulations. [33] The location of the attractive minimum (at $D \approx 3\sigma_p$) is consistent with the peaks in the $g_{cc}(r)$ and $g_{cp}(r)$ plots. The minimum in the effective potentials grows deeper with decreasing ϕ_c because of the denser adsorbed layer as explained in the earlier section. In addition, the minimum at $D \approx 3\sigma_p$ almost disappears at ϕ_c = 0.5 (A6) and the effective potential is purely repulsive for $D > 1\sigma_p$. It is interesting to note that for $D < 1\sigma_p$, the effective potentials seem to be decreasing monotonically at high ϕ_c. At this separation distance, there is no possibility for polymers to remain in the interparticle region and hence the polymer-driven attraction at such close separations may be due to depletion effects. Although depletion attraction is associated primarily with non-adsorbing polymer solutions, it has been observed experimentally that short-ranged depletion attraction can occur between surfaces containing weakly adsorbed polymers. [34] Similar trends of the effect of ϕ_c on the effective potentials are observed for all the other cases (Figures 6.7 – 6.9).

A comparison of the effective potentials in Figure 6.6 ($\sigma_c = 10\sigma_p$) and Figure 6.8 ($\sigma_c = 5\sigma_p$) shows the effect of colloid diameter at constant N = 30 and ρ_p = 0.05. For constant ϕ_c, the minimum in $\beta V_p(r)$ is lower for larger diameters due to the enhanced

polymer adsorption with increasing σ_c. The effect of increasing the polymer segment density can examined by comparing the polymer-induced effective potentials in Figure 6.8 (ρ_p = 0.05) and Figure 6.9 (ρ_p = 0.15) where $\sigma_c = 5\sigma_p$, N = 30 in both figures. The attractive minimum is lower for ρ_p = 0.05 compared to ρ_p = 0.15. This is surprising because one would expect that with increasing ρ_p, the polymer adsorption would increase thereby resulting in a stronger attractive potential. However, this effect would occur only up to a critical segment density beyond which the entropic limitations due to the reduced excluded volume (with increasing ρ_p) available to both the colloids and the polymer chains would become increasingly important. The trends in $\beta V_p(r)$ suggest that the entropic effects begin to dominate as ρ_p is increased from 0.05 to 0.15 resulting in a relatively weaker polymer-induced attractive minimum.

6.4.4 Limitations and extensions of this study

All the above simulations were performed in a cubic simulation box of length $40\sigma_p$. The $g_{cc}(r)$ and $g_{cp}(r)$ plots, especially for $\sigma_c = 10\sigma_p$, do not fully reach the bulk value ($g_{cc}(r) = g_{cp}(r) = 1$) at half the box length, suggesting that larger box dimensions may be required to determine accurately all the features of the radial distribution plots and consequently the effective potentials. Further, the trends in $\beta V_p(r)$ also suggest the presence of a secondary minimum at larger distances. Computational constraints limit the box dimensions; however, we performed simulations for conditions A1-A5 (in Table 6.1) in a larger box of length $70\sigma_p$. The $g_{cc}(r)$, $g_{cp}(r)$ plots are shown in Figure 6.10. Compared to the plots at similar conditions (A1-A5) and box size $40\sigma_p$ (Figure 6.1), the $g_{cc}(r)$ profiles in Figure 6.10 indicate the presence of a small secondary peak at $11\sigma_p < D$

$< 13\sigma_p$. It is interesting to note there is also a secondary peak in the $g_{cp}(r)$ plots at $D \approx 6\sigma_p$ which correlates with the secondary peak in $g_{cc}(r)$ (using an argument similar to that described earlier for the first peak at low ϕ_c). In addition, this secondary peak in $g_{cc}(r)$ manifests as weak secondary minimum in the plots of $\beta V_p(r)$ in Figure 6.11. While these secondary features are not observed in the earlier plots at a smaller box size ($40\sigma_p$), it is noteworthy that there is no significant change with box dimensions in the location and magnitudes of the primary peaks in the distribution plots and the primary minimum in $\beta V_p(r)$.

The use of periodic boundary conditions in simulations of bulk systems allows $g(r)$ to be known only up to half the simulation box size, rendering the inversion problem undetermined. In the direct problem where one is trying to determine $g(r)$ from knowledge of the potential at all r, OZ techniques can be used to extend $g(r)$ beyond the box size. However, while attempting to find $g(r)$ from simulations with an unknown effective potential (as in our case), we make the implicit assumption that $\beta V_p(r) = 0$ beyond half the box size. This is not necessarily obvious at high densities, and large simulation boxes are needed to achieve proper convergence of the effective potentials. In our study, even at a box size of $70\sigma_p$ the effective potentials do not fully converge to zero (see Figure 6.11) suggesting that a further increase in box size may be required. In addition, the inclusion of colloid-colloid and colloid-polymer VDW attractions adds another complication, which occurs at low colloid densities. At low ϕ_c, the colloid-polymer interactions control the CPM structure resulting in the formation of large colloid-polymer flocs. This can be seen in an equilibrated simulation snapshot for the case of $\sigma_c = 10\sigma_p$, $N = 30$, $\rho_p = 0.05$ and $\phi_c = 0.05$ (state A1) shown in Figure 6.12. As a

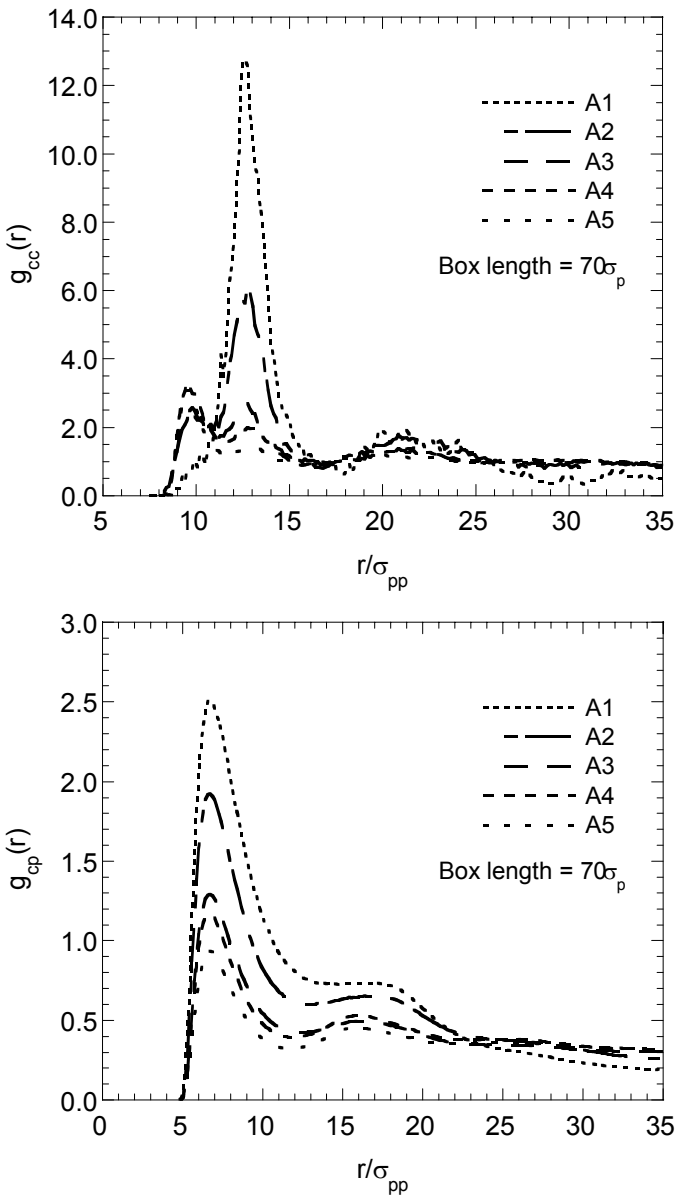

Figure 6.10: The colloid-colloid ($g_{cc}(r)$) and colloid-polymer segment ($g_{cp}(r)$) radial distribution functions, obtained from the binary CPM simulations, for states A1-A5 (Table 6.1). These profiles are obtained from simulations performed in a cubic box of length $70\sigma_p$, compared to earlier results for the same conditions (Figure 6.1) which were for a box size of $40\sigma_p$. $\sigma_c = 10\sigma_p$, $N = 30$ and $\rho_p = 0.05$.

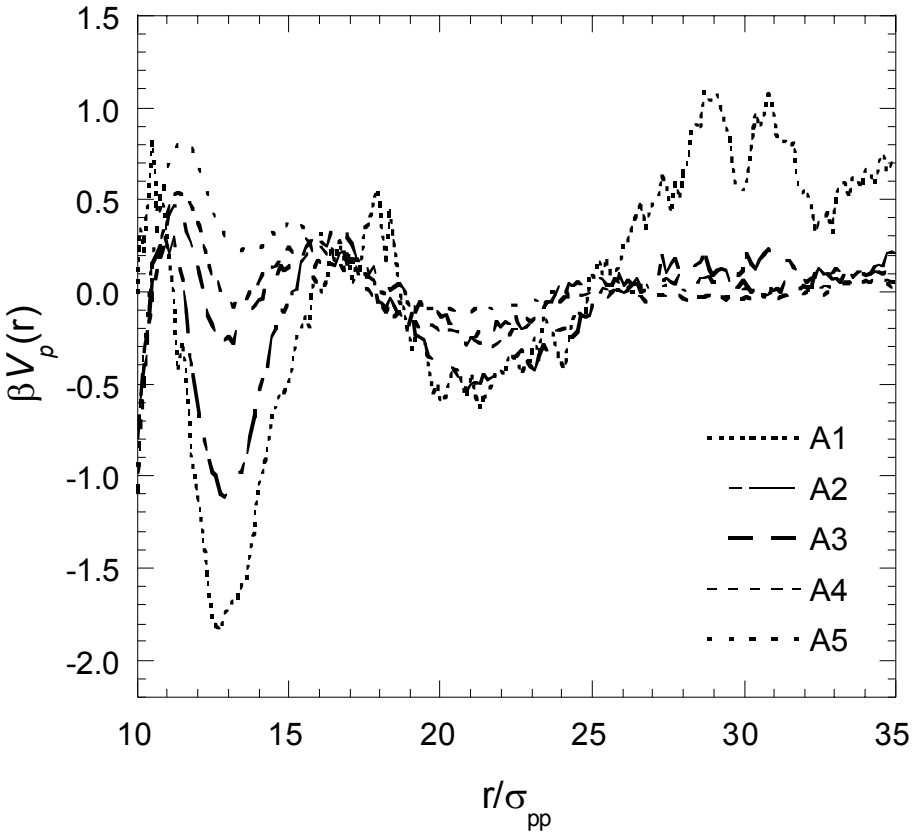

Figure 6.11: The effective one-component colloid potentials, $\beta V_p(r)$, obtained from equation 6.8, for states A1-A5 (Table 6.1). These profiles are obtained from simulations performed in a cubic box of length $70\sigma_p$, compared to earlier results for the same conditions (Figure 6.6) which were for a box size of $40\sigma_p$. $\sigma_c = 10\sigma_p$, $N = 30$ and $\rho_p = 0.05$.

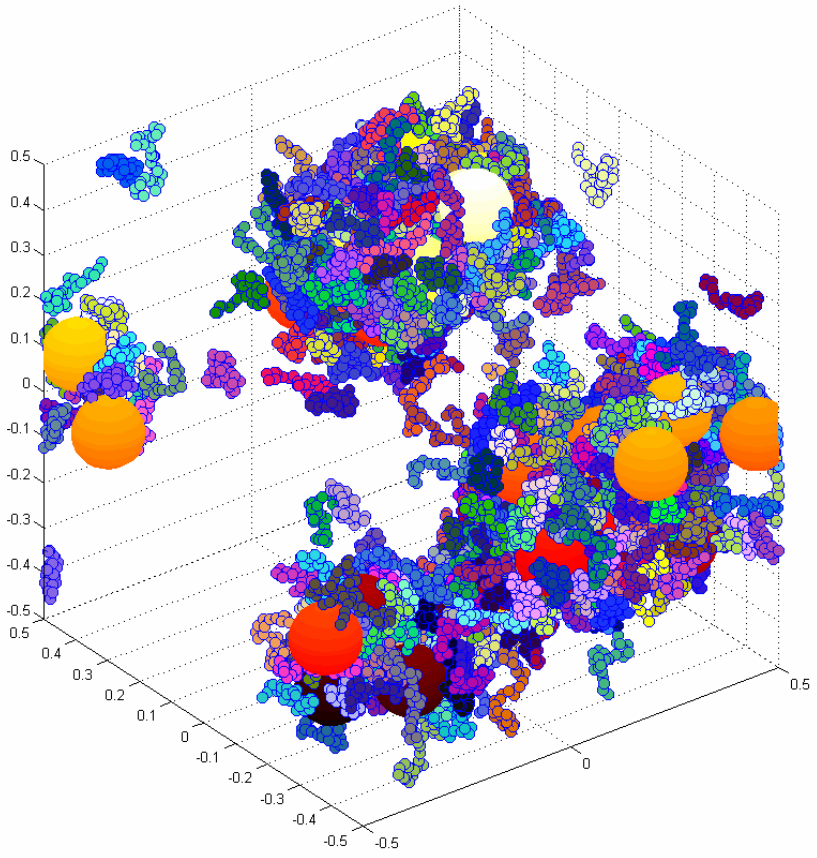

Figure 6.12: Equilibrated configuration snapshot for the case of $\sigma_c = 10\sigma_p$, $N = 30$, $\rho_p = 0.05$ and $\phi_c = 0.05$, Simulation box length= $70\sigma_p$ (state A1).

result, $g_{cc}(r)$ and $g_{cp}(r)$ are less than 1 at distances shorter than half the box size. Even in the simplest of cases where $\rho \to 0$ and $\beta U_{eff}(r) \approx -\ln(g_{cc}(r))$ (from equation 6.7), if $g_{cc}(r) < 1$, then $\beta U_{eff}(r) > 0$ suggesting a repulsive potential at large distances (observed in Figure 6.11). This may well be an artifact of a small box size or the inversion procedure, introduced due to the complexity of the colloid-polymer interactions.

These effective potentials offer important qualitative insights into the complex physics of attractive CPM. However, in order to exploit the advantage of using these potentials in large-scale coarse-grained simulations or in theoretical analysis, it is important to have an explicit expression or parameterization of the potentials. For a hard-sphere CPM wherein the only interaction is a polymer-induced monotonic depletion attraction between the colloids, the effective potentials have been successfully fitted to a form inspired by the Derjaguin approximation.[10] However, such a form could not be fitted to the effective potentials obtained here for LJ colloid-polymer mixtures. While the potentials could be fitted to simple higher order polynomials, these fits would be purely empirical with no physical significance attached to the coefficients. Also, a much larger body of data over a wider range of parameters would be required to fit the effective potentials to functional forms in which the dependence of the coefficients on the various molecular parameters (σ_c, N, ρ_p, ϕ_c) could be established. However, for the purpose of testing the applicability of the inversion procedure and the DH closure approximations to our system, we fitted the effective potentials to a simple n^{th} order polynomial form and calculated $g(r; \beta V_p(r) + \beta U_{cc}(r))$ by performing NVT Monte Carlo simulations for the pure colloid system for a few cases. For example, the $g(r; \beta V_p(r) + \beta U_{cc}(r))$ from the one-component simulations and $g_{cc}(r)$ from the binary CPM simulations for the case σ_c =

$10\sigma_p$, $N = 30$, $\rho_p = 0.05$, $\phi_c = 0.3$ with box size $40\sigma_p$ (State A4 in Table 6.1) are shown in Figure 6.13. It was found, in general, that the $g(r; \beta V_p(r) + \beta U_{cc}(r))$ did not match exactly the $g_{cc}(r)$ from the binary CPM simulations. This raises the question of the applicability of the DH closure to strongly attractive LJ colloid-polymer mixtures. Although the DH closure has been developed for LJ fluids and is known to be accurate over a wide range of densities for LJ fluids as well as mixtures, it has not been used previously in attractive systems with large size asymmetry ($\sigma_c/\sigma_p = 10$ in our case). Increasing the particle diameter increases not only the range of interaction but also the LJ attractive energy. Such long range attractions are not observed in the case of simple fluids. Note that the excellent agreement between $g(r; \beta V_p(r) + \beta U_{cc}(r))$ and $g_{cc}(r)$ from the binary CPM simulations that was obtained by Guzman and de Pablo[10] by using the DH closure for systems with similar size ratios (as in our simulations) was for repulsive LJ systems devoid of any attractive interactions. While initial results suggest that DH closure may not be exact for attractive CPM, further simulations with larger box sizes are required to conclusively verify this. The data obtained from these simulations could also be used to modify the closure approximations to incorporate the effects of polymer-induced attractions (due to bridging and intersegmental attractions).

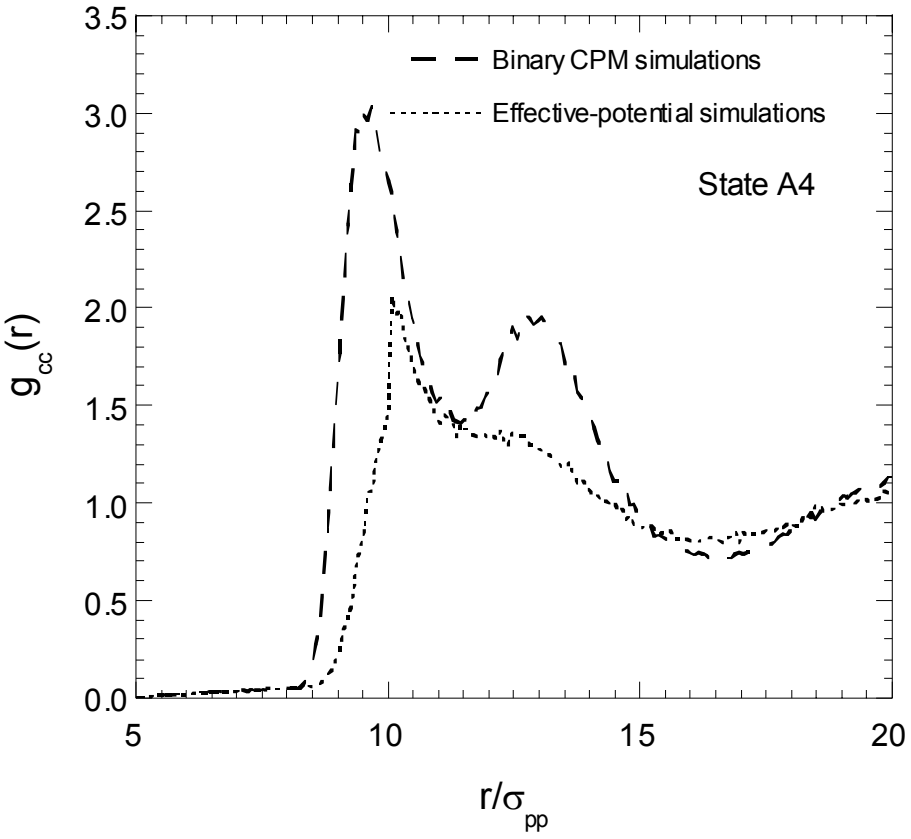

Figure 6.13: Comparison of the colloid-colloid pair distribution functions – $g(r; \beta V_p(r) + \beta U_{cc}(r))$ from the one-component simulations and $g_{cc}(r)$ from the binary CPM simulations for the case $\sigma_c = 10\sigma_p$, $N = 30$, $\rho_p = 0.05$, $\phi_c = 0.3$ with box size $40\sigma_p$ (State A4 in Table 6.1).

6.5 CONCLUDING REMARKS

In this study, we have applied OZ inversion techniques with the DH closure to derive effective one-component potentials for the interaction of colloids suspended in an attractive colloid-polymer mixture. This coarse-graining of the polymer chains would allow modeling and simulation of large-scale colloid-polymer mixtures towards determining the structure and phase behavior of these systems. Our initial results indicate that the effective potentials do not reproduce exactly the pair distribution profiles of the original binary CPM. This could be due to the DH closure approximations which may not be suited ideally for strongly attractive colloid-polymer systems. In addition, larger simulation box sizes than the ones used in this study are required for the binary CPM simulations used to generate the radial distribution plots.

The pair distribution plots and colloid chemical potentials offer important physical insights into the structure and free-energy properties of CPM. In the dilute polymer regime, the polymeric modifiers control the CPM structure at low colloid concentrations. The polymer-induced attractions results in the formation of colloidal flocs. At high colloid-to-polymer concentration ratios, the colloid-colloid interactions determine the structure and polymer effects become relatively unimportant. Also the trends of $\beta\mu_c^{ex}$ versus ϕ_c show a minimum due to the competing effects of (i) attraction due to polymer adsorption and (ii) repulsion due to colloid-colloid excluded volume interactions. This suggests that the polymer-to-colloid concentration ratio is an important design variable for colloid stabilization and self-assembly and could be used to switch between polymer-controlled to colloid-controlled phase behavior in these systems.

6.6 REFERENCES

(1) Asakura, S.; Osawa, F. *J. Chem. Phys.* **1954**, *22*, 1255-1256.

(2) Asakura, S.; Oosawa, F. *J. Polym. Sci.,* **1958**, *33*, 183-192.

(3) Lekkerkerker, H. N. W.; Poon, W. C. K.; Pusey, P. N.; Stroobants, A.; Warren, P. B. *Europhys. Lett.* **1992**, *20*, 559-564.

(4) Gast, A. P.; Hall, C. K.; Russel, W. B. *J. Colloid Interface Sci.* **1983**, *96*, 251-267.

(5) Bolhuis, P. G.; Louis, A. A. *Macromolecules* **2002**, *35*, 1860-1869.

(6) Bolhuis, P. G.; Louis, A. A.; Hansen, J. P.; Meijer, E. J. *J. Chem. Phys.* **2001**, *114*, 4296-4311.

(7) Louis, A. A.; Bolhuis, P. G.; Hansen, J. P.; Meijer, E. J. *Phys. Rev. Lett.* **2000**, *85*, 2522-2525.

(8) Louis, A. A.; Bolhuis, P. G.; Meijer, E. J.; Hansen, J. P. *J. Chem. Phys.* **2002**, *117*, 1893-1907.

(9) Bolhuis, P. G.; Louis, A. A.; Hansen, J. P. *Phys. Rev. Lett.* **2002**, *89*, 128302.

(10) Guzman, O.; de Pablo, J. J. *J. Chem. Phys.* **2003**, *118*, 2392-2397.

(11) Meijer, E. J.; Frenkel, D. *J. Chem. Phys.* **1994**, *100*, 6873.

(12) Meijer, E. J.; Frenkel, D. *Physica A* **1995**, *213*, 130-137.

(13) Sear, R. P.; Frenkel, D. *Phys. Rev. E* **1997**, *55*, 1677-1681.

(14) Tej, M. K.; Meredith, J. C. *J. Chem. Phys.* **2002**, *117*, 5443-5451.

(15) Lekkerkerker, H. N. W.; Poon, W. C. K.; Pusey, P. N.; Stroobants, A.; Warren, P. B. *Europhys. Lett.* **1992**, *20*, 559-564.

(16) Fuchs, M.; Schweizer, K. S. *Phys. Rev. E* **2001**, *64*, 021514.

(17) Fuchs, M.; Schweizer, K. S. *J. Phys.: Condens. Matter* **2002**, *14*, R239-R269.

(18) Eisenriegler, E.; Hanke, A.; Dietrich, S. *Phys. Rev. E* **1996**, *54*, 1134 - 1152.

(19) Wilding, N. B.; Muller, M. *J. Chem. Phys.* **1994**, *101*, 4324.

(20) Lyubartsev, A. P.; Martsinovski, A. A.; Shevkunov, S. V.; Vorontsov-Velyaminov, P. N. *J. Chem. Phys.* **1992**, *96*, 1776-1783.

(21) Escobedo, F.; de Pablo, J. J. *J. Chem. Phys.* **1995**, *103*, 2703-2710.

(22) Hansen, J. P.; McDonald, I. R. *Theory of Simple Liquids*, 2nd ed.; Academic: London, **1986**.

(23) Duh, D.-M.; Henderson, D. *J. Chem. Phys.* **1996**, *104*, 6742-6754.

(24) Mooij, G. C. A. M.; Frenkel, D. *Mol. Phys.* **1991**, *74*, 41-47.

(25) de Pablo, J. J.; Laso, M.; Suter, U. W.; Cochran, H. D. *Fluid Phase Equilib.* **1993**, *83*, 323-331.

(26) Metropolis, N.; Rosenbluth, A. W.; Rosenbluth, M. N.; Teller, A. H.; Teller, E. *J. Chem. Phys.* **1953**, *21*, 1087-1092.

(27) Marla, K. T.; Meredith, J. C. *Langmuir* **2004**, *20*, 1501-1510.

(28) Allen, M. P.; Tildesley, D. J. *Computer Simulation of Liquids*, 1st ed.; Oxford University Press: Clarendon,Oxford, 1987.

(29) Henderson, D.; Sokolowski, S.; Wasan, D. *J. Phys. Stud.* **1998**, *2*, 496.

(30) Pusey, P. N.; Van Megen, W. *Nature* **1986**, *320*, 340-342.

(31) Alder, B. J.; Wainwright, T. E. *J. Chem. Phys.* **1957**, *27*, 1208.

(32) Prausnitz, J. M.; Lichtenthaler, R. N.; de Azevedo, E. G. *Molecular Thermodynamics of Fluid-Phase Equilibria*, 3rd ed.; Prentice-Hall PTR: Upper Saddle River, New Jersey, **1996**.

(33) Marla, K. T.; Meredith, J. C. *Langmuir* **2004**, (submitted).

(34) Ruths, M.; Yoshizawa, H.; Fetters, L. J.; Israelachvili, J. N. *Macromolecules* **1996**, *29*, 7193-7203.

CHAPTER 7

CONCLUSIONS AND RECOMMENDATIONS FOR FUTURE STUDY

The free-energy properties, interaction forces and structure of nanoscale colloid-polymer mixtures have been investigated using Monte Carlo simulation techniques. Computer simulations allow the investigation of the effects of the various molecular parameters over the large variable range and phase space that characterizes colloid-polymer systems. While the accurate calculation of colloid chemical potentials opens the route for detailed phase-behavior simulations of organically modified nanoparticle systems, the polymer-mediated interaction forces between the nanoparticles offer a more direct relation to experiments and provide physical guidelines for design of organic surface modifiers. The simulation results based on the Lennard-Jones model are broadly relevant to systems that are dominated by attractive dispersion interactions.

7.1 CONCLUSIONS

The main advances and findings of this work are summarized below:

- Development of a novel method for calculating colloid chemical potentials in nanoscale colloid-polymer mixtures.
- First simulations of nanocolloid chemical potentials and interaction forces which incorporate *attractive* colloid-polymer and colloid-colloid *dispersion interactions*.
- In attractive colloid-polymer systems, polymer adsorption dominates colloid free-energy properties and interaction forces.
- Empirical scaling relationships have been proposed that describe the dependence of colloid chemical potential on molecular properties of the polymers and colloids.
- Polymer-induced force profiles between nanoparticles differ significantly from previous results in the macroscopic particle limit, when the effect of *curvature* and *attractive interactions* are taken into account.
- Design criteria for effective polymeric modifiers have been identified towards achieving nanoparticle stabilization and self-assembly.

These conclusions are elaborated upon in the following sections.

7.1.1 Thermodynamics of nanoparticle-polymer mixtures

A novel method for calculation of the nanocolloid chemical potentials in pure solvent or in the presence of polymeric modifiers has been developed in this work. This method, based on the expanded ensemble Monte Carlo (EEMC) algorithm, was shown to be accurate using the hard-sphere (HS) model system, which provides a stringent test for the efficiency of EEMC chemical potential calculations. The nanoparticle diameter is

used as the expansion variable and during the course of the EEMC simulation, incremental chemical potentials are generated as the diameter of the colloidal particle varies between zero and maximum diameter. When the incremental chemical potentials from zero to particle size σ_c are summed, the correct chemical potential at size σ_c, measured independently, is recovered. While the EEMC method has been used in this work primarily for calculating colloid chemical potentials (μ_c) in a dilute solution of surface modifiers, this technique is also useful potentially with regard to questions concerning the thermodynamics of mixing in the opposite limit of dispersing nanoparticles in a polymer matrix for nanocomposites applications.

For HS colloid-polymer systems, μ_c increases as a cubic polynomial in σ_c for all polymer molecular weights, reflecting the increase in the probability of steric overlaps and excluded volume. The addition of low molecular weight polymer chains brings about a large reduction in the colloid chemical potential, compared to pure monomer solvent at the same volume fraction. This free-energy reducing effect diminishes asymptotically for longer chains. This behavior shows that even in the absence of attractive colloid-polymer interactions, there is an entropically-derived benefit to dispersing nanocolloids in oligomer or polymer solutions, rather than solvent alone. In addition, the decrease in μ_c also suggests a monotonic improvement in suspension miscibility with increasing chain length (n).

A major advance that has been made in this work is the incorporation of attractive colloid-polymer van der Waals interactions, which are often neglected in theoretical and simulation studies due to the added complexity. When nanoparticles are suspended in a dilute solution of adsorbing polymeric modifiers, the free energy required for particle

insertion decreases with the colloid diameter σ_c (opposite to the HS case) due to the increased attractive energy and surface area available for particle-polymer contacts. However, similar to the case of nonadsorbing modifiers, the μ_c decreases as molecular weight of the adsorbing modifiers increases, albeit for different reasons. This suggests that for both HS and attractive CPM, the colloid concentration at which phase separation occurs would increase with increasing polymer chain length (at constant polymer concentration). For the HS system, the one-phase region necessarily implies a stable dispersion of colloids in nonadsorbing polymer solution. These observations have also been reported in recent theoretical[1,2] and experimental[3] studies of HS colloid-polymer systems. However, in attractive CPM, the colloid-polymer attraction could cause bridging, resulting in the formation of flocs. Hence, the one-phase region could consist of either colloid-polymer flocs or a stable dispersion of colloids in adsorbing polymer solution or a mixture of both.

In attractive systems, the chemical potential is dominated by chain adsorption (Γ_s), and both μ_c and Γ_s show a similar dependence on polymer chain length. This provides a molecular interpretation of the effect of adsorbed organic layers on nanoparticle stability and self-assembly. Since polymer adsorption can be measured by techniques like small angle neutron scattering, the strong correlation between μ_c and Γ_s also provides an indirect route for determining the effect of molecular parameters like polymer chain length and concentration on free-energy properties of the colloid, which are generally not accessible from experiments. In addition, the dependence of chemical potential on n and σ_c was found to be represented well by a power scaling law of the form $\beta\mu_c^{ex} \sim \sigma_c^{3.0} n^b$. The colloid diameter exponent in the above scaling relationship was

close to 3.0 for all cases, independent of the polymer segment density (ρ_p) and colloid-polymer interaction energy (ε_{cp}). On the other hand, the chain length exponent varied greatly with ρ_p and ε_{cp}. Such power law relationships may prove to be useful in interpolating and extrapolating experimental and simulation results for free energy properties of colloid-polymer mixtures and could also guide theoretical model development.

In the dilute polymer regime and at low colloid concentrations (ϕ_c), the polymeric modifiers control the structure and phase-behavior of the CPM. At high colloid-to-polymer concentration ratios, the colloid-colloid interactions determine the structure and polymer effects become relatively unimportant. The colloid chemical potential $\beta\mu_c^{ex}$ as a function of ϕ_c shows a minimum due to the competition between polymer adsorption and colloid-colloid excluded volume interactions. This minimum represents a necessary, but not sufficient condition for phase instability. The polymer-to-colloid concentration ratio is an important design variable for colloid stabilization and self-assembly and could be used to switch between polymer-controlled to colloid-controlled phase behavior in these systems.

7.1.2 Nanoparticle interaction forces: Adsorbed and End-grafted modifiers

Grand canonical MC simulations of interaction forces between nanoparticles in the presence of adsorbing Lennard-Jones homopolymer modifiers reveal a strong correlation between the polymer-induced forces (F_P) and polymer adsorption. An increase in either n, σ_c or ε_{cp} results in increased adsorption and consequently a stronger polymer-induced attraction between the nanoparticles. At smaller nanoparticle diameters,

the polymer adsorption is weak and the homopolymer modifiers have no significant effect on nanoparticle interactions. This suggests that as particle sizes get smaller, polymers that have a relatively stronger affinity for the colloids (higher ε_{cp}) need to be chosen for effective modification. In general, adsorbing modifiers give rise to a short-range repulsion (limited to the first 2-3 monolayers) and long-range attraction between the nanoparticles in the full thermodynamic equilibrium condition over the range of parameters explored.

In the macroscopic limit where the colloidal particles are represented as flat walls, adsorbing polymers give rise to a monotonic attraction at full equilibrium. However, the effect of curvature and the incorporation of colloid-polymer attraction, both of which are important for nanoscale colloidal systems, result in markedly different force profiles suggesting that the well-established results in the macroscopic limit may not be applicable directly to nanoparticle systems.

Grafted homopolymers which have attractive dispersion interactions with the particle surface, give rise to either long-ranged attraction and short-ranged repulsion, or pure repulsion depending on the grafting density (ρ_a^*) and polymer chain length. There is a critical limit of ρ_a^* and n beyond which, increasing either of them would result in an increasingly repulsive polymer-induced force. A higher ρ_a^* is required for stabilization as the particle size increases. The ability of grafted modifiers to induce both attractive and repulsive forces between the nanoparticles makes them useful for both self-assembly as well as stabilization purposes. Also grafted polymers are better suited for stabilization as compared to adsorbing modifiers.

The polymer-induced attraction in both adsorbing and grafted modifiers is attributed primarily to polymer intersegmental interactions and bridging, the relative contributions of which could be adjusted by tuning the colloid-polymer and polymer-polymer interaction (ε_{pp}) energies. The location of the equilibrium spacing between the nanoparticles (corresponding to $F_P = 0$) can be controlled by the molecular parameters n, ε_{cp} and ε_{pp} (and ρ_a^* for grafted modifiers) for both adsorbing and grafted modifiers. This provides a molecular mechanism for thermodynamically-driven nanoparticle self-assembly with controlled lattice spacing – one of the key requirements for the development of photonic and optoelectronic devices based on nanocolloid phenomena.

The polymer chain lengths examined in this work (n = 5 – 50) correspond to molecular weights ranging from 1000 to 30000 depending on the polymer and its persistence length. In addition, taking a single model chain segment to represent several "real polymer" repeat units (≈ 5 nm), the model colloid diameters examined here would range from 5 nm to 75 nm. Although a simple Lennard-Jones potential is used in this work to model the dispersion interactions, the correlation between adsorption and μ_c (as well as interaction forces), and the basic trends in both μ_c and F_P should extend to other power-law polymer-colloid potentials, including attractive Coulombic (electrostatic) and Hamaker (integrated LJ) potentials.

7.2 RECOMMENDATIONS

7.2.1 Monte Carlo simulations of phase behavior of colloid-polymer mixtures

The EEMC method, applied in this work to calculate colloid chemical potentials, makes it possible to simulate the full phase behavior of nanoparticle-polymer mixtures.

The phase behavior simulations can be performed using the Expanded Grand Canonical Ensemble Monte Carlo method combined with Gibbs-Duhem Integration (EGC-GD).[4,5] The colloid insertion and deletion moves required for equilibration of chemical potentials can be performed using the expanded ensemble technique outlined in this work. The basic idea of the EGC-GD method and the algorithm for its application to phase equilibrium simulation of nanocolloid-modifier systems is outlined below. The Gibbs-Duhem equation for phase "I" of a two-component system (colloid-polymer) can be written as

$$d\left(\beta\mu_c\right)^I = h_c{}^I d\beta^I + v_c{}^I \beta^I dP^I , \tag{7.1}$$

where h^I_c and v^I_c are the molar enthalpy and volume respectively and subscript c refers to the colloid. Writing the above equation for the colloid in phases I and II and recognizing that at coexistence $dP^I = dP^{II}$ and $d(\beta\mu_c)^I = d(\beta\mu_c)^{II}$, we can eliminate dP from both equations to get

$$\left[\frac{d\left(\beta\mu_c\right)}{d\beta}\right]_{eq} = \frac{\rho_c^{II} h_c^{II} - \rho_c^I h_c^I}{\rho_c^{II} - \rho_c^I} = \frac{\rho_c^{II} u_c^{II} - \rho_c^I u_c^I}{\rho_c^{II} - \rho_c^I}, \tag{7.2}$$

where ρ^I_c and u^I_c are the molar (or number) density and internal energy of the phase respectively. Numerical integration of equation 7.2 requires an initial coexistence point. For subsequent steps of β and $\beta\mu_c$, the integrand of equation 7.2 can be evaluated by conducting simultaneous EGC simulations, one for each phase. Predictor-corrector methods can be used to carry out the necessary numerical integration.

Algorithm for phase equilibrium calculations of nanocolloid-polymer systems

(i) Specify the relevant simulation parameters: n, σ_c and ρ_p

(ii) Choose an initial temperature and run a series of canonical ensemble (*NVT*) simulations at different colloid densities (ρ_c). A plot of μ_c vs. ρ_c as shown below (Fig. 7.1) should give the μ_c values at the first coexistence point.

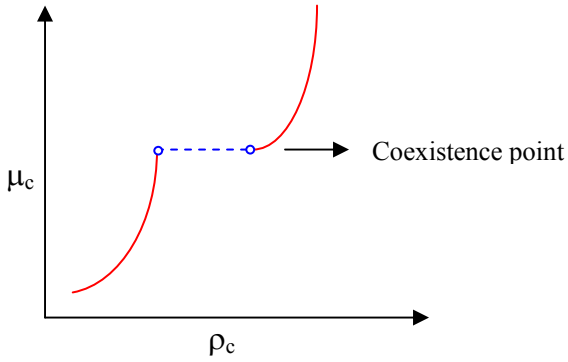

Figure 7.1: Schematic plot of the colloid chemical potential vs. colloid density to get the first coexistence point.

(iii) Run EGC simulations at this coexistence point to get ρ_c and u_c in the two phases. Calculate the slope $[d(\beta\mu_c)/d\beta]_{eq}$ from equation 7.2.

(iv) Make a step increment in β ($\Delta\beta = 1/\Delta T$) and apply a predictor to estimate the new value of $\beta\mu_c$ at the new temperature. The simple forward Euler formula can be used as a predictor, e.g., $\beta\mu_{c,\,i+1} = \beta\mu_{c,\,i} + [d(\beta\mu_c)/d\beta].\Delta\beta$

(v) Initiate two new EGC simulations (one for each phase) at the new temperature and predicted chemical potentials.

(vi) Collect averages of the ρ_c and u_c needed to evaluate the slope at the new state condition.

(vii) Apply a corrector to update the estimate of the chemical potential, using the slope determined from the current running averages. A second order corrector, which allows the flexibility in varying the integration step size, can be used.[4] The general form of the corrector equation is:

$$\beta\mu_{c,k+1} = \beta\mu_{c,k} + A\sum_{i=-1}^{i=1} B_i \left(\frac{d\beta\mu_c}{d\beta}\right)_{k+i}, \qquad (7.3)$$

where $A = h_k/[6(1+r)]$, $B_{-1} = -r^{-1}$, $B_0 = r^{-1} + 4 + 3r$, $B_1 = 2+3r$, $r = h_{k-1}/h_k$ and h is the integration step size.

(viii) Repeat from step (v) till convergence, as indicated by $|\beta\mu_{c,\,k+1} - \beta\mu_{c,\,k}| < \delta$, where δ is the tolerance limit.

In this manner coexistence points can be located at various temperatures to generate T, ρ_c phase diagrams. The phase diagrams, which can be generated as a function of n, σ_c and ρ_p, would enable rational and predictive design of organic modifiers for achieving self-assembly or dispersability of the nanocolloid system in question at the desired concentration.

7.2.2 Integrated Lennard-Jones potentials with density-of-states Monte Carlo

The LJ 6-12 potential captures the generic features of attractive colloid-polymer mixtures well, but the use of LJ potential involves the implicit assumption of considering the entire colloidal particle to be one big molecule. However, in reality a colloidal particle is composed of a large number of atoms or molecules. Hence a more accurate model for the above system would be obtained by integration of the LJ potential between all the atoms in the particle and each polymer segment, in the manner of the Hamaker microscopic approach.[6] This integration results in a potential where the repulsion is longer-ranged and the attraction is shorter-ranged compared to the LJ 6-12 potential.[7] In addition, the attractive minimum also becomes deeper. EEMC simulations with the integrated LJ potential would be an important advance towards accurate modeling of the thermodynamics of CPM.

However, the enhanced colloid-polymer attraction strength in the integrated LJ potential causes the CPM to be stuck in deep free-energy minima during the simulation. This problem gets compounded in the limit of large particle sizes and long polymer chains due to the additional driving force for adsorption leading to deeper minima. This poses significant obstacles for molecular simulations; once the system is trapped in a minimum, conventional algorithms are unable to explore configurations pertaining to other, relevant regions of phase space. In the EEMC method, preweighting factors which control the frequency of visits to the intermediate states are determined by initial trial simulations. For systems with deep attractive minimums, it maybe difficult to accurately determine these weights *a priori*. This problem can be overcome by combining the EE technique with the density-of-states (DOS) Monte Carlo method.[8,9] The main idea of the

DOS method is to accept trial configurations of the system according to a running estimate of the density of states. A random walk in energy space is used to visit each energy level and the density of states function is constructed concurrently during the course of the simulation. This method could potentially overcome the sampling limitations and enable efficient simulation in strongly attractive colloid-polymer mixtures.

7.3 REFERENCES

(1) Fuchs, M.; Schweizer, K. S. *Europhys. Lett.* **2000**, *51*, 621-627.

(2) Fuchs, M.; Schweizer, K. S. *Phys. Rev. E* **2001**, *64*, 021514.

(3) Ramakrishnan, S.; Fuchs, M.; Schweizer, K. S.; Zukoski, C. F. *J. Chem. Phys* **2002**, *116*, 2201.

(4) Escobedo, F. A.; de Pablo, J. J. *J. Chem. Phys.* **1997**, *106*, 2911-2923.

(5) Escobedo, F.; de Pablo, J. J. *J. Chem. Phys.* **1996**, *105*, 4391-4394.

(6) Israelachvili, J. N.; Kott, S. J. *J. Chem. Phys* **1988**, *88*, 7162.

(7) Henderson, D.; Duh, D.-M.; Chu, X.; Wasan, D. *J. Colloid Interface Sci.* **1997**, *185*, 265-268.

(8) Yan, Q.; Faller, R.; de Pablo, J. J. *J. Chem. Phys* **2002**, *116*, 8745-8749.

(9) Wang, F.; Landau, D. P. *Phys. Rev. Lett.* **2001**, *86*, 2050-2053.

VITA

Krishna Tej Marla was born on October 21, 1976 in Hyderabad, India to Padma and M. Veerabhadra Sastry. He did his schooling in St. Xaviers High School, Bombay. He attended D.J. Sanghvi College of Engineering (University of Mumbai), where he obtained his Bachelor's degree in chemical engineering with high honors in 1998. He later obtained his Masters degree in chemical engineering from the Indian Institute of Technology, Mumbai in 2000. His Masters Dissertation focused on supercritical fluid extraction of natural products under the guidance of Prof. Sandip Roy. He joined the School of Chemical & Biomolecular Engineering at Georgia Institute of Technology for pursuing his Ph.D in the fall of 2000. He worked in the area of thermodynamics of nanoscale colloid-polymer mixtures under the guidance of Dr. J. Carson Meredith. He was awarded the "*Ziegler award for the Best Paper*" in 2003 for a research paper that he co-authored with his advisor. He was also a fellow of the Molecular Design Institute (Georgia Tech) for 2002-2003. After graduating with a Ph.D in chemical engineering in Fall 2004, he will work at Intel in Portland, Oregon.